MARMARA UNIVERSITY

INSTITUTE OF SCIENCE

ELECTROCATALYTIC PROPERTIES AND ZN-AIR BATTERY APPLICATION OF MONONUCLEAR AND DINUCLEAR PHTHALOCYANINE COMPLEXES INVOLVING TERTIARY BUTYL AND OXO BRIDGING GROUPS

TARIFA KANIZ

720716921

PhD THESIS

Department of Chemistry

Physical Chemistry Program

ADVISOR

Prof. Dr. Ali Rıza ÖZKAYA

ISTANBUL, 2025

MARMARA UNIVERSITY

INSTITUTE OF SCIENCE

ELECTROCATALYTIC PROPERTIES AND ZN-AIR BATTERY APPLICATION OF MONONUCLEAR AND DINUCLEAR PHTHALOCYANINE COMPLEXES INVOLVING TERTIARY BUTYL AND OXO BRIDGING GROUPS

TARIFA KANIZ

720716921

PhD THESIS

Department of Chemistry

Physical Chemistry Program

ADVISOR

Prof. Dr. Ali Rıza ÖZKAYA

ISTANBUL, 2025

ACKNOWLEDGEMENTS

I express my utmost satisfaction to Almighty Allah, the most benevolent, the merciful, and the gracious, who has given me knowledge, strength, patience and opportunity to complete this research work.

First and foremost, I am tremendously thankful to my advisor, Prof. Dr. Ali Rıza ÖZKAYA, for his indispensable advice, invaluable supervision, continuous support, and patience, during my PhD study. His vast knowledge as well as bountiful experience has inspired me in all the time of my academic research and daily life.

I would like to express my deepest gratitude to Prof. Dr. Zafer ODABAŞ, who took part in the thesis monitoring committee and contributed to the synthesis of the noble phthalocyanine derivatives that I used in my studies. I would also like to thank his student Safinaz Şahin.

I owe a huge debt of gratitude to another member of my thesis monitoring committee, Assoc. Prof. Duygu Akyüz ÇUBUKÇU, for her generous help from the very beginning of my PhD life.

I would like to express my gratitude to Assistant Prof. Efe Baturhan ORMAN for all the guidance, motivation, and instruction he provided me throughout my doctoral studies.

I would also like to thank all my fellow lab mates and research team, especially Özgün AKDAĞ, who helped me get through this difficult period in the most positive way. He is my lifesaver brother from the day we started our research until the last day of my PhD life.

In addition, thanks to my friend Dicle ATILMIŞ, who always stood by my side when times get hard. I am grateful for the laughter, support, and memories we have shared.

Finally, but definitely not the least, I express my gratitude to my dear husband Md. Faruk Hossen; it would be totally impossible for me to finish this study without his treasured support, continuous inspiration, enormous understanding, and encouragement in the past few years. I also want to include the name of my eight-month-old daughter, Yanisha Binte Hossen, because she is the light of my life. I also appreciate all the help and heartwarming kindness I received from the rest of my family.

This study, which examined the electrochemical, spectroelectrochemical, and electro

catalytic properties of novel phthalocyanines in Marmara University, Faculty of Arts and Sciences, Department of Chemistry, Physical Chemistry program, was supported by Marmara University Scientific Research Project Coordination Unit (BAPKO) through the project coded "FDK-2021-10045" with ID “10045”. Experimental measurements were made at Marmara University, Faculty of Arts and Sciences, Department of Chemistry, Electrochemistry Research Laboratory.

I would like to express my gratitude to the Türkiye Bursları-Yurtdışı Türkler ve Akraba Topluluklar Başkanlığı (YTB) for awarding me this fully funded scholarship to pursue my PhD.

I also extend my gratitude to the Scientific and Technological Research Council of Turkey (TÜBİTAK) for its support of this thesis study through the 1001 project numbered 118Z250.

February, 2025

Tarifa Kaniz

TABLE OF CONTENTS

ÖZET

Metallerin ftalosiyanin (MPc) kompleksleri; katalizörler, yarı iletkenler, moleküler elektronik, gaz sensörleri, doğrusal olmayan optikler, fotovoltaik hücreler, elektrokromizm, güneş hücreleri, yakıt hücreleri ve doğrudan metanol yakıt hücreleri gibi alanlarda büyük ilgi görmektedir. Bu bileşikler, 18 π-elektronlu konjuge sistemleri nedeniyle bilimsel, teknolojik, endüstriyel ve tıbbi alanlarda yaygın olarak kullanılmaktadır. Ayrıca, zengin redoks davranışları, kimyasal stabiliteleri, merkezi boşlukta farklı metal bulundurabilmeleri, halka yapılarının değiştirilme kolaylığı ve yüksek metanol toleransları nedeniyle oksijen redoks prosesleri için elektrokatalizör olarak araştırmacıların dikkatini çekmiştir. Bir çok enerji dönüşüm sisteminde elektrokatalitik malzeme olarak kullanılmakta olan ve zengin redoks özellikleri sergileyen MPc kompleksleri yüksek güç yoğunluğuna sahip, uygun maliyetli ve güvenilir enerji dönüşüm sistemlerinin geliştirilmesi için çok önemlidir.

Bu çalışmada, yakıt ve metal-hava pilleri için etkinliği yüksek oksijen elektrokatalizörleri geliştirmek amacıyla, yeni mononükleer ve dinükleer metal ftalosiyanin bileşiklerinin elektrokimyasal redoks özellikleri, iki farklı çözücü ortamında elektroanalitik yöntemler ile ayrıntılı olarak araştırılmıştır. Söz konusu bileşikler genel olarak ligand ve metal temelli redoks prosesleri gösterirken, top tipi dinükleer bileşiklerin, iki MPc birimi arasındaki molekül içi etkileşimler nedeniyle çeşitli karışık değerlikli yükseltgenme ve indirgenme türleri oluşturdukları gözlemlenmiştir.

Gözlenen indirgenme ve yükseltgenme reaksiyonlarının ligand veya metal merkezli olduğunu belirlemek amacıyla eş-zamanlı spektroelektrokimyasal analizler gerçekleştirilmiştir. Daha sonra, bu bileşiklerin oksijen indirgenme ve oksijen yükseltgenme reaksiyonlarındaki elektrokatalitik performansları, yakıt pili ve çinko-hava pili uygulamalarına yönelik olarak asidik ve bazik ortamda genel voltametri (doğrusal taramalı ve dönüşümlü voltametri) ve hidrodinamik voltametri (dönen halka ve dönen halka-disk elektrot voltametrisi) teknikleri ile incelenmiştir.

Oksijen elektrokatalizörü olarak yüksek aktivite gösteren bileşiklerin çinko-hava pili performans testleri galvanodinamik ve galvanostatik tekniklerle gerçekleştirilmiştir. Söz konusu ölçümler, redoks aktif metal içeren top tipi metal ftalosiyaninlerin, yakıt ve çinko-hava pil uygulamalarında katot katalizörü olarak platine alternatif olabileceklerini

göstermiştir. Yüzyüze iki redoks-aktif metal merkezi içeren yapısı nedeniyle, top tipi dinükleer Fe kompleksinin oksijen indirgeme reaksiyonu için oldukça yüksek katalitik aktivite sergilediği anlaşılmıştır.

SUMMARY

ELECTROCATALYTIC PROPERTIES AND ZN-AIR BATTERY APPLICATION OF MONONUCLEAR AND DINUCLEAR PHTHALOCYANINE COMPLEXES INVOLVING TERTIARY BUTYL AND OXO BRIDGING GROUPS

The metal phthalocyanine (MPc) complexes have attracted great interest in fields such as catalysts, semiconductors, molecular electronics, gas sensors, nonlinear optics, photovoltaic cells, electrochromism, solar cells, fuel cells, and direct methanol fuel cells. These compounds are widely used in scientific, technological, industrial, and medical fields due to their 18 π-electron conjugated systems. Additionally, their rich redox behaviour, chemical stability, ability to accommodate different metals in the central cavity, ease of ring modification, and high methanol tolerance have drawn researchers' attention as electro catalysts for oxygen redox processes. MPc complexes, which exhibit rich redox properties and are used as electro catalytic materials in many energy conversion systems, are crucial for developing high-power-density, cost-effective, and reliable energy conversion systems.

In this study, the electrochemical redox properties of novel mononuclear and dinuclear metal phthalocyanine compounds were investigated in detail using electroanalytical methods in two different solvent media to develop highly efficient oxygen electro catalysts for fuel cells and metal-air batteries. While these compounds generally exhibited ligand- and metal-based redox processes, it was observed that the ball-type dinuclear compounds formed various mixed-valence oxidation and reduction species due to intramolecular interactions between the two MPc units.

In situ spectroelectrochemical analyses were conducted to determine whether the observed reduction and oxidation reactions were ligand- or metal-centered. Subsequently, the electro catalytic performance of these compounds in oxygen reduction and oxygen evolution reactions was examined in acidic and basic media using general voltammetry (linear sweep and cyclic voltammetry) and hydrodynamic voltammetry (rotating ring and rotating ring-disk electrode voltammetry) techniques for fuel cell and zinc-air battery applications.

Zinc-air battery performance tests of the compounds exhibiting high activity as oxygen electro catalysts were conducted using galvanodynamic and galvanostatic techniques. These measurements demonstrated that redox-active metal-containing ball-type metal phthalocyanines could serve as alternative cathode catalysts to platinum in fuel cell and

zinc-air battery applications. Due to its rigid cofacial structure containing two face-to-face redox-active metal centers, the ball-type dinuclear Fe complex exhibited remarkably high catalytic activity for the oxygen reduction reaction.

CLAIM FOR ORIGINALITY

ELECTROCATALYTIC PROPERTIES AND ZN-AIR BATTERY APPLICATION OF MONONUCLEAR AND DINUCLEAR PHTHALOCYANINE COMPLEXES INVOLVING TERTIARY BUTYL AND OXO BRIDGING GROUPS

In this thesis study, the mononuclear and dinuclear phthalocyanines, which have been systematically examined, are novel compounds that have not been synthesized before as of the date they were discussed, electrochemical measurements and evaluations carried out to determine their technological usage areas entered the literature for the first time with this thesis study. From this perspective, the study is new and original. Moreover, since the voltammetric, *in situ* spectroelectrochemical, catalytic analyses of the compounds and application in the Zn-air battery, which are the subject of the thesis, as well as the measurements and evaluations for their usability in technological fields such as electrochemical energy conversion and energy storage devices, have been carried out, it can be easily stated that the study can be an example for future research and will make a significant contribution to the literature.

The results of this thesis study and its evaluations were presented as papers at two international conferences:

- "Electrochemical, Spectro-electrochemical, and Electro- Catalytic Properties of Novel Di-nuclear Ball Type Metallo Phthalocyanines Involving Tertiary Butyl and Oxo Bridging Groups, 2021, 10.13140/RG.2.2.19837.49122, 29th Annual Meeting of the International Society of Electrochemistry, Czech Republic, April 2021."
- "Electrochemical, Spectro-electrochemical, and Electro-Catalytic Properties of New Mononuclear Metallo Phthalocyanines Involving Tertiary Butyl and Oxo Bridging Groups, 2021, 10.13140/RG.2.2.31581.54243, 29th Annual Meeting of the International Society of Electrochemistry, Czech Republic, April 2021."
- "Electrochemical and Electro-Catalytic Oxygen Reducing Properties of Metal Phthalocyanines Involving Tertiary Butyl and Oxo Bridging Groups. Tarifa Kaniz et al., J BiosensBioelectron 2019, Volume 10, 13th International Conference on Electrochemistry in Barcelona, Spain at 27-28 May, 2017".

The results of this thesis were also published in 2 articles within the scope of SCI.

- Published articles are; “Electrochemical and *In-situ* exhibited spectroelectrochemical properties of novel 4,40.625*pt′*0.625*pt*-(3,5-di-tert-butyl-1,2- phenylene) bis(oxy) substituted ball-type phthalocyanine compounds. Synthetic Metals 297 (2023) 117408.”
- “Electrochemical and in-situ spectroelectrochemical properties of novel mononuclear 2,4-di-tert-butyl-6-(3,4-dicyanophenoxy) phenolate substituted metallophthalocyanine compounds. Polyhedron, 1 October, 2023, 116541.”

SYMBOLS

π	: Pi
e^-	: Electron
n	: Number of electrons transferred
^oC	: Degrees Celsius
σ	: Sigma
J_L	: Current density
E_p	: Peak potentials
$E_{1/2}$	: Half peak potentials
ΔE_p	: Peak potentials differences
E_o	: Starting potential
I_{pc}	: Cathodic peak current
I_{pa}	: Anodic peak current
V	: Scanning speed
I_{pa}/I_{pc}	: Peak currents ratio
nm	: Nanometer
mV	: Millivolt
λ	: Wavelength
D	: Diffusion coefficient
~	: Approximately
M	: Molarity
I	: Current
Abs	: Absorbance
O_2	: Oxygen

ABBREVIATIONS

M	: Metal
Pc	: Phthalocyanine
MPc	: Metal Phthalocyanine
M_2Pc_2	: Ball Type Dinuclear Phthalocyanine
DMSO	: Dimethyl Sulfoxide
DCM	: Dichloro Methane
CV	: Cyclic Voltammetry
SWV	: Square Wave Voltammetry
DPV	: Differential Pulse Voltammetry
LSV	: Linear Sweep voltammetry
SCA	: Spectro Chrono Amperometry
RDE	: Rotating Disc Electrode
RRDE	: Rotating Ring Disc Electrode
SCE	: Saturated Calomel Electrode
TBAP	: Tetrabutylammonium perchlorate
UV	: Ultraviolet
UV-Vis	: Ultraviolet-visible area
HOMO	: Highest Occupied Molecular Orbital
LUMO	: Lowest Unoccupied Molecular Orbital
LMCT	: Ligand to Metal Charge Transfer
MLCT	: Metal to Ligand Charge Transfer
IR	: Infrared
Nf	: Nafion
VC	: Vulcan XC-72
FC	: Fuel Cells
PEMFC	: Proton Exchange Membrane Fuel Cells
DMFC	: Direct Methanol Fuel Cell
GCE	: Glassy Carbon Electrode
ORR	: Oxygen Reduction Reaction
OER	: Oxygen Evolution Reaction

LIST OF FIGURES

LIST OF TABLES

1. INTRODUCTION

This thesis has three main sections: general theoretical information in which almost all the properties, characteristics, usages and importance of general phthalocyanine compounds were discussed; experimental information in which the electrochemical, spectroelectrochemical and electro catalytic properties of the novel phthalocyanine compounds are explained and application in Zinc air battery is the third part in which the best experimented novel catalysts were applied in the battery. In order to determine the technological usage areas, the compounds discussed in this thesis study examined using electrochemical methods were two types- monomeric species with a single phthalocyanine nucleus containing a metal atom in the center and another one was dimeric ball type dinuclear species with two phthalocyanine nucleus.

It is considerably tough to identify the characteristics of the redox couples thoroughly with individual voltammetric experiments. On that account, the voltammetric investigation along with *in-situ* spectro-electrochemical investigation were carried out at voltammetrically determined constant potentials. At applicable steady potentials at the time of electrolysis of the compounds, *in-situ* spectro-electrochemical experiment has a crucial significance in the understanding of redox procedures. Throughout the experiment, all the changes occurred at spectra, pointed out that the procedures are ligand or metal based. The redox properties of the compounds have relatively analyzed by voltammetry and *in-situ* spectro-electrochemical methods in two different solvent media of non-coordinating dichloromethane solution (DCM) along with coordinating dimethyl sulfoxide solution (DMSO) and as the supporting electrolyte, tetrabutylammonium perchlorate (TBAP) has used.

During these measurements, the parameters that may affect the electrochemical behavior of the compounds were investigated. Such as;

1. The effect of both redox-active as well as redox-inactive metal centers was examined for mononuclear and binuclear phthalocyanine compounds.
2. The effects of the two different solution system on the electrochemical behavior of these compounds.
3. The effect of substituents.

4. The effects of electron donor/releasing species.
5. The reversibility/irreversibility of the electrochemical reactions of the phthalocyanine compounds
6. The presence and effect of aggregated species.
7. The effect and relationship between redox behavior and molecular structure.

The linear sweep voltammetry carried out using rotating disk electrode (RDE) and rotating ring-disk electrode (RRDE) with the bipotentiostat system. The examined complexes have shown their usability as electro catalysts for oxygen reduction reaction (ORR) in fuelcell applications and oxygen evolution reaction (OER). Acidic and alkaline media were used for investigating ORR along with OER experiments of these compounds. The Koutecky-Levich investigation of ORR induced by novel phthalocyanines were calculated. Galvanodynamic with galvanostatic methods were used to investigate the properties of Zn-air battery (ZAB) of phthalocyanine catalyst. Charge as well as discharge study of novel phthalocyanine catalysts were investigated.

1.1. General Information About Phthalocyanines

Phthalocyanines have 18-π electron heterocyclic system and they are aromatic macrocyclic compounds. Phthalocyanine with these 18 electrons cloud delocalized over an alignment of alternated carbon and nitrogen atoms. They are structurally similar to natural porphyrins such as vitamin B12, hemoglobin and chlorophyll. They are in the class of macromolecular substances but they are not found in nature and are obtained synthetically in the laboratory environment. They are capable of assembling almost 70 several cations (metallic and nonmetallic) in their ring cavity. As seen in **Figure 1**, they have a two-dimensional geometry and are composed of four isoindole units with a central cavity large enough to accommodate many metal ions linked by a ring of nitrogen atoms [1]. The peripheral hydrogen atoms of the phthalocyanines are substituted by functional groups like alkyl, amine, aryl, alkoxy, halogens, hydroxyl, nitrosyl, thiol etc. and thus phthalocyanines have many derivatives (**Figure 1**). Phthalocyanines containing a metal atom in the middle of the molecule are called MPc while two- dimensional metal-free phthalocyanines are called dihydrogen phthalocyanine - H_2Pc or just phthalocyanine Pc.

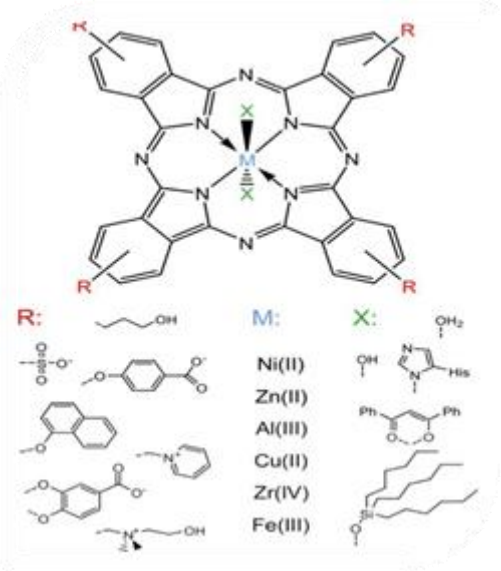

Figure 1 Chemical structures of metal free and metal phthalocyanine[10]

Because of the approachability of oxidation states which is focused on the phthalocyanine unit or on the central metal of the metal-phthalocyanine, they display an exceptional electrochemical nature. Redox behavior can be affected by the coordination of metal phthalocyanine which is banded one/two axial ligands. It can be also affected by aggregation properties of phthalocyanines [5].

1.2. Physical and chemical properties of phthalocyanines

Different MPc have synthesized both by the introduction of different central ions on the macro ring and by the substitution of different functional groups into the ring.

Pc have chemical and thermal stability. They do not undergo significant decomposition in air up to 400-500 °C. In vacuum, most metal complexes do not decompose before 900 °C. They are resistant to strong acids and bases. Only under the influence of strong oxidants (dichromate or serum salts) does the structure of the macro ring deteriorate by breaking down into phthalic acid or phthalamide.

Pc can be prepared from aromatic o-dicarboxylic acids or amide, imide and nitrile derivatives of these acids. If the carboxyl groups are not directly attached to the unsaturated aromatic group, synthesis of Pc is not possible. In addition, another necessary condition for the synthesis of Pc is the presence of double bonds between carbon atoms carrying carboxyl or cyano groups.

Pc molecule has a highly tight structure and consists of four iminoisoindoline units. The

product yield in the synthesis of H_2Pc is lower than that of MPc. The reason for this is that the metal ion that present in the structure during the production of MPc increases the product yield with the coordination effect.

The hydrogen atoms of iminoisoindoline, which forms the center of the Pc molecule, easily replace the metal ion, providing the formation of MPcs. The chemical properties of Pcs largely depend on its central atom. There are generally two types of MPcs. The first group is called "electrovalent phthalocyanines", this group generally includes alkali and alkaline earth metals, they are insoluble in organic solvents, they cannot sublimate at high temperatures in vacuum, when treated with dilute inorganic acids, aqueous alcohol, or even water, the metal ion is easily separated from the molecule and metal-free Pcs are formed. The second group is called "covalent phthalocyanines", the complexes of this group are more stable than the electrovalent ones. They are partially soluble in hot solvents such as chlornaphthalene and quinoline. Some types can sublimate in an inert environment, in vacuum, at 400-500 °C without decomposing. When treated with other inorganic acids other than nitric acid, there is no change in their structure. This is because the bond between the metal and the Pc molecule is very strong.

The stability of Pc depends on the correspondence between the diameter of the central cavity and the diameter of the metal ion. The cavity diameter of the Pc molecule is 1.35 Å. If the ionic diameter of the metal is significantly larger or smaller than the cavity diameter of the molecule (1.35 Å), the metal can be easily separated from the Pc molecule. Solubility is important for Pcs. They are both large and planar, the molecules cluster easily. For this reason, Pcs are poorly soluble in water or organic solvents. The low solubility of Pc is a disadvantage. To eliminate this, Pc derivatives can be synthesizedby adding bulky or long chain groups to the peripheral positions of the Pc skeleton, thusincreasing solubility.

1.3. Spectrochemical properties of phthalocyanines

Pcs give characteristic absorption peaks in the visible and ultraviolet regions. In *UV-Vis* measurements of Pcs in the 10^{-4}-10^{-5} M concentration range in known organic solvents, electronic absorption called Q band is observed in the range of 600-700 nm, resulting from intense π-π^* transitions. This range is also a characteristic region to distinguish MPc from H_2Pc. H_2Pcs give two bands in the range of 600-700 nm [2]. In addition,

there may be differences in the spectrum depending on the solvent concentration and polarity.An example of UV-visible spectrum for H_2Pc is shown in **Figure 2** [5].

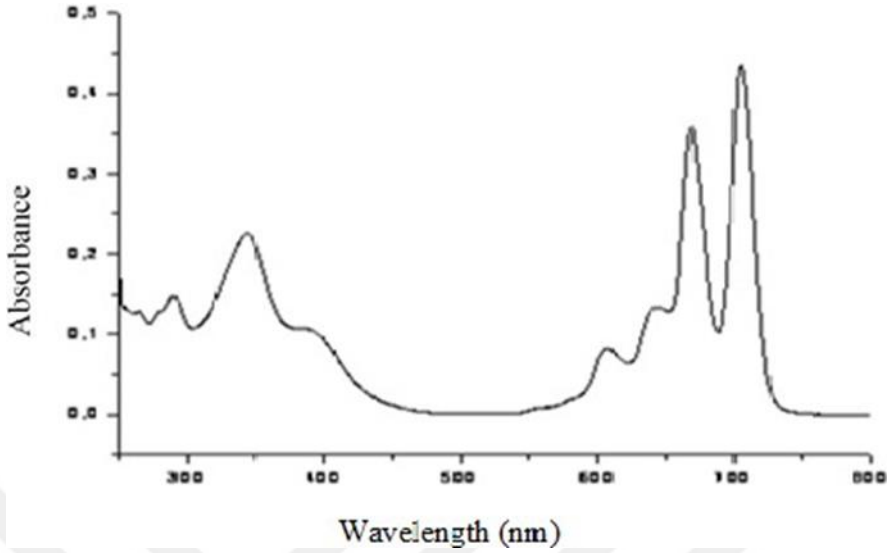

Figure 2 UV-visible spectrum for metal-free phthalocyanine.

Metal phthalocyanines give a single intense Q band in the same region. UV visible spectrum for MPc is shown in **Figure 3** [5]. $\pi \rightarrow \pi^*$ transitions in MPc, it varies depending on the metal ion as well as the solvent concentration and polarity [3]. In general, a strong band at 675 nm, a shoulder at 640 nm and a weak band at 610 nm are observed in the *UV-vis* spectra of MPc taken in chloroform.

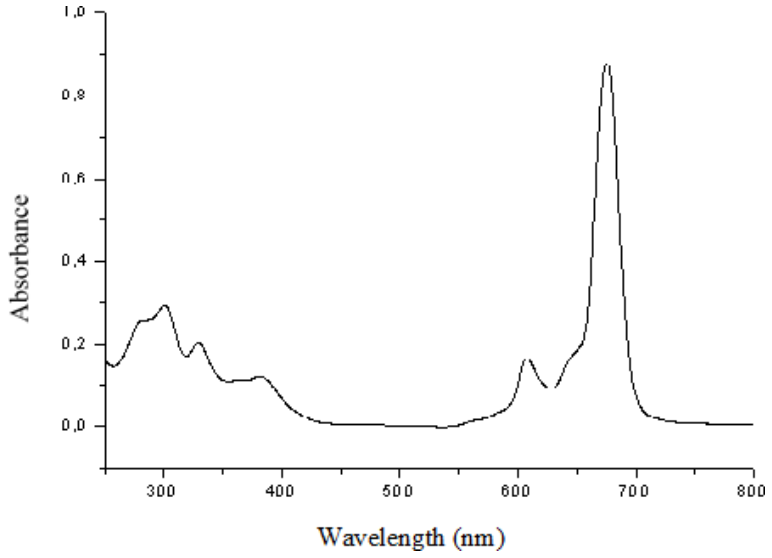

Figure 3 UV-visible spectrum for metal phthalocyanine.

These bands arise from monomeric Pc. It is seen that in polar solvents such as methanol, the intensity of the Q band at 675 nm decreases considerably and a new band form at

630 nm. This is due to aggregate formation. Characteristic Soret bands (B band) are observed around 300 nm in the *UV-vis* spectra of Pc.

Synthesis of Pc dissolved in suitable solvents enabled NMR measurements. The point to be considered in the H-NMR spectra is that the NH protons in the Pc nucleus shift to a stronger field from TMS, under the influence of the aromatic 18π-electron system in the planar structure. In addition, there is a broadening of the peaks in the H-NMR spectrum of Pcs depending on the solvent concentration and aggregation [4].

The large number of bands observed in the FT-IR spectra of Pcs also the size of the macrocyclic system makes it difficult to characterize all bands. The IR spectra of metal and metal free phthalocyanines are very similar. An important difference arises from the -NH vibrations in the inner side of the Pc. In metal free phthalocyanines, a weak -NH band is observed at 3280 cm^{-1}.

1.4. Aggregation behavior of phthalocyanines

Pcs can aggregate to a greater or lesser range and this aggregation of Pcs may affect the redox potentials behavior. Various factors such as pH, ionic strength, temperature, and the amount of electrolyte in the solution significantly affect it. Pcs with large π electron systems, which are in the macrocycle class, tend to cluster in water or organic solvents and form dimers or aggregated species at higher orders. This aggregation may occur as a result of the interactions of co-planar macrocyclic rings with van der Waals forces, p-stacking interactions and solvent effects. Aggregation phenomenon significantly affects the spectral, photo physical, photochemical, redox processes and solubility of Pc compounds, and therefore their use in different technological applications. For this reason, it is very important to elucidate the effect of the aggregation behavior of Pc compounds on their electrochemical properties and to examine the changes such as decrease or increase in the aggregation behavior with the application of changing electrical potential from the other window. In six-coordinated MPc species, aggregation is generally not observed because the molecules are far apart due to the effect of axially linked ligands [5].

1.5. Electrochemical properties of phthalocyanines

The electrochemical properties of Pcs basically arise from the interactions between the central metal ion and the 18π-electron system and the effects of different substituents on

these interactions. In Pc complexes with the 18π-electron system, the ring system is in the -2 oxidation state (Pc^{2-}), while the metal ion in the center is generally +2 charged (M^{2+}). Thus the successive one e^- transfer reactions occurring in the Pc ring, Pc (-3), Pc (-4), Pc (-5) and Pc (-6) are formed by reduction, and Pc (-1) and Pc (0) are formed by oxidation. On the other hand, some transition metals as for example Fe(II), Co(II) and Mn(II) in the center give redox reactions, while Ni(II), Zn(II) and Cu(II) do not give redox reactions [6]. The reduction reaction of the Pc ring is generally electrochemically reversible, while the oxidation reactions are generally electrochemically irreversible. For Pcs that do not contain a redox active metal center, the difference between the first reduction potential and the first oxidation potential is approximately 1.5 V. This value arises from the energy difference between the highest energy occupied molecular orbital (HOMO) and the lowest energy empty molecular orbital (LUMO). It is important to determine from the electrochemical behavior of redox-active metal complexes, especially whether the first oxidation redox couple will occur from the metal or from the ring [7]. The solvent environment and environmental conditions in which phthalocyanines are located change the electrochemical behavior of some species. In particular, the electrochemical behavior of [Co(II)Pc (-2)] and [Fe(II)Pc (-2)] species changes considerably when a solvent with coordinative feature is used or a solvent without coordinative feature is used. For example, the [Co(II)Pc (-2)] species tends to be oxidized to the $[Co(III)Pc (-2)]^+$ form or the $[Co(II)Pc (-1)]^+$ form. Donor solvents favor the formation of $[Co(III)Pc (-2)]^+$ species along with the formation of six-coordinated species. If such donor solvents are not available, oxidation of Co(III) is prevented and oxidation of the ring occurs first. Therefore, in voltammetric measurements performed in DMSO/TBAP environment, the first oxidation and first reduction events of redox active metals (such as M= Fe, Co and Mn) are probably metal-centered, corresponding to the pairs $[M(II)Pc(-2)]/[M(III)Pc (-2)]^+$ and $[M(II)Pc(-2)]/[M(I)Pc (-2)]^-$ respectively, while the second reduction must be ring-centered. However, spectroelectrochemical measurements are carried out in order to clearly evaluate the redox events of such MPc complexes. Different solvent systems should be studied in order to understand the redoxevents in more detail. As for example, cobalt metal, which has the ability to make 6 coordination bonds, exists in the DMSO solvent system as a balance of two species in the form of [Co(II) Pc (−2)] + DMSO ↔ [DMSO-Co(II)Pc (−2)]. When the results obtained in polar solvent systems such as

DMSO and DMF, which have coordinative properties, and non-polar solvent systems such as DCM, which do not have coordinative properties, are compared, it is seen that the metal center is more stabilized at high oxidation levels in coordinated polar solvent systems. It is seen in the literature that as the oxidation number decreases, the ability to coordinate decreases. In this case, axially bonded anionic species such as acetate, chlorate, perchlorate and solvents such as polar DMSO, which have similar coordination properties, are easily separated in the reduction process with decreasing oxidation numbers. The existence of this situation causes different redox processes with coordinated species to be observed in electrochemical measurements. This is generally understood with split redox couples. For these reasons, it is more likely that the first reduction and first oxidation events in the DMSO coordinated solvent system are metal-based. Redox active metals with high coordination numbers, such as iron and manganese, also exhibit similar behavior. The existence of a coordinated species and an uncoordinated species in this equilibrium is understood by the split redox pairs occurring at different half-peak potential values. Another important difference when using a solvent system such as donor DMSO is that all redox processes shift in the negative direction. This situation can be explained by theincrease in electron density on the ring. Another tendency observed for some complexesis their aggregation character, which is the broadening or splitting of redox waves. However, it is not possible to make a definitive decision about the relationship of redox couples to aggregation-disaggregation events based only on electrochemical measurements.

1.6. Application Areas of Phthalocyanines

Pc compounds, which were initially used only as dyestuffs, have found many different applications in many fields of industry and especially in medicine in recent years. Using their coloring properties, it is used in the coloring of aluminum, as a pigment in the coloring of PVC, epoxy resin, plastic and fireproof plastic materials, as a fabric dye in textiles, in the coloring of paper, soap, detergent and cement, in the production of printing ink and in the production of indicators. Pcs are used in the oxidation of phenol compounds in wastewater, desulfurization in oil and increasing the octane number of gasoline. In addition, phthalocyanines have begun to be used to obtain clean energy, such as decomposing water into O_2 and H_2 with the photocatalytic effect, reducing CO_2 to methanol and some other organic compounds, and successful results have been

achieved. Pcs have the potential to be used as an alternative to the very expensive heterogeneous pt catalyst in fuel cell applications due to their electro catalytic effect on the reduction of oxygen. For this reason, intensive research has been carried out on this subject with Pcs in recent years. Applications of phthalocyanines in the field of medicine are also important. Phthalocyanine sodium sulfonates are used to mark cancerous cells by staining them. Additionally, copper phthalocyanine (CuPc) blue and ascorbic acid are used together to prepare an indicator that shows the completion of sterilization. Other uses of phthalocyanines are- photocopy machines, optical computer read-write disks and related information storage systems, laser dyes, liquid-crystal color display applications, photovoltaic battery elements, oxidizing saturated hydrocarbons at low temperatures, electro catalysts, Langmuir-Blodget films [8]. Most of these uses arerelated to both the broad and flat p-conjugation system of phthalocyanine compounds and the type of central metal atom.

1.7. Electro catalytic performances of phthalocyanines in electrochemical oxygen reduction

O_2 is a diatomic molecule composed of two oxygen atoms, each with the electronic configuration $1s^2\ 2s^2\ 2p^4$. **Figure 4** shows the molecular orbital diagram of the O_2 molecule in its ground state [7].

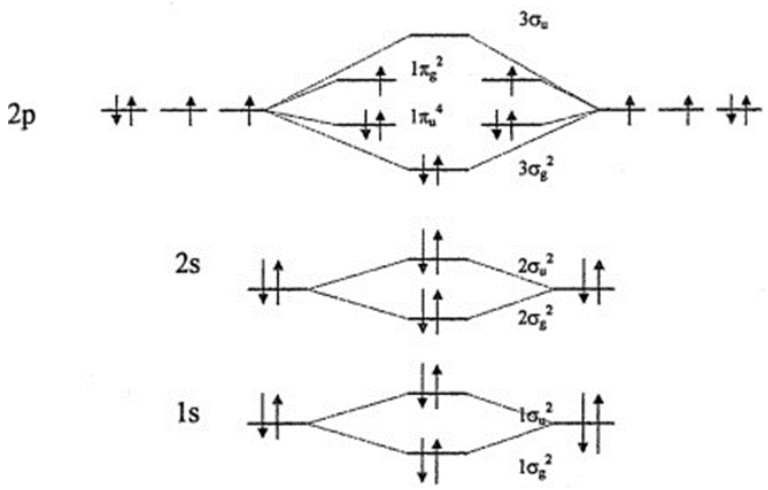

Figure 4 Molecular orbital diagram of the O_2 molecule in the ground state.

In the ground state, O_2 has 2 unpaired electrons in π_g antibonding orbital and 6 electrons in $3\sigma_g$ and $1\pi_u$ orbitals. When the oxygen molecule gains 2 electrons and then after reduction, these electrons enter $1\pi_g$ antibonding orbital. When more than two electrons

are gained, bond breaking occurs. In terms of thermodynamics, the 4-electron reduction of oxygen is an exothermic event and the standard reduction potential is +0.40 V compared to the normal hydrogen electrode. However, oxygen's tendency to gain 1 electron is quite low, so the first electron transfer step occurs slowly and this step constitutes the rate-determining step.

The electrochemical reduction of oxygen provides a model for the cathodic reaction in PEM fuel cells, called proton exchange membrane or polymer electrolyte membrane fuel cells. For this reason, it is researched with great interest in the literature [9]. One of the most important problems experienced in fuel cells is the lack of a highly efficient and cheap electro catalyst that can be used instead of platinum in oxygen reduction. Therefore, intensive research is being carried out to develop an alternative catalyst to platinum that can reduce oxygen at a sufficiently positive potential with low overvoltage. Pc complexes are the subject of much research today, as they have the potential to be used as an alternative to the very expensive heterogeneous platinum catalyst in applications related to fuel cells, due to their electro catalytic effect on the reduction of oxygen [10]. In oxygen reduction, initial electron transfer is the slow step. In the presence of transition metal complexes in organic solvents, oxygen reduction due to the formation of intermediate product $M\text{-}O_2^-$ occurs by the transfer of multiple electrons and at remarkably low negative potentials [11]. Zagal and his colleagues examined the reduction mechanism of oxygen in aqueous media catalyzed by iron phthalocyanine andsuggested the Fe(III)Pc(-2)/Fe(II)Pc (-2) redox reaction as the initial step [1 2]. Tafel slopes of -40 and -120 mV observed in the low and high overvoltage regions of the polarization curve of oxygen reduction, respectively, showed that the 2nd and 3rd steps were slow steps that determined the rate [13].

Collman and his group investigated for the first time the electro catalytic activities in oxygen reduction of metal porphyrin complexes in dimeric structure with two porphyrin rings positioned face to face. It has been reported that two porphyrin rings are brought face to face with 4-atom bridges, and dimeric cobalt porphyrins adsorbed on the graphite electrode surface catalyze oxygen reduction through a mechanism in which 4 electrons are transferred. It has been stated that when cobalt metal is replaced with nickel, palladium or copper, oxygen is reduced to hydrogen peroxide via a 2-electron mechanism. A similar result was obtained when the distance between the two porphyrin

rings was increased by changing the bridges. Considering the experimental results, Collman and his colleagues proposed a mechanism in which cobalt metal centers are reduced as the first step in oxygen reduction and then the per Oxo complex (PCo^{III}-O^{-}-O^{-}-$Co^{III}P$) is formed [13]. Studies with Pcs show that, although there are exceptions, oxygen reduction generally occurs as reduction to 4-electron water under the catalysis of iron phthalocyanine and as reduction to 2-electron hydrogen peroxide under the catalysis of cobalt phthalocyanine.

1.8. Oxygen reduction reaction (ORR) and oxygen evolution reaction (OER)

ORR is the reaction that occurs at the cathode in proton exchange membrane (PEM) fuel cells as well as direct methanol fuel cells (DMFCs). According to the thermodynamics and kinetics of ORR, if the electrolyte is an acidic aqueous solution then the ORR reaction would be,

$O_2 + 4H^+ + 4e^- = H_2O$ **1.1**

$O_2 + 2H^+ + 2e^- = H_2O_2$ **1.2**

$H_2O_2 + 2H^+ + 2e^- = 2H_2O$ **1.3**

According to the thermodynamics and kinetics of ORR, if the electrolyte is alkaline aqueous solution then the ORR reaction would be,

$O_2 + H_2O + 4e^- = 4OH^-$ ····· **1.4**

$O_2 + H_2O + 2e^- = HO_2^- + OH^-$ ····· **1.5**

The $1e^-$, $2e^-$, and $4e^-$ reduction pathways have unique significance, depending on the applications. The $4e^-$ direct pathway is hugely preferred in fuel cell procedures. The $2e^-$ reduction pathway is applied in industry for H_2O_2 production. The $1e^-$ reduction pathway is of importance in the exploration of the ORR mechanism [5].

Because of the importance of biology, chemistry, and technology; Oxygen evolution electro catalysis has gained huge attention. OER is fundamentally an electro catalytic reaction. The transition metals are commonly unstable in acidic media, their relatively low cost and long term corrosion resistance in alkaline solution makes them attractive, alternative OER materials [15]

According to the thermodynamics and kinetics mechanism of OER in acidic

electrolyte,

$$* + H_2O \rightarrow OH^* + H^+ + e^- \cdots\cdots 1.6$$

$$OH^* \rightarrow O^* + H^+ + e^- \cdots\cdots 1.7$$

$$O^* + H_2O \rightarrow OOH^* + H^+ + e^- \cdots\cdots 1.8$$

$$OOH^* \rightarrow * + O_2 + H^+ + e^- \cdots\cdots 1.9$$

According to the thermodynamics and kinetics mechanism of OER in basicelectrolyte,

$$* + OH^- \rightarrow OH^* + e^- \cdots\cdots 1.10$$

$$OH^* + OH^- \rightarrow O^* + H_2O + e^- \cdots\cdots 1.11$$

$$O^* + OH- \rightarrow OOH^* + e^- \cdots\cdots 1.12$$

$$OOH^* + OH- \rightarrow * + O_2 + H_2O + e^- \cdots\cdots 1.13$$

Here * designate the active site of the catalyst. OH*, O* and OOH* indicate adsorbed intermediates species.

1.9. Zinc(Zn) air battery

Battery has recognized for its capacity to smoothly convert and store electrical energy. From a fossil fuel based technology our society has been in transition to a clean energy technology. Recently, Zn-air batteries have attracted immense interest. It is comparatively the most sophisticated technology among all the various kinds of metal air batteries. Therefore, for future energy uses and applications, Zn air batteries hold the finest promise. Having high theoretical energy density of 1086 Wh kg^{-1} which is almost five times greater than the present Li-ion battery, Zn air batteries suggest the highest available energy density of any primary battery technology [51]. In view of having exclusive molecular structure along with redox properties, Pc complexes have exhibited exceptional performance while they had applied in Zn air battery system.

1.10. Electrochemical analysis methods- Cyclic Voltammetry (CV)

Voltammetry technique is an analysis technique that examines and evaluates the characteristics of current intensity-voltage curves, called voltammograms, obtained under appropriate conditions from solutions of electroactive organic and inorganic

substances that can be oxidized and/or reduced in various environments [14]. This technique generally based on applying a voltage excitation signal whose value changes over time between a polarizable working electrode and a reference electrode in the electrochemical cell, and measuring the current between the working electrode and the auxiliary electrode in three-electrode cells, and between the working electrode and the reference electrode in two-electrode cells [15]. The change of applied potential in CV over time is shown in **Figure 5** [16].

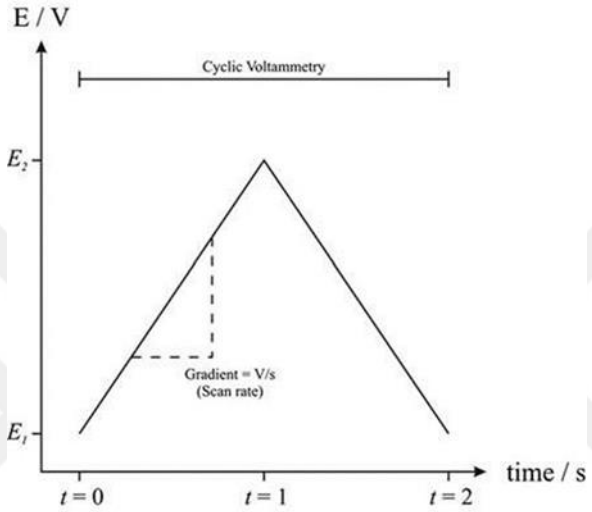

Figure 5 Variation of applied potential with time in cyclic voltammetry.

In the CV technique; the voltage sweep applied to the working electrode in a certain direction (positive or negative) up to a certain potential value, and the potential sweep direction is reversed at the same sweep speed. Forward and reverse scanning speeds are generally kept the same, but measurements can be taken at different scanning speeds if desired. Important parameters in CV are cathodic peak potential (Epc), anodic peak potential (Epa), cathodic peak current (Ipc) and anodic peak current (Ipa) [17]. The current-potential curve for cyclic voltammogram is shown in **Figure 6** [17].

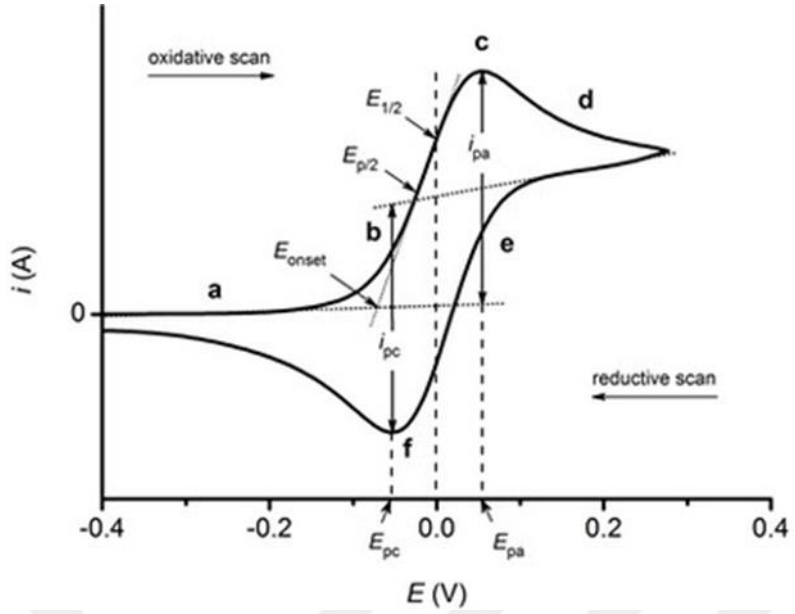

Figure 6 Current-potential curve for cyclic voltammogram.

With the CV technique, it is understood at what potentials and in how many steps a system is reduced or oxidized, whether it is electrochemically reversible, and whether the reduction or oxidation products are stable [18]. In a reversible electrochemical reaction, when an oxidation occurs during the anodic potential scan, when the scan is reversed, the product formed during the oxidation is reduced again at the electrode, so a peak in this direction is also observed. The same is true for a reversible reduction reaction observed during the cathodic potential scan. In an electrochemical reaction that is reversible and not accompanied by chemical reactions, there is a voltage difference of 59/n mV between Epa and Epc (n is the number of electrons transferred) and at the same time Ipa and Ipc intensities are equal to each other. As the reversibility of the electrode reaction decreases, anodic and cathodic peaks are observed at potentials farther from each other and more broadly. In a fully irreversible electrode reaction, the anodic and cathodic peaks are very far away from each other and none of their parts face each other and they have completely lost their symmetry, or the back peak is not observed and disappears completely [19]. The peak current for reversible reactions is given by the Randles-Sevcik equation;

at 25 °C:

$$I = 2.69 \times 10^{5} n^{3/2} C_{p} D^{1/2} \nu^{1/2} \qquad \textbf{1.14}$$

For irreversible reactions, the peak current is given by the following equation:

$$I = 2.99 \times 10^5 \, n \left(\alpha n_p\right)^{1/2} C . \mathrm{D}^{1/2} \nu^{1/2} \qquad \textbf{1.15}$$

In these equations; I_p is the current density, α is the electron transfer coefficient, n is the total number of electrons transferred, D is the diffusion coefficient, C is the concentration of the electroactive material and v is the scanning rate, n_a is the number of electrons transferred in the rate-determining step and α_c is the electron transfer coefficient [21]. The CV method has three-electrode system which includes a working electrode, reference electrode and counter electrode. With an additional circuit, the potential is controlled between the working electrode and the reference electrode; but the current passing through the cell is measured between the working electrode and the counter electrode.

Supporting Electrolyte;

The current resulting from migration is undesirable in voltammetry and makes it difficult to explain the results obtained, so efforts are made to minimize it to a negligible extent. For this, an excessive amount of electrolyte, called supporting electrolyte, which does not participate in electrode reactions, is added into the electrolysis solution. Now the electroactive material is ensured to be transported to the electrode surface only by diffusion. The supporting electrolyte is often anion and cation stable ionic compounds such as alkali metal salts that are difficult to oxidize or reduce. Since all ions in the solution carry electricity, the contribution of the reduced or oxidized ion compared to the supporting electrolyte is neglected and the migration of the reacting ion is neglected.

Working Electrode or Indicator Electrode;

These are electrodes whose potential changes linearly during measurement. In general, the surface areas of the working electrodes used are kept small to increase polarization. In voltammetry, a working electrode must have high conductivity, it should not cause any reaction (inert) within the studied potential range, the negative potential window should be wide for scans in the cathodic direction and it should be easy to take into the desired shape and be easy to process.

Reference Electrode;

It is a half-cell whose electrode potential is clearly known. The potential of the reference electrode remains fairly unchanged, serving as a comparison to other electrodes in the cell. Since the internal resistance of this electrode is very high, no current flows. That is, all current flows from the auxiliary (counter) electrode to the working electrode. Always act as the anode in potentiometric measurements. (Ag/AgCl Electrode, Hg/Hg_2Cl_2 (Calomel) Electrode, Standard (Normal) Hydrogen Electrode (SHE=NHE)). An ideal reference electrode must have a reversible character and comply with the Nernst equation. Its potential should be minimally affected by all changes on the system and should not change over time. There should be no change in its potential even though a very small amount of current passes through it, and it should have ideal non-polarizable properties. The potential should not be affected much by changes in the test conditions (temperature, pressure, etc.).

Auxiliary (Counter) Electrode;

The third electrode is the auxiliary (counter) electrode that allows electricity to come from the source and be transferred through the solution to the working electrode. The auxiliary electrode has no effect on the reaction in the working electrode, it creates a source pool for electrons and thus allows current to flow from the battery. Generally, its potential is not measured and it is chosen from noble metals such as Pt. It has a considerably larger surface area compared to the working electrode.

In voltammetry, the limits of the potential range that can be applied to the electrode to determine the electrochemical behavior of any substance depend on some variables such as the types of working electrode, solvent and electrolyte used. The electrolyte used in an electrochemical cell can be a very simple aqueous solvent, a solution of salt mixtures, a solid or even a gas. In general, an electrolyte contains several different components, and each of these components affects the measurement made in the cell. However, what is important is the presence of the solvent. The most important feature sought in solvents is that they have a high dielectric constant. The most used solvents and dielectric constants are; water, 80; DMSO is 46.7 and ACN is 37.5. If solvents with lower polarity are used in voltammetric studies, supporting electrolyte is added to the medium to ensure sufficient conductivity. Various salts, acids and bases can be used as supporting electrolytes in aqueous media.

In addition, under normal conditions, the concentration of dissolved oxygen molecules

in a solution in equilibrium with air is $2x10^{-4}$ M. Oxygen at this concentration is highly electroactive and gives a distinct peak. In order to remove oxygen from the environment, an inert gas, usually nitrogen or argon, must be passed through the cell for a long time.

The electrochemical cells used for general voltammetric measurements are made to work with 5–50 mL of solution. Electrodes are attached to the cap made of Teflon. N_2 gas is passed through the solution with the help of a thin pipe. The cell is made of glass that does not adsorb on the surface.

1.11. Differential Pulse Voltammetry (DPV)

Pulse voltammetry is used to increase the sensitivity of voltammetric measurements. It enables detection even at concentrations below 10^{-8} M by greatly changing the ratio of faradic and non-faradic currents. Different pulse techniques are generally based on gradual changes in current or potential. A gradual potential change is applied to the working electrode sequentially over a certain period of time. When the potential is instantaneously increased by a certain step, the faradic current decreases slowly, while the non-faradic working electrode charging current suddenly decreases exponentially. Thus, the faradic current recorded during the pulse will be significantly separated from the non-faradic current. The most important difference between different pulse techniques is the different stimulation signals applied and current recording methods.

DPV is a very useful pulse technique used in the determination of small amounts of organic or inorganic species. In this technique, a constant value potential pulse is added to the linear potential increase and applied to the working electrode for a certain period of time, as seen in **Figure 7 [**21]. The currentpassing through the working electrode is recorded before and after the pulse, the first current is subtracted from the second and its graph is plotted against the applied potential. The peak current of the peaks in a DPV voltammogram are proportional to theconcentration of the substance being analyzed.

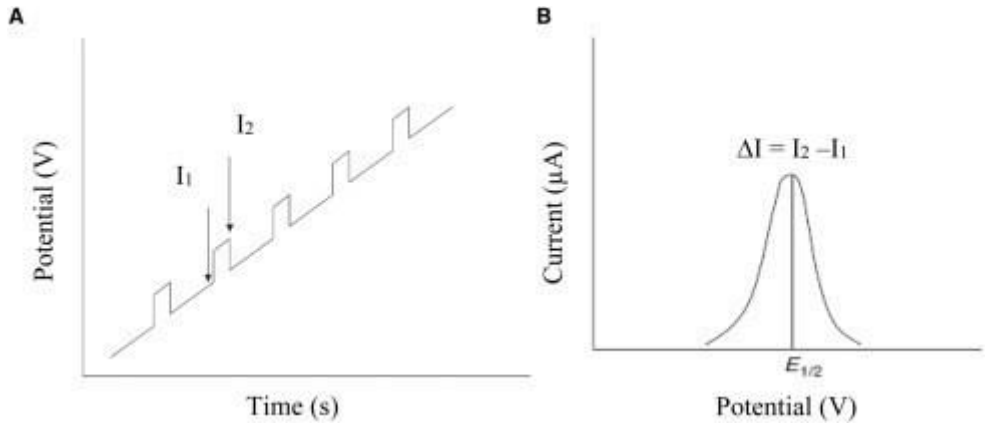

Figure 7 (A) variation of the applied potential in DPV; **(B)** Typical voltammogram response obtained in DPV.

Square wave voltammetry (SWV);

SWV is a large amplitude differential measurement technique. It is a waveform formed by combining the steps into a symmetrical square wave. For each square wave conversion, the current is measured twice, at the end of the forward pulse and at the end of the reverse pulse [25-27]. The voltammogram results in very precise sensitivity and effective separation. The detection limit is approximately 10^{-8} M. The speed of the technique allows it to increase the number of samples analyzed, which is desired in many clinical applications.

1.12. Spectroelectrochemistry

In spectroelectrochemical techniques, spectroscopic measurements are performed under electrochemical control, and both techniques collect their data complementary to each other. This technique is based on measurement of absorbance, transmittance or reflectance. A mechanism used in spectroelectrochemical analysis is shown in **Figure 8** [22]. In this technique, a thin layer quartz cell with a triple electrode system placed insideis used as an electrochemical cell. The working electrode and the solution must be permeable to allow light transmission [24-28].

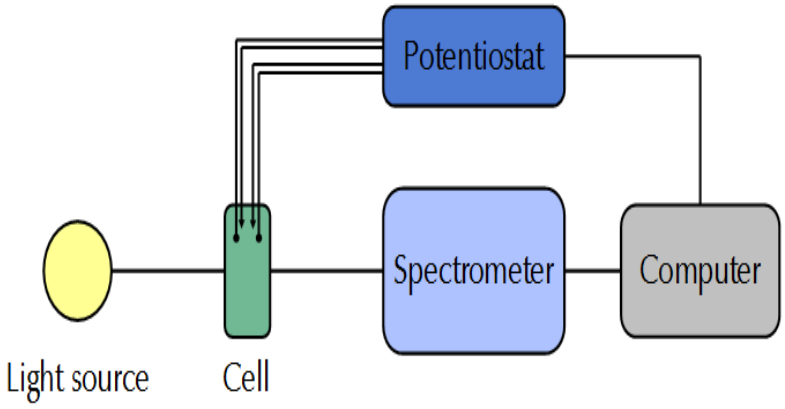

Figure 8 Spectroelectrochemical analysis experimental setup.

1.13. Rotating disk Electrode (RDE)Voltammetry

RDE is a hydrodynamic working electrode used in a three- electrode system. This electrode is rotated in the electrolyte solution during electrochemical measurements, thus ensuring the flow of the electroactive species in the solution to the electrode surface. RDE is used to elucidate reaction mechanisms related to redox chemistry. The electrode is placed in an inert polymer or resin that is non-conductive and is connected to an electric motor that performs the rotation. The disk is generally made of a noble metal or glassy carbon material, like other electrode materials. By rotating the electrode, the flow of the electroactive species to the electrode surface is ensured, and the flow rate is controlled by the rotation speed of the electrode. In the RDE technique, various events such as multi-electron transfer, slow electron transfer kinetics, adsorption/desorption steps and electrochemical reaction mechanisms can be examined by applying linear scanning voltammetry and other techniques at various electrode rotation speeds [29].

RDE current density for the redox reaction of an oxidant species (O) is expressed as **Equation 1.16**; where, n is the number of electrons transferred in the redox reaction, c_o (mol/cm^3) is the concentration of the electroactive species, m is the order of the reaction relative to the O species, and J_L is the limit current density.

$$J = n F c_o^m [(J_L - J)/J]_L^m \quad \textbf{1.16}$$

The equivalent obtained by arranging this equation is,

$$1/J^{1/m} = 1/J_K^{1/m} + 1/J^{1/m} / J_L \quad \textbf{1.17}$$

where J_K is the kinetically controlled current density and is expressed by the following equation:

$$J_K = n F c_o k^o \exp [-\alpha n_\alpha F (E-E^{o'})/RT] \quad \textbf{1.18}$$

In the above equation; k^o(cm/s) is the heterogeneous standard rate constant, F is the Faraday constant, α is the electron transfer coefficient, n_α is the number of electrons transferred in the rate-determining step, and E and E^o are the electrode potential and standard redox potential, respectively. Limit current density J_L expressed as,

$$J_L = 0.201 n F D^{2/3} \upsilon^{-1/6} \Omega^{1/2} c_o \quad \textbf{1.19}$$

In this equation; υ (cm^2/s) is the kinematic viscosity of the solution, Ω is the rotation speed of the electrode and D is the diffusion coefficient of the electroactive species.

Equation 1.16 becomes simpler for a first-order reaction and is expressed as the Koutecky-Levich equation as follows:

$$1/J = 1/J_K + 1/J_L \quad \textbf{1.20}$$

The Koutecky-Levich equation is a useful equation that is frequently used to determine first JL and then the number of electrons transferred. If a first-order reaction is corrected for diffusion effects, the following equation is obtained for J_K:

$$J_K = (J J_L) / (J_L - J) \quad \textbf{1.21}$$

In this case, there is a relationship between the E potential applied to the rotating disk electrode and the kinetic current density, determined by the Tafel equation given below:

$$E = E_{eq} - (2.3 RT/\alpha n F) \log J_K \quad \textbf{1.22}$$

With the help of this equation, the Tafel slope and hence the kinetic parameter α_n can be determined by taking advantage of the change of kinetic current density with the applied electrode potential.

RRDE is an electrode used in hydrodynamic voltammetry and consists of two working electrodes. All the features described above for RDE also apply to the disk electrode of

RRDE. In the RRDE voltammetry method, the products or intermediate products formed as a result of the reduction or oxidation of the electroactive species that reach the electrode surface during the rotation process reach the ring electrode and are reduced or oxidized depending on the potential applied there. Therefore, this technique provides significant advantages in elucidating electrochemical reaction mechanisms. This technique can be applied in various ways. Generally, when linear scanning voltammetry is applied on the disc electrode, the potential of the ring electrode is kept constant at a value at which the resulting intermediate or product can be reduced or oxidized [31,32]. A polarization curve recorded for ORR with the RRDE voltammetry technique is shown as an example in **Figure 9.**

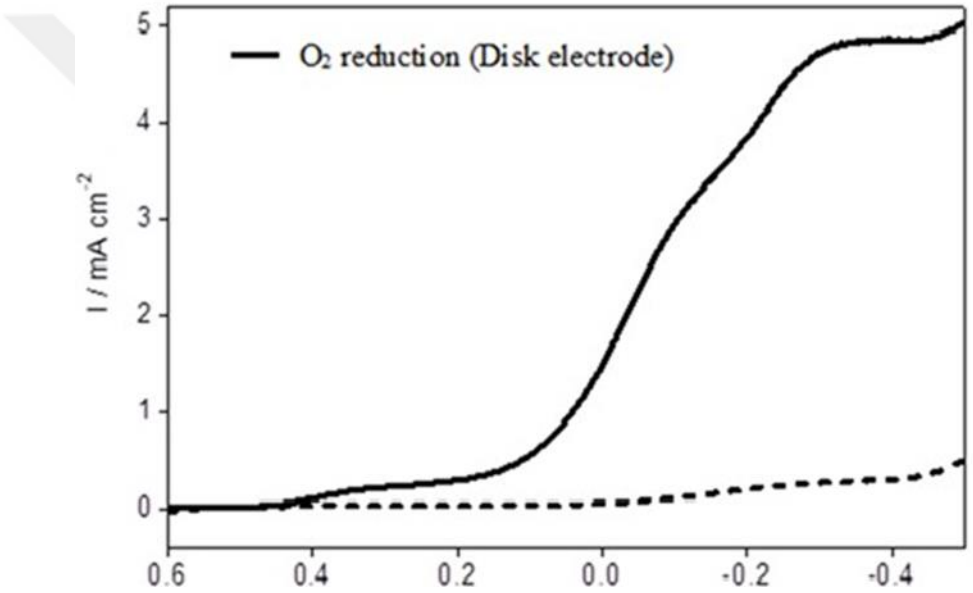

Figure 9 A polarization curve with the RRDE voltammetry technique (E/V vs. SCE).

RRDE voltammetry is a very useful method in determining the basic properties of electro catalysts used in fuel cells. For example, during ORR, which is electrochemically catalyzed at the cathode of PEMFC, hydrogen peroxide may be formed as an undesirable intermediate or by-product and damages the internal components of PEMFC. For this reason, it is desired that ORR electro catalysts produce as little hydrogen peroxide as possible. The tendency of an electrochemical ORR catalyst to form hydrogen peroxide can be determined by the RRDE voltammetry method. For this purpose, the glassy carbon disc is coated with an electro catalyst in the form of a thin layer and polarized to realize ORR. Since the intermediate product formed by rotating the electrode reaches the platinum ring electrode, the potential of

this electrode is kept constant at a value that can detect the hydrogen peroxide that may be formed. With such an application, the percentage of hydrogen peroxide formed can be determined, as well as the total number of electrons transferred in ORR and the mechanism of ORR can be elucidated. All the electrons transferred at a certain potential and the percentage of hydrogen peroxide formed are calculated by the following equations [33-35]:

$$n_t = 4I_D / [I_D + (I_R/N)] \quad \textbf{1.23}$$

$$H_2O_2\% = 100(4 - n_t)/2 \quad \textbf{1.24}$$

2. MATERIAL AND METHOD

In this thesis, mononuclear and ball type dinuclear Pc compounds were examined. In the first stage, electrochemical and spectroelectrochemical properties of all compounds in solutions were investigated. In the second stage, the electro catalytic activities of phthalocyanine compounds in ORR and OER were investigated in order to determine their usability as electro catalysts in fuel cell applications. In the last stage, the best Pc catalysts were applied in Zn air battery and compared with Pt catalyst.

2.1. Chemicals and reagents

The molecular structure of phthalocyanine compounds, which are the used of this thesis study, is given in **Figure 10**. Two separate groups of phthalocyanine compounds were used which synthesized by different researchers.

(a) Mononuclear 2,4-di-tert-butyl-6-(3,4-dicyanophenoxy) phenolate substituted cobalt, iron, manganese, nickel and zinc [CoPc (**1a**), Fe(OAc)Pc (**1b**), Mn(OAc)Pc (**1c**), NiPc (**1d**) and ZnPc(**1e**)] phthalocyanine compounds (**Figure 10** (**A**)). Synthesis and electrochemical characterization of these complexes have been published in the literature.

(b) 4,4'-(3,5-di-tert-butyl-1,2-phenylene) bis(oxy) substituted Co_2Pc_2 (**2a**), $Fe_2(OAc)_2Pc_2$ (**2b**), $Mn_2(OAc)_2Pc_2$ (**2c**), Ni_2Pc_2 (**2d**), Zn_2Pc_2 (**2e**) ball-type phthalocyanine compounds (**Figure 10** (**B**)), synthesis and electrochemical characterization of these compounds have been published in the literature.

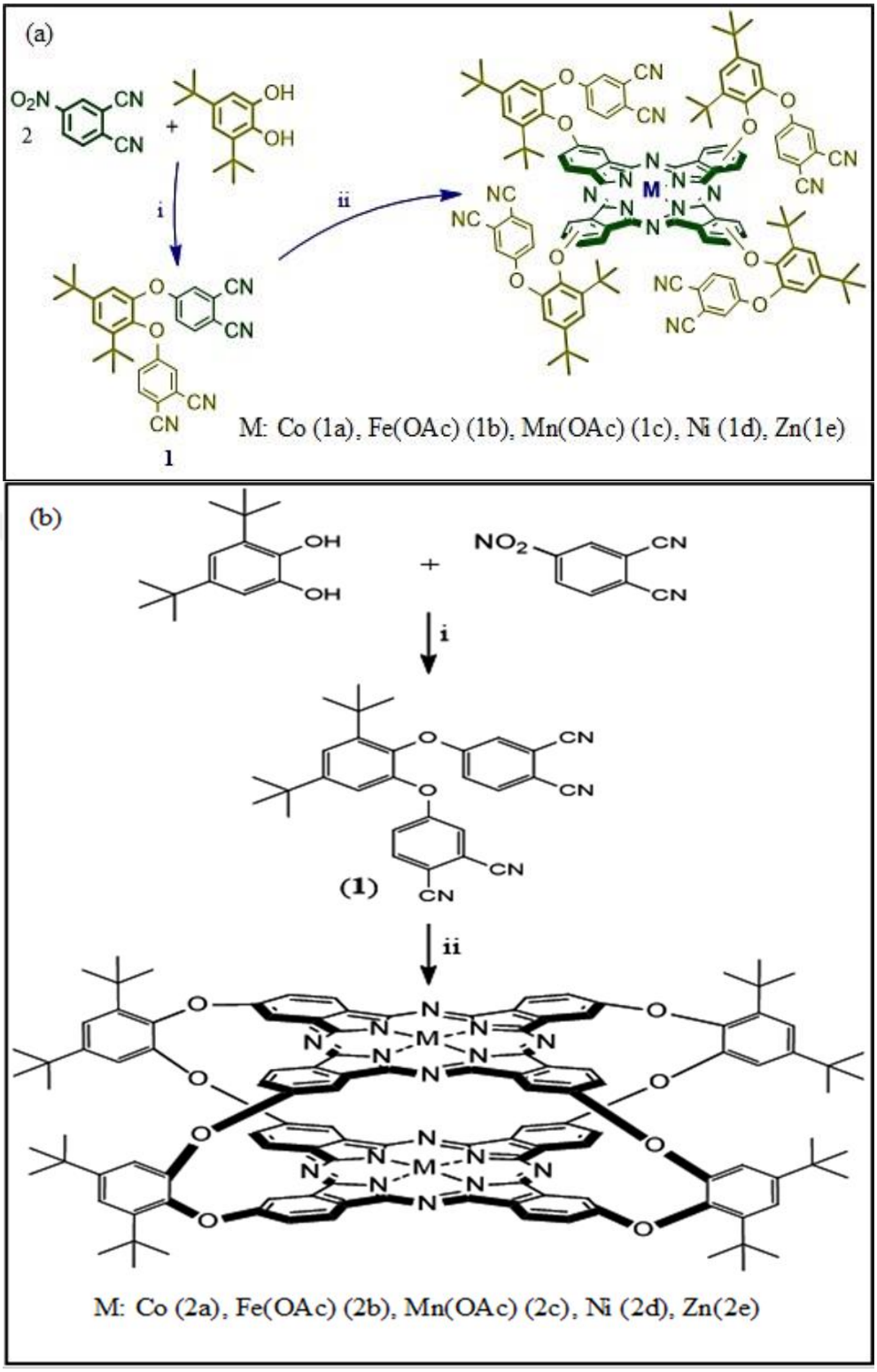

Figure 10 Molecular structures of phthalocyanine compounds that are the used of this thesis study.

Electrochemically pure tetrabutylammonium perchlorate (TBAP) (Fluka brand) was used as the carrier electrolyte, high purity DMSO and DCM (Merck brand) were used as

the solvent. In electro catalytic studies, 5% Nafion (Nf) solution, active carbon VC, Graphene (G), graphene oxide (GO), fullerene (Fl), timcal (Tm) and commercial Pt catalyst mixed with activated carbon were used.

Chromic acid and ultra-distilled water (at 18.2 mega ohm-cm resistance) were used to clean all glassware used in the study. For preparing electrolyte solution in electro-catalytic studies, ultra-distilled water and high purity Merck brand H_2SO_4 (≥ %98.0) were used. High purity Merck brand methanol was used in methanol tolerance measurements. Additionally, hydrogen peroxide (high purity Merck) was added to the electrolyte medium in some measurements. For the formation of catalysts, commercial 40% Pt/C from Sigma- Aldrich, %10 Nafion-PFTE solution from Aldrich, KOH pellets from Merck, tetrahydrofuran from Sigma-Aldrich, zinc acetate from Sigma-Aldrich, carbon gas diffusion layer from GDL, MTI Corp., polypropylene membrane from MTI Corp. and zinc plate from Alfa-Easar were used.

2.2. Electrodes and materials

Experiments were carried out in three-electrode electrochemical and spectroelectrochemical cells. Platinum disk electrode, glassy carbon electrode (GCE), RDE, RRDE and platinum cage electrode were used as working electrodes in the analyses. A spiral platinum wire was used as the auxiliary electrode and a SCE was used as the reference electrode. In catalytic measurements, RDE and RRDE were used modified with phthalocyanine complexes and support materials (Nf and VC, F, G, GO, Tm). N_2 gas atmosphere was provided for voltammetric measurements that required anaerobic conditions and for aerobic conditions, the environment was saturated with O_2 gas.

2.3. Devices

Electrochemical, spectroelectrochemical and electro catalytic measurements were carried out with Gamry Reference 600 potentiostat/galvanostat double potentiostat and Ocean Optics HR2000+ model *UV-Vis* spectrophotometer devices in the M.Ü. Department of Chemistry, Faculty of Arts and Sciences. Bandelin Brand ultrasonic bath was used for homogenization during the preparation of the catalysts. During the application of dynamic RDE and RRDE voltammetry techniques, Pine brand MSRCE model electrodes and a micropipette were used to modify the electrodes.

2.4. Method

During the determination of the redox properties of the phthalocyanine complexes, voltammograms were recorded using CV, DPV and SWV techniques in suitable organic solvent environment, and these voltammograms were analyzed to determine the peak potentials (Ep), half-peak potentials (E1/2), electrochemical data such as peak potential separations (ΔEp), peak currents (Ipc and Ipa) and peak current ratio (Ipa/Ipc).

Simultaneous spectroelectrochemistry technique was used to determine whether the reduction and oxidation reactions took place on the phthalocyanine ring or in the metal center. With this technique, spectral changes during the formation of reduction and oxidation and UV-Vis spectra of these compounds were recorded.

In the final stage of the study, RDE voltammetry and RRDE voltammetry techniques were used. The ORR was examined in the glassy carbon electrode system modified and unmodified with the examined complexes, using a rotating ring (Pt)-disk (C) double working electrode with the bipotentiostat system, and in this way, the electro catalytic activities of the complexes in ORR were investigated.

2.5. Electrochemical measurements

For CV, DPV and SWV measurements of all Pc (**1a-1e** and **2a-2e**) complexes (**Figure 10**);Pt disk electrode was used. These voltammetric measurements were performed in a high purity DMSO and/or DCM solvent system containing TBAP carrier electrolyte at 0.1 M concentration. SCE is used as reference electrode and the analyst is separated from the solution by a double-layer bridge. The analyst concentration prepared to examine its properties is $5x10^{-4}$ M. In addition, high purity nitrogen gas was passed through the solution for 20 minutes in order to expel oxygen, and a nitrogen atmosphere was provided by keeping the inert gas over the solution during the measurement.

2.6. Simultaneous spectroelectrochemical measurements

In-situ spectroelectrochemical was conducted by a computer which was connected from the outside with an "Ocean Optics HR2000 UV-Vis spectrophotometer" arranged with the galvanostat/potentiostat with three electrode arrangement at 25°C. A transparent Pt gauze was acted as the working electrode.

The optical changes that the products of electrochemically produced redox processes show in the visible region of the UV-Vis spectrum cause color changes. For this purpose, colorimetric analysis was performed with simultaneous electro colorimetric measurements and this colorfulness was shown on a two-dimensional plane.

2.7. Electro catalytic measurements

A triple electrode system was used in electro catalytic measurements. In electro catalytic measurements, the solution was mixed with the help of a stirrer during electrolysis. To prepare catalysts from phthalocyanine complexes, whose electro catalytic activity in oxygen reduction will be determined, 5% Nf solution and VC, Fl, G, GO, Tm were used as support material and ethyl alcohol was used as solvent. Appropriate mixtures of the phthalocyanine complexes were prepared, and after the resulting catalyst mixture was homogenized in an ultrasonic bath for 30 minutes, an appropriate amount (106 $\mu g/cm^{-2}$ phthalocyanine compound) was placed on the RDE and RRDE electrodes with the help of a micro pipette.

After preparing suitable modified electrodes to examine the electro catalytic activities of phthalocyanine compounds, CV, RDE voltammetry and RRDE voltammetry techniques were used with the triple electrode system. In these measurements, 0.5 M aqueous sulfuric acid was utilized as the electrolyte. These same measurements were performed with commercially prepared carbon-supported platinum catalysts and the results were compared. To determine the methanol tolerances of the prepared catalysts or modified electrodes, electro catalytic RDE and RRDE measurements were repeated in sulfuricacid aqueous solution containing 1.0 M methanol.

In RRDE measurements, an electrode consisting of a glassy carbon disc electrode with a diameter of 5.61 mm with a Pt ring electrode with an efficiency of 38% was used as the working electrode. The measurements were carried out at a temperature of 25 °C and in a 0.5 M sulfuric acid aqueous solution saturated with oxygen gas, with a modified GCE

(5 mm diameter) at a rotation speed of 2500 rpm. During these measurements, the carbon disc electrode was polarized with a potential scanning rate of 0.005 Vs^{-1}, while the potential of the platinum ring electrode was kept constant at 0.95 V against SCE. Using the measured current densities of the disk and ring electrodes, all the electrons transmitted including the percentage of H_2O_2 or H_2O formed were calculated. For OER techniques, 0.1 M KOH solution was used. For certain time period (half an hour), the catalyst active material (40% wt.), VC (50% wt.) and Nafion/PTFE solution (10% wt.) were sonicated for homogenization and formed as an ink in tetrahydrofuran (THF). An appropriate amount of catalyst (106 $\mu g/cm^{-2}$) was placed on freshly polished glassy carbon electrode (GCE) with the help of a micro pipette.

In the initial stage of these measurements, the same experiments were carried out with the catalyst mixture containing only support material and commercially purchased catalysts containing carbon-supported platinum. In the light of the results, the most optimum electro catalytic results were obtained for the catalyst mixtures prepared with the above-described ratios.

3. FINDINGS AND DISCUSSION

3.1. Studies with Mono (1a–1e) substituted complexes

Electrochemical, simultaneous spectroelectrochemical and electro catalytic ORR performances of mononuclear peripherally tetra substituted metallophthalocyanines **(1a–1e)** derivatives bearing 4-dicyanophenoxy) phenolate groups on the peripheral positions; were determined by using techniques CV, SWV, CA and simultaneous UV-Vis spectroelectrochemical in suitable solvent environments, where spectral changes are observed. Using these techniques, the electron transfers and electro catalytic oxygen reduction behaviors of Pc complexes have been elucidated in detail [6]. Generally, using only voltammetry technique is insufficient to determine redox events. Therefore, simultaneous spectroelectrochemical, simultaneous electro colorimetric, hydrodynamic RDE and bipotentiostatic RRDE measurements of phthalocyanine complexes provide additional support for the determination of redox events and play an important role in understanding their electrochemical and electro catalytic properties.

3.2. Investigation of electrochemical and spectroelectrochemical behaviors of Mono (1a–1e) substituted complexes in solution environment

In order to determine the electrochemical behavior of mono substituted cobalt, iron, manganese, nickel and zinc [CoPc (**1a**), Fe(OAc)Pc (**1b**), Mn(OAc)Pc (**1c**), NiPc (**1d**) and ZnPc(**1e**)] phthalocyanine compounds (**Figure 10** (**A**)) compounds, CV and SWV methods were used using a platinum working electrode in solution environments containing DMSO/TBAP and DCM/TBAP.

With these techniques, voltammetric data such as peak potentials (E_p), half-peak potentials ($E_{1/2}$), ratio of anodic and cathodic peak currents (I_{pa}/I_{pc}) and the difference between the first oxidation and first reduction half-peak potentials ($\Delta E_{1/2}$) were obtained and voltammograms of the complexes were recorded.

The results of the electrochemical characterization of these compounds are given in **Table 1** and **Table 2**, and it has been observed that they generally form reversible one-electron metal and/or Pc ligand-induced redox peaks. When the similarities in the general redox behavior of metal phthalocyanines are examined; It is understood that and that CoPc (**1a),** Fe(OAc)Pc **(1b)** and Mn(OAc)Pc (**1c)** compounds show similar redox properties among themselves. These results show that NiPc (**1d)** and ZnPc (**1e)**

compounds; they act as redox inactive metal centers, with all events showing three or four reductions and one or two oxidation pairs centered on the Pc core [36-40]. By adding di-tert-butyl groups to the substituents, the solubility of metal phthalocyanines in DMSO has increased, thus redox responses of (**1a-1e)** pcs are recorded in DMSO/TBAP electrolyte. These 1a-1e pcs have more electron releasing nature because these Pcs possess the shorter classical bridge. This first reduction event occurring in the Pc core corresponds to the LUMO (lowest energy orbital) and is shown as M(II)Pc (-2) + e^{-}↔ [M(II)Pc (-3)]$^{-}$. Likewise, the first oxidation event that occurs in the Pc core is shown as M(II)Pc (-2) ↔[M(II)Pc (- 1)] $^{+}$ + e^{-} and corresponds to HOMO (highest energy orbital). In general, as the polarization strength of the metal center increases, the reduction of the compound becomes easier and its oxidation becomes more difficult [36]. These redox inactive compounds; The electrochemical characteristic measured in DMSO, was overly close tothe DCM/TBAP system **(Table 1 and 2)**. Generally, the fact that the absorbance value of the Q band of Pc compounds decreases without any shift and is accompanied by the formation of a new band in the 500-600 nm range is an indication that redox events occur in the Pc ring. These characteristic spectrum changes help elucidate the voltammetrically determined ligand-centered redox processes of these compounds. Phthalocyanine complexes undergo sequential one-electron reduction and oxidation events. Elucidating these metal-centered or ligand-centered events is only possible by using simultaneous spectroelectrochemical measurements together with voltammetric measurements. It was also concluded that it is not possible to fully evaluate the nature of redox processes only by voltammetric measurements. Thus, the electrolysis of the complexes (**1a-1e)** was carried out at appropriate constant potentials, and the effect of solvents on redox behavior was tried to be understood by recording simultaneous (in- situ) spectroelectrochemical measurements. The voltammetric behavior of these redox- inactive complexes [NiPc (**1d**), ZnPc (**1e**)] were quite different from the redox-active (Fe, Co and Mn) complexes. For this reason, electrochemical measurements of redox-active complexes were first carried out in the non-polar DCM/TBAP system and polar DMSO system, and then simultaneous (in-situ) spectroelectrochemical measurements wererecorded to understand the effect of solvents on their spectral behavior.

Table 1 Data on the electrochemical characterization of 1a-1e compounds in DMSO/TBAP solution medium.

Complex	Redox Process	Label	[a]$E_{1/2}$ (V)	[b]ΔE_p	[c]a_p/I_{pc} (V)	[d]$\Delta E_{1/2}$ (V)
Fe(OAc)Pc	$[Fe(IV)(OAc)Pc(-2)]^+/[Fe(IV)(OAc)Pc(-1)]^{2+}$	[e]O2	0.85	-	-	0.75
	$Fe(III)(OAc)Pc(-2)/[Fe(IV)(OAc)Pc(-2)]^+$	O1	0.26	65	0.90	
	$Fe(III)(OAc)Pc(-2)/[Fe(II)(OAc)Pc(-2)]^-$	R1	-0.49	70	0.88	
	$[Fe(II)(OAc)Pc(-2)]^-/[Fe(I)(OAc)Pc(-2)]^{2-}$	R2	-1.11	75	0.92	
	$[Fe(I)(OAc)Pc(-2)]^{2-}/[Fe(I)(OAc)Pc(-3)]^{3-}$	R3	-1.20	70	0.85	
	Nitrile Reduction	[e]R4	- 1.42	75	0.88	
CoPc	$Co(II)Pc(-2)^+/[Co(III)Pc(-1)]^{2+}$	[e]O2	0.98	-	-	0.86
	$Co(II)Pc(-2)/[Co(III)Pc(-2)]^+$	O1	0.46	75	0.80	
	$Co(II)Pc(-2)/[Co(I)Pc(-2)]^-$	R1	-0.40	70	0.85	
	$[Co(I)Pc(-2)]^-/[Co(I)Pc(-3)]^{2-}$	R2	-0.82	80	0.80	
	Nitrile Reduction	R3	-1.39	65	0.95	
Mn(OAc)Pc	$Mn(IV)(OAc)Pc(-2)^+/[Mn(IV)(OAc)Pc(-1)]^{2+}$	[e]O2	1.08	-	-	0.60
	$Mn(III)(OAc)Pc(-2)/[Mn(IV)(OAc)Pc(-2)]^+$	O1	0.44	90	0.80	
	$Mn(III)(OAc)Pc(-2)/[Mn(II)(OAc)Pc(-2)]^-$	R1	-0.16	65	0.88	
	$Mn(II)(OAc)Pc(-2)^-/[Mn(I)(OAc)Pc(-2)]^{2-}$	R2	-0.77	60	0.90	
	$[Mn(I)(OAc)Pc(-2)]^{2-}/[Mn(I)(OAc)Pc(-3)]^{3-}$	R3	-1.42	80	0.85	
	Nitrile Reduction	R4	-1.61	65	0.95	
NiPc	$Ni(II)Pc(-2)/[Ni(II)Pc(-1)]^+$	[e]O1	0.92	-	-	1.67
	$Ni(II)Pc(-2)/[Ni(II)Pc(-3)]^-$	R1	-0.75	85	0.80	
	$[Ni(II)Pc(-3)]^-/[Ni(II)Pc(-4)]^{2-}$	R2	-1.14	65	0.95	
	Nitrile Reduction	R3	-1.63	70	0.88	
ZnPc	$Zn(II)Pc(-2)/[Zn(II)Pc(-1)]^+$	[e]O1	0.81	-	-	1.62
	$Zn(II)Pc(-2)/[Zn(II)Pc(-3)]^-$	R1	-0.81	60	0.98	
	$[Zn(II)Pc(-3)]^-/[Zn(II)Pc(-4)]^{2-}$	R2	-1.20	90	0.80	
	Nitrile Reduction	R3	-1.65	65	0.95	

[a]: $E_{1/2} = (E_{pa} + E_{pc})/2$ at 0.100 V s^{-1}.

[b]: $\Delta E_p = E_{pa} - E_{pc}$ at 100 mV s^{-1}.

[c]: I_{pa}/I_{pc} for reduction processes at 0.100 V s^{-1} scan rate.

[d]: $\Delta E_{1/2} = E_{1/2}$(first oxidation) - $E_{1/2}$ (first reduction). It represents the HOMO-LUMO gap for Zn and Ni, but the charge transfers transitions for Fe, Mn and Co involving redox-active metal centers.

[e]: These redox couples could be detected only by square wave voltammetry. ΔEp value could not bedetermined due to ill-defined and/or irreversible nature of the redox process.

Table 2 Data on the electrochemical characterization of mononuclear tetra substituted 1a-1e compounds in DCM/TBAP solution medium.

Complex	Redox process	Label	[a]$E_{1/2}$ (V)	[b]ΔE_p	[c]I_{pa}/I_{pc} (V)	[d]$\Delta E_{1/2}$ (V)
Fe(OAc)Pc	Fe(III)(OAc)Pc(-2)/[Fe(III)(OAc)Pc(-2). Fe(III)(OAc)Pc(-1)]$^+$	O1	0.89	85	0.80	0.58
	Fe(III)(OAc)Pc(-2)/[Fe(III)(OAc)Pc(-2). Fe(II)(OAc)Pc(-2)]$^-$	R1	-0.22	75	0.85	
	Fe(III)(OAc)Pc(-2).Fe(II)(OAc)Pc(-2)]$^-$/ [Fe(II)(OAc)Pc(-2)]$_2^{2-}$	R2	-0.64	65	0.98	
	Fe(II)(OAc)Pc(-2)]$_2^{2-}$/[Fe(II)(OAc)Pc(-3). Fe(II)(OAc)Pc(-2)]$^{3-}$	R3	-1.12	65	0.95	
CoPc	[Co(II)Pc(-1)]$^+$/ [Co(III)Pc(-1)]$^{2+}$	O2	1.07	80	0.80	0.83
	Co(II)Pc(-2)/[Co(II)Pc(-1)]$^+$	O1′(O1″)	0.60(0.92)	-	-	
	Co(II)Pc(-2)/[Co(I)Pc(-2)]$^-$	R1	-0.23	60	0.98	
	[Co(I)Pc(-2)]$^-$ / [Co(I)Pc(-3)]$^{2-}$	R2	-1.08	65	0.95	
	Nitrile Reduction	R3	-1.44	75	0.85	
Mn(OAc)Pc	Mn(III)(OAc)Pc(-2)/[Mn(III)(OAc)Pc(-1)]$^+$	[e]O1	1.12	-	-	1.21
	Mn(III)(OAc)Pc(-2)/ [Mn(II)(OAc)Pc(-2)]$^-$	R1	-0.09	65	0.90	
	[Mn(II)(OAc)Pc(-2)]$^-$/[Mn(I)(OAc)Pc(-2)]$^{2-}$	R2	-0.94	75	0.85	
	Mn(I)(OAc)Pc(-2)]$^{2-}$/[Mn(I)(OAc)Pc(-3)]$^{3-}$	[e]R3	-1.12	-	-	
NiPc	Ni(II)Pc(-2)/[Ni(II)Pc(-1)]$^+$	O1	0.95	65	0.95	1.72
	Ni(II)Pc(-2)/[Ni(II)Pc(-3)]$^-$	R1	-0.77	60	0.98	
	[Ni(II)Pc(-3)]$^-$/[Ni(II)Pc(-4)]$^{2-}$	R2	-1.18	60	0.98	
ZnPc	Zn(II)Pc(-2)/[Zn(II)Pc(-1)]$^+$	O1′(O1″)	0.54(0.77)	65(70)	0.95(0.88)	1.44
	Zn(II)Pc(-2)/[Zn(II)Pc(-3)]$^-$	R1	-0.86	85	0.80	
	[Zn(II)Pc(-3)]$^-$/[Zn(II)Pc(-4)]$^{2-}$	R2	-1.13	85	0.80	

[a]: $E_{1/2} = (E_{pa} + E_{pc})/2$ at 0.100 V s^{-1}.
[b]: $\Delta E_p = E_{pa} - E_{pc}$ at 100 mV s^{-1}.
[c]: I_{pa}/I_{pc} for reduction processes at 0.100 V s^{-1} scan rate.
[d]: $\Delta E_{1/2} = E_{1/2}$(first oxidation) - $E_{1/2}$ (first reduction). It represents the HOMO-LUMO gap for Zn and Ni, but the charge transfer transitions for Fe, Mn and Co involving redox-active metal centers.
[e]: These redox couples could be detected only by square wave voltammetry. ΔEp value could not be determined due to ill-defined and/or irreversible nature of the redox process.

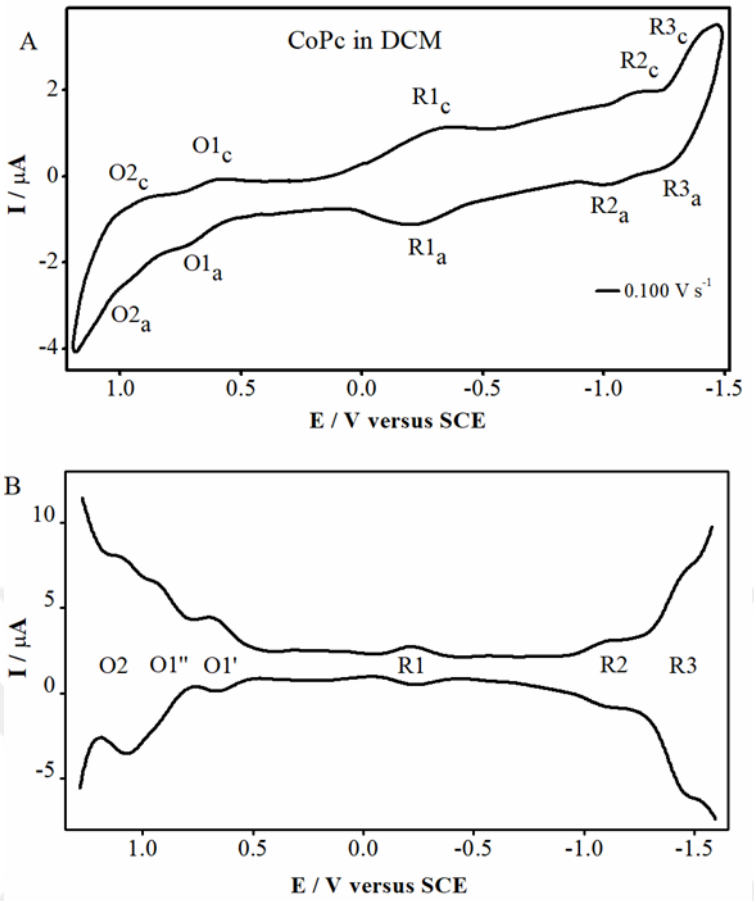

Figure 11 (A) CV and **(B)** SWV voltammograms of CoPc (**1a**) complex ($5.0x10^{-4}$ M) DCM/TBAP solution medium.

Figure 11 represents CVs along with SWVs of CoPc **(1a)** in DCM/TBAP solution medium. The compound CoPc **(1a)** goes through three one electron reductions (R1 at -0.23V, R2 at - 1.08V and R3 at - 1.44V versus SCE) and also two one electron oxidation procedures. Despite that, the first oxidation procedure splits into two waves (O1′ at 0.60V and O1″ at 0.92V versus SCE), probably due to the presence of aggregated species. The reduction of R3 at -1.44 V derives from the nitrile groups at the open ends of the complex. Moreover, the second oxidation and the first reduction procedures of Co could be assigned to the $[Co(II)Pc\ (-1)]^{+}/[Co(III)Pc\ (-1)]^{2+}$ and $Co(II)Pc(-2)/[Co(I)Pc\ (-2)]^{-}$ in DCM, respectively while the rest procedures to the Phthalocyanine ring. The Ipa/Ipc proportion with the scan rate was almost unity which suggests the perfect diffusion

controlled electron transfer mechanism of the procedures (**Table 2**). ΔEp values ranged 60 to 80 mV pointed purely diffusion-controlled mass transfer and reversible electron transfer nature of these redox pairs. The chemical-electrochemical reversibility of the redox procedures was also verified, mostly, by SWV in the forward and reverse scans (**Figure 11B**).

While the first reduction and oxidation events of compounds with a redox active metal center in polar solvents such as DMF and DMSO occur in the metal center, in nonpolar solvents such as DCM and THF, this first oxidation event occurs in the Pc ring [40, 41]. In addition, as a result of the interaction between the Co-d and Pc ligand-molecular orbitals, the LUMO energy for this complex is highly negative compared to the NiPc (**1d)** and ZnPc**(1e)** complexes, and the initial ring-centered reduction event occurs at a highly negative potential. Therefore, the second and ongoing ring-based reduction processes are generally outside the existing negative potential window and cannot be observed as expected. [40]. The electrochemical behavior of CoPc **(1a)** in the polar DMSO/TBAP solvent system, which has a coordinative property, is quite different from the voltammetric measurements performed in the DCM/TBAP environment. However, the half-wave potentials $E_{1/2}$ of redox processes vary significantly depending on the nature of the solvent. The $E_{1/2}$ value of -0.40 V for the first reduction pair R1 observed in the DMSO/TBAP solvent system is quite negative compared to the $E_{1/2}$ value of -0.23 V found for the DCM solvent environment. While the 1st oxidation and 1st reduction events, which exhibit reversible and diffusion-controlled redox events, are metal-centered, the other events must be ring-centered. The spectral behaviors of Mn, Fe and Co derivatives in solvents with low dielectric constant are also quite different. For example, in nonpolar DCM, the first oxidation process is ligand-centered, [Co(II)Pc (- 2)]/[Co(II)Pc (-1)] +, while in the polar DMSO solvent environment, which has a coordinative feature, the first oxidation processes occur metal-centered. Cobalt metal is known to be more stable in the Co(III) form, and is easily oxidized from the 2+ oxidation state to the 3+ form at a much lower potential value, because of the coordination feature of the DMSO solvent [40-46].

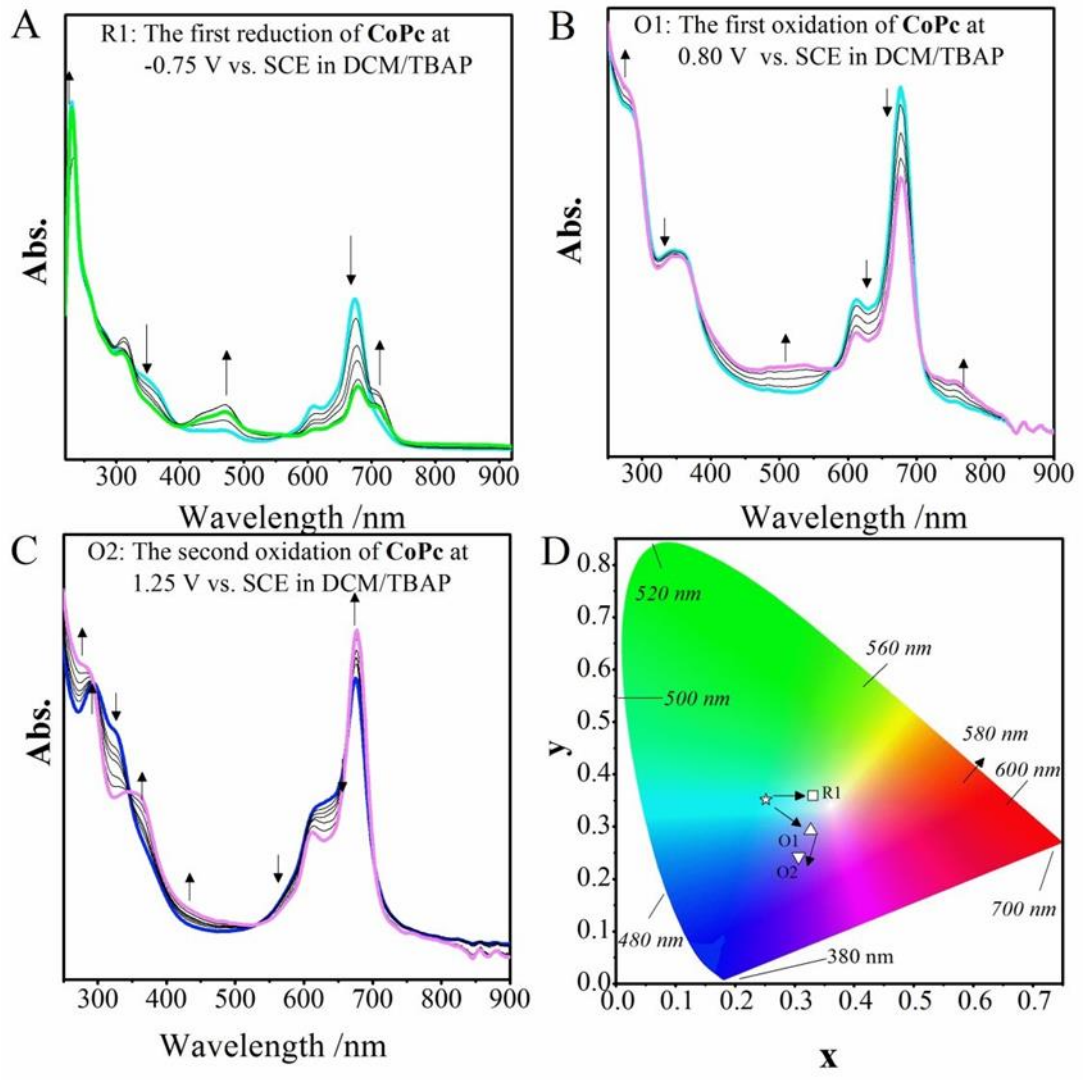

Figure 12 In situ UV-*Vis* spectral and electro colorimetric changes of CoPc (**1a**) complex (5.00 x 10^{-5} M) in DCM/TBAP solution medium, recorded by applying constant potential according to SCE.

Spectroelectrochemical studies were also applied to verify the assignments of the redox processes of CoPc **(1a)**. In situ UV-Vis spectral variations were observed in both non-coordinating solvent DCM and coordinating polar solvent DMSO. **Figure 12** exhibits the spectral variations throughout the number one reduction process of CoPc **(1a)** at − 0.75Vversus SCE in DCM/TBAP which is related to the redox procedure marked R1 in **Figure 12** A new band at 470 nm seems at the same time the Q band at 673 nm shifts to 710 nm. This is feature of [Co(I)Pc (−2)] − monoanionic species [33,34]. The spectral changes have clear cut isosbestic points at 398, and 565 nm. As it shows in situ electrocolorimetrically recorded chromaticity scheme in **Figure 12D**, the changes of color from turquoise (x=0.251 and y=0.351) to light green (x = 0.331 and y = 0.359) of

the solution. The shifting of the Q band and the formation of a new band at 470 nm designate the formation of [Co(I)Pc (−2)] − species, at the same time this changes confirm the CV assignment of the pair R1 to Co(II)Pc(−2)/[Co(I)Pc (−2)] − procedure. **Figure 12B** shows in situ UV Vis spectral variations recorded throughout the first oxidation procedure. The sharp Q band at 675 along with a vibrational band at 608 nm decrease (**Figure 12B**) whereas two other new peaks within the range of 400–500 nm and 753 nm increase. These spectral variations produce a change in color from turquoise to blue (x=0.326 and y=0.292) (**Figure 12D)** and form sharp1 isosbestic points at 361, 581, and 702 nm. Over the first oxidation procedure in DCM/TBAP electrolyte system, all these spectral variations suggest a ring based oxidation reaction, Co(II)Pc (-2)/[Co(II)Pc (-1)] +. During further oxidation at 1.25 V vs. SCE, the Q band at 652 nm decreases while a new band at 460 nm appears. These kind of spectral changes are unique for a metal based oxidation for CoPc **(1a)** complexes [35,36]. Moreover, this is also support the CV assignment of [Co(II)Pc (-1)] $^{+}$/[Co(III)Pc (-1)] $^{+}$ for O2 pair of CoPc **(1a)** in **Figure 12**.

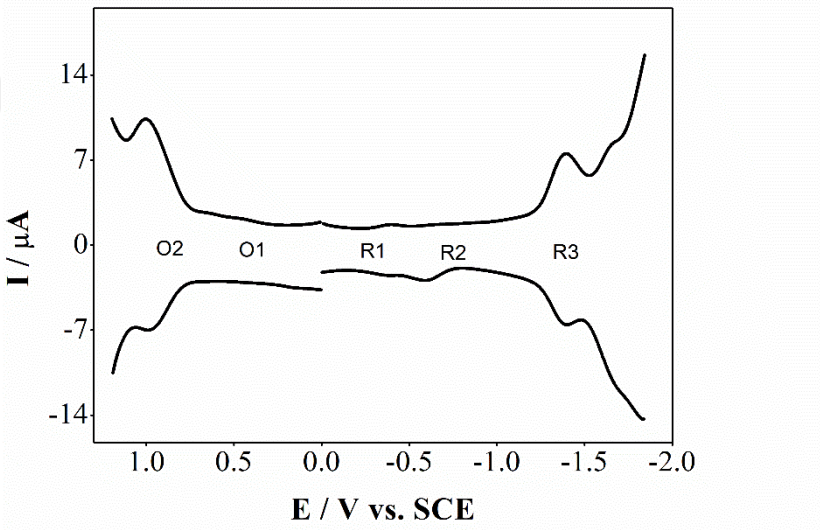

Figure 13 SWV voltammograms of CoPc (**1a**) complex ($5.0x10^{-4}$ M) in DMSO/TBAP solution medium.

For investigating the solvent effect of the complexes, Voltammetric analysis of CoPc **(1a)** were conducted in a coordinating polar solvent DMSO/TBAP too (**Figure 13** and **Table 1).** According to the number of redox signals, the voltammetric feedback of Co in DMSO/TBAP and DCM/TBAP are quite close to each other. This one undergoes three well resolved diffusion controlled and reversible reduction processes and two

oxidation processes. The values for ΔEp are range between 65 to 80 mV which indicates thatevery electron transfer procedures are electrochemically reversible (**Table 1**). Each reduction process of CoPc **(1a)** are surely diffusion controlled with unity of relevant Ipa/Ipc ratios. Despite that, the nature of the solvent is also one of the factors on which the "half wave potentials" of all redox procedures are dependent. Because of the donor character of DMSO, the "half wave potential" of number one reduction procedure is slightly moved negatively from - 0.23 V to - 0.40 V by coordinating DMSO solvent, even though both procedures are metal based as Co(II) / Co(I). Hence, the nitrile based third reduction procedure of CoPc **(1a)** takes place almost at the similar potential in DMSO as well as DCM. So, only by the metal-based procedure, the shifting effect of potential of the polar solvent DMSO is demonstrated. It is may be analyzed as a predicted consideration since in CoPc **(1a)**, metal center Co(II) likely prefers six coordination and that'show, in CoPc **(1a),** donor type DMSO particles are coordinated in the axial direction to the metal center Co. For the first oxidation procedure of the compound, the half wave potential is moved negatively from 0.60V to 0.46V by coordinating DMSO solvent. Hence, in such circumstances, the number one oxidation procedure is metal based at the same time, the other procedure is ligand based. But for nonpolar solvent as DCM, the number one oxidation procedure takes place on the Phthalocyanine ring [30,37]. So in DMSO, the first oxidation couples as well as the second one also might be occupying to the Co(II)Pc (- 2) / [Co(III)Pc (- 2)] + as well as [Co(III)Pc (- 2)] + / [Co(III)Pc (- 1)]2+, respectively. Moreover, six co-ordinate Metal Phthalocyanine species are kept separate by the axially bound ligands so that they basically do not aggregate [30,37]. Consequently, for the first reduction and first oxidation procedures, the character of the electron transfer procedures are perfectly diffusion controlled. Furthermore, the peaks noted throughout the forward and reverse square wave voltammetric scans suggested electrochemical reversibility of those pairs [38]. The symmetry of all the peaks recordedthroughout the forward and reverse SWV scans indicated the chemical along with electrochemical reversibility of these procedures. According to the **Table 1** the number two oxidation procedure O_2, was spotted only by SWV.

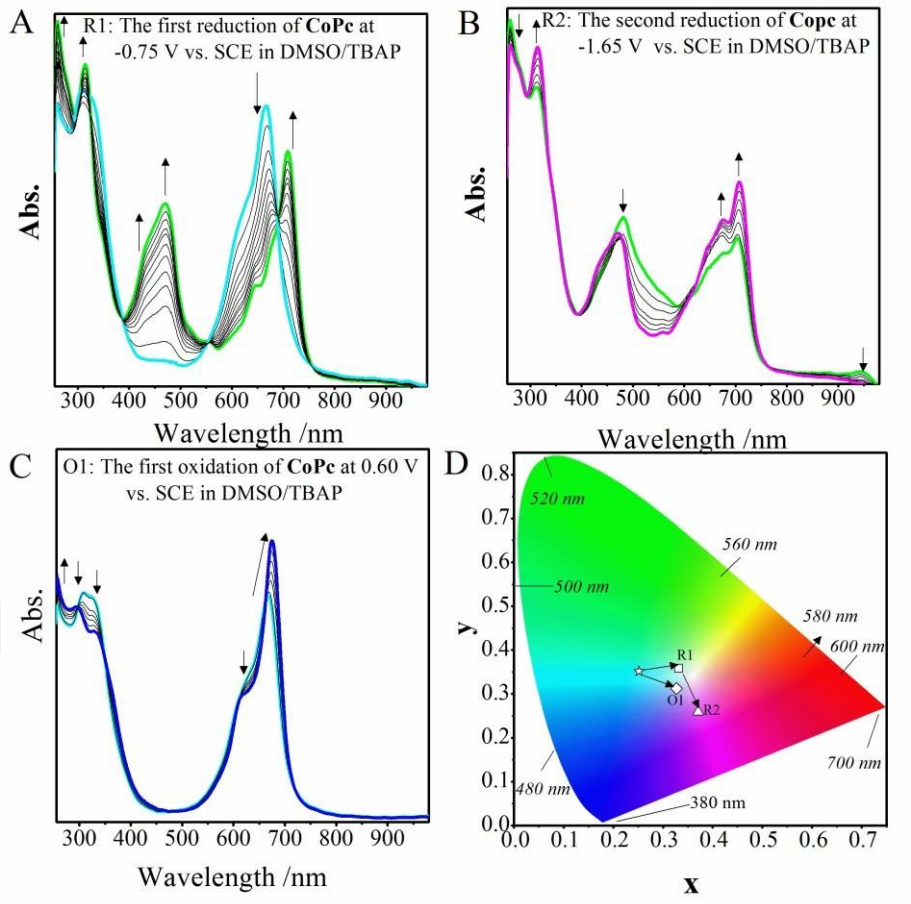

Figure 14 In situ UV-*Vis* spectral and electro colorimetric changes of CoPc (**1a**) complex (5.00 x 10^{-5} M) in DMSO/TBAP solution medium, recorded by applying constant potential according to SCE.

For investigating the solvent effect and making comparison of CoPc **(1a)** in DMSO/TBAP and DCM/TBAP solution medium, UV-*vis* spectral variations also carried out in DMSO/TBAP (**Figures. 14A-14D)**. The starting spectrum with turquoise color in **Figure 14A** was a bit broad being different from that in **Figure 14A** which was causedby the formation of aggregated species in DMSO/TBAP electrolyte system [40-45]. However, throughout the number one oxidation procedure (O1), all the changes recorded were entirely different than those in DCM indicating a ring based oxidation reaction. **Figure 14A** illustrates in situ UV vis spectral variations throughout the number one reduction of CoPc **(1a)** at -0.75 V versus SCE in DMSO/TBAP, correspondingto the redox procedure labelled R1 in **Table 1**. The Q band at 667 nm shifts to 710 nm, while a new band at 472 nm appears. The spectral variations have clear cut isosbestic points at 375, 556 and 696 nm. According to the chromacity scheme in **Figure 14D**, a change in color from turquoise (x=0.251 and y=0.351) to light

green (x=0.332 and y=0.357). The shifting of the Q band and the formation of a new band at 472 nm recommend the formation of [Co(I)Pc (2)] − species which proved the CV assignment of the couple Co(II)Pc(-2)/[Co(I)Pc (-2)] − (R1) procedure. [40-42] The color changes from light green to purple (x = 0.371 and y = 0.259) as given in the chromaticity diagram in **Figure 14D**. **Figure 14C** shows spectroelectrochemical changes for the former oxidation procedure (O1). The Q band at 666 nm increases with redshift to 675 nm which is unique of a metal based oxidation in CoPc **(1a)** complexes and thereby, supports the voltammetric assignment of Co(II)Pc (- 2) / [Co(III)Pc (- 2)] $^{+}$ for O1 pair of CoPc **(1a)** (Table **1**). [35,36,43] It also provides clear isosbestic points at 296, 349, 485,610 and 662 nm. The changing color from turquoise to light blue (x = 0.326 and y = 0.312) (**Figure 14D)**. The following second oxidation procedure was out of the available limited positive potential range of DMSO/TBAP electrolyte, this is why it could not be observed as expected.

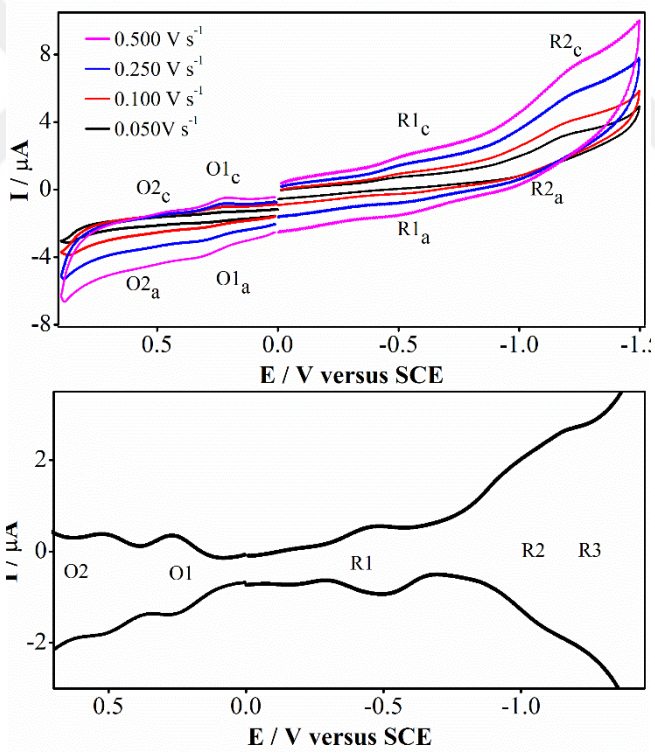

Figure 15 (A) CV and (**B)** SWV voltammograms of Fe(OAc)Pc (**1b**) complex ($5.0x10^{-4}$ M) in DMSO/TBAP solution medium.

Voltammetric experiment of Fe(OAc)Pc (**1b**) compound was also carried out in DMSO/TBAP and DCM/TBAP solutions (**Figure 15** and **Table 1).** Each of the reduction and oxidation combinations, electron transfer procedures along with redox

behaviors are in harmony with the literature [41,42]. The voltammetric feedback of (1b) compound in DMSO is quite close to that in DCM. Although, all redox responses shift to more negative potentials in DMSO because of its polarization effect. $\Delta E_{1/2}$ value for the Fe(OAc)Pc (**1b**) complexes are largely in keeping with those of the formerly published phthalocyanine compounds [41, 42] (**Table 1**).

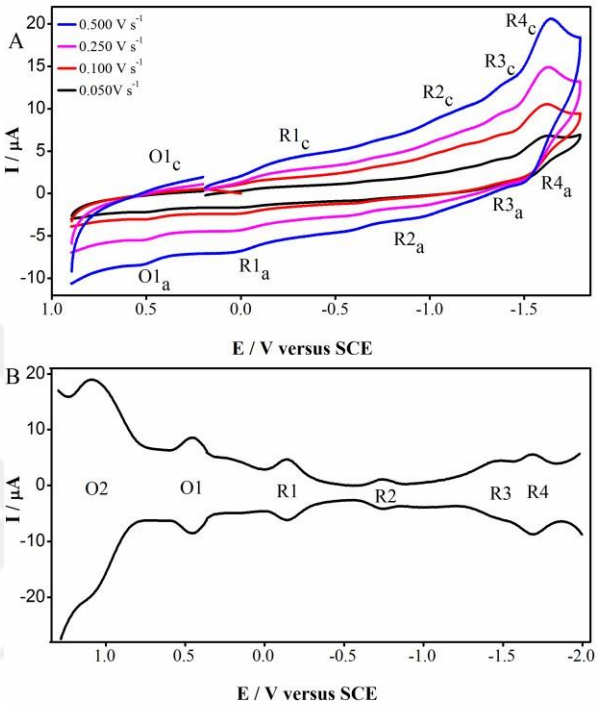

Figure 16 (A) CV and (**B)** SWV voltammograms of Mn(OAc)Pc (**1c**) complex in DMSO/TBAP.

Figure 16 shows the CVs and SWVs of Mn(OAc)Pc **(1c)** in DMSO/TBAP. The related electrochemical data are tabulated for this solvent in **Table 1**. Each and every redox procedure is reversible electrochemically in coordinating DMSO/TBAP electrolyte. Mn(OAc)Pc **(1c)** provides four clear-cut diffusion controlled and reversible reduction procedures (R1 at - 0.16V, R2 at - 0.77V, R3 at 1.43V and R4 at -1.61V versus SCE) and two oxidation couples (O1 at 0.44 V and O2 at 1.08 V versus SCE). The former two reduction procedures and the first oxidation procedure are possibly metal based [Mn(III)(OAc)Pc(-2)]/[Mn(II) (OAc)Pc (-2)] $^{-}$, [Mn(II) (OAc)Pc (-2)] $^{-}$/ [Mn(I)(OAc)Pc (-2)]$^{2-}$ and Mn(III)(OAc)Pc(-2)/[Mn(IV)(OAc)Pc (-2)] $^{+}$ processes, respectively. On the contrary, the third reduction and the second oxidation processes are attributed to the ligand based [Mn(I)(OAc)Pc(-2)]$^{2-}$/[Mn(I)(OAc)Pc (-3)]$^{3-}$ and Mn(IV)(OAc)Pc (-2) $^{+}$/[Mn(IV)(OAc)Pc (-1)]$^{2+}$, processes correspondingly. ΔEp values

for these processes were within the range of 60–90 mV at various scan rates from 0.050 to 0.500 Vs^{-1}, demonstrating reversible electrochemical behavior. The couples showed totally diffusion controlled mass transfer behavior with roughly unit values of the Ipa/Ipc ratios. This reversible behavior was also verified by the affinity in the forward and reverse SWVs (**Figure 16B**). The number two oxidation procedure could be detected only by SWV due to the appearance of the process at the end of the available potential window (**Figure 16B**). Because of the polarization effect of DMSO, each redox pairs of Mn have slightly much negative half-wave potentials in coordinating DMSO/TBAP electrolyte than those in non-coordinating DCM/TBAP electrolyte. Although, the R2 redox couples do not conform to typical shifting behavior.

The first oxidation process of Fe(OAc)Pc (**1b**) is possibly metal-based Fe(III)(OAc)Pc(-2)/[Fe(IV)(OAc)Pc (-2)] $^{+}$ which is as same as Mn(OAc)Pc (**1c**), Mn(III)(OAc)Pc(-2)/[Mn(IV)(OAc)Pc (-2)] $^{+}$. In comparison with CoPc (**1a**) and Fe(OAc)Pc (**1b**) complexes, for CV and SWV method, the shifting of redox potential for Mn(OAc)Pc (1c) compound is minor if coordinating DMSO/TBAP electrolyte is applied in place of non-coordinating DCM/TBAP electrolyte which would be connected with the variation of the coordinating properties of axial sites of these compounds. Hence, due to the arrange of axial position by the neutralizing and/or donor solvent molecules, the potentials of MPcs are greatly affected. Metal ions in Fe(OAc)Pc (**1b**) and Mn(OAc)Pc (**1c**) complexes containing iron and manganese metal centers, the oxidation state of manganese center is 3^{+} in Mn(OAc)Pc (**1c**), whereas the metal center is in the oxidation state of 2+ in CoPc (**1a**). Because of the essentiality of neutralization of the oxidation state three (3+), one axial sites of Mn(OAc)Pc (**1c**) and Fe(OAc)Pc (**1b**) is occupied by OAc in DMSO and DCM. Moreover, these results were supported by observing carbonyl groups of Fe and Mn in IR spectroscopy. However, in case of CoPc (**1a**), the axial sites for fifth and sixth coordination's are engaged with the donor solvent dimethyl sulfoxide excluding dichloromethane. When comparing the solvent effect, it was observed that generally coordinated polar solvents such as DMSO shifted the Q band to the low energy region due to its high refractive indexes. It was observed from the analysis of the voltammetric and spectroelectrochemical action of the complexes that nickel and zinc exhibit only Pc ring based redox procedures.

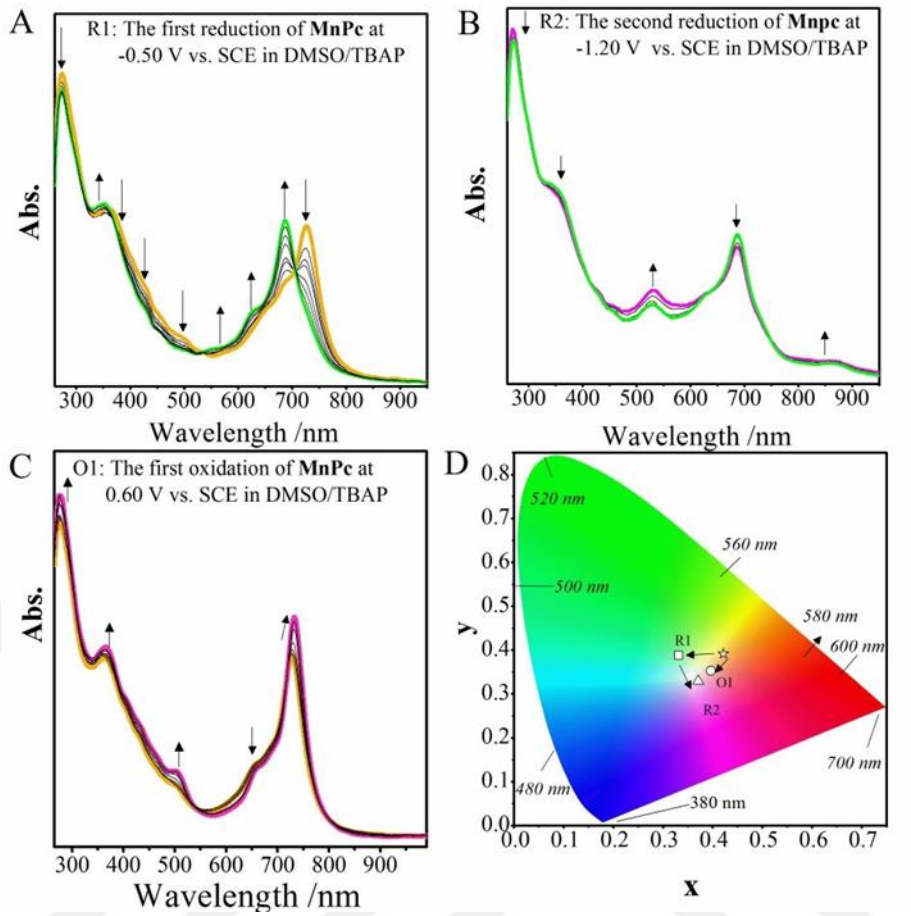

Figure 17 In situ UV-Vis spectral and electro colorimetric changes of Mn(OAc)Pc (**1c**) complex (5.00 x 10^{-5} M) in DMSO/TBAP solution medium, recorded by applying constant potential according to SCE.

Figures 17A–17D represents UV Vis spectral variations also collaboratively recorded chromaticity scheme of compound 1c in DMSO/TBAP. Throughout the number one reduction of Mn(OAc)Pc **(1c)** at - 0.50V versus SCE, the Q band shifted at 726 nm to 686nm plus formed new bands at 569 nm and 621 nm which is also known as the charge transfer region. These changes approve the output of [Mn(II)(OAc)Pc (-2)]$^{-}$ species from Mn(III)(OAc)Pc (-2) species. These spectral variations are associated by the formation of three new bands at 621, 686, and 569 nm [34,43]. As illustrated in **Figure 17D**, the changing of color from orange (x=0.421 and y=0.391) to light green (x=0.332 and y=0.387) and form clear isosbestic points at 371, 525, and 706 nm. In the process of the second reduction of Mn(OAc)Pc **(1c)** at - 1.20V versus SCE, one new band formed at 530 nm and another band decreased at 686 nm. Those changes represent a metal based reduction to [Mn(I)(OAc)Pc (-2)]$^{2-}$ from [Mn(II)(OAc)Pc (- 2)]$^{-}$ species (**Figure 17B)**. According to **Figure 17D,** these spectral changes produce a

change in color from green to light pink (x=0.371 and y=0.329). **Figure 17C** presents the spectral changes upon the first oxidation process at 0.60V versus SCE. Throughout this process, the Q band shifted at 728 nm to 732 nm and a new band formed at 498 nm which also supports the output from Mn(III)Pc (-2) to [Mn(IV)Pc (-2) species (**Figure 17C**). The changes in color from orange to light pink (x=0.396 and y=0.352) in **Figure 17D.** For first oxidation O1, these kind of spectral variations are characteristics for a metal based oxidation, additionally it confirms the voltammetric assignment to Mn(III)(OAc)Pc(-2)/[Mn(IV)(OAc)Pc (-2)]$^{+}$ of this process in **Figure 17.**

Additionally, similar systematic potential shifts were observed as a result of the comparison of electrochemical measurements made in DCM and DMSO solvent environments. In measurements made with the DMSO solvent system, it was observed that the redox couples of nickel and zinc metal complexes shifted more negatively than DCM due to their donor properties. These redox inactive compounds were also measured in DMSO and results electrochemical characteristics, very similar to the DCM/TBAP system.

To differentiate the common characteristics of Phthalocyanine ring based redox procedures, the voltammetric analysis of NiPc **(1d)** was firstly illustrated. Voltammetric experiments of NiPc **(1d)** compound were analyzed in DCM/TBAP **(Figure 18)**. At every single scan rate, the relevant Ipa/Ipc ratios are unity which indicates that diffusion controlled reduction pairs of NiPc **(1d)**. It shows two clear-cut diffusion-controlled as well as reversible reduction combinations (R1 = - 0.77V and R2 = - 1.18V versus SCE) and one oxidation pairs (O1 at 0.95V versus SCE) at different scan rates from 0.050 to 0.500 Vs^{-1}. SWVs distinctly show reversibility of the redox processes in the chemical and electrochemical measurements (**Figure 18B**). For the redox pairs, ΔEp data at 0.100 Vs^{-1} scan rate range normally between 60 to 65 mV which proves the electrochemical reversibility of the electron transfer procedures (**Table 2**).

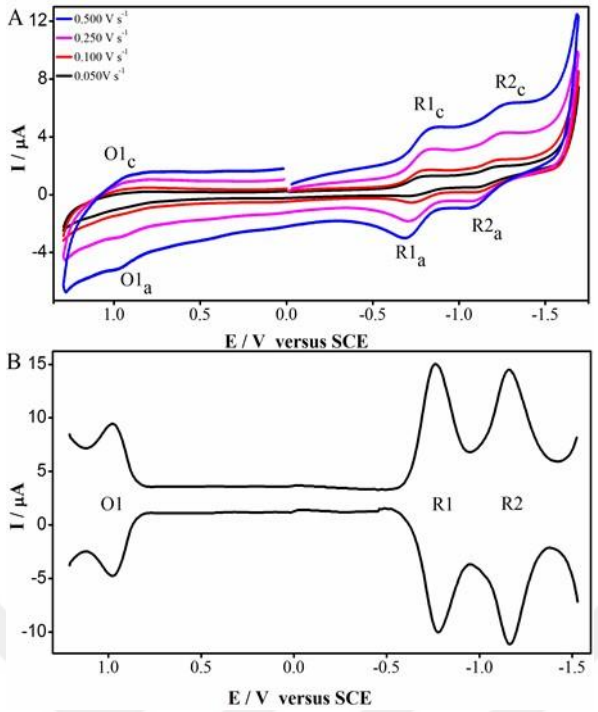

Figure 18 (A) CV and **(B)** SWV voltammograms of NiPc (**1d**) complex ($5.0x10^{-4}$M) in DCM/TBAP solution medium.

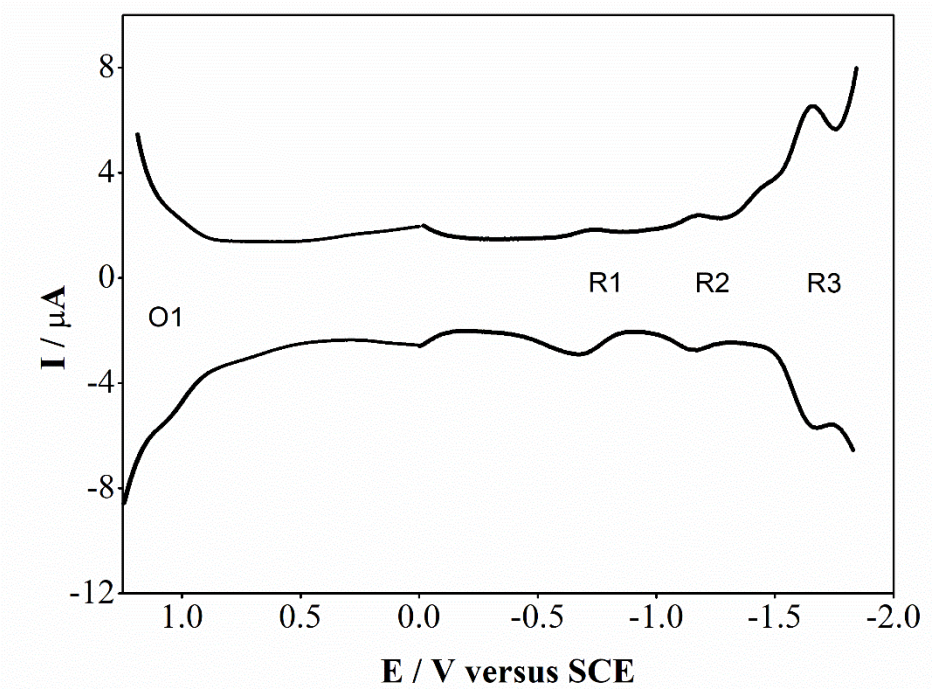

Figure 19 SWV voltammograms of NiPc (**1d**) complex ($5.0x10^{-4}$ M) in DMSO/TBAP solution.

For investigating the solvent effect on the electrochemical behavior of the complex, voltammetric analyses of NiPc **(1d)** compound were analyzed in DMSO/TBAP

electrolyte system too (**Table 1 and Figure 19**)**.** The electron transfers procedures along with redox behaviors of each of the reduction and oxidation combinations are in harmony with the literature [44-48]. The voltammetric feedback of NiPc **(1d)** compound in DMSO is quite close to that in DCM. Although, all redox responses shift to more negative potentials in DMSO as a consequence of its polarization effect. $\Delta E_{1/2}$ value for the NiPc **(1d)** complexes are largely in consonance with the formerly published phthalocyanine compounds [48]

By using voltammetric measurements singly, it is fairly impossible to point out the nature of the redox couples perfectly. Meanwhile, the voltammetric analyses were supported with *in situ* spectroelectrochemical analysis, performed throughout the controlled potential electrolysis of complex at voltammetrically determined constant potentials. The spectral changes monitored during these measurements permitted us to make the assignment of the redox methods, that is, either these processes are metal based or ligand based. The general trend in the spectral changes of **NiPc (1d)** with redox inactive metal center species is assumed to be different from those of the MPcs having redox active metal centers. Predictably, the spectral changes of these compounds were different from those of the MPcs having redox active metal centers. Predominantly, the formation of a new absorption band within the range of 550–650 nm and lowering in the main Q band absorption without a shift and simultaneously throughout the redox procedures of these complexes was detected. These kind of spectral transformation were particular for Phthalocyanine ring based redox procedures and hence, offered considerable evidence for electrochemically allocated ligand based character of the redox procedures of redox inactive compounds [49].

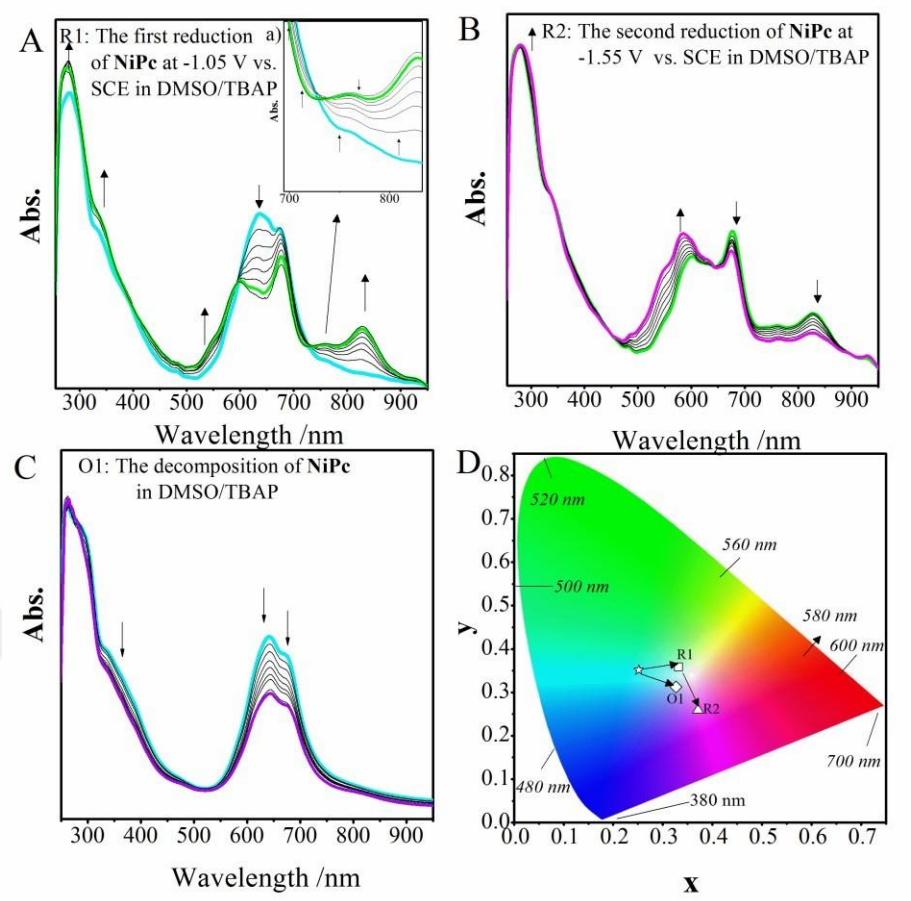

Figure 20 In situ UV-Vis changes of NiPc (**1d**) complex (5.00 x 10^{-5} M) in DMSO/TBAP

Figure 20A–20D illustrates UV-*Vis* spectral changes along with chromaticity diagram of NiPc (**1d**) in DMSO/TBAP. The intensity of the band at 633 nm decreases whereas it increases from 780 nm to 900 nm at 830 nm in the process of the first reduction reaction at -1.05 V. Nevertheless, moving isobestic points have been identified (**Figure 20A** inset). Observation of moving isobestic points in spectroelectrochemical measurements of mononuclear metal centered phthalocyanine complexes is an indication of aggregation. The changing of color from turquoise (x=0.251 and y=0.351) to light green (x=0.332 and y=0.357) as has been seen in the chromacity scheme in **Figure 20D**. Over the additional reduction at - 1.55V versus. SCE, the Q band at 661 nm decreased without shift (**Figure 20B**) indicates the continuation of aggregation process. This procedure is simply presented to Ni(II)Pc (- 2)/[Ni(II)Pc (-3)]$^{-}$ redox couple. As represented by the chromaticity diagram in **Figure 20D**, a distinct change of color from light green to light pink was produced by the process (x = 0.371 and y = 0.259). **Figure 20C** presents in situ UV *Vis* spectral changes at the time of the first oxidation

procedure. The slow decrease in intensity of the band at 652 nm was also observed which is as well as followed by the lessen in the B band. Despite that, after the oxidation procedure, spectroelectrochemical measurements would not productive in the allocation of these compounds due to the decomposition of the monocationic [Ni(II)Pc (-1)] $^{+}$ species, besides their unstable situation over the circumstances of constant potential application, in contrast to potential sweep at constant potentials more positive than 1.05 V vs. SCE. A sharp changing color from original turquoise to light bluish pink (x=0.326 and y=0.312) resulted in this decomposition process **(Figure 20D)** [26]

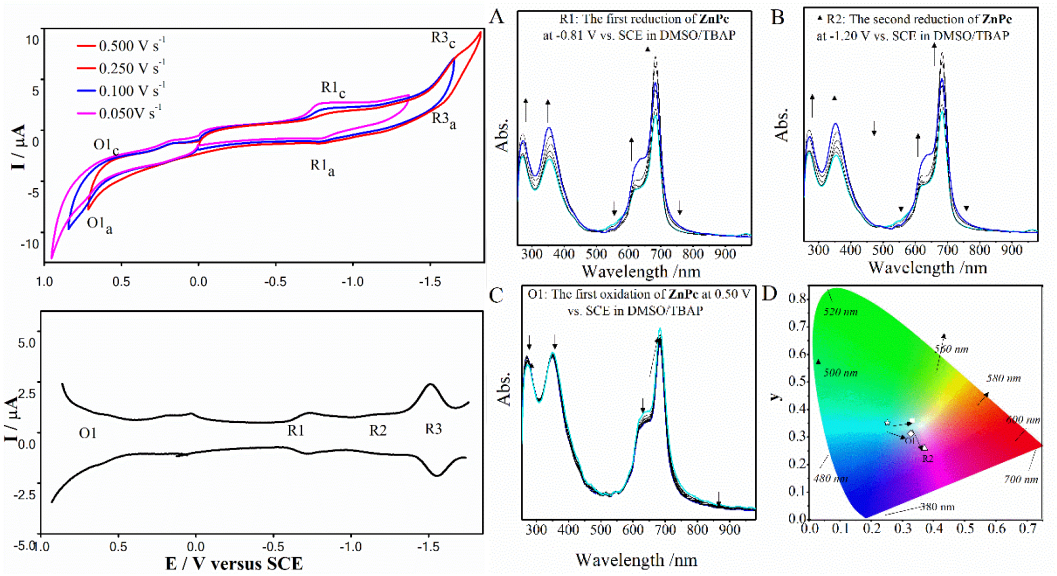

Figure 21 (**A**) CV and (**B**) SWV voltammograms of ZnPc (**1e**) complex (5.0x10-4 M) in DMSO/TBAP solution medium. (**C**) In situ UV-Vis spectral and electro colorimetric changes of ZnPc (**1e**) complex (5.00 x 10-5 M) in DMSO/TBAP solution medium, recorded by applying constant potential according to SCE.

For NiPc (**1d**) and ZnPc (**1e**) the first reduction occurs at a less negative potential value of the redox couple, while the earliest oxidation occurs at a lower positive potential value **(Table 1).** The main reason for this voltammetric difference is that complexes with electroactive metals such as CoPc **(1a)**, Fe(OAc)Pc **(1b)** and Mn(OAc)Pc **(1c)** have d orbital levels at the energy levels between the lowest energy empty molecular orbital (LUMO) and the highest energy filled molecular orbital (HOMO). Thus, complexes with such metal centers both easily accept and give electrons [39].

According to the data listed in **Table 1 and 2,** voltammetric responses of the redox inactive complexes NiPc **(1d)** and ZnPc**(1e)** in DMSO/TBAP electrolyte were quite equal to those in DCM/TBAP electrolyte. Based on **Table 1 and 2,** the redox processes

of ZnPc **(1e) has** occurred at slightly negative potentials than this of NiPc **(1d).** Because of the dissimilarities in the polarizing effects of metal centers, the variation between the half wave potentials of NiPc **(1d)** and ZnPc **(1e)** were observed. Varying from 1.40 to 1.72 V, $\Delta E_{1/2}$ data are basically consistent with the data reported in literature for NiPc **(1d)** and ZnPc **(1e)**. The MPc species which have redox inactive metal center, number one reduction of the Phthalocyanine ligand, metal(II)Phthalocyanine (-2) + electron$^-$ = [metal(II)Phthalocyanine (-3)] $^-$, associated with the place of the "Lowest Unoccupied Molecular Orbital" (LUMO), at the same time number one oxidation of the ligand metal(II)Phthalocyanine (-2) =[metal(II)Phthalocyanine (-1)] + electron$^-$ is involved with the place of the "Highest Occupied Molecular Orbital" (HOMO) [28,29]. So that, $\Delta E_{1/2}$ values of these compounds reflect their HOMO-LUMO gaps. In addition, these compounds display two / three reduction pairs along with one or two oxidation pairs which suggest each and every redox procedure are Pc ring based of these complexes [30-32]. ΔE_p values ranged from 60 to 90 mV, indicates that every electron transfer procedures are electrochemically reversible. The peak currents progress lineally with the square root of scan rates varying from 0.025 to 0.250 Vs^{-1} for these compounds has recommended absolutely diffusion controlled character of the procedures.

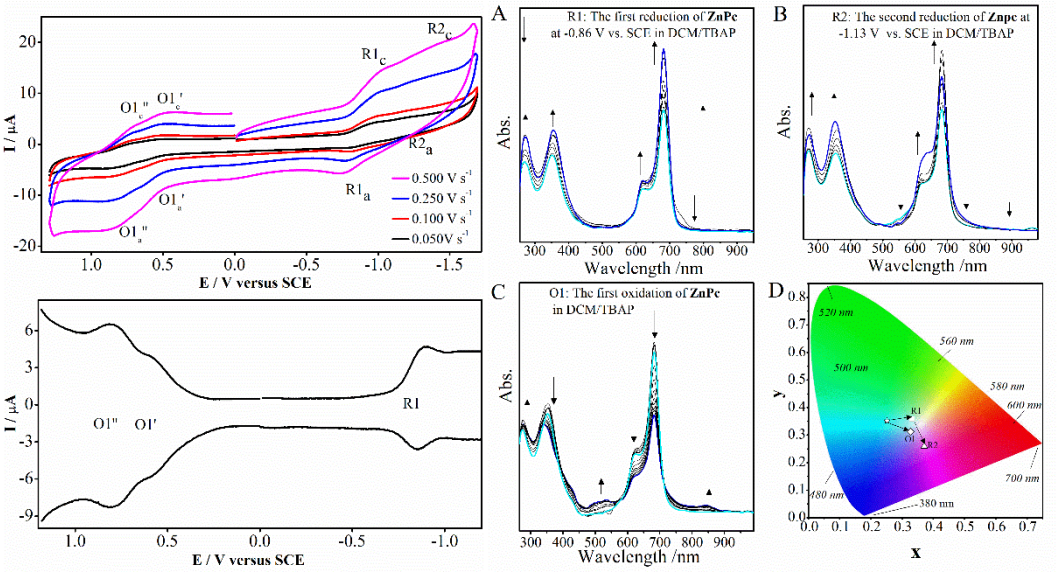

Figure 22 (**A**) CV and (**B**) SWV voltammograms of ZnPc (**1e**) complex (5.0x10-4 M) in DCM/TBAP solution medium. (**C**) In situ UV-Vis spectral and electro colorimetric changes of ZnPc (**1e**) complex (5.00 x 10-5 M) in DCM/TBAP solution medium, recorded by applying constant potential according to SCE.

Redox behaviors of NiPc **(1d)** and ZnPc **(1e)** were distinctly different in contrast with CoPc **(1a)**, Fe(OAc)Pc **(1b)** and Mn(OAc)Pc **(1c)**, because the previous group having redox inactive metal centers which exhibited only Phthalocyanine ring based one electron redox procedures, when the rest with redox active metal centers group showed both Phthalocyanine ring and metal based one electron redox procedures. Besides, if we compare the redox potentials in DMSO and DCM, we can notice that because of the electron donorproperty of DMSO, the peaks in the redox active metal centers group are found at much negative potentials in terms of those in the redox inactive metal centers group [51,52]. Therefore, for electing their area of application in electrochemical technologies, recognition of the character of all redox procedures is highly essential. From that perspective, electrochemical actions of CoPc **(1a)**, Fe(OAc)Pc **(1b)** and Mn(OAc)Pc **(1c)** complexes were performed in solution and the analysis results are listed in **Table 1** and **2**. The first oxidation and the first reduction processes of CoPc **(1a)**, Fe(OAc)Pc **(1b)** and Mn(OAc)Pc **(1c)** were observed to occur at significantly less positive and less negative potentials, respectively, as compared to those of NiPc **(1d)** and ZnPc **(1e)** (**Table 1**).The main reason of this dissimilarity in the voltammetric performance of the former group is MPcs such as CoPc **(1a)**, Mn(OAc)Pc **(1c)** and Fe(OAc)Pc **(1b)** which have a metal center having energy levels laying between the LUMO and HOMO of the Phthalocyanine ligand, mostly show both metal based and

ring based redox procedures. In case of polar solvents as for example DMSO and DMF, for a MPc together with a redox active metal center, the number one oxidation and reduction procedures are presumed to take place on the metal center, yet, the number one oxidation procedure takes place on the Phthalocyanine ring in nonpolar solvents as for example THF and DCM [55-58].

The redox behavior of these redox-active complexes [CoPc **(1a)**, Fe(OAc)Pc **(1b)** and Mn(OAc)Pc **(1c)**) is quite different from the redox-inactive complexes [NiPc (**1d**), ZnPc (**1e**)]. CoPc **(1a)**, Fe(OAc)Pc **(1b)** and Mn(OAc)Pc **(1c)** complexes show both ligand and metal-centered electron transfer processes due to the electro-active metal centers they have. Therefore, in order to decide on the use of such complexes in the field of electrochemical technologies, it is important to define their characteristic redox properties in detail. For CoPc **(1a)**, Fe(OAc)Pc **(1b)** and Mn(OAc)Pc **(1c)** complexes, the first reduction of the redox couple happens at lower negative potential value, while the 1st oxidation occurs atlower positive potential value **(Table 1 and 2).** The main reason for this voltammetric difference is that complexes with electroactive metals such as CoPc **(1a)**, Fe(OAc)Pc **(1b)** and Mn(OAc)Pc **(1c)** have d orbital levels at the energy levels between the lowest energy empty molecular orbital (LUMO) and the highest energy filled molecular orbital (HOMO). Thus, complexes with such metal centers both easily accept and give electrons.

When the effect of the solvent systems used for CoPc **(1a)** and Mn(OAc)Pc **(1c)** compounds on the electrochemical behavior was compared, when DMSO was used as the solvent system for Mn(OAc)Pc **(1c),** the shift in the half-wave potentials ($E_{1/2}$) obtained by CV was less. The redox potentials of MPcs are significantly affected by the occupation of the axial position by donor solvent molecules with coordination properties. While the oxidation state of the manganese center is 3+ valence, the cobalt metal center is 2+ valence. As a result of the decreasing oxidation number, the coordination number of its compounds also decreases [52]. Therefore, the OAc ion binds from the axial position of the Mn and Fe compounds, and for CoPc **(1a)** compound with coordination numbers 6 and 5, the donor DMSO solvent binds from the axial position. Simultaneous spectral measurements provide a clearer understanding of this situation.

3.3. Investigation of the electro catalytic performances for Oxygen reduction reaction (ORR) of Mono Substituted (1a-1e) complexes in acidic medium

In addition to the above-mentioned electrochemical and simultaneous UV-Vis spectroelectrochemical measurements, RDE and RRDE voltammetry with a double potentiostat system was also used. The catalytic experiments of the examined compounds in the ORR were examined by LSV. Catalytic measurements were carried out in acidic environment for PEMFC applications.

Electro catalytic activities of the CoPc **(1a)**, Fe(OAc)Pc **(1b)** and Mn(OAc)Pc **(1c)** NiPc **(1d)**, ZnPc **(1e)** complexes towards ORR were tested by the RDE technique at 2500 rotations per minute (rpm). The RDE polarization curves of VC/Nf/Pc, Fl/Nf/Pc, GO/Nf/Pc, G/Nf/Pc and Tm/Nf/Pc modified glassy carbon working electrodes were recorded in 0.5 M H_2SO_4 aqueous electrolyte solution with oxygen purging for 30 min. The potential scanning range was from 0.70 to -0.50 V vs. SCE with a scan rate of 0.005 Vs^{-1}. The onset potential (E_o) where the current begins to increase, and the limiting diffusion current density (J_L) can be taken as the measures of catalytic activity. The potential at which the current density reaches 0.100 mA cm^{-2} was taken as E_o. **Table 3** sums up the electro catalytic behavior of Pc-based catalysts.

Table 3 Electro catalytic activities of 1a-1e complexes for ORR according to the parameters of onset potential (E_o), diffusion current density (J_L) and half-wave potential ($E_{1/2}$) (according to SCE).

Complex	E_o [a] V (vs. SCE)	J_L / mA cm^{-2}	$E_{1/2}$ / V (vs. SCE)
Fe(OAc)Pc/Vc/Nf	0.39	3.75 (0.76)	0.06 (-0.25)
CoPc/Vc/Nf	0.40	1.34 (0.58)	0.23 (-0.06)
Mn(OAc)Pc/Vc/Nf	0.08	2.22	-0.11
NiPc/Vc/Nf	0.01	2.44	-0.20
ZnPc/Vc/Nf	0.03	1.51	-0.14
Fe(OAc)Pc/Fl/Nf	0.46	1.85 (3.19)	0.30 (-0.02)
CoPc/Fl/Nf	0.38	3.85 (0.71)	0.05 (-0.29)
Mn(OAc)Pc/Fl/Nf	0.30	1.94	0.10
NiPc/Fl/Nf	0.29	1.65	0.11
ZnPc/Fl/Nf	0.20	0.42	0.12
Fe(OAc)Pc/GO/Nf	0.45	3.66 (0,57)	0.05 (-0.27)
CoPc/GO/Nf	0.49	0.60 (1.44)	0.37 (-0.02)
Mn(OAc)Pc/GO/Nf	0.26	2.75	0.02
NiPc/GO/Nf	0.12	2.24	-0.06
ZnPc/GO/Nf	0.25	1.62	-0.07
Fe(OAc)Pc/G/Nf	0.44	3.74	-0.01
CoPc/G/Nf	0.58	1.00	-0.02
Mn(OAc)Pc/G/Nf	0.35	0.90	-0.06
BO-NiPc/G/Nf	-0.05	0.95	-0.20
BO-ZnPc/G/Nf	-0.13	0.75	-0.29
Fe(OAc)Pc/Tm/Nf	0.28	2.90 (0.74)	-0.05 (-0.30)
CoPc/Tm/Nf	0.33	0.54 (1.04)	0.19 (-0.14)
Mn(OAc)Pc/Tm/Nf	0.41	0.98	-0.11
NiPc/Tm/Nf	0.07	0.78	-0.17
ZnPc/Tm/Nf	-0.16	0.27	-0.18

[a] The potential at which the current density reaches to 0.100 mA cm^{-2} was taken as the onset potential, Eo.

These compounds are widely used as oxygen reduction reaction catalysts in fuel cells [70-75]. Fe/Fl/Nf, Fe/VC/Nf, Fe/GO/Nf, Fe/G/Nf and Fe/Tm/Nf with their redox active metal center, show better catalytic efficiency according to both their starting potential and limit current densities (**Table 3**). In particular, the measured parameters for the FePc/Fl/Nf-based catalyst indicate a remarkable catalytic activity for any mononuclear MPc complex. Considering the high 5.04 mA cm^{-2} limit diffusion current density of the Fe/Fl/Nf-based catalyst and its catalytic activity starting at positive potential (E_o value 0.46 V), it shows high ORR performance. Therefore, it appears to provide a mechanism for the reduction of ORR, which is desired for fuel cell applications, by a 4-electron mechanism, with H_2O as the prime product. On the other hand, the relatively lower

catalytic activities of NiPc **(1d)** and ZnPc **(1e)** compounds can be interpreted as the fact that their redox inactive metal centers do not undergo reduction and oxidation.

Because of the huge mesoporous distribution, excellent electrical characteristics and economic price, carbon blacks have widely utilized in the region of electrochemistry. Carbon blacks are commonly acquired by thermal decomposition of hydrocarbons originate from petroleum sources. As catalyst supports in electrochemical l experiments, various carbon blacks, for example Fl, acetylene black, Ketjen Black, Black Pearl or VC, GO, G and Tm have utilized extensively. On account of having sufficient surface area (> 250 m^2 g^{-1}) as well as great electric conductivity (> 2.77 Scm^{-1}), Fl has drawn attention out of all the carbon blacks. Generally, the applications of carbon pertain to interfacial interactions, wherein various reactants and ions come into contact with the carbon surface. Consequently, significant attention has been dedicated to investigating how the surface chemical characteristics of carbon and carbon blacks, influence the electrochemical action of energy conversion and storage appliances. As molecular allotropes of carbon, fullerenes demonstrate a multitude of fascinating phenomena that arise from their π-electron properties, which can be conveniently modified through chemical processes. The significant curvature of the conjugated π-electron systems present in these hollow spheres has enabled a diverse range of chemical interactions, leading to the synthesis of numerous derivatives. This characteristic renders the Fl family a highly versatile foundational element in materials that hold considerable significance in the fields of physics, chemistry, and biology.

The family of fullerenes embodies a unique molecular configuration of carbon, attracting considerable attention for its outstanding chemical and physical attributes. The molecule Buckminsterfullerene (C60), known for its remarkable stability, was first identified in 1985. C60 is the prototypical representative of the Fl family and may be classified as the third allotrope of carbon, succeeding graphite and diamond. Each Fl is characterized by an even number of carbon atoms that are distributed over the surface of a sealed, hollow cage. Each atom forms trigonal connections with three neighboring atoms, with three out of the four valence electrons participating in sp2 σ-bonding. The residual electrons are distributed across π-molecular orbitals that encompass both the external and internal surfaces of the molecule. The resulting π- electron density cloud is comparable to that which envelops graphite sheets. The σ framework outlines a

polyhedral network featuring 12 pentagons and m hexagons, where m can take any value including zero, except for one, in line with Euler's law. Furthermore, the development and characteristics of various curved carbon structures that exist as structural intermediates between the expansive flat graphitic sheets and the diminutive hollow fullerenes, including nanotubes and Bucky onions, have garnered significant attention.

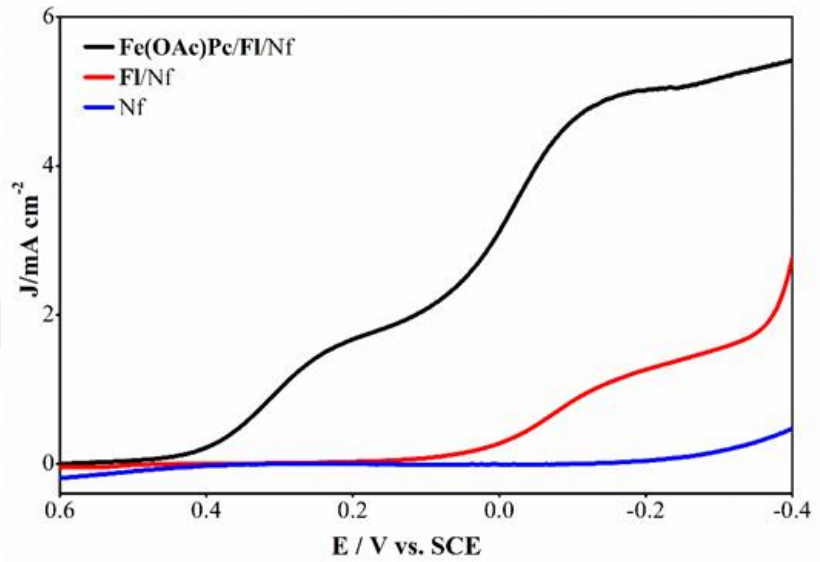

Figure 23 RDE curve for Fe(OAc)Pc (**1b**)/Fl/Nf modified electrodes in 0.5 M H_2SO_4 solution.

The presence of a clearly defined limiting current plateau, as demonstrated in **Figure 23**, is commonly observed. This is due to the homogeneous arrangement of electro catalytic sites on the electrode's surface. Conversely, when the active sites are not uniformly distributed on ink-type electrodes that possess a thin porous coating, the polarization curves can appear inclined or bell-shaped.

LSVs in 0.5 M H_2SO_4 aqueous solution saturated with oxygen gas at a rotation speed of 2500 rpm using the rotating disk voltammetry technique, are shown in **Figure 23**. When the ORR performances of glassy carbon electrodes modified only with Nf or Fl/Nf (**Figure 23**) are compared with the measurements made for (**1a-1e)** complexes, they show that Pc modified catalysts give better ORR performance according to both the starting potentials and limit current densities parameters. This is probably due to the fact that the MPcs in the catalyst mixture are uniformly distributedin the Fl. The Figure also clearly shows that the catalyst layer structure has a remarkable effect on catalytic

performance.

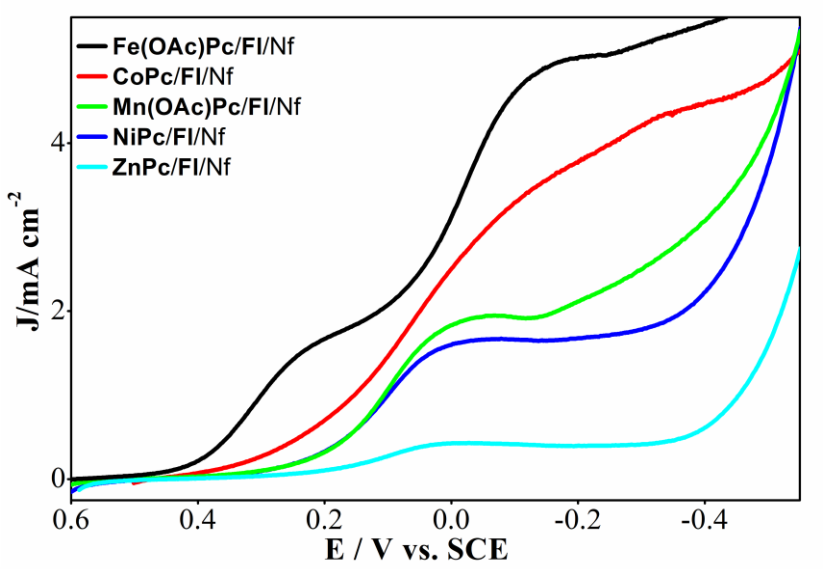

Figure 24 RDE polarization curves recorded with MPc/Fl/Nf (M= Fe, Co, Mn, Ni and Zn) modified glassy carbon electrodes in 0.5 M H_2SO_4 solution saturated with O_2 for electro catalytic ORR (Rotation speed: 2500 rpm).

The catalytic performances of Fe(OAc)Pc (**1b**), CoPc (**1a**) and Mn(OAc)Pc (**1c**) on GO/Nf/Pc, G/Nf/Pc and Tm/Nf/Pc modified rotating (2500 rpm) glassy carbon electrodes towards ORR are much better as compared to those of mononuclear NiPc (**1d**) and ZnPc(**1e**). The limit current densities for Fe(OAc)Pc (**1b**), CoPc (**1a**) and Mn(OAc)Pc (**1c**) are considerably high. On the contrary, NiPc (**1d**) and ZnPc (**1e**) have a very low limit current density. In addition, E_o values for Fe(OAc)Pc (**1b**), CoPc (**1a**) and Mn(OAc)Pc (**1c**) are more positive than those of NiPc (**1d**) and ZnPc (**1e**.

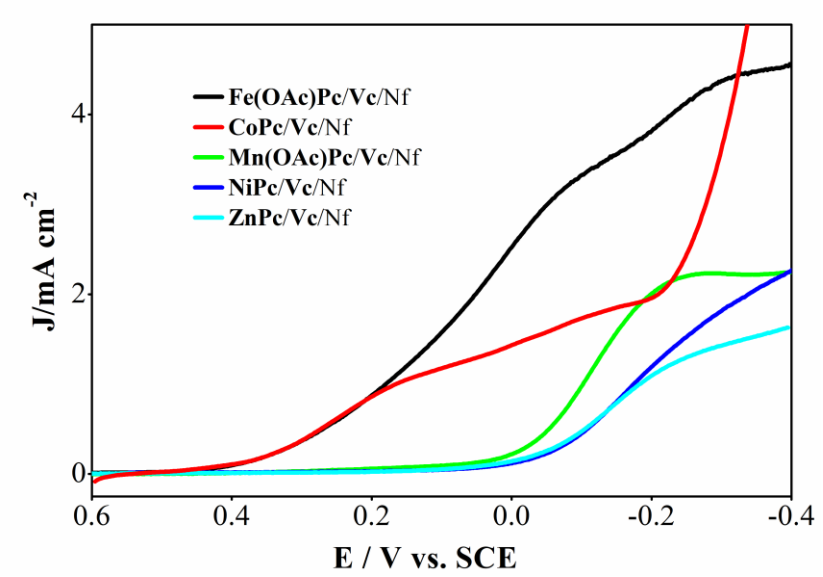

Figure 25 RDE curves for MPc/VC/Nf modified electrodes in 0.5 M H_2SO_4 solution

In **Figure 25**, it is clearly seen that catalytic performances of Fe(OAc)Pc (**1b**), Mn(OAc)Pc (**1c**) and CoPc (**1a**) on VC/Nf/Pc modified rotating (2500 rpm) glassy carbon electrodes towards ORR are much better as compared to those of mononuclear NiPc (**1d**) and ZnPc (**1e**). The limit current densities for Fe(OAc)Pc (**1b**), CoPc (**1a**) and Mn(OAc)Pc (**1c**) are considerably high. On the contrary, NiPc (**1d**) and ZnPc (**1e**) have a very low limit current density. In addition, E_o values for Fe(OAc)Pc (**1b**), CoPc (**1a**) and Mn(OAc)Pc (**1c**) are more positive than those of NiPc (**1d**) and ZnPc (**1e**).

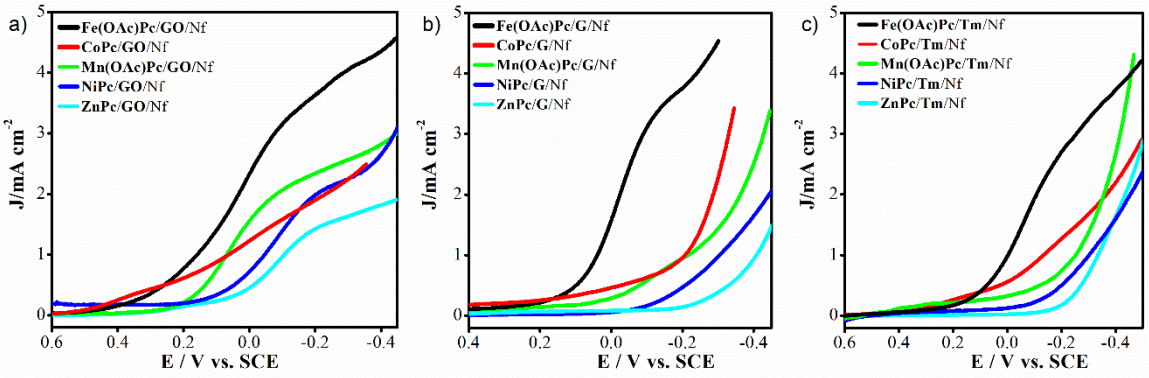

Figure 26 RDE polarization curves recorded with MPc/GO/Nf, MPc/G/Nf and MPc/Tm/Nf modified glassy carbon electrodes in 0.5 M H_2SO_4 solution saturated with O_2 for electro catalytic ORR (Rotation speed: 2500 rpm).

The electro catalytic reduction of oxygen on metallophthalocyanines occurs via a redox-catalysis mechanism, wherein the ability to bind oxygen and the redox potential of the

central metal ions are of paramount importance. During the adsorption of the oxygen molecule, the metal ion at the center of the phthalocyanine ring undergoes oxidation, thereby facilitating the reduction of oxygen. Conversely, the metal centers in NiPc (**1d**) and ZnPc (**1e**) are characterized as redox-inactive, indicating that they do not undergo oxidation or reduction during electro catalytic measurements, as evidenced by their established electrochemical behavior. Consequently, the superior catalytic performance of Fe(OAc)Pc (**1b**) and CoPc (**1a**), in comparison to other complexes, can be ascribed to the presence of a redox-active metal center and its unique ability to coordinate with the dioxygen molecule.

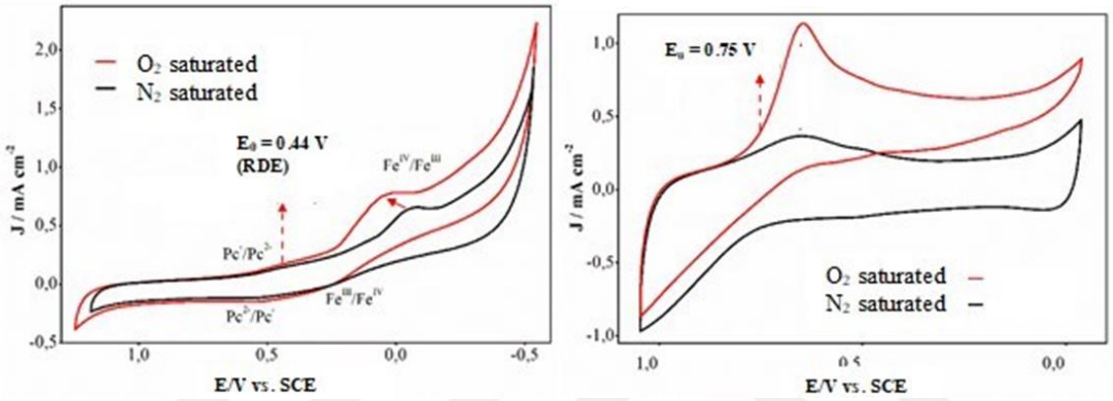

Figure 27 Cyclic voltammograms of the Pt/VC/Nf and Fe(OAc)Pc/Fl/Nf complex adsorbed on glassy carbon electrodes in 0.5 M H_2SO_4, purged with N_2 or saturated with O_2

The pertinent cyclic voltammograms for the Fe(OAc)Pc/Fl/Nf based catalysts are illustrated in **Figure 27**. Additionally, the onset potentials identified during the RDE tests are indicated on the voltammograms with arrows, facilitating the correlation between catalytic activity and redox potentials, as the ORR initiates at these onset potentials.

In line with expectations, the mononuclear complex Fe(OAc)Pc/Fl/Nf reveals a conventional redox couple, identified as a Fe^{III}/Fe^{IV} redox process. Fe(OAc)Pc/Fl/Nf catalyst containing mononuclear phthalocyanine complex in saturated N_2 medium showed first Fe^{III}/Fe^{IV} transition in the oxidation direction and then Pc^{2-}/Pc^{-} transition as second oxidation. Fe(OAc)Pc/Fl/Nf catalyst showed first Pc^{-}/Pc^{2-} reduction and then Fe^{IV}/Fe^{III} reduction in cathodic scanning. The half-peak potential of Fe^{III}/Fe^{IV} and Fe^{IV}/Fe^{III} redox processes was determined as $E_{1/2}$=0.08 V. In addition, the half-peak potential of Pc^{2-}/Pc^{-} and Pc^{-}/Pc^{2-} redox pairs were obtained with $E_{1/2}$=0.42 V. In the 0.5

M H_2SO_4 solution saturated with O_2, firstly Fe^{III}/Fe^{IV} transition and secondly Pc^{2-}/Pc^{-} transition were observed in the direction of oxidation similar to N_2 environment. While the half-peak potential of Fe^{III}/Fe^{IV} and Fe^{IV}/Fe^{III} redox couples is $E_{1/2}$=0.12 V in the solution medium saturated with O_2, the half-peak potential of Pc^{2-}/Pc^{-} and Pc^{-}/Pc^{2-} redox couples is $E_{1/2}$=0.45 V.

In our study, RRDE polarization curves of VC/Nf/Pc and Fl/Nf/Pc electrodes modified with different Pc compounds were made with a modified glassy carbon disk and platinum ring electrodes polarized at a constant potential of 0.95 V according to SCE. Here it is modified with Fe(OAc)Pc (**1b)**, which is thought to show the highest catalytic activity. The RRDE measurement obtained for the modified glassy carbon disc electrode is shown as an example (**Figure 28**). These polarization curves enable the determination of the contribution of hydrogen peroxide formation during ORR and the number of electrons transferred.

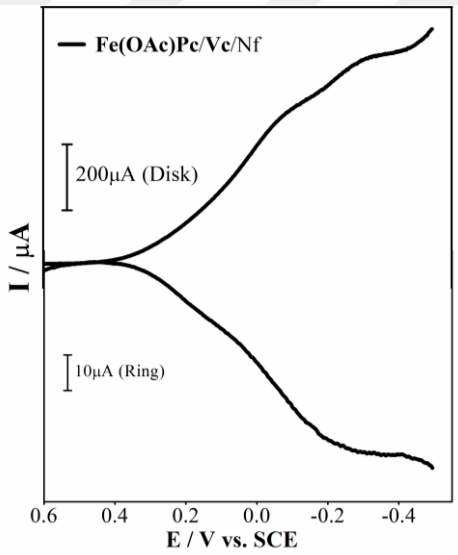

Figure 28 RRDE polarization curves recorded with Fe(OAc)Pc/Vc/Nf modified rotating (2500 rpm) glassy carbon disc in 0.5 M H_2SO_4 solution saturated with O_2 for electro catalytic ORR (potential scan rate: 0.005 V s^{-1}).

While ORR can be formed in a single step by 4-electron reduction to give water, it can also be reduced in two steps, where first the hydrogen peroxide intermediate product is formed and then water is formed by 2-electron transfer. In fuel cell applications, the optimal approach involves the generation of water via a four-electron process. Consequently, it is essential to ascertain the total number of electrons transferred, denoted as n_t, as well as the proportion of hydrogen peroxide, should it be produced.

The ring currents were assessed to determine the quantity of H_2O_2 produced by each catalyst. It was noted that the ring currents commenced at the same potentials as the onset potentials for the ORR observed in the disk, suggesting that H_2O_2 generation is occurring. The bell-shaped profile of the ring current is indicative of H_2O_2 formation on non-noble metal catalysts and activated carbon.

The ORR in an acidic environment can occur as either a four-electron process resulting in the formation of H_2O or as a two-electron reduction leading to the production of H_2O_2. It is preferable for the reaction to proceed to completion, yielding H_2O through a four-electron transfer mechanism. In instances of low catalytic activity, oxygen is reduced to H_2O_2 through a two-electron mechanism; however, this peroxide can subsequently undergo further reduction via an additional two-electron process to yield H_2O. Consequently, it is essential to ascertain the n_t value, which will allow for the assessment of hydrogen peroxide's contribution. To evaluate the role of hydrogen peroxide formation during the ORR on each catalyst, RRDE measurements were conducted using a glassy carbon disk electrode modified with VC/Nf/Pc and a platinum ring electrode set at 0.95 V versus SCE. An example of the RRDE measurement utilizing the Fe(OAc)Pc/VC/Nf modified glassy carbon disk electrode is illustrated in **Figure 29**.

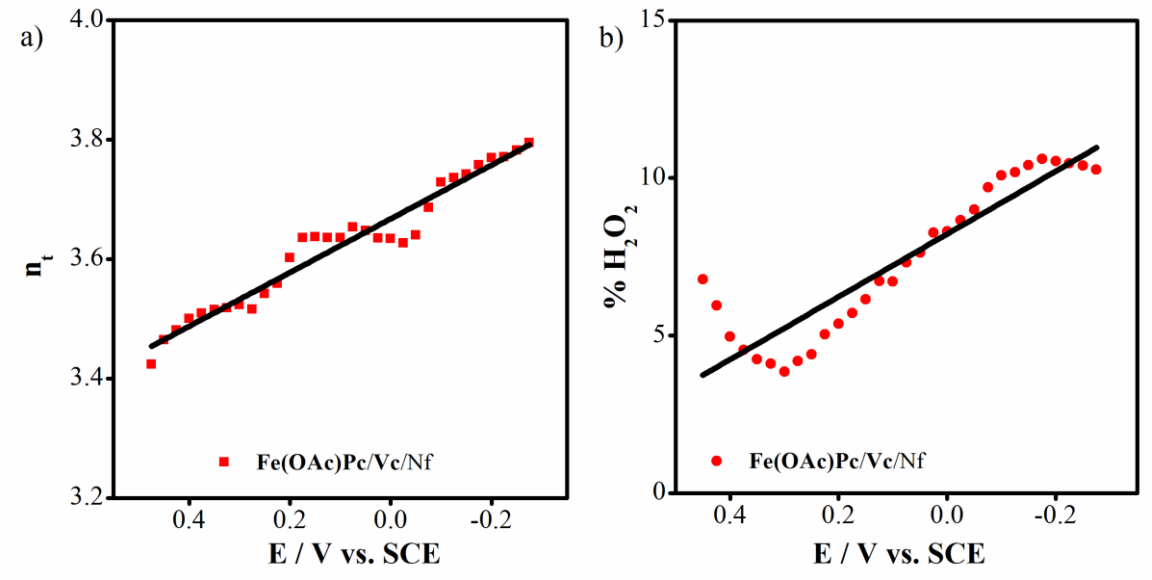

Figure 29 (A) Variation of the total number of electrons transferred with the disk potential for VC/Nf/Pc modified electrodes **(B)** Variation of the % H_2O_2 formedfor VC/Nf/Pc modified electrodes with the disk potential (according to Ering = 0.95V vs SCE)

The n_t and the percentage of hydrogen peroxide produced at a given potential were determined by the following equations:

$$n_t = 4\, I_D / [I_D + (I_R/N)] \quad (1)$$

$$\%H_2O_2 = 100\,(4 - n_t)/2 \quad (2)$$

where N, I_D, and I_R are the collection efficiency, disk current and ring current, respectively. **Figure 29A and 29B** show the number of electrons and $\%H_2O_2$ generated at different potentials for each catalyst, respectively. The total electron count, n_t, indicates that the ORR occurring on the Fe(OAc)Pc/VC/Nf based electrode generates a greater quantity of water in comparison to hydrogen peroxide. The n_t value rises with an increase in potential, reaching 3.80 comprising 89% H_2O and 11% H_2O_2) at the limiting diffusion current plateau, therebyestablishing water as the primary product.

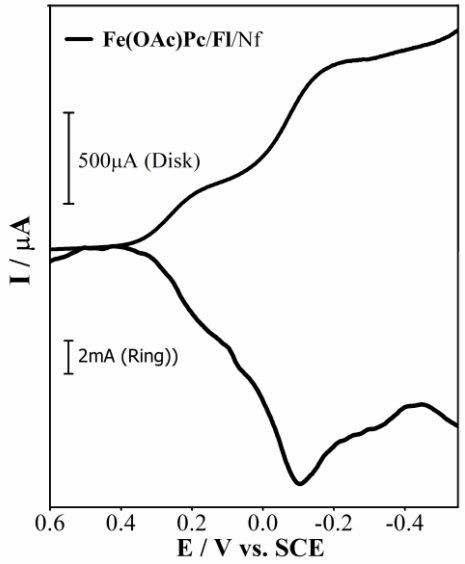

Figure 30 RRDE polarization curves recorded with Fe(OAc)Pc/Fl/Nf modified rotating (2500 rpm) glassy carbon disc in 0.5 M H_2SO_4 solution saturated with O_2 for electro catalytic ORR (potential scan rate: 0.005 V s^{-1}).

In accordance with calculation, the ORR for all catalysts proceeds through a four-electron pathway that produces only water, in addition to two separate two-electron pathway that first generate hydrogen peroxide, which is then convert into water. In contrast, Fe(OAc)Pc/Fl demonstrates enhanced electro catalytic efficiency relative to Fe(OAc)Pc/Vc, particularly in terms of current and potential measurements relevant to the ORR. It is particularly evident that the ORR facilitated by the Fe(OAc)Pc/Fl -based electrode generates a substantially greater quantity of water in contrast to that of hydrogen peroxide. Regarding Fe(OAc)Pc/Fl, an increase in voltage corresponds to a rise in the n_t value, reaching 3.85 (90% H_2O and 10% H_2O_2) at the limiting diffusion current plateau, thereby indicating that water being the predominant product. **Figure 31A and 31B** clearly demonstrates the rise in the ring current at potentials ranging from 0.30 and −0.25 V versus SCE.

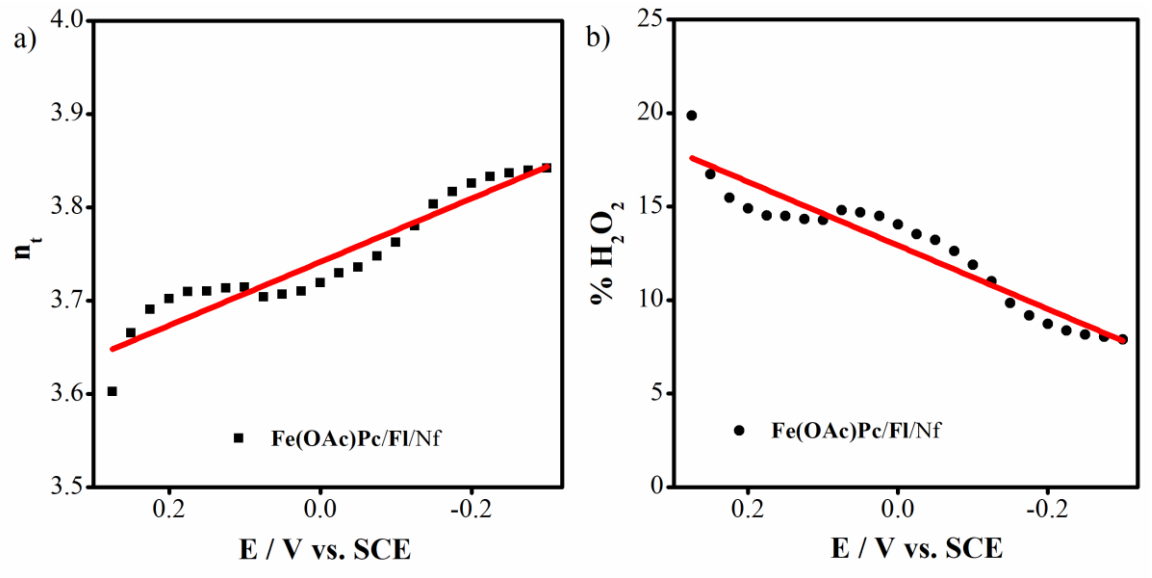

Figure 31 (A) Variation of the total number of electrons transferred with the disk potential for Fl/Nf/Pc modified electrodes **(B)** Variation of the % H_2O_2 formed for Fl/Nf/Pc modified electrodes with the disk potential (according to Ering = 0.95 V vsSCE)

Figures 31A and 31B illustrate the quantity of electrons and the percentage of H_2O_2 produced at various potentials for each catalyst. The total number of electrons, denoted as n_t, indicates that the ORR occurring on the Fe(OAc)Pc/Fl/Nf based electrode yields a greater volume of water in comparison to hydrogen peroxide. As the potential increases, the n_t value rises, reaching 3.85 (with 93% attributed to H_2O and 7% to H_2O_2) at the limiting diffusion current plateau, thereby establishing water as the predominant product.

In a direct methanol fuel cell (DMFC), the diffusion of methanol from the anode to the cathode can negatively affect the fuel cell's performance, especially when the cathode is composed of platinum. Nevertheless, metal N4 chelates have been identified as selective catalysts that exhibit a notable tolerance to methanol in the context of the ORR.

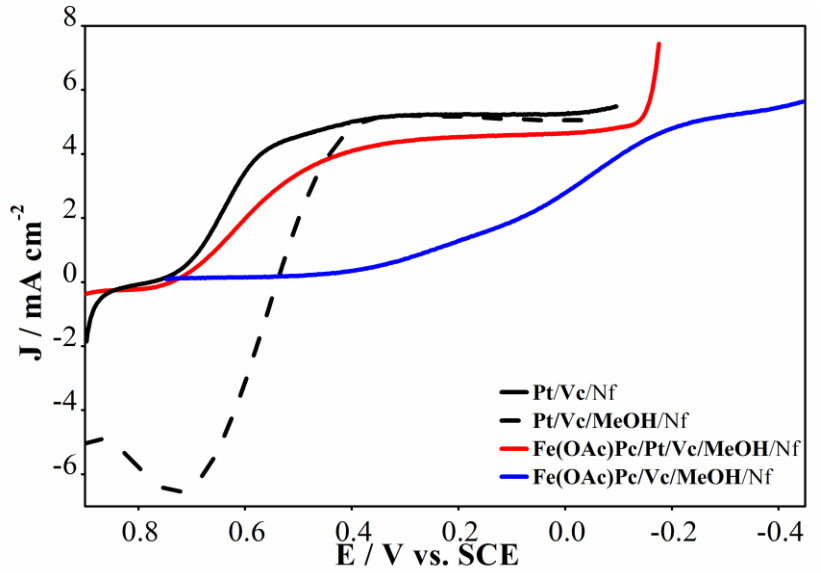

Figure 32 RDE polarization curves recorded with Pt/Vc/Nf, Fe(OAc)Pc/Vc/Nf and Fe(OAc)Pc/Pt/Vc/Nf modified glassy carbon electrodes in 0.5 M H_2SO_4 solution saturated with O_2 for electro catalytic ORR in the presence and absence ofmethanol (Rotation speed: 2500 rpm).

Methanol tolerance of Fe(OAc)Pc/Vc/Nf based catalyst was also determined and compared with that of Pt-based one. **Figure 32** shows the polarization curves obtainedin O_2 saturated electrolyte in the presence and absence of methanol for the Pt, Fe(OAc)Pc/Vc/Nf and Pt/Fe(OAc)Pc/Vc/Nf based catalysts. At an electrode composed of Fe(OAc)Pc/Vc/Nf, the polarization curve for the ORR remains unchanged despite the inclusion of 1.0 M methanol in the electrolyte. In contrast, at a platinum-based electrode, the introduction of 1.0 M methanol in theelectrolyte results in a shift of the oxygen reduction potentials to more negative values. A notable methanol oxidation current is detected across a broad spectrum of potential, resulting in the complete inhibition of the catalytic activity of the Pt-based catalyst for the ORR within the potential range of 0.50–0.80 V versus SCE. While the methanol tolerance exhibited by the Fe(OAc)Pc/Vc/Nf-based catalyst surpasses that of the Pt-based catalyst, it is regrettable that the ORR on the Fe(OAc)Pc/Vc/Nf-based catalyst still takes place at more negative potentials in the presence of methanol when compared to the Pt-based catalyst. Furthermore, a significant quantity of hydrogen peroxide (H_2O_2) is generated, even though the Fe(OAc)Pc/Vc/Nf modified electrode primarily facilitates the ORR through a four-electron mechanism in regions of high over potential. So, the methanol tolerance of Pt/ Fe(OAc)Pc/Vc/Nf -based dual catalyst during ORR was also determined

and compared with that of Pt-based one. As shown in **Figure 32**, in the presence of methanol, electro catalytic activity of the Fe(OAc)Pc/Pt/Vc/Nf -based dual catalyst is much better than that of the Pt-based one at all potentials. The findings of our research demonstrated that the straightforward incorporation of an appropriate Fe(OAc)Pc into Nf and carbon-supported platinum significantly improves the methanol tolerance of platinum for the ORR, indicating a promising and economical alternative for DMFC applications.

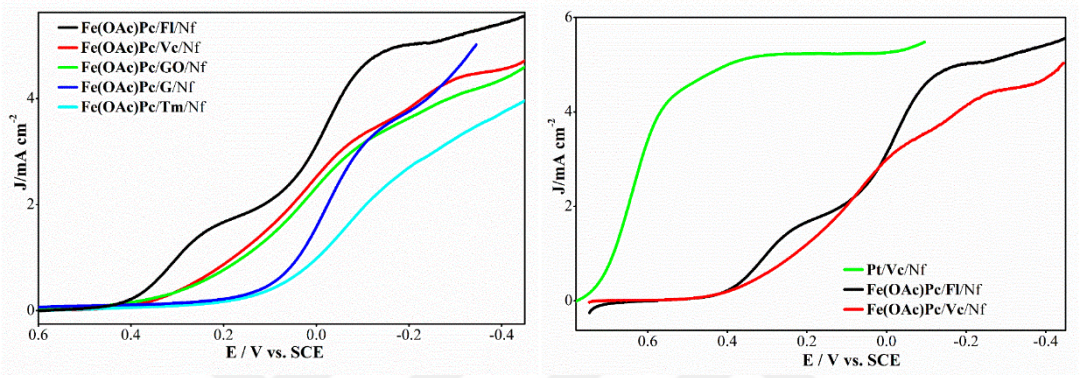

Figure 33 (A) RDE polarization curves recorded with Fe(OAc)Pc/Vc/Nf, Fe(OAc)Pc/Fl/Nf, Fe(OAc)Pc/GO/Nf, Fe(OAc)Pc/G/Nf and Fe(OAc)Pc/Tm/Nf modified glassy carbon electrodes in 0.5 M H_2SO_4 solution saturated with O_2 for electro catalytic ORR (Rotation speed: 2500 rpm). **(B)** RDE polarization curves recorded with Pt/Vc/Nf, Fe(OAc)Pc/Vc/Nf ve Fe(OAc)Pc/Fl/Nf modified glassy carbon electrodes in 0.5 M H_2SO_4 solution saturated with O_2 for electro catalytic ORR (Rotation speed: 2500 rpm).

Amongst Pc compounds used in this study, Fe(OAc)Pc/Fl/Nf and Fe(OAc)Pc/Vc/Nf showed remarkable catalytic activity towards ORR in acidic medium. The distinctive catalytic performance of Fe(OAc)Pc/Fl/Nf and Fe(OAc)Pc/Vc/Nf are attributed to the redox-active behavior of the metal center. It appears that, in the case of a redox-active metal center, the interaction between the metal center and O_2 molecule is enhanced **Table 4** summarizes the electro catalytic performance of Fe(OAc)Pc (**1b**) based catalystsfor ORR.

Table 4 Electro catalytic activities of Fe(OAc)Pc **(1b)** complexes for ORR according to the parameters of onset potential (E_o), diffusion current density (J_L) and half-wave potential ($E_{1/2}$) (according to SCE).

Catalysts	E_o[a] V (vs. SCE)	J_L / mA cm^{-2}	$E_{1/2}$ / V (vs. SCE)
Fe(OAc)Pc/Fl/Nf	0.44	1.85 (3.19)	0.30 (-0.02)
Fe(OAc)Pc/Vc/Nf	0.39	3.75 (0.76)	0.06 (-0.25)
Fe(OAc)Pc/GO/Nf	0.45	3.66 (0.57)	0.05 (-0.27)
Fe(OAc)Pc/G/Nf	0.44	3.74	-0.01
Fe(OAc)Pc/Tm/Nf	0.28	2.90 (0.74)	-0.05 (-0.30)

[a] The potential at which the current density reaches to 0.100 mA cm^{-2} was taken as the onset potential .

3.4. Investigation of the electro catalytic performances for Oxygen reduction reaction (ORR) of Mono Substituted (1a-1e) compounds in alkali medium

The electro catalytic activities of the complexes in the context of oxygen electro catalysis were evaluated utilizing CV, RDE, and RRDE voltammetry techniques within an air half-cell containing a 0.1 M KOH solution. The CV and RDE measurements were conducted with a Gamry Reference 600 potentiostat/galvanostat, while a Pine Instrument Company AFMSRCE modulator speed rotator was utilized for the RDE experiments. The electrolyte solution for the electro catalytic measurements was prepared using ultra- pure water and potassium hydroxide. A GCE and a polishing kit for this electrode were acquired from Pine Instruments for the RDE measurements. These measurements were conducted with a glassy carbon diskof 5 mm in diameter in an oxygen-saturated 0.1 M KOH aqueous solution under quasi- stationary conditions, utilizing a sweep rate of 5 mV/s at a temperature of 25°C. The counter electrode employed was a platinum spiral, while the reference electrode used was a SCE. High-purity N_2 and O_2 were employed to deoxygenate the solution and to saturate it with oxygen, respectively, for a minimum duration of 30 minutes before each experimental run. In the course of the RRDE measurements, a bipotentiostat, which consists of two Gamry Reference 600 potentiostat/galvanostats, was utilized to regulate the potentials of both the disk and the ring. The working electrode comprised a glassy carbon disk with a diameter of 5 mm and a platinum ring electrode with a composition of 37% platinum. RRDE experiments were conducted at a rotation speed of 2500 rpm in an O_2-saturated 0.1 M KOHsolution. The catalyst preparation utilized high-purity chemicals,

including Commercial 40% Pt/C from Sigma-Aldrich, VC XC-72 from Cabot Co., Fl, GO, G, Tm, a 10% Nafion-PFTE solution from Aldrich, KOH pellets from Merck, tetrahydrofuran from Sigma-Aldrich, ethanol from Merck, and ultra-pure water. The catalyst ink, comprising 40% by weight of catalyst active material, VC XC-72, Fl, GO, G, Tm (50% by weight), along with a Nafion/PTFE solution (10% by weight), was subjected to sonication in THF for thirty minutes to achieve homogenization. A specified volume of this ink was then applied to a freshly polished GCE using a micropipette, resulting in a catalyst loading of 106 μg cm^{-2}. Similarly, a mixture containing 10% by weight of Nafion and 90% by weight of commercial Pt/C (a 40% Pt-VC XC-72 blend) was suspended in ethanol and sonicated for thirty minutes to prepare the platinum-based catalyst, which was subsequently coated onto the GCE following the same procedure.

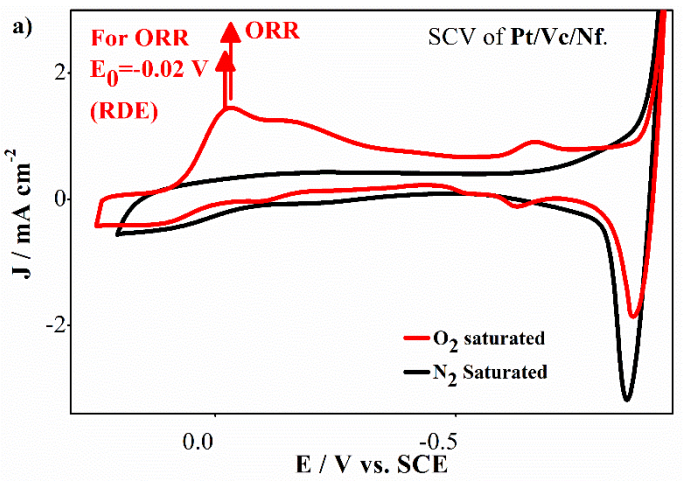

Figure 34 Cyclic voltammograms of the Pt/VC complex adsorbed on glassy carbon electrodes in 0.1 M KOH, purged with N_2 or saturated with O_2 (scan rate 5 mVs^{-1})

The electro catalytic activities of the Pt/C and Fe(OAc)Pc complex for the ORR were initially assessed using CV. The cyclic voltammograms for electrodes modified with Pt/C and Fe(OAc)Pc (**1b**) **(Figure 34 and 35)** were obtained in 0.1 M KOH solutions saturated with either N_2 or O_2, employing a scan rate of 5 mV/s. The peak currents associated with the ORR in the voltammograms indicate that the Fe(OAc)Pc(**1b**) complex effectively interacts with molecular oxygen, attributed to the redox-active nature of the Fe^{2+} core. Additionally, a comparison of the voltammograms for the Fe(OAc)Pc (**1b**) complex in N_2- and O_2-saturated environments distinctly demonstrates

that the oxidation of the Fe(OAc)Pc (**1b**) complex at approximately -0.20 V is reversible and coincides with the signal of the O_2 molecule. When the Fe(III)/Fe(IV) redox transition takes place at low positive potentials, the highly acidic Fe(IV) species interact favorably with dioxygen, resulting in a relatively low over potential for the ORR.

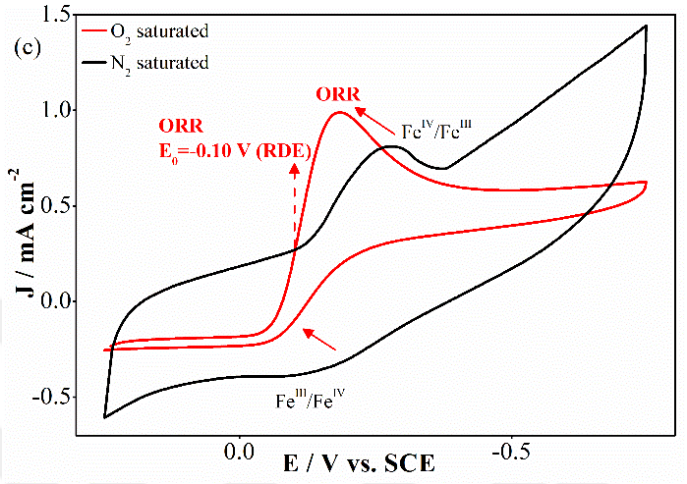

Figure 35 Cyclic voltammograms of the Fe(OAc)Pc/Fl/Nf complex adsorbed on glassy carbon electrodes in 0.1 M KOH, purged with N_2 or saturated with O_2 (scan rate 5 mVs^{-1})

The electro catalytic performance of the catalyst materials for the ORR was examined using the RDE technique, as illustrated in **Figure 36.** The polarization curves for the ORR of each catalyst were obtained at a rotation speed of 2500 rpm, with a scan rate of 5 mV/s in oxygen-saturated 0.1 M KOH solutions. The E_o, defined as the point at which the current begins to rise, along with the J_L, were utilized as indicators of catalytic activity. The potential corresponding to a current density of 0.100 mA cm^{-2} was designated as E_o. **Table 5** presents a summary of the electro catalytic performance of MPc-based catalysts for the ORR. The findings distinctly demonstrate that the catalytic activity of the Fe(OAc)Pc (**1b**), CoPc (**1a**), and Mn(OAc)Pc (**1c**) complexes significantly surpasses that of NiPc (**1d**) and ZnPc (**1e**)

Table 5 Electro catalytic activities of (**1a-1e)** complexes for ORR according to the parameters of onset potential (E_o), diffusion current density (J_L) and half-wave potential ($E_{1/2}$) (according to SCE).

Catalysts	E_o V (for ORR/V)	J_L / mA cm^{-2}	$E_{1/2}$ / V (vs SCE)
Fe(OAc)Pc/Vc/Nf	-0.09	5.77	-0.25
CoPc/Vc/Nf	-0.10	2.34	-0.24
Mn(OAc)Pc/Vc/Nf	-0.10	4.82	-0.38
NiPc/Vc/Nf	-0.20	2.00	-0.35
ZnPc/Vc/Nf	-0.22	1.35	-0.39
Fe(OAc)Pc/Fl/Nf	-0.10	5.84	-0.23
CoPc/Fl/Nf	-0.13	5.38	-0.26
Mn(OAc)Pc/Fl/Nf	-0.12	6.63	-0.33
NiPc/Fl/Nf	-0.19	2.69	-0.40
Fe(OAc)Pc/GO/Nf	-0.11	3.80	-0.25
CoPc/GO/Nf	0.05	2.49	-0.23
Mn(OAc)Pc/GO/Nf	-0.14	3.18	-0.33
NiPc/GO/Nf	-0.15	2.92	-0.33
ZnPc/GO/Nf	-0.17	2.26	-0.31
Fe(OAc)Pc/G/Nf	-0.13	2.31	-0.30
CoPc/G/Nf	-0.08	0.70	-0.23
Mn(OAc)Pc/G/Nf	-0.11	1.31	-0.37
NiPc/G/Nf	-0.25	0.95	-0.35
ZnPc/G/Nf	-0.16	0.74	-0.35
Fe(OAc)Pc/Tm/Nf	-0.18	5.00	-0.31
CoPc/Tm/Nf	0.02	2.61	-0.32
Mn(OAc)Pc/Tm/Nf	-0.12	2.90	-0.34
NiPc/Tm/Nf	-0.26	2.51	-0.42
ZnPc/Tm/Nf	-0.21	1.74	-0.34

In order to evaluate the ORR activity, RDE tests of carbon samples in O_2 saturated and 0.1 M KOH electrolyte, under a rotation rate of 2500 rpm were performed at scan rate of 5 mV s^{-1}.

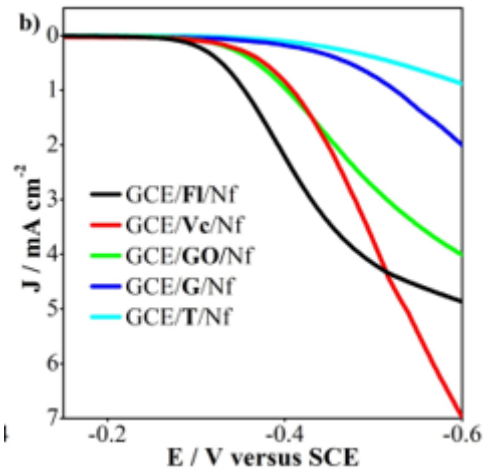

Figure 36 RDE polarization curves recorded with Vc/Nf, Fl/Nf, GO/Nf, G/Nf and Tm/Nf modified glassy carbon electrodes in 0.1 M KOH solution saturated with $O_2$for electro catalytic ORR (Rotation speed: 2500 rpm

By comparison, the redox active and redox inactive metals had also been tested under the same test conditions, as shown **Figure 37** Obviously, the ORR activities of the Fe(OAc)Pc/Vc/Nf, CoPc/Vc/Nf and Mn(OAc)Pc/Vc/Nf are much higher than those of NiPc/Vc/Nf and ZnPc/Vc/Nf in the whole process of cathodic oxygen reduction, the ORR values of current densities for Fe(OAc)Pc/Vc/Nf, CoPc/Vc/Nf and Mn(OAc)Pc/Vc/Nf at the all potentials are larger than those NiPc/Vc/Nf and ZnPc/Vc/Nf. The J_L (5.77 mA cm^{-2}) of the Fe(OAc)Pc/Vc/Nf is larger than those of CoPc/Vc/Nf (2.34 mA cm^{-2}), NiPc/Vc/Nf (2.00 mA cm^{-2}) and ZnPc/Vc/Nf (1,02 mA cm^{-2}). Moreover, the E_0 and $E_{1/2}$ of the Fe(OAc)Pc/Vc/Nf complex are -0.09 V and 0.25 V, respectively. These values of the Fe(OAc)Pc/Vc/Nf complex is nearly equal to those of Pt/C catalyst (E_0 = -0.02V and $E_{1/2}$ = -0.17 V, respectively).

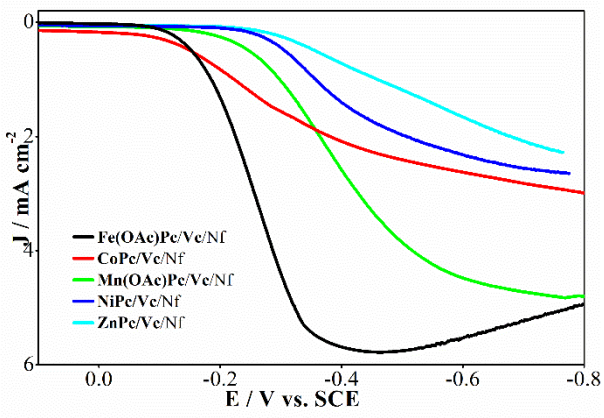

Figure 37 RDE polarization curves recorded with Fe(OAc)Pc/Vc/Nf, CoPc/Vc/Nf, Mn(OAc)Pc/Vc/Nf, NiPc/Vc/Nf and ZnPc/Vc/Nf modified glassy carbon electrodes in 0.1 M KOH solution saturated with O_2 for electro catalytic ORR (Rotation speed: 2500 rpm).

ORR activity of these Fe(OAc)Pc/Fl/Nf, CoPc/Fl/Nf, Mn(OAc)Pc/Fl/Nf and NiPc/Fl/Nf were evaluated in 0.1 M KOH aqueous solution. The half-wave potential ($E_{1/2}$) of Fe(OAc)Pc/Fl/Nf positively shifts 20 mV compared to that of NiPc/Fl/Nf and the current density of Fe(OAc)Pc/Fl/Nf at 5.84 V (vs. SCE) is much higher than that of NiPc/Fl/Nf (**Figure 38** and **Table 5**). **Figure 38** shows that Fe(OAc)Pc/Fl/Nf possesses an onset potential of -0.10 V (vs. SCE), superior to that of NiPc/Fl/Nf (-0.19 V vs. SCE).

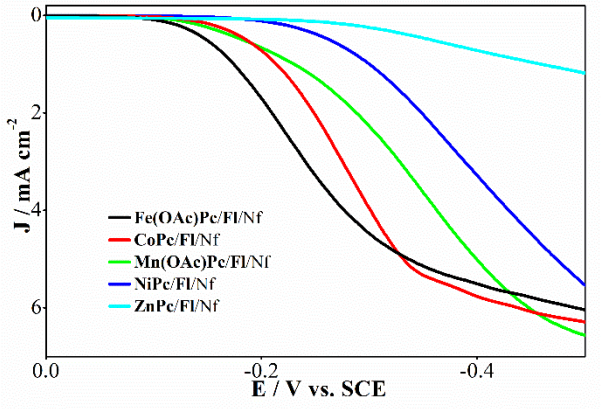

Figure 38 RDE polarization curves recorded with Fe(OAc)Pc/Fl/Nf , CoPc/Fl/Nf, Mn(OAc)Pc/Fl/Nf and NiPc/Fl/Nf modified glassy carbon electrodes in 0.1 M KOHsolution saturated with O_2 for electro catalytic ORR (Rotation speed: 2500 rpm).

By comparison, the redox active and redox inactive metals had also been tested under the same test conditions, as shown **Figure 39** Obviously, the ORR activities of the

Fe(OAc)Pc/GO/Nf , Fe(OAc)Pc/G/Nf and Fe(OAc)Pc/Tm/Nf are much higher than those of NiPc/GO/Nf, ZnPc/GO/Nf, NiPc/G/Nf, ZnPc/G/Nf and NiPc/Tm/Nf, ZnPc/Tm/Nf in the whole process of cathodic oxygen reduction, the ORR values of current densities for Fe(OAc)Pc/GO/Nf , CoPc/GO/Nf and Mn(OAc)Pc/GO/Nf at the all potentials are larger than those NiPc/GO/Nf and ZnPc/GO/Nf. The J_L (3.80 mA cm^{-2}) of the Fe(OAc)Pc/GO/Nf is larger than those of CoPc/GO/Nf (2.49 mA cm^{-2}), NiPc/GO/Nf (2.92 mA cm^{-2}) and ZnPc/GO/Nf (2.26 mA cm^{-2}). Moreover, the E_0 and $E_{1/2}$ of the Fe(OAc)Pc/GO/Nf complex are -0.11 V and -0.25 V, respectively. These values of the Fe(OAc)Pc/GO/Nf complex are nearly equal to those of Fe(OAc)Pc/G/Nf catalyst (E_0 = -0.13V and $E_{1/2}$ = -0.30 V, respectively).

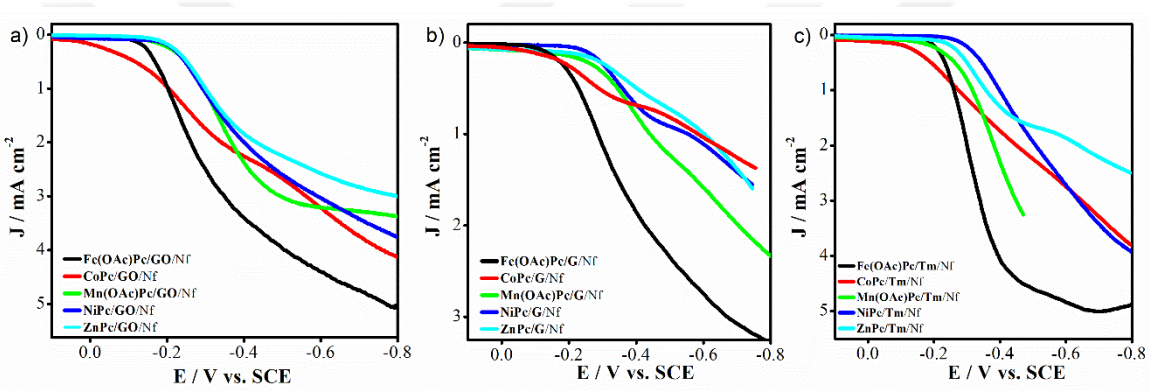

Figure 39 RDE polarization curves recorded with **(a)** M/GO/Nf **(b)** M/G/Nf **(c)** M/Tm/Nf (M= Fe(OAc), Co, Mn(OAc), Ni, Zn) modified glassy carbon electrodes in 0.1 M KOH solution saturated with O_2 for electro catalytic ORR (Rotation speed: 2500 rpm).

Table 6 Electro catalytic activities of Fe(OAc)Pc **(1b)** complexes for ORR according to the parameters of onset potential (E_o), diffusion current density (J_L) and half-wave potential ($E_{1/2}$) (according to SCE).

Catalysts	E_o V (For ORR/V)	J_L / mA cm^{-2}	$E_{1/2}$ / V (vs SCE)
Fe(OAc)Pc/Fl/Nf	-0.10	5.84	-0.23
Fe(OAc)Pc/Vc/Nf	-0.09	5.77	-0.25
Fe(OAc)Pc/GO/Nf	-0.11	3.80	-0.25
Fe(OAc)Pc/G/Nf	-0.13	2.31	-0.30
Fe(OAc)Pc/Tm/Nf	-0.18	5.00	-0.31

To further examine the ORR electro catalytic activity of the catalysts, RDE curves of Fe(OAc)Pc/Vc/Nf, Fe(OAc)Pc/Fl/Nf, Fe(OAc)Pc/GO/Nf, Fe(OAc)Pc/G/Nf and Fe(OAc)Pc/Tm/Nf catalysts were performed as presented in **Figure 40**. The onset and half-wave potentials for Fe(OAc)Pc/Fl/Nf (-0.10 V and -0.23 V) were close to that for Fe(OAc)Pc/Vc/Nf (-0.09 V and -0.25 V), and more positive than that for Fe(OAc)Pc/GO/Nf, Fe(OAc)Pc/G/Nf and Fe(OAc)Pc/Tm/Nf indicating that Fe(OAc)Pc/Fl/Nf possesses a highly efficient ORR electro catalytic activity. Fullerene stands differing from sp^2-conjugated graphene and carbon nanotubes and has great electronic structure with smaller HOMO–LUMO gaps, the ability of modification of the material's surface, high conductivity and appropriate wettability. Because of the distinctive features of Fl, that are increasingly being identified and applied by the electro catalysis researchers. It also has the advantageous electron affinity that facilitates the modifying the electronic structure in other substances along with the ability for on-demand chemical alterations and the capability for intermolecular self-assembly into micro and Nano structures. Together with all of these, the precise atomic and molecular structures have provided Fl with unique advantages as bi-functional catalyst, which are not available in other carbon based materials [32]

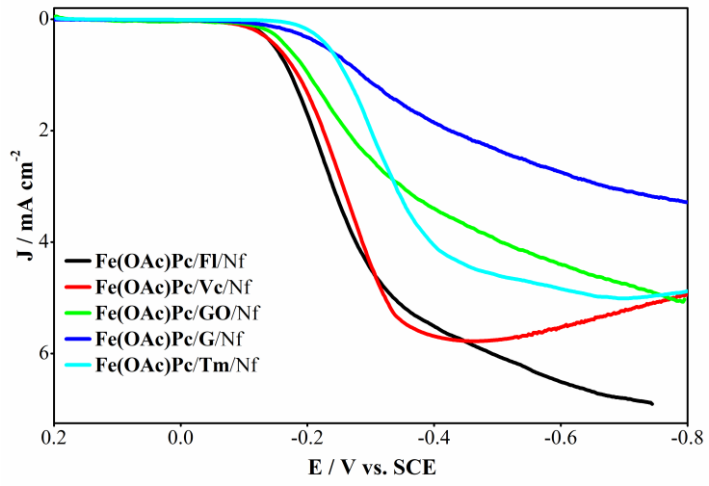

Figure 40 RDE polarization curves recorded with Fe(OAc)Pc/VC/Nf,Fe(OAc)Pc/Fl/Nf, Fe(OAc)Pc/GO/Nf, Fe(OAc)Pc/G/Nf and Fe(OAc)Pc/Tm/Nf modified glassy carbon electrodes in 0.1 M KOH solution saturated with O_2 for electro catalytic ORR (Rotation speed: 2500 rpm).

Table 7 Electro catalytic activities of Pt/Vc and Fe(OAc)Pc **(1b)** complexes for ORR according to the parameters of onset potential (E_o), diffusion current density (J_L) and half-wave potential ($E_{1/2}$) (according to SCE).

Catalysts	E_oV (For ORR/V)	J_L / mA cm^{-2}	$E_{1/2}$ / V (vs SCE)
Pt/Vc/Nf	-0.02	5.94	-0.17
Fe(OAc)Pc/Vc/Nf	-0.09	5.77	-0.25
Fe(OAc)Pc/Fl/Nf	-0.10	5.84	-0.20

To further examine the ORR electro catalytic activity of the catalysts, RDE curves of Fe(OAc)Pc/Fl/Nf, Fe(OAc)Pc/VC/Nf and Pt/C/Nf catalysts were performed as presented in **Figure 41**. The onset and half-wave potentials for Fe(OAc)Pc/Fl/Nf (-0.10 V and -0.20 V) were close to that for benchmark Pt/C (-0.02 V and -0.17 V), and more positive than that for Fe(OAc)Pc/Vc/Nf, indicating that Fe(OAc)Pc/Fl/Nf possesses a highly efficient ORR electro catalytic activity.

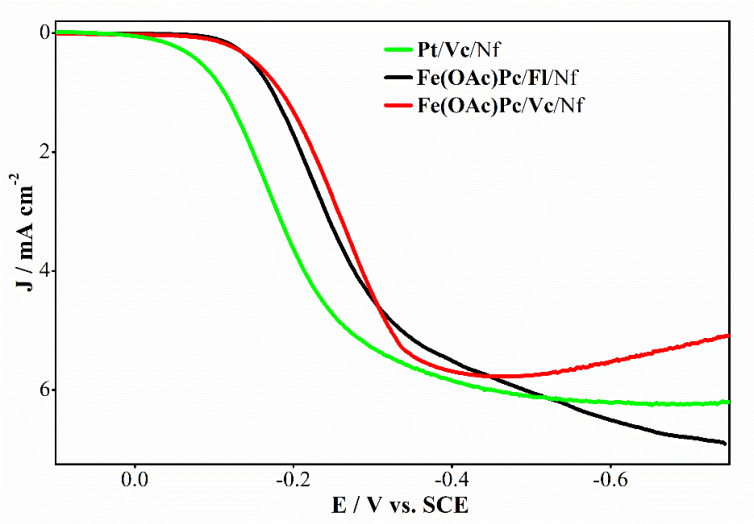

Figure 41 RDE polarization curves recorded with Pt/Vc/Nf, Fe(OAc)Pc/VC/Nf and Fe(OAc)Pc/Fl/Nf modified glassy carbon electrodes in 0.1 M KOH solution saturated with O_2 for electro catalytic ORR (Rotation speed: 2500 rpm).

In conclusion, novel ORR catalyst of fuel cell cathode, the Fe(OAc)Pc/Fl/Nf has demonstrated prominent ORR activity, high durability, small electrochemical impedance and good tolerance to fuel molecule in 0.1 M KOH. Thus, the Fe(OAc)Pc/Fl/Nf complex is a promising candidate to solve the problems of sluggish ORR kinetics, high cost of precious metal catalysts and low durability of traditional catalysts for fuel cells and metal-air batteries

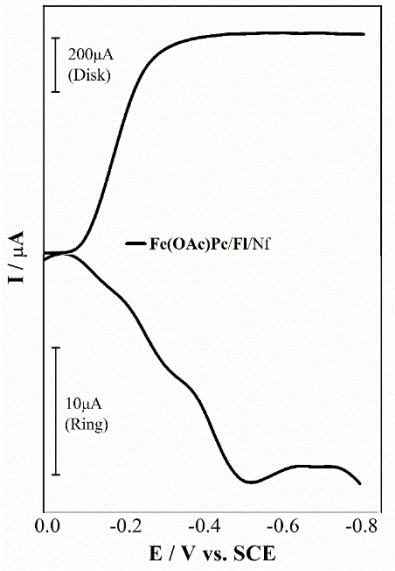

Figure 42 RRDE polarization curves recorded with Fe(OAc)Pc/Fl/Nf modified rotating (2500 rpm) glassy carbon disc in 0.1 M KOH solution saturated with O_2 for electro catalytic ORR (potential scan rate: 0.005 V s^{-1}).

Figure 42 shows the RRDE polarizations of the Fe(OAc)Pc/Fl based catalysts. The RRDE measurements confirm the notably high catalytic efficiency of the Fe(OAc)Pc/Fl-based catalyst. While a relatively lower ring current serves as an important indicator for a high n_t value, it does not serve as a definitive assurance. According to Equation 1.25, the n_t value is a parameter that relies on both the ring and disk currents, as well as the collection efficiency. Utilizing the results from the RRDE experiments, the total number of electrons transferred, n_t, along with the percentage of the produced species, OH^- and HO_2^- ions, were determined through Equations 1.25 and 1.26.

$$n_t = 4\, I_D / [I_D + (I_R/N)] \qquad \textbf{1.25}$$

$$\%HO_2^- = [2\,(I_R/N)] / [I_D + (I_R/N)] \qquad \textbf{1.26}$$

where N, I_D, and I_R are the collection efficiency, disk current and ring current, respectively.

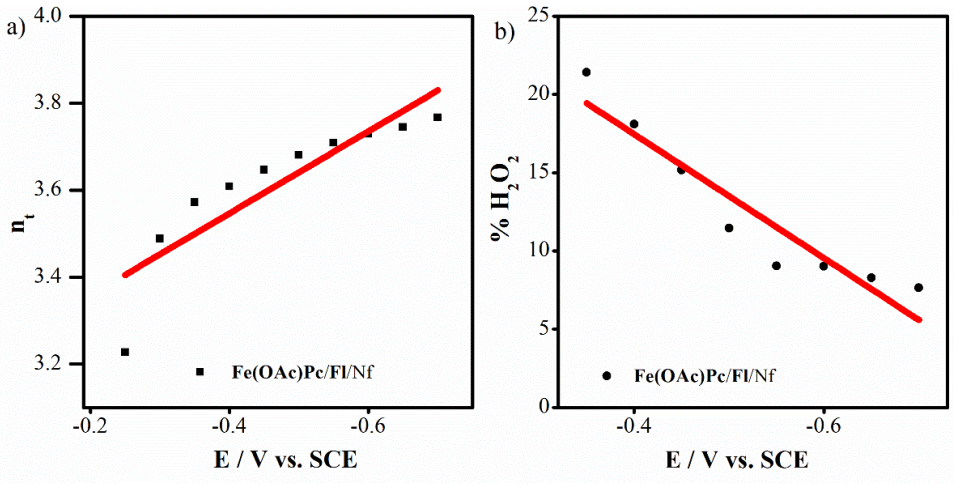

Figure 43 (A) Variation of the total number of electrons transferred with the disk potential for Fe(OAc)Pc/Fl modified electrodes **(B)** Variation of the % H_2O_2 formed for Fe(OAc)Pc/Fl modified electrodes with the disk potential (according to Ering = 0.5 V vs SCE)

The n_t values and the rates of hydrogen peroxide, along with the resulting hydroxide ions, are depicted in **Figures 43A and 43B** as a function of the applied potential. It is observed that the n_t values increase from 3.50 to 3.78 when the potential shifts from 0.00 V to -0.60 V for the catalysts based on Fe(OAc)Pc/Fl. At the same time, the ratio of HO_2^- and OH^- ions produced shifts from 20% to 5.0% and from 80% to 95%, respectively. These results imply that, akin to the Fe(OAc)Pc/Fl catalyzed ORR, the reaction primarily proceeds through a single-step mechanism involving a direct four-electron transfer, yielding only OH^- ions. Additionally, a two-step mechanism characterized by 2 + 2 electron transfers occur simultaneously, initially generating HO_2^- intermediates, which are then converted to OH^- ions. The degree of this process varies across different catalytic sites, depending on the voltage applied. On specific surfaces, the series and the direct four-electron pathways may function simultaneously. The decline in the proportion of HO_2^- ions as over potential increases may be linked to the enhanced catalytic reduction of HO_2^- (formed during the first step of the series pathway) to OH^- ions at higher over potentials. The formation of the peroxide ion does indeed weaken it, leading to the establishment of an O–O single bond. The bond must be broken to facilitate further reduction to hydroxide ions. At the limiting diffusion current plateau of -0.60 V, the n_t value is determined to be 3.8, comprising 94% OH^- and 6% HO_2^- for the Fe(OAc)Pc/Fl catalyzed ORR, which predominantly produces hydroxide ions. Additionally, the Koutecky-Levich analysis shows that the calculated number of

electrons is 3.96 at a potential of -0.40 V. It is significant to note that the values obtained from the Koutecky-Levich analysis are somewhat higher than those measured using the RRDE technique. A minor variation may arise from various factors, including the mass or thickness and the surface roughness of the electrode. Nevertheless, the elevated n_T values observed from both RDE and RRDE measurements distinctly demonstrate that Fe(OAc)Pc/Fl effectively catalyzes the ORR by generating a substantial quantity of OH^- ions while producing a minimal amount of HO2- ions at an exceptionally high rate. In the case of the Fe(OAc)Pc/Fl catalyzed ORR, the production percentages of OH- and HO_2^- ions are recorded at 89% and 11%, respectively, at a potential of 0.40 V. This indicates that the Fe(OAc)Pc/Fl catalyst effectively suppresses the generation of the HO_2^- intermediate, leading the electro catalytic ORR to predominantly proceed via the direct four-electron pathway.

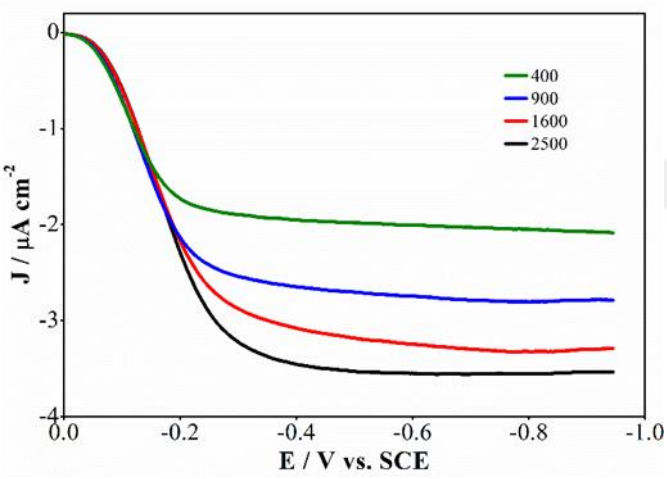

Figure 44 RDE voltammograms recorded with Fe(OAc)Pc/Fl/Nf modified glassy carbon electrodes in 0.1 M KOH solution for electro catalytic ORR at various rotation speeds.

The electrons that transferred in the ORR were referred as n and it was calculated from the Koutecky Levich (K-L) equations which is,

$$1/j = 1/jk + 1/jL = 1/(Bw1/2) + 1/jk \qquad \textbf{1.27}$$

$$B = 0.2nFC_o(D_o)^{3/2} v^{-1/6} \qquad \textbf{1.28}$$

Here, j (mA/cm^2) = Measured current density,

jK (mA/cm^2) = Kinetic current density,

jL (mA/cm^2) = Diffusion-controlled current density,

v = Angular velocity of the rotating disk

and w = 2πN, N = Linear rotating speed (rpm),

n = Total number of transferred electrons in ORR,

F = Faraday constant,

C_0 = Bulk concentration of O_2,

D_0 = Diffusion coefficient of O_2,

v = Kinematic viscosity of the electrolyte. In this analysis, the electrode process for the ORR is regarded as first-order concerning the reactant. This hypothesis was corroborated by the linear trend observed between 1/J and 1/w1/2 at various potentials. K-L plots were created using the corresponding RDE data at the potentials of -0.35 V, -0.45 V, -0.55 V, -0.65 V, -0.75 V, and -0.85 V (**Figure 45**). The n values for these potentials were found to be 3.79, 3.67, and 3.96, respectively, as calculated from the K-L slope, 1/B, of each linear graph. In a basic aqueous medium, the ORR may occur through a direct four-electron mechanism that exclusively produces OH^-, or through two consecutive two-electron mechanisms that first generate a hydro peroxide intermediate (HO^{2-}) before yielding hydroxide ions. To better understand the mechanism that leads to the formation of OH^- ions, RRDE measurements were performed, as it is inadequate to rely solely on RDE measurements. The RRDE voltammograms were recorded at a scan rate of 5 mVs^{-1} and a rotation speed of 2500 rpm in a 0.1 M KOH aqueous electrolyte saturated with oxygen. Throughout the measurements, the potential of the glassy carbon disk was varied from +0.20 V to -0.60 V, while the ring potential was held constant at +0.50 V versus the SCE.

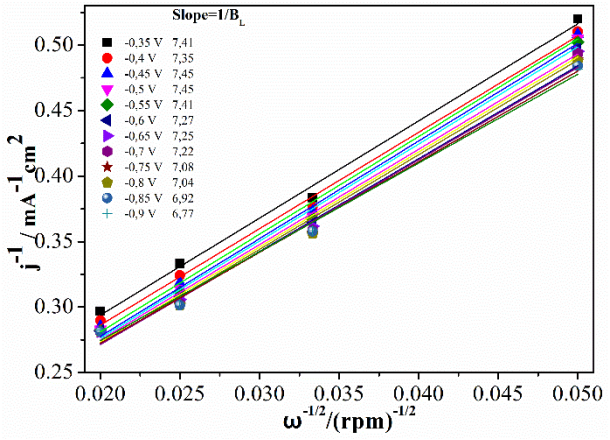

Figure 45 Koutecky-Levich plot of Fe(OAc)Pc/Fl **(1b)** catalyst for the various potentials.

In **Figure 45**, the closeness of the regression curves indicates that the studied potential range has reached the limit diffusion current density. It is seen that the limit current decreases as it approaches zero from E=-0.35 V and it is no longer possible to accurately determine the total number of electrons transferred using Koutecky-Levich curves. Because the limit current value is variable. As a result of this, as the value of E=-0.35 V approaches zero, the total number of electrons transferred at the determined potentials changes at a high rate with the potential changes. B=0.03552277 ≈ 0.0355 mA calculated as cm-2 $(rpm)^{-1/2}$. Thus, using equation 3, the total number of electrons transferred could be calculated for each potential value.

Table 8 Parameters obtained using the Koutecky-Levich plot of the Fe(OAc)Pc/Fl/Nf catalyst for ORR in KOH medium.

Potentials (E/V)	J_K^{-1}	J_K mA cm^{-2}	$(n_t.B)^{-1}$	$(n_t.B)$	n_T
-0.35	0.14	6.87	7.41	0.13	3.79
-0.40	0.13	7.18	7.35	0.13	3.82
-0.45	0.13	7.58	7.45	0.13	3.77
-0.50	0.12	7.77	7.45	0.13	3.77
-0.55	0.12	7.80	7.41	0.13	3.80
-0.60	0.12	7.73	7.27	0.13	3.86
-0.65	0.12	7.79	7.25	0.13	3.88
-0.70	0.12	7.85	7.22	0.13	3.89
-0.75	0.12	7.69	7.08	0.14	3.97
-0.80	0.13	7.66	7.04	0.14	3.99
-0.85	0.13	7.45	6.92	0.14	4.06
-0.90	0.13	7.20	6.77	0.14	4.15

$B=0.03552277 \approx 0.0355$ mA cm^{-2} $(rpm)^{-1/2}$

The mathematical expression of B_L ($B_L=B.n_T$) taken as the Levich constant, expressed as $1/B_L$, corresponds to the slopes of the Koutecky-Levich curves shown in Figure 46. Taking B= 0.0355 mA as cm^{-2} $(rpm)^{-1/2}$, the total number of electrons transferred was calculated for each potential value and shown in **Table 8**. The dependence of the Levich constant B_L on the potential for each potential value shows that the total number of electrons transferred and the active surface area vary with the potential (**Figure 46**).This variation may be due to errors in the repeatability of the polarization curves due to the adsorption of oxygen in different modes or possible errors in measuring the volume of the catalyst ink or determining the electrode area. Therefore, since the ratio of ring and disk currents does not depend on the surface area of the catalyst layer or the amountof catalyst on the electrode, the RRDE technique was used to determine the totalnumber of electrons transferred accurately or with little error.

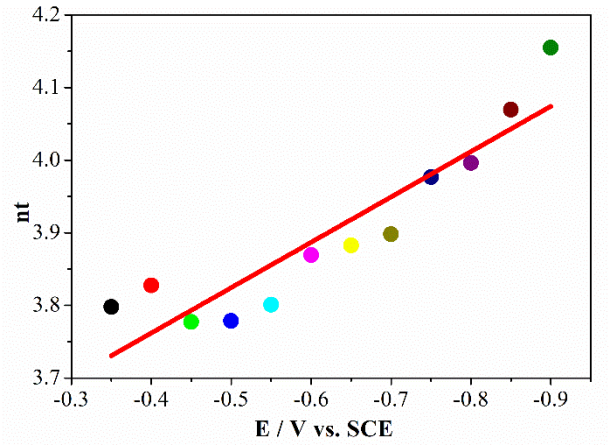

Figure 46 Total number of transferred electrons (n_T) calculated by the Koutecky-Levich plot for the Fe(OAc)/Fl/Nf modified electrode in 0.1 M KOH solution saturated with O_2 for electro catalytic ORR.

The slopes obtained from the Koutecky-Levich curves in the Koutecky-Levich graph in **Figure 45** and the total number of electrons transferred are calculated for each potential value and are shown in **Table 8** and **Figure 45**. In addition, when the total number of electrons transferred during the reaction obtained by the rotating disk ring electrode voltammogram for the Fe(OAc)Pc/Fl/Nf modified electrode and the Koutecky-Levich analysis were compared, the total number of transferred electrons calculated by both methods was compared to each other, was found to be close (**Figure 43**, **Table 8** and **Figure 45**). Due to the fact that the total number of electrons transferred is close to four, it was concluded that the oxygen reduction reaction in the 0.1 M KOH solution saturated with O_2 mostly occurs via a single-step four-electron mechanism. Fe(OAc)Pc/Fl/Nf catalyst attracts attention due to its high electro catalytic effect.

3.5. Investigation of the electro catalytic performances for Oxygen evolution reaction (OER) of Mono Substituted (1a-1e) compounds in alkali medium

OER as a counter reaction plays a key role for the water electrolysis, organic synthesis and metal electro winning. The OER is a complex multistep reaction, which requires a considerably large over potential to the actual process that distinctly reduces the process efficiency. Noble metallic oxides such as IrO_2 have attracted intensive attention due to their high electro catalytic activity for OER. However, their application is limited by low service life in aggressive aqueous solutions and high cost. An ongoing aim of electro catalytic research is to increase the electro catalytic activity and stability while reducing the cost.

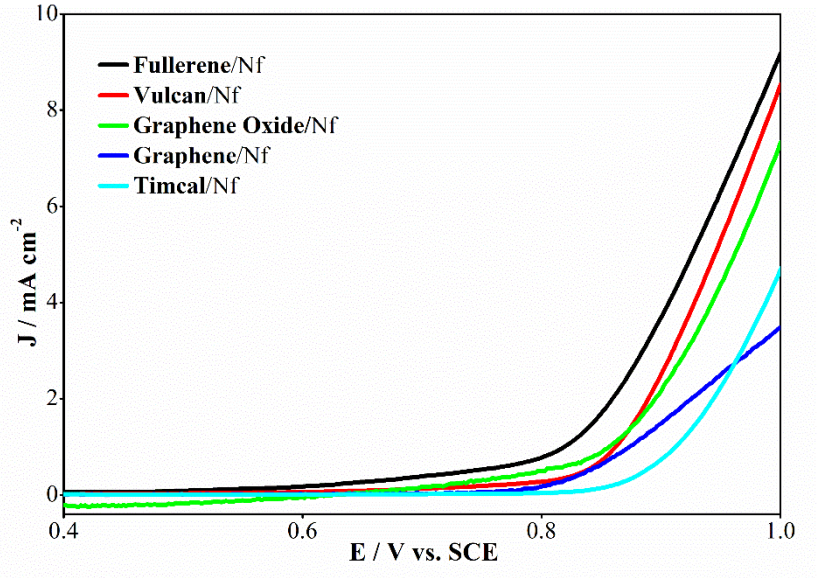

Figure 47 RDE voltammograms of carbons modified electrodes in 0.1 M KOH solution

In order to evaluate the OER activity, RDE tests of carbon samples in O_2 saturated and 0.1 M KOH electrolyte, under a rotation rate of 2500 rpm were performed at scan rateof 5 mV s^{-1}.

Table 9 Electro catalytic OER performances of catalyst materials.

Catalysts	E_o V (For OER/V)	J / mA cm^{-2}
Fe(OAc)Pc/Vc/Nf	0.26	1.33
CoPc/Vc/Nf	0.53	0.71
Mn(OAc)Pc/Vc/Nf	0.42	0.56
NiPc/Vc/Nf	0.54	0.55
ZnPc/Vc/Nf	0.55	0.22
Fe(OAc)Pc/Fl/Nf	0.25	5.84
CoPc/Fl/Nf	0.27	3.19
Mn(OAc)Pc/Fl/Nf	0.40	3.16
ZnPc/Fl/Nf	0.62	0.44

By comparison, the redox active and redox inactive metals had also been tested under the same test conditions, as shown **Figure 48**. Obviously, the OER activities of the Fe(OAc)Pc/Vc/Nf, CoPc/Vc/Nf and Mn(OAc)Pc/Vc/Nf are much higher than those of NiPc/Vc/Nf and ZnPc/Vc/Nf in the whole process of cathodic oxygen reduction, the OER values of current densities for Fe(OAc)Pc/Vc/Nf, CoPc/Vc/Nf and Mn(OAc)Pc/Vc/Nf at the all potentials are larger than those NiPc/Vc/Nf and ZnPc/Vc/Nf. The J_L (1.33 mA cm^{-2}) of the Fe(OAc)Pc/Vc/Nf is larger than those of CoPc/Vc/Nf (0.71 mA cm^{-2}), NiPc/Vc/Nf (0.55 mA cm^{-2}) and ZnPc/Vc/Nf (0.22 mA cm^{-2}). Moreover, the E_0 of the Fe(OAc)Pc/Vc/Nf complex is 0.26 V.

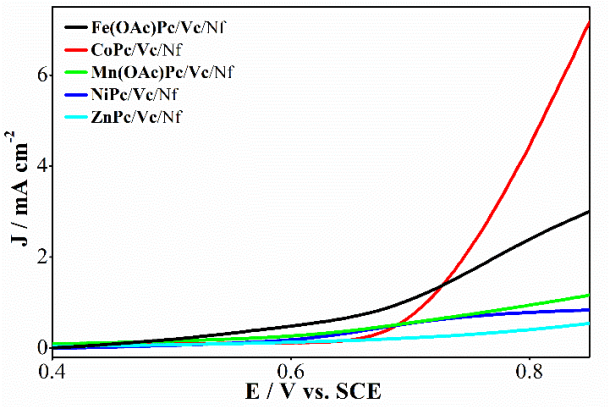

Figure 48 RDE voltammograms recorded with MPc/Vc/Nf (M= Fe,Co,Mn,Ni andZn) modified glassy carbon electrodes in 0.1 M KOH solution for electro catalytic OER (Rotation speed: 2500 rpm).

OER activity of these Fe(OAc)Pc/Fl/Nf, CoPc/Fl/Nf, Mn(OAc)Pc/Fl/Nf and ZnPc/Fl/Nf were evaluated in 0.1 M KOH aqueous solution. E_0 of Fe(OAc)Pc/Fl/Nf positively shifts 40 V compared to that of NiPc/Fl/Nf and the E_0 of Fe(OAc)Pc/Fl/Nf

at 0.25 V (vs. SCE) is much higher than that of ZnPc/Fl/Nf (**Figure 49** and **Table 9**).

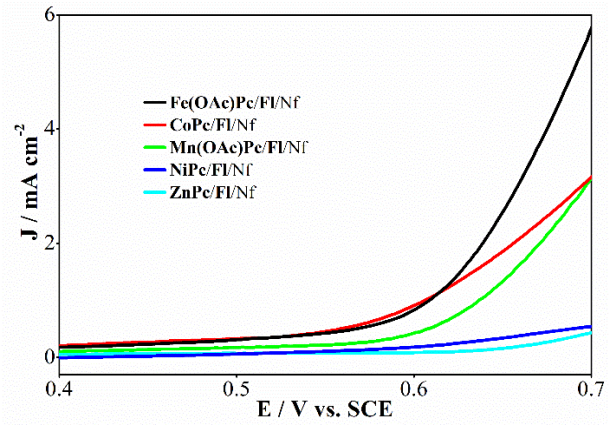

Figure 49 RDE voltammograms recorded with MPcs [M=Fe , Co, Mn, Ni and Zn] modified glassy carbon electrodes in 0.1 M KOH solution for electro catalytic OER (Rotation speed: 2500 rpm).

Table 10 Electro catalytic OER performances of catalyst materials.

Catalysts	**E_o V** (vs SCE)	**J / mA cm^{-2}** (vs SCE)
Fe(OAc)Pc/Fl/Nf	0.25	5.84
Fe(OAc)Pc/Vc/Nf	0.26	1.33
Fe(OAc)Pc/GO/Nf	0.27	1.36
Fe(OAc)Pc/G/Nf	0.39	0.80
Fe(OAc)Pc/Tm/Nf	0.37	0.59

To further examine the OER electro catalytic activity of the catalysts, RDE curves of Fe(OAc)Pc/Vc/Nf, Fe(OAc)Pc/Fl/Nf, Fe(OAc)Pc/GO/Nf, Fe(OAc)Pc/G/Nf and Fe(OAc)Pc/Tm/Nf catalysts were performed as presented in **Figure 50**. The onset potentials for Fe(OAc)Pc/Vc/Nf (0.26 V) was close to that for Fe(OAc)Pc/Fl/Nf (0.25 V), and more positive than that for Fe(OAc)Pc/GO/Nf, Fe(OAc)Pc/G/Nf AND Fe(OAc)Pc/Tm/Nf indicating that Fe(OAc)Pc/Vc/Nf possesses a highly efficient OER electro catalytic activity.

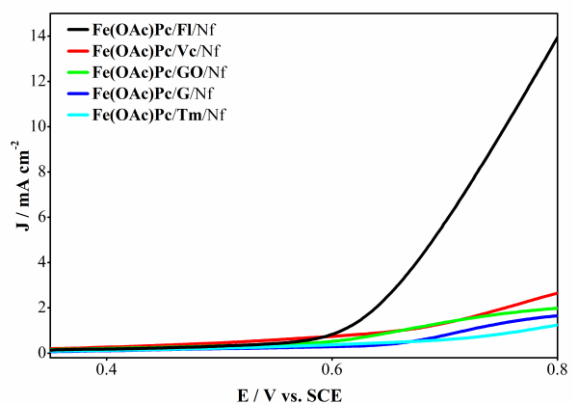

Figure 50 RDE voltammograms recorded with Fe(OAc)Pc/VC/Nf, Fe(OAc)Pc/Fl/Nf, Fe(OAc)Pc/GO/Nf, Fe(OAc)Pc/G/Nf and Fe(OAc)Pc/Tm/Nf modified glassy carbon electrodes in 0.1 M KOH solution for electro catalytic OER (Rotation speed: 2500 rpm).

In **Figure 51**, RDE' recorded in O_2 saturated 0.1M KOH solution for electro catalytic OER of IrO_2/Nf, Pt/Vc/Nf, Fe(OAc)Pc/Fl/Nf and Fe(OAc)/Vc/Nf catalysts. When J_L values of the catalysts at E=0.70 V are compared, Fe(OAc)/Vc/Nf J_L=1.33 mA cm^{-2} catalyst IrO_2/Nf - J_L=10.35 mA cm^{-2}, Pt/Vc/Nf - J_L=6.05 mA cm^{-2}. It is seen in **Figure 51** that it has lower current density than J_L=6.05 mA cm^{-2} and Fe(OAc)Pc/F1/Nf- J_L=5.84 mA cm^{-2} catalysts. When the electro catalytic activity results obtained with the catalysts used in the oxygen oxidation reaction, which takes place in the 0.1M KOH solution saturated with O_2 in an environment similar to the operating conditions of the zinc air battery, are compared, the electro catalytic performance close to the IrO_2/Nf catalyst, which is seen as the best catalyst in the literature, is Fe(OAc)Pc/Fl. This catalyst appears to be usable in zinc air battery systems. The current density of the Fe(OAc)Pc/Fl/Nf catalyst at E=0.70 V is close to the current density of J=5.84 mA cm^{-2} catalyst Pt/Vc/Nf J=6.05 mA cm^{-2}. It is seen that the IrO_2/Nf J=10.35 mA cm^{-2} catalyst is quite good in this parameter. As expected, IrO_2/Nf and Pt/Vc/Nf catalysts give better results in the current density parameter. Fe(OAc)Pc/Fl/Nf catalyst contains a mononuclear structure with a current density value closest to IrO_2/Nf and Pt/Vc/Nf catalysts, which show good catalytic effect in the oxygen oxidation reaction in basic medium, considering the current density at E=0.70 V. attention as a catalyst. However, as E=0.70 V goes more positive, it is seen in **Figure 51** that the current density of the Fe(OAc)Pc/Fl/Nf catalyst is higher than thecurrent density of the Pt/Vc/Nf catalyst.

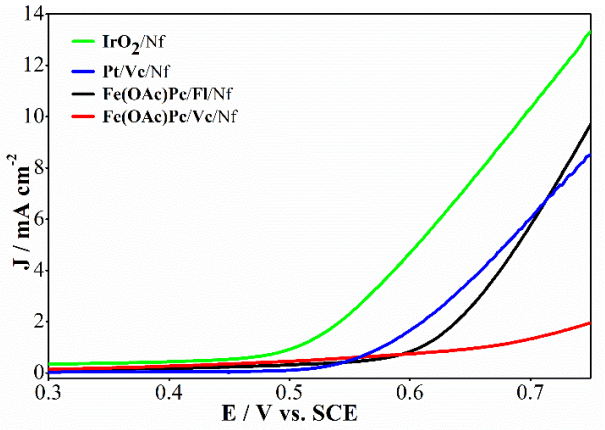

Figure 51 RDE voltammograms in 0.1 M KOH for OER (Rotation speed: 2500 rpm).

Table 11 Electro catalytic OER performances of catalyst materials.

Catalysts	E_o V (vs. SCE)	J / mA cm^{-2}
IrO2/Nf	0.15	10.35
Pt/Vc/Nf	0.49	6.05
Fe(OAc)Pc/Vc/Nf	0.26	1.33
Fe(OAc)Pc/Fl/Nf	0.25	5.84

As expected, the initiation potential of the IrO_2/Nf catalyst E_o=0.15 V is quite negative and good compared to other catalysts. If the initiation potential of the Pt/Vc/Nf catalyst is E_o=0.49 V, it is more positive than the Fe(OAc)Pc/Fl/Nf E_o=0.25 V and Fe(OAc)/Vc/Nf E_o=0.26 V catalysts and this catalyst showed a weaker catalytic effect (**Table 11**). Fe(OAc)Pc/Fl/Nf catalyst was seen as the closest catalyst to IrO_2/Nf catalyst in the starting potential parameter. Fe(OAc)Pc/Fl/Nf catalyst draws attention with its good electro catalytic effect among catalysts containing mononuclear structure when both initiation potential and current density parameters are taken into account. Thus, Fe(OAc)Pc/Fl/Nf catalyst can be used as an electro catalyst in Zinc Air battery systems due to its effective and remarkable catalytic performances in oxygen oxidation reaction in both acidic and basic environments saturated with O_2.

3.6. SEM and EDS spectrum of Mono Substituted Fe(OAc)Pc (1b) compound

The scanning electron microscopy (SEM) images for VC XC-72, Fe(OAc)Pc (**1b**), and the composite Fe(OAc)Pc/VC/Nafion are presented in **Figure 52(A-C**). It is found that the morphology of VC is spherical (**Figure 52A**). These results showed a homogeneous but irregular electrodeposit material where the presence of the starting elements can be

noticed. **Figure 52A** and **52B** demonstrate the size of the particle of catalyst active material (VC and Fe(OAc)Pc (**1b**)) are close to each other. Many Fe(OAc)Pc (**1b**) particles connect with VC forming Fe(OAc)Pc/VC (**Figure 52C**). In the carbon based supporting material, Fe(OAc)Pc (**1b**) complex spread homogeneously. Microstructure analysis by SEM indicates that the Fe(OAc)Pc(**1b**) particles are irregular bulk (**Figure 52C**).

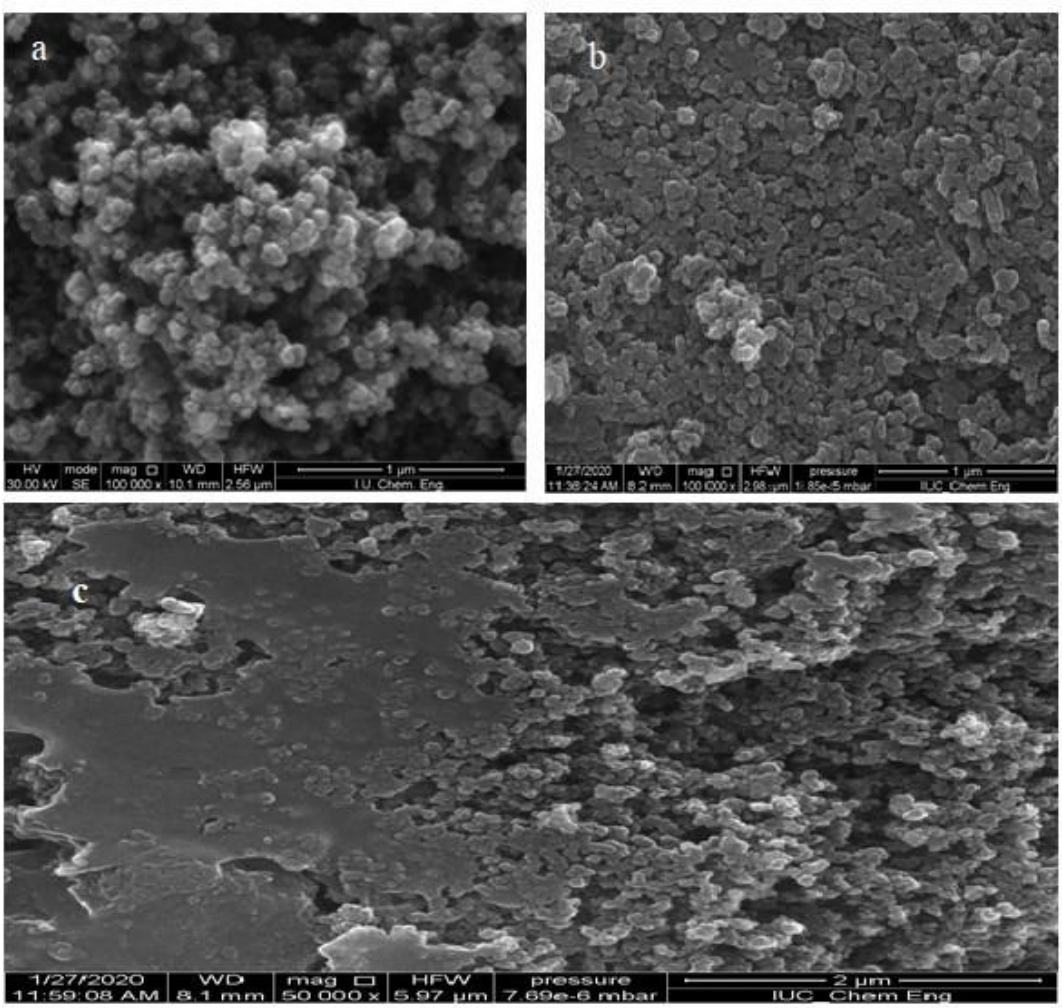

Figure 52 The scanning electron microscopy (SEM) images of **(A)** VC **(B)** Fe(OAc)Pc **(1b) (C)** Fe(OAc)Pc/Vc

Figure 53A displays the EDS spectra of carbon, nitrogen, oxygen and iron contents of the FePc-based catalyst. The elemental mapping of C, N, Fe and overall distribution of the Fe(OAc)Pc /Vc are presented in Figure **53B**. It is worth to mention that VC is the largest portion comparing all other particles found in the sample. Analysis through EDS-mapping substantiates the consistent distribution of iron atoms in the Fe(OAc)Pc(**1b**) structure that is spread across the Vc.

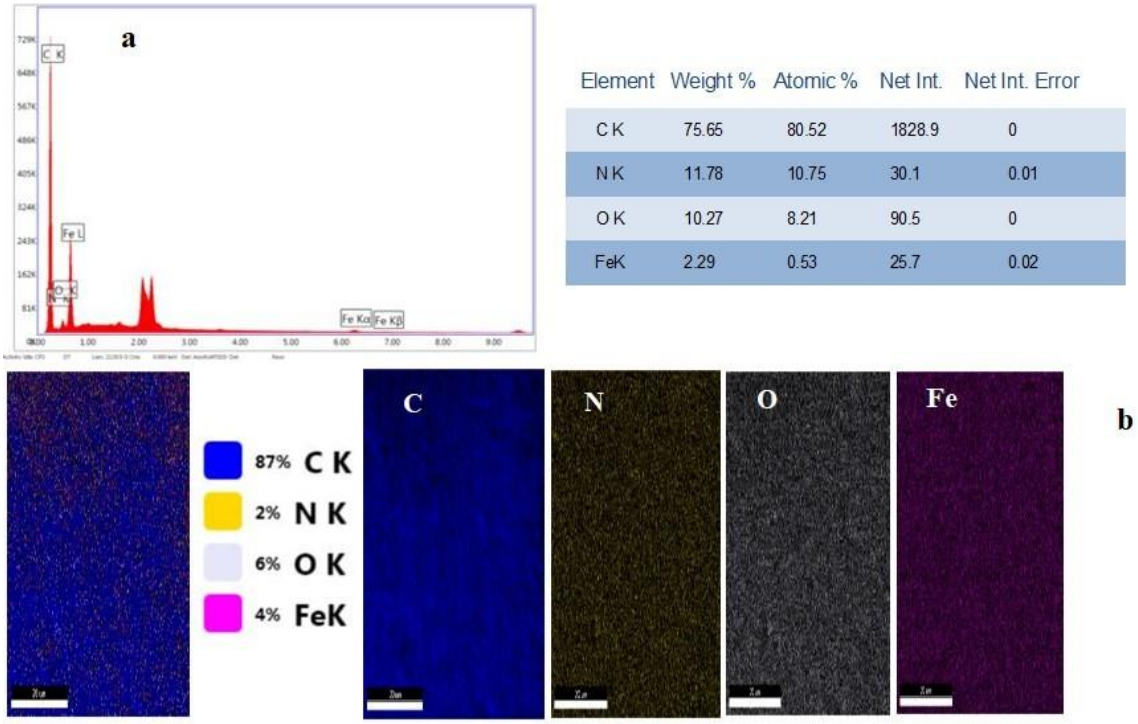

Figure 53 (A) EDS spectrum and **(B)** EDS elemental mapping of C, N, O, Fe and overall distribution on the outer surface of Fe(OAc)Pc/VC.

The morphology and size of the Fl, Fe(OAc)Pc (**1b**) and Fe(OAc)Pc /Fl/Nf were studied by SEM analysis (**Figure 54**). The SEM images of Fl, Fe(OAc)Pc (**1b**) and Fe(OAc)Pc / Fl/Nf showed spherical particles. Some agglomerates, which resulted from aggregation of primary particles, are observable in the SEM images. This agglomeration gives an increase in the size of particles.

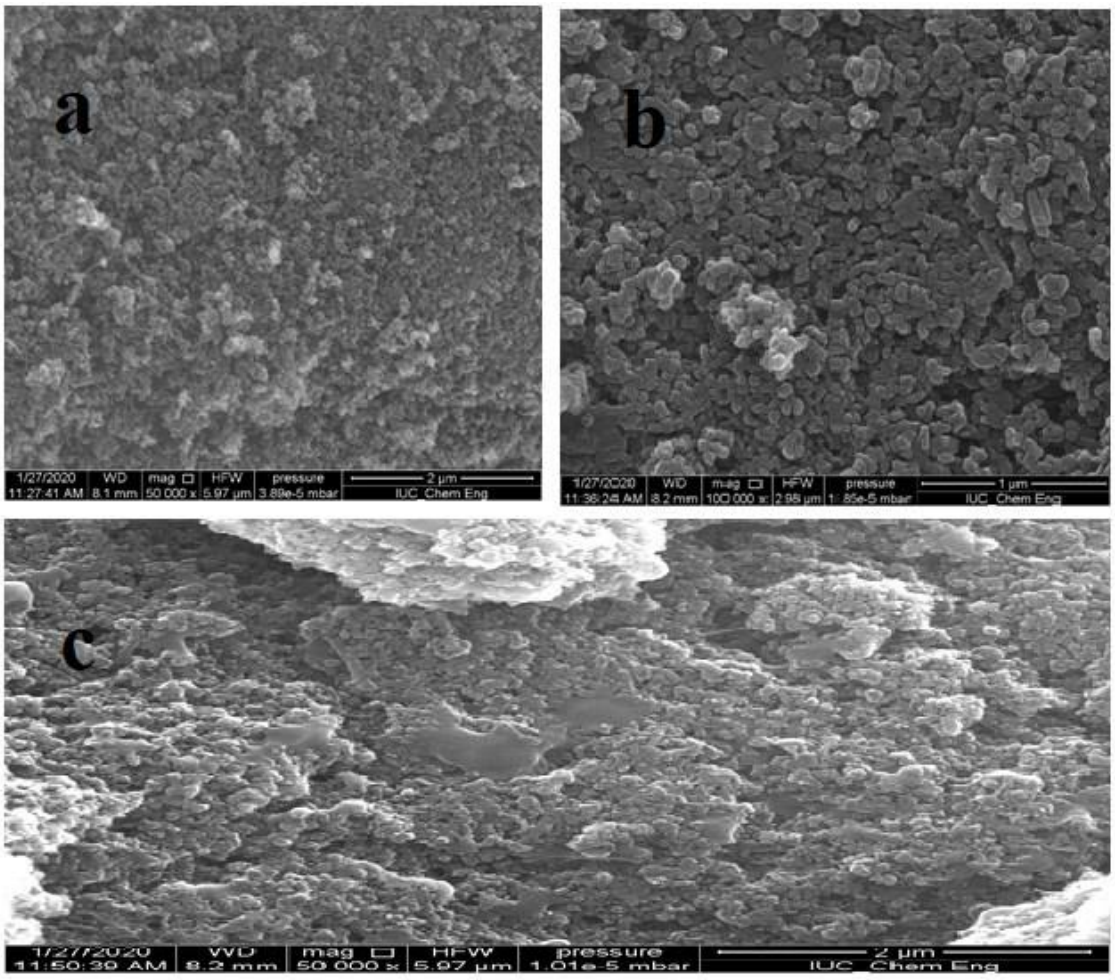

Figure 54 SEM images of **(A)** Fl **(B)** Fe(OAc)Pc **(1b) (C)** Fe(OAc)Pc/ Fl.

Figure 55 displays the EDS spectra of carbon, nitrogen, oxygen and iron contents of the Fe(OAc)Pc (**1b**) -based catalyst. The elemental mapping of C, N, Fe and overall distribution of the Fe(OAc)Pc/Fl mixture are presented in **Figure 55B**. Analysis through EDS-mapping substantiates the consistent distribution of iron atoms in the Fe(OAc)Pc (**1b**) structure that is spread across the Fl. It is worth to mention that Fl is the largest portion comparing all other particles found in the sample.

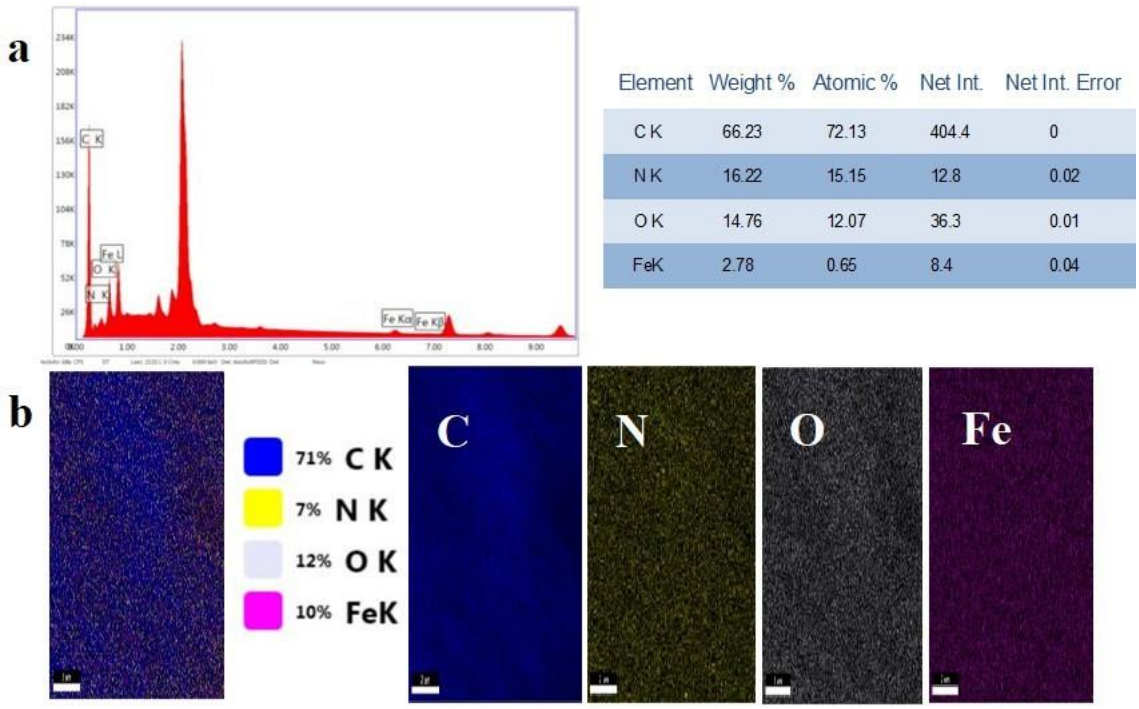

Figure 55 (A) EDS spectrum and **(B)** EDS elemental mapping of C, N, O, Fe and overall distribution on the outer surface of Fe(OAc)Pc/Fl.

3.7. Investigation of electrochemical and spectroelectrochemical behaviors of Ball Type Dinuclear (2a–2e) substituted complexes in solution environment

Ball-type Pcs consisting of two metal centers have captivated great attention in recent times, as a consequence of their interesting properties such as electrochemical, spectroscopic, electrical, electro catalytic [74], optical [75] and gas sensing properties [76] resulting from intense interaction between two metal centers and/or the face-to-face Pc rings [77]. These properties of ball-type Pcs can transform sharply in terms of the central metal [78], the bridging links [79], the distance between the two Pc units [80] and the presence or absence of axial ligands [81]. In the present work, we aimed to extend our studies with the newly synthesized dinuclear phthalocyanine complexes [Co_2Pc_2 (**2a**), $Fe_2(OAc)_2Pc_2$ (**2b**), $Mn_2(OAc)_2Pc_2$ (**2c**), Ni_2Pc_2 (**2d**) and Zn_2Pc_2 (**2e**)] with novel 4,4 '- (3,5-di-tert-butyl- 1,2-phenylene) bis (oxy) moieties and make new benefactions by determination of the effects of interaction between two metal centers and/or the face-to-face Pc rings, the effects of the bridging links on the electrochemical properties of these complexes. On that account, at the first stage of this work, the redox properties of the complexes have been comparatively analyzed by the voltammetric methods and in-situ spectroelectrochemistry in coordinating DMSO solvent media and as the supporting electrolyte, TBAP has used.

Table 12 Data on the electrochemical characterization of (**2a-2e)** compounds in DMSO/TBAP

Complex	Redox process	Label	$^{a}E_{1/2}$	$^{b}\Delta E_p$	$^{c}I_{pa}/I_{pc}$	$^{d}\Delta E_{1/2}$	$^{e}\Delta E_s$
Co_2Pc_2	$[Co(II)Pc(-2).Co(III)Pc(-2)]^{+}/[Co(III)Pc(-2)]^{2+}$	O2	0.46	80	0.85		0.30
	$[Co(II)Pc(-2)]_2/[Co(II)Pc(-2).Co(III)Pc(-2)]^{+}$	O1	0.16	85	0.80	0.54	
	$[Co(II)Pc(-2)]_2/[Co(II)Pc(-2).Co(I)Pc(-2)]^{-}$	R1	-0.38	100	0.80		0.27
	$[Co(II)Pc(-2).Co(I)Pc(-2)]^{-}/[Co(I)Pc(-2)]_2^{2-}$	R2	-0.65	90	0.82		
	$[Co(I)Pc(-2)]_2^{2-}/[Co(I)Pc(-3).Co(I)Pc(-2)]^{3-}$	R3	-1.40	65	0.94		0.30
	$[Co(I)Pc(-3).Co(I)Pc(-2)]^{3-}/[Co(I)Pc(-3)]_2^{4-}$	R4	-1.70	70	0.92		
$Fe_2(OAc)Pc_2$	$[Fe(III)(OAc)Pc(-2)]_2/[Fe(IV)(OAc)Pc(-2)]_2^{2+}$	[f,g]O1,O2	0.22	-	-	0.52	0.52
	$[Fe(III)(OAc)Pc(-2)]_2/[Fe(III)(OAc)Pc(-2).Fe(II)(OAc)Pc(-2)]^{-}$	R1	-0.30	80	0.80		
	$[Fe(III)(OAc)Pc(-2).Fe(II)(OAc)Pc(-2)]^{-}/[Fe(II)(OAc)Pc(-2)]_2^{2-}$	R2	-0.52	75	0.92		
	$[Fe(II)(OAc)Pc(-2)]_2^{-2}/[Fe(I)(OAc)Pc(-2)]_2^{4-}$	[f,g]R3,R4	-0.78	-	-		
	$Fe(I)(OAc)Pc(-2)]_2^{-4}/[Fe(I)(OAc)Pc(-2).Fe(I)(OAc)Pc(-3)]^{5-}$	R5	-1.43	65	0.92		
$Mn_2(OAc)Pc_2$	$[Mn(IV)(OAc)Pc(-2)]_2^{2+}/[Mn(IV)(OAc)Pc(-1).Mn(IV)(OAc)Pc(-2)]^{3+}$	[f]O3	0.98	-	-		
	$[Mn(III)(OAc)Pc(-2)]_2/[Mn(IV)(OAc)Pc(-2)]_2^{2+}$	[f,g]O1 O2	0.26	-	-	0.41	
	$[Mn(III)(OAc)Pc(-2)]_2/[Mn(III)(OAc)Pc(-2).Mn(II)(OAc)Pc(-2)]^{-}$	R1	-0.15	75	0.92		0.29
	$[Mn(III)(OAc)Pc(-2).Mn(II)(OAc)Pc(-2)]^{-}/[Mn(II)(OAc)Pc(-2)]_2^{2-}$	R2	-0.44	-	-		
	$[Mn(II)(OAc)Pc(-2)]_2^{2-}/[Mn(II)(OAc)Pc(-2).Mn(I)(OAc)Pc(-2)]^{3-}$	R3	-0.75	80	0.90		0.21
	$[Mn(II)(OAc)Pc(-2).Mn(I)(OAc)Pc(-2)]^{3-}/[Mn(I)(OAc)Pc(-2)]_2^{4-}$	[f]R4	-0.96	75	0.85		
	$[Mn(I)(OAc)Pc(-2)]_2^{4-}/[Mn(I)(OAc)Pc(-3).Mn(I)(OAc)Pc(-2)]^{5-}$	R5	-1.36	65	0.92		0.27
	$[Mn(I)(OAc)Pc(-3).Mn(I)(OAc)Pc(-2)]^{5-}/[Mn(I)(OAc)Pc(-3)]_2^{6-}$	[f]R6	-1.63	68	0.94		
Ni_2Pc_2	$[Ni(II)Pc(-2)]_2/[Ni(II)Pc(-1)]_2^{2+}$	O1	0.90	75	0.80	1.60	0.50
	$[Ni(II)Pc(-2)]_2/[Ni(II)Pc(-2).Ni(II)Pc(-3)]^{-}$	R1	-0.70	60	0.80		
	$[Ni(II)Pc(-2).Ni(II)Pc(-3)]^{-}/[Ni(II)Pc(-3)]_2^{2-}$	R2	-1.20	65	0.95		
	$[Ni(II)Pc(-3)]_2^{2-}/[Ni(II)Pc(-4)]_2^{4-}$	R3	-1.37	65	0.92		
	$[Ni(II)Pc(-4)]_2^{4-}/[Ni(II)Pc(-5)]_2^{6-}$	R4	-1.55	75	0.95		
Zn_2Pc_2	$[Zn(II)Pc(-1).Zn(II)Pc(-2)]^{+}/[Zn(II)Pc(-1)]_2^{2+}$	O2	0.76	70	0.85		0.22
	$[Zn(II)Pc(-2)]_2/[Zn(II)Pc(-1).Zn(II)Pc(-2)]^{+}$	O1	0.54	75	0.80	0.96	
	$[Zn(II)Pc(-2)]_2/[Zn(II)Pc(-2).Zn(II)Pc(-3)]^{-}$	R1	-0.42	60	0.95		0.32
	$[Zn(II)Pc(-2).Zn(II)Pc(-3)]^{-}/[Zn(II)Pc(-3)]_2^{2-}$	R2	-0.74	65	0.92		
	$[Zn(II)Pc(-3)]_2^{2-}/[Zn(II)Pc(-4).Zn(II)Pc(-3)]^{3-}$	R3	-1.41	65	0.95		

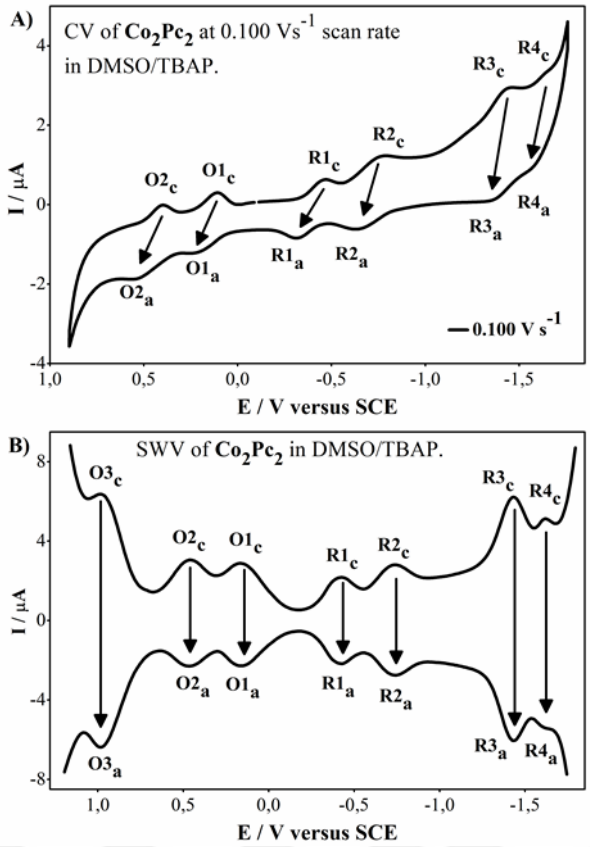

Figure 56 (A) CV and **(B)** SWV voltammograms of Co_2Pc_2 (**2a**) complex (5.0x10-4 M) in DMSO/TBAP solution medium.

Figure 56 shows the CVs and SWVs of Co_2Pc_2 **(2a)** in DMSO/TBAP. The related electrochemical data are tabulated for this solvent in **Table 12**. Co_2Pc_2 **(2a)** provides four clear-cut diffusion controlled and reversible reduction procedures (R1 at - 0.38 V, R2 at - 0.65 V, R3 at 1.40 V and R4 at -1.70 V versus SCE) and two oxidation couples (O1 at 0.16 V and O2 at 0.46 V versus SCE). Controlled potential electrolysis was applied at relevant potentials to determine the number of electrons transferred for each redox process. The number of electrons transferred for each redox process is approximately equal to unity showed by the coulometric studies of voltammetric couples. For the two cofacial Pc rings and metal centers, the reactions in the voltammogram are step wise one electron processes, which indicates that the splitting of the molecular orbitals takes place because of the remarkable interaction between the two Pc rings and/or two metal centers in Co_2Pc_2 **(2a)** and thus the redox processes occur at different potentials of each Pc ring and/or metal center in this complex [12].

The metal center in a Co_2Pc_2 **(2a)** is redox active because of the presence of d-orbital

levels in the HOMO–LUMO gap [73-75]. The electrochemistry of cobalt Pcs is divided into two categories based on its medium of solution as donor solvents and non donor solvents. The prime variation between them is the metal or the ring is oxidized first. By coordinating along the axis, donor solvents firmly recommend the oxidation of Co(II) to Co(III) to form six coordinate species [76]. Whether this kind of donor solvents are not present, then oxidation to Co(III) is reserved and ring oxidation occurs first. At the same time; the first reduction process is metal based both in donor as well as non donor solvents [76-78]. So The former two reduction procedures are possibly metal based $[Co(II)Pc(-2)]_2$/[Co(II)Pc (-2). Co(I)Pc (-2)]$^-$ and [Co(II)Pc (-2). Co(I)Pc(-2)]$^-$/$[Co(I)Pc (-2)]_2^{2-}$ processes, respectively. Furthermore, the former two oxidation procedures are also possibly metal based $[Co(II)Pc(-2)]_2$/[Co(II)Pc (-2). Co(III)Pc (-2)]$^+$ and Co(II)Pc (- 2). Co(III)Pc (-2)]$^+$/$[Co(III)Pc (-2)]^{2+}$ processes, respectively. On the contrary, the third and fourth reduction processes are attributed to the ligand based correspond to the splitting of the Pc (-2) / Pc (-3) redox pair $[Co(I)Pc(-2)]_2^{2-}$/[Co(I)Pc (-3). Co(I)Pc (-2)]$^{3-}$ and [Co(I)Pc (-3). Co(I)Pc(-2)]$^{3-}$/$[Co(I)Pc (-3)]_2^{4-}$ processes correspondingly; in view of the fact that each molecule of Co_2Pc_2 **(2a)** includes two Co(II) centers and the voltammetric analysis was accomplish in DMSO–TBAP solution. The redox potentials of MPcs are significantly influenced by the coordination of the axial position of donor and/or neutralizing solvent molecules. While the manganese and iron center may have 3+ valence in the oxidation state, but the cobalt metal center has 2+ oxidation state. The presence of cobalt metal initially as Co (II) is due to the cobalt metal preferring six coordination number by connecting DMSO from its axial positions in the donor polar solvent DMSO/TBAP medium, the UV-*vis* spectral and IR spectroscopy have provided support for this situation. In IR spectroscopy, due to the binding of the acetate group, the carbonyl peak had seen in $Mn_2(OAc)_2Pc_2$ **(2c)** and $Fe_2(OAc)_2Pc_2$ **(2b)** complexes which were not observed in the Co_2Pc_2 **(2a)** complex. This indicates that the cobalt metal was present in the Co (II) valence state. ΔEp values for these processes were within the range of 65–100 mV at various scan rates from 0.050 to 0.250 Vs^{-1}, demonstrating quasi reversible electrochemical behavior. The couples showed totally diffusion controlled mass transferbehavior with roughly unit values of the Ipa/Ipc ratios. This reversible behavior was also verified by the affinity in the forward and reverse SWVs [79] (**Figure 56A**). The difference between the half-peak potentials of

R1 and O1 for Co_2Pc_2 **(2a)** ($\Delta E_{1/2}$) was low (0.54) V. This kind of voltammetric nature results from strong intermolecular interactions between the two Pc rings and/or metal centers connected cofacially at two sides with four arms, and consistent with the rigid structure of Co_2Pc_2 **(2a)** [80] (**Table 12)**. The ΔEs data which reflect the mixed-valence splitting in V, for the redox processes of all MPcs are presented in **Table 12**. These results confirm the delocalization of charge among the cofacial MPc units as well as the formation of electrochemically stable oxidized and reduced mixed valence species [72].

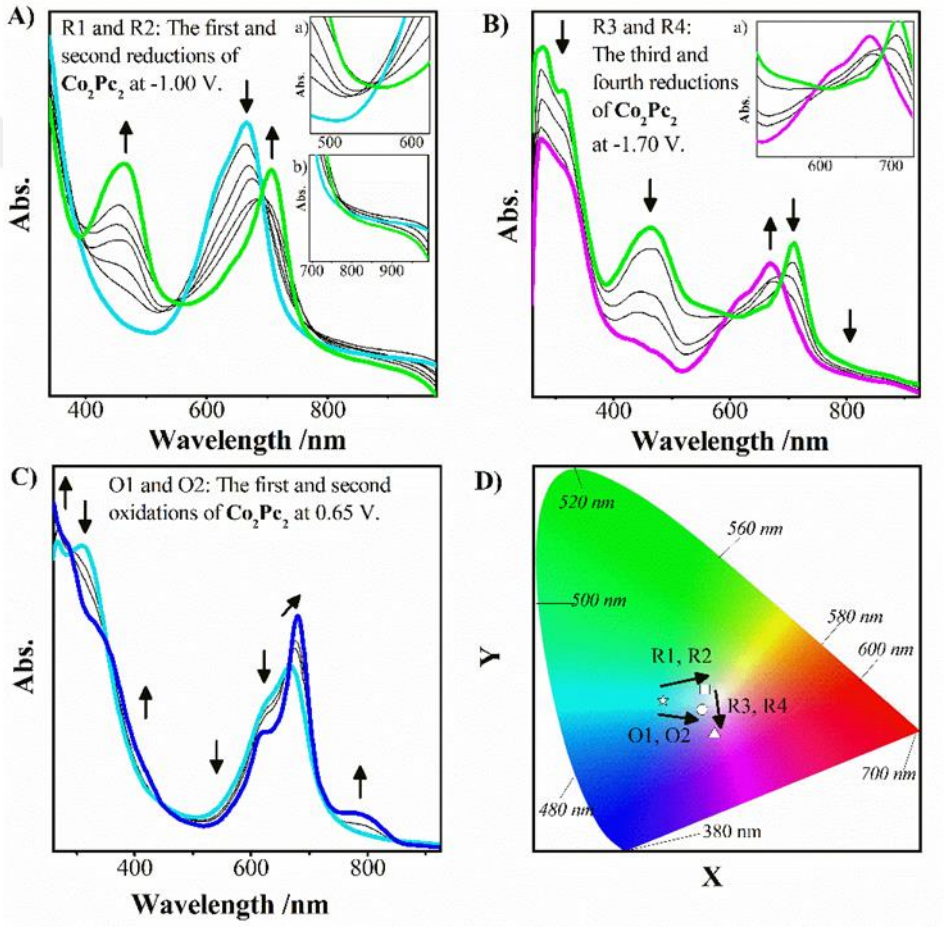

Figure 57 In situ UV-*Vis* spectral and electro colorimetric changes of Co_2Pc_2 (**2a**) complex (5.00×10^{-5} M) in DMSO/TBAP solution medium, recorded by applying constant potential according to SCE.

By using voltammetric measurements singly, it is fairly impossible to point out the nature of the redox couples perfectly. Meanwhile, the voltammetric analyses were supported with in situ spectroelectrochemical analysis, performed throughout the controlled potential electrolysis of complex at voltammetrically determined constant

potentials. The spectral changes monitored during these measurements permitted us to make the assignment of the redox methods, that is, either these processes are metal based or ligand based. **Figures. 57A–57D** represents UV-Vis spectral variations also collaboratively recorded chromaticity scheme of compound **Co_2Pc_2 (2a)** in DMSO/TBAP. Throughout the number one reduction of **Co_2Pc_2 (2a)** at -0.60V versus SCE, the Q band at 665 nm decreased and shifted to 708 nm, formed a new band at 469 nm. Itshows a broad shoulder at around 622 nm resulting from intramolecular coupling and interactions. These spectral variations are associated by the formation of a new band at 469 nm [79]. These changes approve the output of [Co (II) Pc (-2). Co (I) Pc (-2)] $^{-}$ species from [Co (II) Pc (-2)] ^{2} species. These spectral changes approve the arrangement of Co(II)·Co(I) mixed valence species [72, 73]. Co(II)·Co(I) and Co(I)·Co(I) both species display Q band along with metal to ligand charge transfer (MLCT) [74,75]. The new band at 469 nm can be placed for MLCT from Co(I) to the Pc ring. This process results with the formation of unstable isosbestic points as a response of splitting in the CV voltamogram indicated the properties of ball-type phthalocyanine complexes (**Figure 57A** inset). As illustrated in **Figure 57D**. the changing of color from turquoise (x=0.332 and y=0.357) to light green (x=0.332 and y=0.357). In the process of the second reduction of Co_2Pc_2 **(2a)** at -1.55V versus SCE, there was an increase in the absorption of the band at 450 nm upon further reduction in **Figure 57B**. At the starting point, the Q band at 615 nm decreases with red shift and a new band at 724 nm forms and the band at 450 nm increases **(Figure 57C).** These spectral variations illustrate the formation of Co(I) ·Co(I) species [76]. Unstable isobetic points continued in the second reduction process shows the properties of ball-type phthalocyanine complexes. Previous studies of our group support this approach [76, 79]. These variations are accompanied by an exceptional increase in absorption between 400–500 nm. According to **Figure 57D,** these spectral changes produce a change in color from green to purple (x=0.351 and y=0.259). **Figure 57C** presents the spectral changes upon the first oxidation process at 0.60V versus. SCE. Throughout this process, the Q band shifted at 669 nm to 679 nm and form clear isosbestic points at 354, 454, 667 and 812 nm which also support the output from [Co (II) Pc (-2)]2 to [Co(II)Pc (-2). Co (III) Pc (-2)] + species (**Figure 57C**). The changes in color from light blue to light purple (x=0.326 and y=0.312) in **Figure 57D.** For first oxidation O1, these kind of spectral variations are characteristics for a metal based oxidation, additionally it confirms the voltammetric

assignment to [Co (II) Pc (-2)] 2 / [Co(II)Pc (-2). Co (III) Pc (-2)] + of this process in **Figure 57**. Spectral changes of oxidation process in the phthalocyanine ring could not be recorded due to the narrow anodic working window of the DMSO / TBAP system. Electrochemical and spectroelectrochemical studies have shown that the first two reductions and first two oxidation reactions of dinuclear cobalt phthalocyanine complexes in the coordinating donor polar solvent such as DMSO, are probably metal derived **(Table 12).**

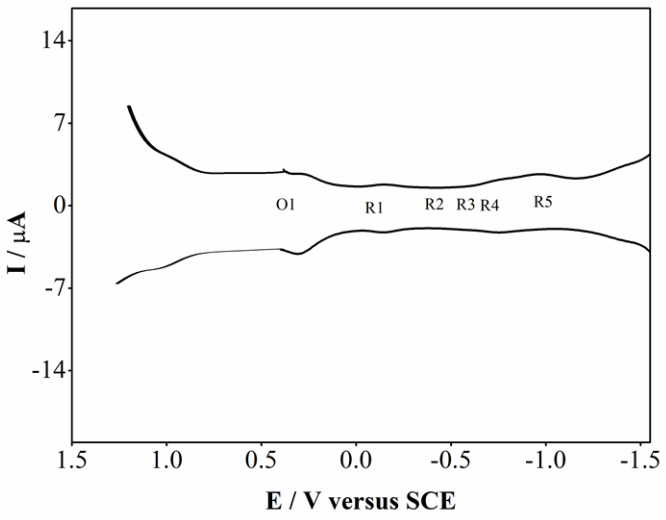

Figure 58 SWV voltammograms of $Fe_2(OAc)_2Pc_2$ (**2b**) complex (5.0x10-4 M) in DMSO/TBAP solution medium.

$Fe_2(OAc)_2Pc_2$ **(2b)** complex provides five diffusion controlled and reversible reduction procedures (R1 at - 0.30 V, R2 at - 0.52 V, R3 and R4 at -0.78 V and R5 at -1.43 V versus SCE) and two oxidation couples (O1 and O2 at 0.22 V versus SCE) (**Table 12 and Figure 58**). The CPC measurements indicated that the number of electrons transferred was unity for the first (R1), second (R2) and fifth (R5) reduction couples. The incident of one-electron redox processes of R1, R2, and R5 couples implies that there is distinct interaction between the two FePc units in $Fe_2(OAc)_2Pc_2$ **(2b).** Most likely, because of their very negative peak potentials near the solvent-limited potential region, it was not workable to find out truly the number of electrons engaged in two oxidation couples (O1 and O2) and two reduction couples (R3 and R4). Although, the area or chargeunder the relevant peaks assumes that each of these redox processes involves thetransfer of two electrons. The interaction between the two Pc rings and/or two metal centers in a dimer possibly generates the splitting of molecular orbitals

consequently significant changes in redox potentials [77-79]. The Ipa/Ipc proportion with the scan rate was almost unity which suggests the perfectly diffusion controlled electron transfer mechanism of the procedures (**Table 12**). ΔEp values ranged 65 to 85 mV pointed purely diffusion controlled mass transfer and reversible electron transfer nature of these redox pairs.

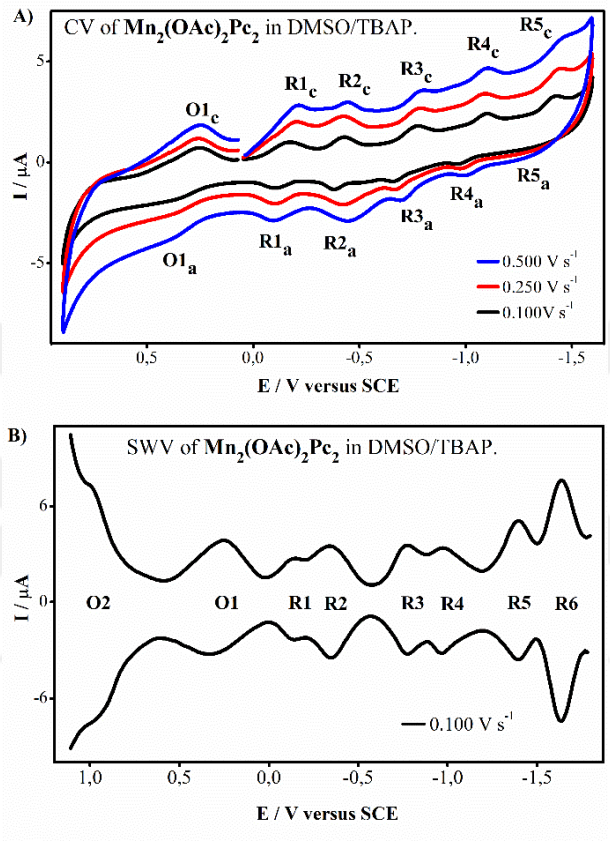

Figure 59 (A) CV and **(B)** SWV voltammograms of $Mn_2(OAc)_2Pc_2$ (**2c**) complex ($5.0x10^{-4}$ M) in DMSO/TBAP solution medium.

Figure 59 shows the CVs of $Mn_2(OAc)_2Pc_2$ **(2c)** in DMSO/TBAP. The related electrochemical data are tabulated for this solvent in **Table 12**. $Mn_2(OAc)_2Pc_2$ **(2c)** provides six clear-cut diffusion controlled and reversible reduction procedures (R1 at -0.15V, R2 at - 0.44V, R3 at -0.75 V, R4 at -0.96 V, R5 at -1.36 V and R6 at -1.63 V versus SCE) and three oxidation couples (O1 and O2 at 0.26 V versus SCE). The former four reduction procedures are possibly metal based [Mn(III)(OAc)Pc (-2)]$_2$/[Mn(III)(OAc)Pc (-2). Mn(II)(OAc)Pc (-2)]$^-$, [Mn(III)(OAc)Pc (-2). Mn(II)(OAc)Pc(-2)]$^-$/[Mn(II)(OAc)Pc(-2)]$_2^{2-}$, [Mn(II)(OAc)Pc(-2)]$_2^{2-}$ /[Mn(II)(OAc)Pc (-2). Mn(I) (OAc)Pc (-2)]$^{3-}$ and [Mn(II)(OAc)Pc (-2). Mn(I)(OAc)Pc(-

2)]$_2^{3-}$/[Mn(I)(OAc)Pc (-2)]$_2^{4-}$ processes, respectively. And for oxidation process, former two oxidation procedures are possibly metal based [Mn(III)(OAc)Pc(-2)]$_2$/[Mn(IV)(OAc)Pc (-2)]$_2^{2+}$ process. On the contrary, the fifth and sixth reduction and the third oxidation processes are attributed to the ligand based [Mn(I)(OAc)Pc(-2)]$_2^{4-}$/[Mn(I)(OAc)Pc(-3).Mn(I)(OAc)Pc(-2)]$^{5-}$, [Mn(I)(OAc)Pc(-3).Mn(I)(OAc)Pc(-2)]$^{5-}$/[Mn(I)(OAc)Pc(-3)]$^{6-}$ and [Mn(IV)(OAc)Pc(-2)] $^{2+}$/[Mn(IV)(OAc)Pc(-1).Mn(IV)(OAc)Pc(-2)]$^{3+}$ processes correspondingly. ΔEp values for R1, R3, R4, R5 and R6 processes were within the range of 65–80 mV at various scan rates from 0.050 to 0.500 Vs−1, demonstrating reversible electrochemical behavior and the couples showed totally diffusion controlled mass transfer behavior with roughly unit values of the Ipa/Ipc ratios. This reversible behavior was also verified by the affinity in the forward and reverse SWVs (**Figure 59B**). The last reduction procedures (R6) could be detected only by SWV due to the appearance of the process at the end of the available potential window (**Figure 59B**). The difference between the half-peak potentials ($\Delta E_{1/2}$) of R1 and O1 for $Mn_2(OAc)_2Pc_2$ **(2c)** was low (0.41). $\Delta E_{1/2}$ value for the $Mn_2(OAc)_2Pc_2$ **(2c)** complex is mostly in agreement with those of the previously reported Pc complexes [80, 81].

The voltammetric behavior of Ni_2Pc_2 **(2d)** was considerably different from that of $Mn_2(OAc)_2Pc_2$ **(2c)** and **Ni_2Pc_2 (2d)** provides four diffusion controlled and reversible reduction procedures (R1 at - 0.70 V, R2 at - 1.20 V, R3 at -1.37 V and R4 at -1.53 V versus SCE) and one oxidation procedure (O1 at 0.90 V versus SCE). The CPC measurements indicated that the number of electrons transferred was unity for the first (R1) and second (R2) reduction couples, and two for the third (R3), fourth reduction couples (R4) and first oxidation (O1) processes. The Ipa/Ipc proportion with the scan rate was almost unity which suggests the perfectly diffusion controlled electron transfer mechanism of the procedures (**Table 12**). ΔEp values ranged 65 to 85 mV pointed purely diffusion controlled mass transfer and reversible electron transfer nature of these redox pairs. The potential separations between R2, R3 and R3, R4 of Ni_2Pc_2 **(2d)** are 0.17 and 0.28V respectively **(Table 12**). These data are slightly lower than those of Zn_2Pc_2 **(2e)** which recommended that mixed valence reduced species of Ni_2Pc_2 **(2d)** are not as stable as Zn_2Pc_2 **(2e).** The variation between stability of the mixed valence

reduced species of Zn_2Pc_2 **(2e)** and Ni_2Pc_2 **(2d)** probably belonged to the difference in intramolecular distance between the two MPc units in these complexes. It apparently suggested that the binding of two Pc rings at two sides in the ball type dinuclear complexes Zn_2Pc_2 **(2e)** and Ni_2Pc_2 **(2d)** cause intramolecular interactions between their two MPc units [19].

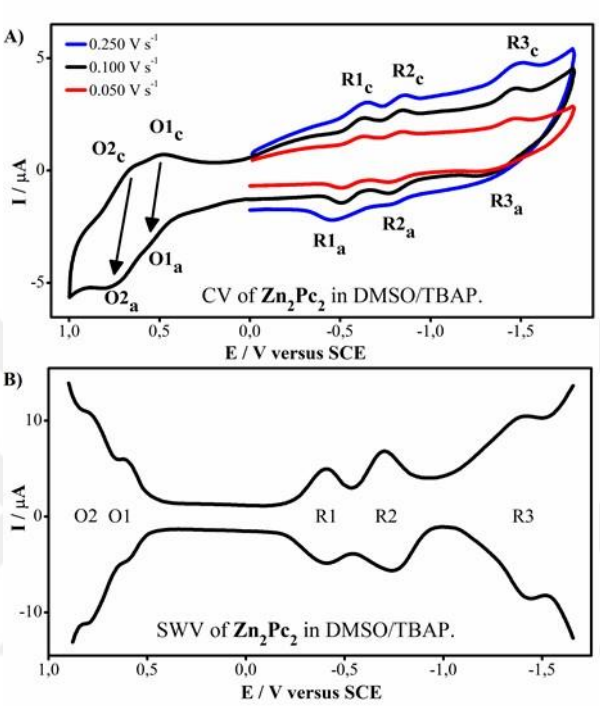

Figure 60 (A) CV and **(B)** SWV voltammograms of Zn_2Pc_2 (**2e**) complex ($5.0x10^{-4}$ M) in DMSO/TBAP solution medium.

To differentiate the common characteristics of Phthalocyanine ring based redox procedures, the voltammetric analysis of Zn_2Pc_2 **(2e)** was firstly illustrated. Voltammetric measurements of Zn_2Pc_2 **(2e)** compound were performed in DMSO/TBAP **(Figure 60)**. At every single scan rate, the relevant Ipa/Ipc ratios are unity which indicates that diffusion controlled reduction pairs of Zn_2Pc_2 **(2e).** It shows three clear-cut diffusion- controlled as well as reversible reduction pairs (R1 at - 0.42V, R2 at – 0.74V and R3 at -1.41V versus SCE) and two oxidation pairs (O1 at 0.54V and O2 at 0.76V versus SCE) at different scan rates from 0.050 to 0.250 Vs−1. SWVs distinctly show reversibility of the redox processes in the chemical and electrochemical measurements (**Figure 60B**). For the redox pairs, ΔEp data at 0.100 Vs^{-1} scan rate range normally between 60 to 75 mV which proves the electrochemical reversibility of the electron transfer procedures (**Table 12**). All redox processes of Zn_2Pc_2 **(2e)** are Pc ring-

based since Zn(II) is redox inactive in MPcs [32]. The CPC studies indicated that each broadly separated redox process requires the transfer of one electron which recommends that the reduction or oxidation of each Zinc Phthalocyanine unit in Zn_2Pc_2 **(2e)** take places at a different potential, by cause of the interaction between the two cofacial Zinc Phthalocyanine units and consequently the splitting of the molecular orbitals (**Table 12**). From the earlier studies, it is understandable that the Zn(II) metal center is not redox active in metallo Phthalocyanines, so that all redox processes of Zn_2Pc_2 **(2e)** are ligand-based [33, 34]. It is stated that the transfer of one electron instead of two electrons at each step takes place at different potentials as a result of the interaction between the two ZnPc units and thus the separation of the molecular orbitals, for each Zn_2Pc_2 **(2e)** complex. All reduction and oxidation pairs, electron transfer procedures along with redox behaviors are in harmony with the literature. So that, $E_{1/2}$ values of these compounds reflect their HOMO- LUMO gaps. $E_{1/2}$ value for the Zn_2Pc_2 **(2e)** complexes (0.96 V) are mostly in agreement with those of the previously reported Pc complexes (**Table 12**).

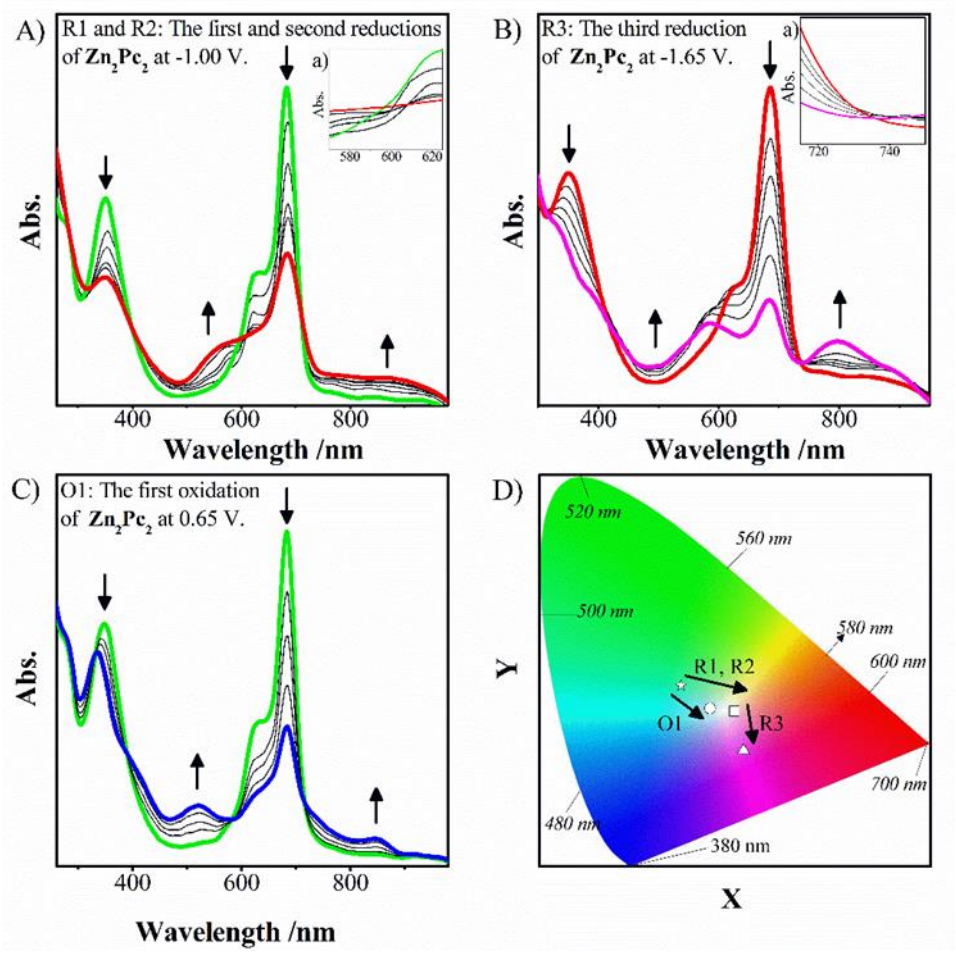

Figure 61 In situ UV-*Vis* spectral and electro colorimetric changes of Zn_2Pc_2 (**2e**) complex (5.00×10^{-5} M) in DMSO/TBAP solution medium.

The general trend in the spectral changes of Zn_2Pc_2 **(2e)** with redox inactive metal center species is assumed to be different from those of the MPcs having redox active metal centers. Predictably, the spectral changes of these compounds were different from those of the MPcs having redox active metal centers. The formation of a new band around 880 nm during the first reduction process, R1, (-0.60 V) increase in the absorption between 500–600 nm during the first reduction process, R1, and the decrease in the split Q band with the red shift of the one at 687 nm to 705 nm during the second reduction process, R2, (**Figure 61A, 61B)**, these spectral changes along with the increase in the absorption between 500–600 nm, are unique for ring reduction. The changing of color from light green (x=0.271 and y=0.391) to light pinkish orange (x=0.373 and y=0.337) as has been seen in the chromacity scheme in **Figure 61D.** This process can be easily presented to [Zn(II)Pc (-2)]2 /[Zn(II)Pc (-2). Zn(II)Pc (-3)]$^-$. The shifts noticed here should be due to the changes in the intramolecular interactions between the two Pc rings in ball type dinuclear structure, upon reduction. Predominantly, the formation of a new absorption band within the range of 550–650 nm and lowering in the main Q band absorption without a shift and simultaneously throughout the redox procedures of these complexes was detected [32- 36]. These kind of spectral transformation were particular for Phthalocyanine ring based redox procedures and hence, offered considerable evidence for electrochemically allocated ligand based character of the redox procedures of redox inactive compounds [33-36]. As Nevertheless, moving isobestic points have been identified (**Figure 61B** inset). This process can be easily presented to [Zn(II)Pc (-2). Zn(II)Pc (- 3)]$^-$ /Zn(II)Pc (-3)]2^{2-} redox couple. In **Figure 61D**, the changing of color from light pinkish orange (x=0.373 and y=0.337) to pink (x = 0.391 and y = 0.250) as has been seen in the chromacity scheme. **Figure 61C** presents *in-situ* UV-Vis spectral changes at the time of the first oxidation procedure. The slow decrease in intensity of the band at615 nm and 705 were also observed which is as well as followed by the lessen in the B band. A sharp changing color from original light green to turquoise (x = 0.326 and y = 0.342) resulted for this decomposition process **(Figure 61D).**

The redox potentials of MPc's are significantly affected by the axial position occupied by the coordination property of donor and / or neutralizing solvent molecules. While the oxidation state of the manganese and iron center can be 3+, the cobalt metal center has

2+ oxidation steps. Cobalt metal is initially found as Co (II) is due to the fact that the cobalt metal chooses six as the coordination number by binding DMSO from its axial positions in the donor polar solvent DMSO / TBAP environment, the measurements made in simultaneous Spectral and IR spectroscopy provide a clear understanding of this situation. In the IR Spectroscopy, the carbonyl peak observed in the $Mn_2(OAc)_2Pc_2$ **(2c)** and $Fe_2(OAc)_2Pc_2$ **(2b)** complexes were not observed in the Co_2Pc_2 **(2a)** complex due to the binding of the acetate group. This shows that cobalt metal is in the Co (II) valence step since it does not bind acetate anion in the center of the complex before redox processes.

3.8. Investigation of the electro catalytic performances for Oxygen reduction reaction (ORR) of Ball Type Dinuclear Substituted (2a-2e) complexes in acidic medium

Electro catalytic activities of the $Fe_2(OAc)_2Pc_2$ (**2a**), Co_2Pc_2 (**2b**), $Mn_2(OAc)_2Pc_2$ (**2c**), Ni_2Pc_2 (**2d**) and Zn_2Pc_2 (**2e**) complexes towards ORR were tested by the RDE technique at 2500 rotations per minute (rpm). The RDE polarization curves of VC/Nf/Pc, Fl/Nf/Pc, GO/Nf/Pc, G/Nf/Pc and Tm/Nf/Pc modified glassy carbon working electrodes were analyzed in 0.5 M H_2SO_4 aqueous electrolyte solution with oxygen purging for 30 min. The potential scanning range was from 0.70 to -0.50 V vs. SCE with a scan rate of $0.005\,Vs^{-1}$. The onset potential (E_o) where the current begins to increase, and the limiting diffusion current density (J_L) can be taken as the measures of catalytic activity. The potential at which the current density reaches 0.100 mA cm^{-2} was taken as E_o. **Table 13** summarizes the electro catalytic performance of Pc-based catalysts for ORR.

Table 13 Electro catalytic activities of **2a-2e** complexes for ORR according to the parameters of onset potential (E_o), diffusion current density (J_L) and half-wave potential ($E_{1/2}$) (according to SCE).

Catalysts	E_o [a] V (vs SCE)	J_L / mA cm^{-2}	$E_{1/2}$ / V (vs SCE)
$Fe_2(OAc)_2Pc_2$/Vc/Nf	0.52	2.78 (1.29)	0.34 (0.01)
Co_2Pc_2/Vc/Nf	0.51	1.45 (2.12)	0.32 (0.01)
Ni_2Pc_2/Vc/Nf	0.09	0.66 (2.12)	-0.01 (-0.16)
Zn_2Pc_2/Vc/Nf	0.02	1.95	-0.22
$Fe_2(OAc)_2Pc_2$/Fl/Nf	0.54	3.05 (1.19)	0.36 (0.01)
Co_2Pc_2/Fl/Nf	0.52	2.48 (1.84)	0.29 (0.03)
$Mn_2(OAc)_2Pc_2$/Fl/Nf	0.27	1.58 (2.64)	0.16 (0.03)
Ni_2Pc_2/Fl/Nf	0.29	3.15	0.01
Zn_2Pc_2/Fl/Nf	0.18	2.06	-0.03
$Fe_2(OAc)_2Pc_2$/GO/Nf	0.48	2.26 (0.19)	0.31 (-0.08)
Co_2Pc_2/GO/Nf	0.41	4.02	-0.01
$Mn_2(OAc)_2Pc_2$/GO/Nf	0.30	3.31	-0.02
Ni_2Pc_2/GO/Nf	0.18	3.95	-0.12
Zn_2Pc_2/GO/Nf	0.24	3.14	-0.12
$Fe_2(OAc)_2Pc_2$/G/Nf	0.46	0.98 (4.18)	0.18 (-0.24)
Co_2Pc_2/G/Nf	0.68	0.44 (3.37)	0.56 (-0.07)
$Mn_2(OAc)_2Pc_2$/G/Nf	0.59	0.38 (2.79)	0.50 (-0.15)
Ni_2Pc_2/G/Nf	0.66	0.32 (1.66)	0.60 (-0.17)
Zn_2Pc_2/G/Nf	0.63	0.29 (0.47)	0.58 (-0.26)
$Fe_2(OAc)_2Pc_2$/Tm/Nf	0.37	4.95	-0.05
Co_2Pc_2/Tm/Nf	0.43	0.72 (1.87)	0.25 (-0.12)
$Mn_2(OAc)_2Pc_2$/Tm/Nf	0.10	1.75	-0.03
Ni_2Pc_2/Tm/Nf	0.22	2.28	-0.26
Zn_2Pc_2/Tm/Nf	0.10	1.72	-0.29

a The potential at which the current density reaches to 0.100 mA cm-2 was taken as the onset potential, Eo.

Figure 62 illustrates a distinct limiting current plateau, which is typically well-defined. This phenomenon is linked to the uniform distribution of electro catalytic sites across the electrode surface. In contrast, when the active sites are unevenly distributed on ink-type electrodes featuring a thin porous coating, the resulting polarization curves tend to exhibit inclined or bell-shaped characteristics.

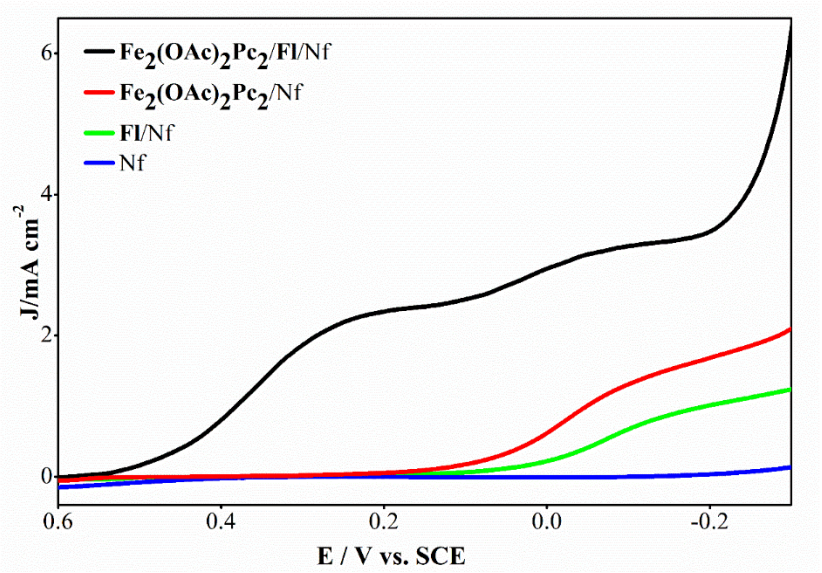

Figure 62 RDE polarization curves recorded with $Fe_2(OAc)_2Pc_2$/Fl/Nf, $Fe_2(OAc)_2Pc_2$/Nf, Fl/Nf, Nf modified glassy carbon electrodes in 0.5 M H_2SO_4 solutionsaturated with O_2 for electro catalytic ORR (Rotation speed: 2500 rpm).

In **Figure 63**, it is clearly seen that catalytic performances of $Fe_2(OAc)_2Pc_2$ **(2b)** and Co_2Pc_2 **(2a)** on VC/Nf/Pc modified rotating (2500 rpm) glassy carbon electrodes towardsORR are much better as compared to those $Mn_2(OAc)_2Pc_2$ **(2c),** Ni_2Pc_2 **(2d)** and Zn_2Pc_2 **(2e).** The limit current densities for $Fe_2(OAc)_2Pc_2$ **(2b)** and Co_2Pc_2 **(2a)** and $Mn_2(OAc)_2Pc_2$ **(2c)** are considerably high. On the contrary, Ni_2Pc_2 **(2d)** and Zn_2Pc_2 **(2e)** have a very low limit current density. In addition, E_o values for $Fe_2(OAc)_2Pc_2$ **(2b)** and Co_2Pc_2 **(2a)** and $Mn_2(OAc)_2Pc_2$ **(2c)** are more positive than those of Ni_2Pc_2 **(2d)** and Zn_2Pc_2 **(2e)**.

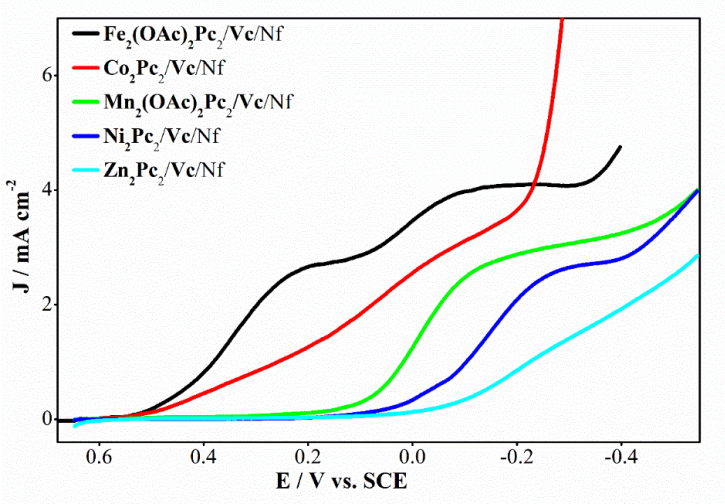

Figure 63 RDE polarization curves recorded with M_2Pc_2/VC/Nf Nf (M= Fe, Co, Mn, Ni and Zn) modified glassy carbon electrodes in 0.5 M H_2SO_4 solution saturated with O_2 for electro catalytic ORR (Rotation speed: 2500 rpm).

The catalytic performances of $Fe_2(OAc)_2Pc_2$ **(2b)** and Co_2Pc_2 **(2a)** and $Mn_2(OAc)_2Pc_2$ **(2c)** on Fl/Nf/Pcmodified rotating (2500 rpm) glassy carbon electrodes towards ORR are much betteras compared to those of Ni_2Pc_2 and Zn_2Pc_2 (**Figure 64).** The limit current densities for $Fe_2(OAc)_2Pc_2$ **(2b)** and Co_2Pc_2 **(2a)** and $Mn_2(OAc)_2Pc_2$ **(2c)** are considerably high. On the contrary, Ni_2Pc_2 **(2d)** and Zn_2Pc_2 **(2e)** have a very low limit current density. In addition, E_o values for $Fe_2(OAc)_2Pc_2$ **(2b)** and Co_2Pc_2 **(2a)** and $Mn_2(OAc)_2Pc_2$ **(2c)** are more positive than those of Ni_2Pc_2 **(2d)** and Zn_2Pc_2 **(2e)**.

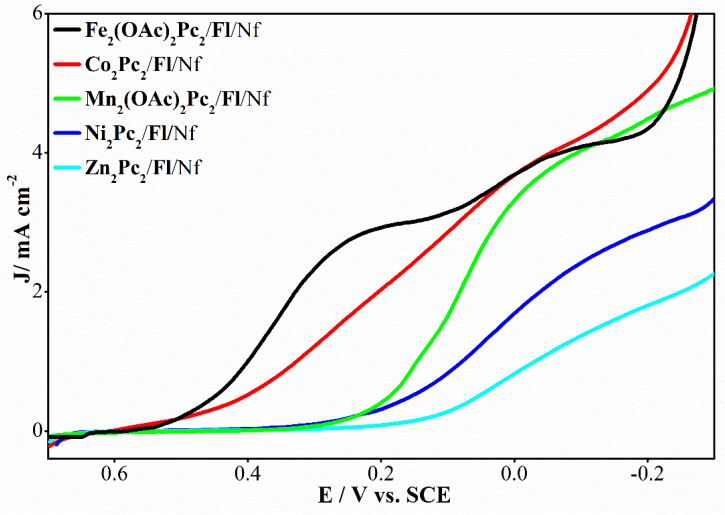

Figure 64 RDE polarization curves recorded with M_2Pc_2/Fl/Nf Nf (M= Fe, Co, Mn, Ni and Zn) modified glassy carbon electrodes in 0.5 M H_2SO_4 solution saturated with O_2 for electro catalytic ORR (Rotation speed: 2500 rpm).

The catalytic performances of $Fe_2(OAc)_2Pc_2$ **(2b)** and Co_2Pc_2 **(2a)** and $Mn_2(OAc)_2Pc_2$ **(2c)** on GO/Nf/Pc, G/Nf/Pc, Tm/Nf/Pc modified rotating (2500 rpm) glassy carbon electrodes towards ORR are much better as compared to those of Ni_2Pc_2 **(2d)** and Zn_2Pc_2 **(2e)**. The limit current densities for $Fe_2(OAc)_2Pc_2$ **(2b)** and Co_2Pc_2 **(2a)** and $Mn_2(OAc)_2Pc_2$ **(2c)** are considerably high. On the contrary, Ni_2Pc_2 **(2d)** and Zn_2Pc_2 **(2e)** have a very low limit current density. In addition, E_o values for $Fe_2(OAc)_2Pc_2$ **(2b)** and Co_2Pc_2 **(2a)** and $Mn_2(OAc)_2Pc_2$ **(2c)** are more positive than those of Ni_2Pc_2 **(2d)** and Zn_2Pc_2 **(2e)**. **(Figure 65).**

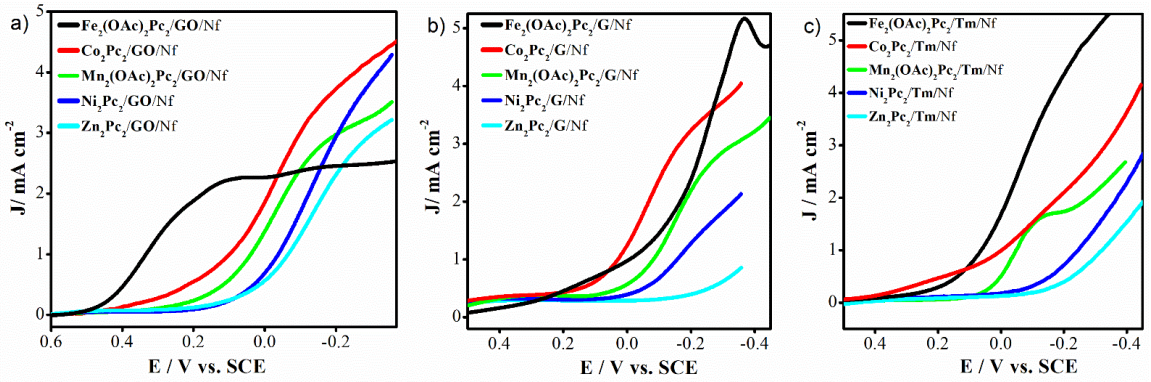

Figure 65 RDE polarization curves recorded with M_2Pc_2/GO/Nf, M_2Pc_2/G/Nf and M_2Pc_2/Tm/Nf, (M= Fe, Co, Mn, Ni and Zn) modified glassy carbon electrodes in 0.5 M H_2SO_4 solution saturated with O_2 for electro catalytic ORR (Rotation speed: 2500 rpm).

It has been proposed by certain scholars that the electro catalytic reduction of oxygen on metallophthalocyanines is facilitated through a redox-catalysis process. In this context, the binding affinity of oxygen and the redox potential of the central metal ions are of paramount importance. The central metal ion within the phthalocyanine ring undergoes oxidation by the adsorbed oxygen molecule, resulting in its subsequent reduction. In contrast, the metal centers found in Ni_2Pc_2 **(2d)** and Zn_2Pc_2 **(2e)** are characterized by their redox inactivity, remaining unaffected by oxidation or reduction during the electro catalytic measurement conditions, as indicated by their recognized electrochemical behavior. Consequently, the enhanced catalytic activity of $Fe_2(OAc)_2Pc_2$ **(2b)** and Co_2Pc_2 **(2a),** relative to other complexes, can be linked to the existence of a redox-active metal center, which is capable of binding dioxygen molecules due to its distinctive coordinating properties.

The relevant cyclic voltammograms for Pt/Vc, $Fe_2(OAc)_2Pc_2$/Vc/Nf and

$Fe_2(OAc)_2Pc_2$/Fl/Nf based catalysts are presented in **Figure 66.** The onset potentials determined during RDE tests on the voltammograms are indicated as arrows to easily establish the relationship between catalytic activity and redoxpotentials, since ORR begins at the onset potentials.

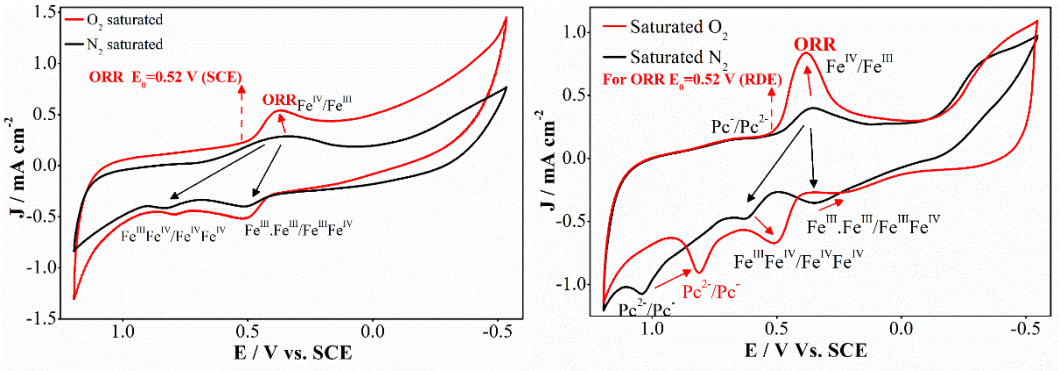

Figure 66 Cyclic voltammograms of the **(A)** $Fe_2(OAc)_2Pc_2$/VC/Nf **(B)** $Fe_2(OAc)_2Pc_2$/Fl/Nf complex adsorbed on glassy carbon electrodes in 0.5 M H_2SO_4, purged with N_2 or saturated with O_2

As expected, mononuclear complex $Fe_2(OAc)_2Pc_2$/Fl/Nf displays an ordinary redox couple which is assigned to a Fe^{III}/Fe^{IV} redox process. $Fe_2(OAc)_2Pc_2$/Fl/Nf catalyst containing mononuclear phthalocyanine complex in saturated N_2 medium showed first Fe^{III}/Fe^{IV} transition in the oxidation direction and then Pc^{2-}/Pc^{-} transition as second oxidation. $Fe_2(OAc)_2Pc_2$/Fl/Nf catalyst showed first Pc^{-}/Pc^{2-} reduction and then Fe^{IV}/Fe^{III} reduction in cathodic scanning. The half-peak potential of Fe^{III}/Fe^{IV} and Fe^{IV}/Fe^{III} redox processes was determined as $E^{1/2}$=0.08 V. In addition, the half-peak potential of Pc^{2-}/Pc^{-} and Pc^{-}/Pc^{2-} redox pairs were obtained with $E^{1/2}$=0.42 V. In the 0.5 M H_2SO_4 solution saturated with O_2, firstly Fe^{III}/Fe^{IV} transition and secondly Pc^{2-}/Pc^{-} transition were observed in the direction of oxidation similar to N_2 environment. While the half-peak potential of Fe^{III}/Fe^{IV} and Fe^{IV}/Fe^{III} redox couples is $E^{1/2}$=0.12 V in the solution medium saturated with O_2, the half-peak potential of Pc^{2-}/Pc^{-} and Pc^{-}/Pc^{2-} redox couples is $E^{1/2}$=0.45 V.

It is necessary to determine the n_t value, and also the contribution of hydrogen peroxide. To determine the influence of hydrogen peroxide production during the ORR on each catalyst, RRDE measurements were executed using a glassy carbon disk electrode modified with VC/Nf/Pc and a platinum ring electrode maintained at 0.95 V versus the (SCE). An example of the RRDE measurement with the $Fe_2(OAc)_2Pc_2$/VC/Nf modified

glassy carbon disk electrode is depicted in **Figure 67.**

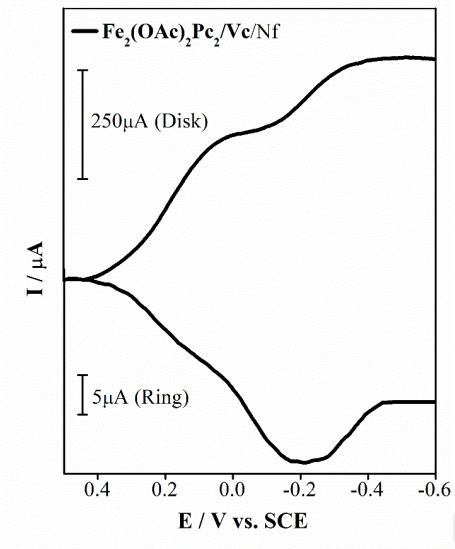

Figure 67 RRDE polarization curves recorded with $Fe_2(OAc)_2Pc_2$/VC/Nf modified rotating (2500 rpm) glassy carbon disc in 0.5 M H_2SO_4 solution saturated with O_2 for electro catalytic ORR (potential scan rate: 0.005 V s^{-1}).

Measurements of the ring currents were conducted to evaluate the volume of hydrogen peroxide generated by each catalyst. It was found that the initiation of the ring currents coincided with the onset potentials for the ORR in the disk, which implies that hydrogen peroxide production is indeed taking place. The characteristic bell-shaped curve of the ring current is associated with hydrogen peroxidegenerated on non-noble metal catalysts and activated carbon.

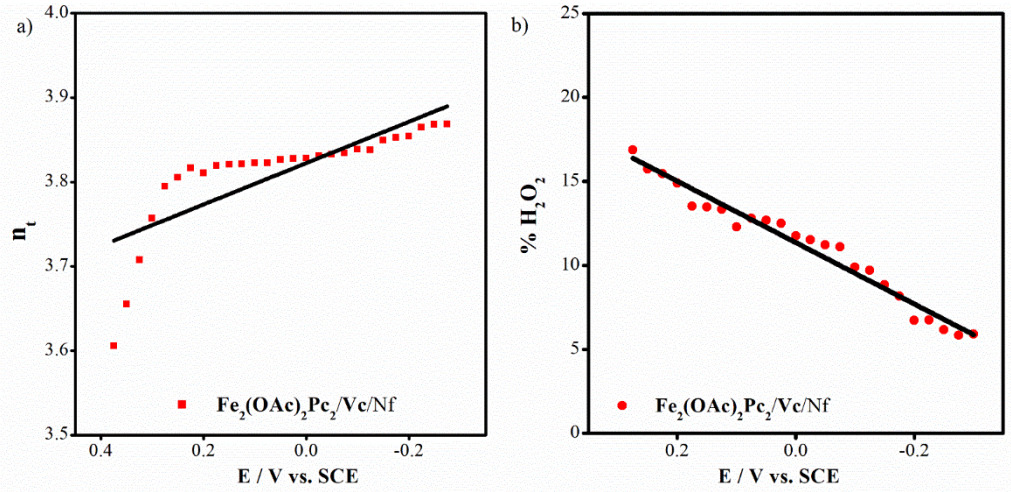

Figure 68 (A) Variation of the total number of electrons transferred with the disk potential for $Fe_2(OAc)_2Pc_2$/VC/Nf modified electrodes **(B)** Variation of the % H_2O_2 formed for $Fe_2(OAc)_2Pc_2$/VC/Nf modified electrode with the

disk potential (according to Ering = 0.95 V vs SCE)

The n_t and the percentage of hydrogen peroxide produced at a given potential were determined by the following equations:

$$n_t = 4\, I_D / [I_D + (I_R/N)] \quad 1.29$$

$$\%H_2O_2 = 100\,(4 - n_t)/2 \quad 1.30$$

where N, I_D, and I_R are the collection efficiency, disk current and ring current, respectively. **Figure 68A and 68B** show the number of electrons and $\%H_2O_2$ generated at different potentials for each catalyst, respectively. The number of total electrons, nt, suggesting that ORR on the $Fe_2(OAc)_2Pc_2$/VC/Nf based electrode produces higher amounts of water compared to hydrogen peroxide. The nt value increases with increasing potential and becomes 3.87 (89% H_2O and 11% H_2O_2) at the limiting diffusion current plateau, leading to the production of water as the main product.

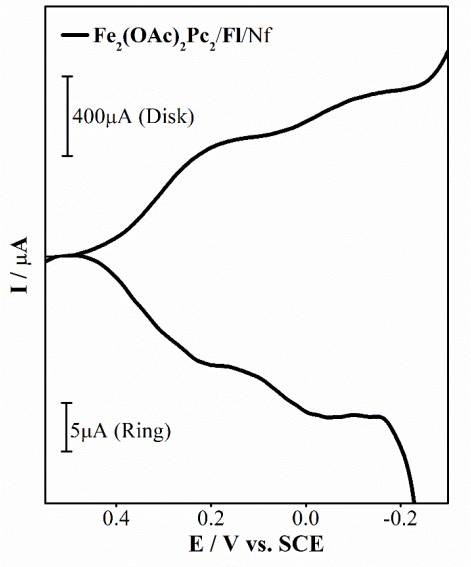

Figure 69 RRDE polarization curves recorded with $Fe_2(OAc)_2Pc_2$/Fl/Nf modified rotating (2500 rpm) glassy carbon disc in 0.5 M H_2SO_4 solution saturated with O_2 for electro catalytic ORR (potential scan rate: 0.005 V s^{-1}).

Figure 70A and 70B show the number of electrons and $\%H_2O_2$ generated at different potentials for each catalyst, respectively. The number of total electrons, n_t, suggesting that ORR on the $Fe_2(OAc)_2Pc_2$/Fl/Nf based electrode produces higher amounts of water compared to hydrogen peroxide. The nt value increases with increasing potential and becomes 3.96 (96% H_2O and 4% H_2O_2) at the limiting diffusion current plateau,

leading to the production of water as the main product.

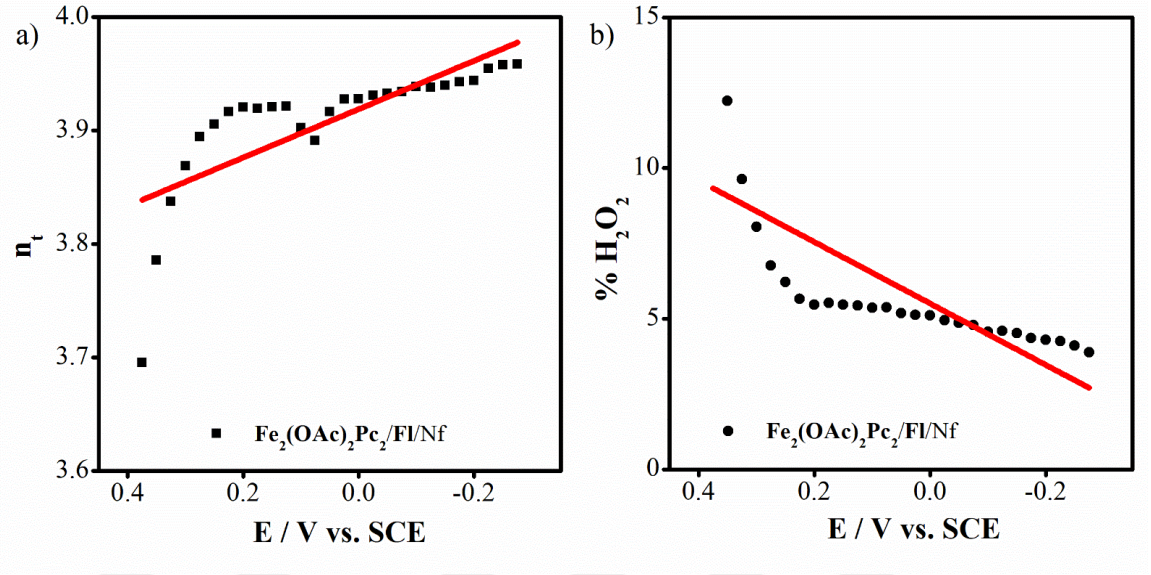

Figure 70 (A) Variation of the total number of electrons transferred with the disk potential for $Fe_2(OAc)_2Pc_2$/Fl/Nf modified electrodes **(B)** Variation of the % H_2O_2 formed for $Fe_2(OAc)_2Pc_2$/Fl/Nf modified electrodes with the disk potential (accordingto Ering = 0.95 V vs SCE)

In the operation of a DMFC, the transfer of methanol from the anode to the cathode can compromise the overall performance of the fuel cell, particularly when platinum is present at the cathode. On the other hand, metal N4 chelates are recognized for their selectivity as catalysts and their ability to withstand the presence of methanol during the ORR.

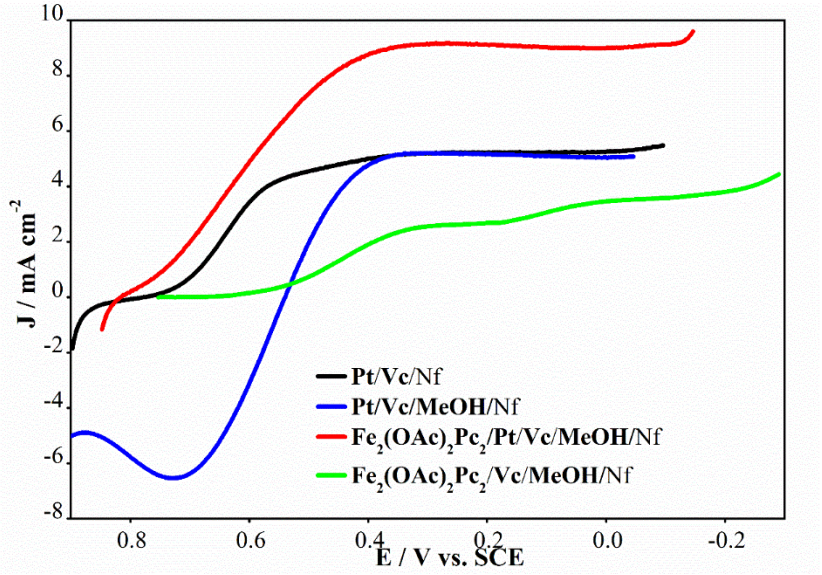

Figure 71 RDE polarization curves recorded with Pt/Vc/Nf, $Fe_2(OAc)_2Pc_2$/Vc/Nf and $Fe_2(OAc)_2Pc_2$/Pt/Vc/Nf modified glassy carbon electrodes in 0.5 M H_2SO_4 solution saturated with O_2 for electro catalytic ORR in the presence and absence of methanol (Rotation speed: 2500 rpm).

Methanol tolerance of $Fe_2(OAc)_2Pc_2$/Vc/Nf based catalyst was also determined and compared with that of Pt-based one. **Figure 71** shows the polarization curves obtainedin O_2 saturated electrolyte in the presence and absence of methanol for the Pt-, $Fe_2(OAc)_2Pc_2$/Vc/Nf and Pt/$Fe_2(OAc)_2Pc_2$/Vc/Nf -based catalysts. Indeed, at a $Fe_2(OAc)_2Pc_2$/Vc/Nf -based electrode, the polarization curve of ORR is not affected by the presence of 1.0 M methanol in the electrolyte. On the contrary of $Fe_2(OAc)_2Pc_2$/Vc/Nf, at a platinum-based electrode, the presence of 1.0 M methanol in the electrolyte leads to a shift in the oxygen reduction potentials towards negative values. Significant methanol oxidation current is observed over a wide range of potential, and thus, the catalytic activity of Pt-based catalyst for ORR is completely blockaded by methanol over the potential range of 0.50–0.80 V vs. SCE. Although the methanol tolerance of the $Fe_2(OAc)_2Pc_2$/Vc/Nf -based catalyst is much better than that of the Pt-based one, unfortunately, ORR on the $Fe_2(OAc)_2Pc_2$/Vc/Nf -based catalyst still occurs at more negative potentials in the presence of methanol, as compared to Pt-based one. In addition, considerable amount of H_2O_2 is produced although the $Fe_2(OAc)_2Pc_2$/Vc/Nf modified electrode catalysts ORR mainly through the four-electron mechanism in high over potentials region. So, the methanol tolerance of Pt/ $Fe_2(OAc)_2Pc_2$/Vc/Nf -based dual catalyst during ORR was also determined and compared with that of Pt-based one. As shown in **Figure 71**, in the presence of

methanol, electro catalytic activity of the Pt/$Fe_2(OAc)_2Pc_2$/Vc/Nf -based dual catalyst is much better than that of the Pt-based one at all potentials. The results of our study indicated that the addition of a suitable $Fe_2(OAc)_2Pc_2$ **(2b)** in a simple manner to Nf and carbon supported platinum results in remarkable enhancement in the methanol tolerance of platinum for ORR, suggesting a good and cost-effective alternative for DMFC applications.

Table 14 Electro catalytic activities of $Fe_2(OAc)_2Pc_2$ (**2b**) complexes for ORR accordingto the parameters of onset potential (E_o), diffusion current density (J_L) and half-wave potential ($E_{1/2}$) (according to SCE).

Catalysts	E_o V (SCE)	J_L/ mA cm^{-2}	$E_{1/2}$ / V (SCE)
$Fe_2(OAc)_2Pc_2$/Fl/Nf	0.54	3.05 (1.19)	0.36 (0.01)
$Fe_2(OAc)_2Pc_2$/Vc/Nf	0.52	2.78 (1.29)	0.34 (0.01)
$Fe_2(OAc)_2Pc_2$/GO/Nf	0.48	2.26 (0.19)	0.31 (-0.08)
$Fe_2(OAc)_2Pc_2$/G/Nf	0.46	0.98 (4.18)	0.18 (-0.24)
$Fe_2(OAc)_2Pc_2$/Tm/Nf	0.37	4.95	-0.05

a The potential at which the current density reaches to 0.100 mA cm-2 was taken as the onset potential, Eo.

Amongst Pc compounds used in this study, $Fe_2(OAc)_2Pc_2$/Fl/Nf and $Fe_2(OAc)_2Pc_2$/Vc/Nf showed remarkable catalytic activity towards ORR in acidic medium. The distinctive catalytic performance of $Fe_2(OAc)_2Pc_2$/Fl/Nf and $Fe_2(OAc)_2Pc_2$/Vc/Nf are attributed to the redox-active behavior of the metal center. It appears that, in the case of a redox-active metal center, the interaction between the metal center and O_2 molecule is enhanced. **Table 14** summarizes the electro catalytic performance of $Fe_2(OAc)_2Pc_2$-based catalysts for ORR.

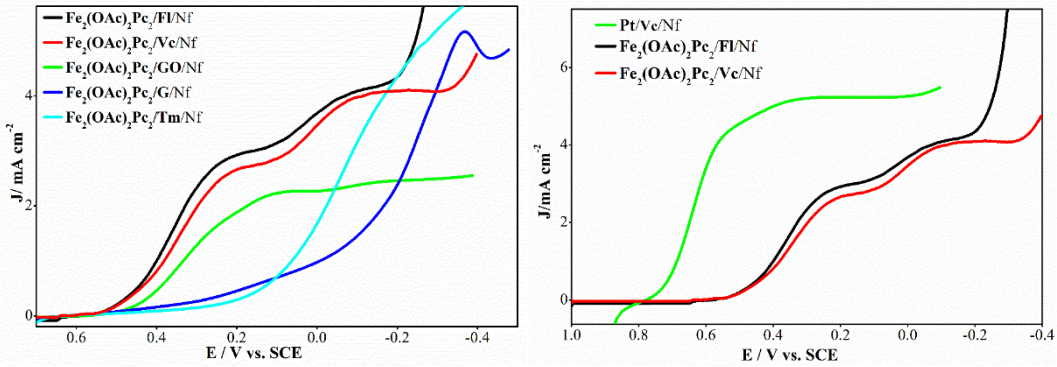

Figure 72 RDE polarization curves of **(A)** $Fe_2(OAc)_2Pc_2$/Vc/Nf, $Fe_2(OAc)_2Pc_2$/Fl/Nf, $Fe_2(OAc)_2Pc_2$/GO/Nf, $Fe_2(OAc)_2Pc_2$/G/Nf and $Fe_2(OAc)_2Pc_2$/Tm/Nf **(B)** Pt/Vc/Nf, $Fe_2(OAc)_2Pc_2$/Vc/Nf ve $Fe_2(OAc)_2Pc_2$/Fl/Nf modified glassy carbon electrodes in 0.5 M H_2SO_4 solution saturated with O_2 for electro catalytic ORR in the presence and absence of methanol (Rotation speed: 2500 rpm).

3.9. Investigation of the electro catalytic performances for Oxygen reduction reaction (ORR) of Ball Type Dinuclear Substituted (2a-2e) complexes in alkali medium

The electro catalytic performances of the complexes in oxygen electro catalysis were measured by CV, RDE and RRDE voltammetry were utilized to measure the electro catalyticactivities of the complexes in the air half-cell in 0.1 M KOH solution.

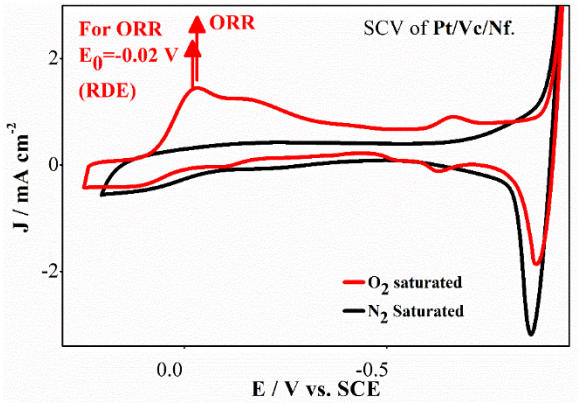

Figure 73 Cyclic voltammograms of the Pt/Vc complex adsorbed on glassy carbon electrodes in 0.1 M KOH, purged with N_2 or saturated with O_2 (scan rate 5 mVs^{-1})

The initial evaluation of the electro catalytic performance of the Pt/C and $Fe_2(OAc)_2Pc_2$ complexes for the ORR was conducted through CV. The cyclic voltammograms for the electrodes modified with Pt/C and $Fe_2(OAc)_2Pc_2$ **(2b)** (**Figures 73** and **74**) were recorded in 0.1 M KOH solutions that were saturated with N_2 or O_2, utilizing a scan rate

of 5 mV/s. The peak currents associated with the ORR in the voltammograms indicate that the $Fe_2(OAc)_2Pc_2$ **(2b)** complex exhibits a strong interaction with molecular oxygen, driven by the redox-active properties of the Fe^{2+} core. Furthermore, a detailed comparison of the voltammograms for the $Fe_2(OAc)_2Pc_2$ **(2b)** complex in both nitrogen- and oxygen-saturated solutions reveals that the oxidation process near -0.20 V is reversible and coincides with the O_2 molecule's signal. Additionally, during the low positive potential redox transition from Fe(III) to Fe(IV), the highly acidic Fe(IV) species effectively interact with dioxygen, resulting in a relatively low over potential for the ORR, RDE was utilized to measure the electro catalytic ORR activities of the catalyst **(Figure 75**). The ORR polarization curves for each catalyst were obtained at a rotation speed of 2500 rpm and a scan rate of 5 mV/s in oxygen-saturated 0.1 M KOH solutions. The onset potential (E_o), defined as the point at which the current begins to rise, along with the J_L, were utilized as indicators of catalytic activity. The potential corresponding to a current density of 0.100 mA cm^{-2} was designated as E_o. **Table 15** presents a summary of the electro catalytic performance of MPc-based catalysts for ORR. The findings clearly demonstrate that the catalytic activity of the complexes $Fe_2(OAc)_2Pc_2$ **(2b),** Co_2Pc_2 **(2a)** and $Mn_2(OAc)_2Pc_2$ **(2c)** significantly surpasses that of Ni_2Pc_2 **(2d)** and Zn_2Pc_2 **(2e).**

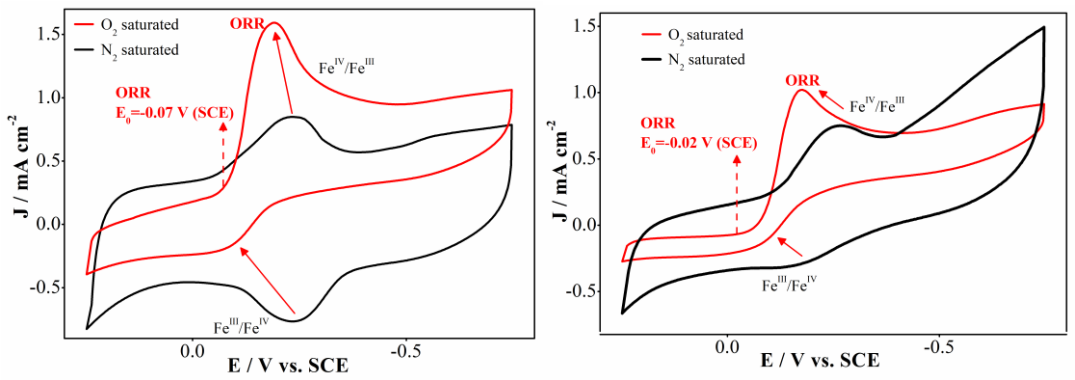

Figure 74 Cyclic voltammograms of the **(A)** $Fe_2(OAc)_2Pc_2$/Vc/Nf **(B)** $Fe_2(OAc)_2Pc_2$/Fl/Nf complex adsorbed on glassy carbon electrodes in 0.1 M KOH, purged with N_2 or saturated with O_2 (scan rate 5 mVs^{-1}).

Table 15 Electro catalytic activities of (**2a-2e**) complexes for ORR according to the parameters of onset potential (E_o), diffusion current density (J_L) and half-wave potential ($E_{1/2}$) (according to SCE).

Catalysts	**E_oV (vs. SCE)**	**J_L / mA cm^{-2}**	**$E_{1/2}$ /(vs. SCE)**
$Fe_2(OAc)_2Pc_2$/Vc/Nf	-0.07	7.40	-0.20
Co_2Pc_2/Vc/Nf	-0.09	5.30	-0.23
$Mn_2(OAc)_2Pc_2$/Vc/Nf	-0.10	5.62	-0.28
Ni_2Pc_2/Vc/Nf	-0.17	2.11	-0.29
Zn_2Pc_2/Vc/Nf	-0.15	3.49	-0.34
$Fe_2(OAc)_2Pc_2$/Fl/Nf	-0.02	6.74	-0.17
Co_2Pc_2/Fl/Nf	-0.05	4.31	-0.18
$Mn_2(OAc)_2Pc_2$/Fl/Nf	-0.08	5.63	-0.21
Ni_2Pc_2/Fl/Nf	-0.08	4.28	-0.23
Zn_2Pc_2/Fl/Nf	-0.15	4.81	-0.30
$Fe_2(OAc)_2Pc_2$/GO/Nf	-0.06	3.28	-0.22
Co_2Pc_2/GO/Nf	-0.10	3.80	-0.24
$Mn_2(OAc)_2Pc_2$/GO/Nf	-0.12	1.63	-0.24
Zn_2Pc_2/GO/Nf	-0.10	2.73	-0.32
$Fe_2(OAc)_2Pc_2$/G/Nf	-0.07	2.16	-0.28
Co_2Pc_2/G/Nf	-0.16	1.13	-0.28
$Mn_2(OAc)_2Pc_2$/G/Nf	-0.23	1.29	-0.32
Zn_2Pc_2/G/Nf	-0.26	2.69	-0.43
$Fe_2(OAc)_2Pc_2$/Tm/Nf	-0.16	4.95	-0.28
Co_2Pc_2/Tm/Nf	-0.06	3.57	-0.30
$Mn_2(OAc)_2Pc_2$/Tm/Nf	-0.12	3.25	-0.35
Ni_2Pc_2/Tm/Nf	-0.21	1.59	-0.33
Zn_2Pc_2/Tm/Nf	-0.26	1.91	-0.39

In order to evaluate the ORR activity, RDE tests of carbon samples in O_2 saturated and 0.1 M KOH electrolyte, under a rotation rate of 2500 rpm were performed at scan rateof 5 mV $s^{-1.}$

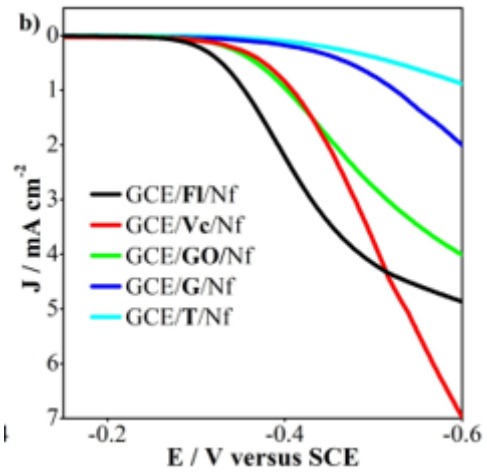

Figure 75 RDE voltammograms recorded with Vc/Nf, Fl/Nf, GO/Nf, G/Nf ve Tm/Nf modified glassy carbon electrodes in 0.1 M KOH solution for electro catalytic ORR (rotation speed 2500rpm)

By comparison, the redox active and redox inactive metals had also been tested under the same test conditions, as shown **Figure 76**. Obviously, the ORR activities of the $Fe_2(OAc)_2Pc_2$/Vc/Nf, Co_2Pc_2/Vc/Nf and $Mn_2(OAc)_2Pc_2$/Vc/Nf are much higher than those of Ni_2Pc_2/Vc/Nf and Zn_2Pc_2/Vc/Nf in the whole process of cathodic oxygen reduction, the ORR values of current densities for $Fe_2(OAc)_2Pc_2$/Vc/Nf, Co_2Pc_2/Vc/Nf and $Mn_2(OAc)_2Pc_2$/Vc/Nf at the all potentials are larger than those Ni_2Pc_2/Vc/Nf and Zn_2Pc_2/Vc/Nf. The J_L (5.77 $mAcm^{-2}$) of the $Fe_2(OAc)_2Pc_2$/Nf is larger than those of Co_2Pc_2/Vc/Nf (2.34 mA cm^{-2}), Ni_2Pc_2/Vc/Nf (2.00 mA cm^{-2}) and Zn_2Pc_2/Vc/Nf (1,02 mA cm^{-2}). Moreover, the E_0 and $E_{1/2}$ of the $Fe_2(OAc)_2Pc_2$/Vc/Nf complex are -0.09 V and -0.25 V, respectively. These values of the $Fe_2(OAc)_2Pc_2$ /Vc/Nf complex are nearly equal to those of Pt/C catalyst (E_0 =-0.02V and $E_{1/2}$ =-0.17 V, respectively).

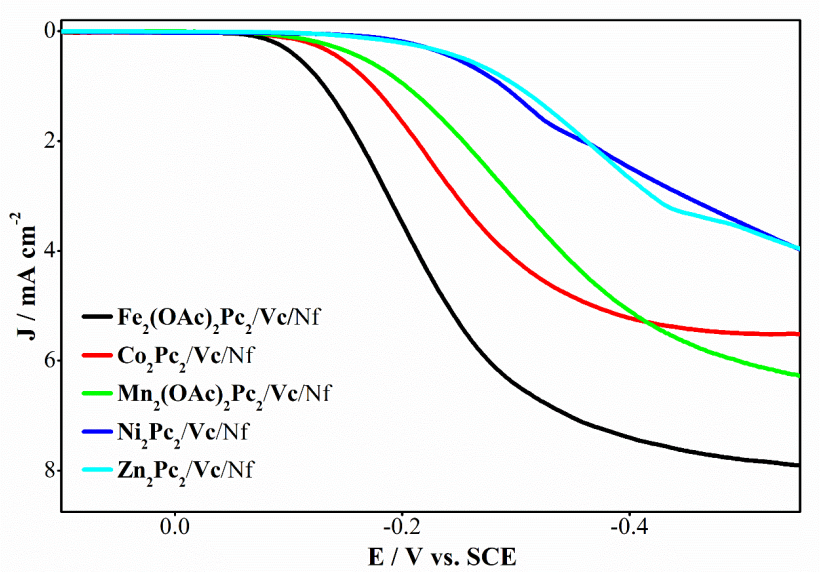

Figure 76 RDE voltammograms recorded with $Fe_2(OAc)_2Pc_2$ (**2b**), Co_2Pc_2 (**2a**) and $Mn_2(OAc)_2Pc_2$ (**2c**) Ni_2Pc_2 (**2d**) ve Zn_2Pc_2 (**2e**) modified glassy carbon electrodes in 0.1 M KOH solution for electro catalytic ORR (rotation speed 2500rpm).

ORR activity of these $Fe_2(OAc)_2Pc_2$/Fl/Nf, Co_2Pc_2/Fl/Nf, $Mn_2(OAc)_2Pc_2$/Fl/Nf and Ni_2Pc_2/Fl/Nf were evaluated in 0.1 M KOH aqueous solution. The half-wave potential ($E_{1/2}$) of $Fe_2(OAc)_2Pc_2$/Fl/Nf positively shifts 20 mV compared to that of Ni_2Pc_2/Fl/Nf and the current density of $Fe_2(OAc)_2Pc_2$/Fl/Nf at 5.84 V (vs. SCE) is much higher than that of Ni_2Pc_2/Fl/Nf (**Figure 77** and **Table 15**). **Figure 77** shows that $Fe_2(OAc)_2Pc_2$/Fl/Nf possesses an onset potential of -0.10 V (vs. SCE), superior to that of Ni_2Pc_2/Fl/Nf (-0.19 V vs. SCE).

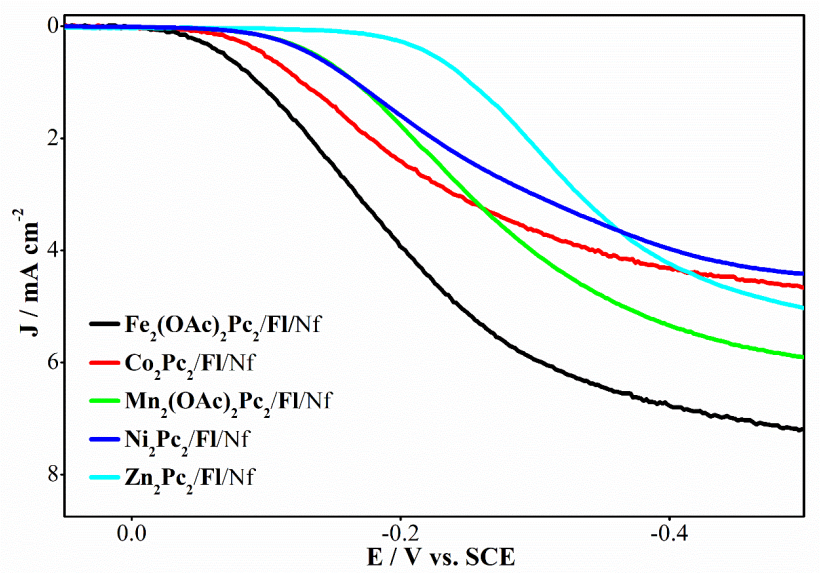

Figure 77 RDE voltammograms recorded with $Fe_2(OAc)_2Pc_2$ (**2b**), Co_2Pc_2 (**2a**) and $Mn_2(OAc)_2Pc_2$ (**2c**) Ni_2Pc_2 (**2d**) ve Zn_2Pc_2 (**2e**) modified glassy carbon electrodes in 0.1 M KOH solution for electro catalytic ORR (rotation speed 2500rpm).

By comparison, the redox active and redox inactive metals have also been tested under the same test conditions, as shown Figure 77. Obviously, the ORR activities of the $Fe_2(OAc)_2Pc_2$/GO/Nf, $Fe_2(OAc)_2Pc_2$/G/Nf and $Fe_2(OAc)_2Pc_2$/Tm/Nf are much higher than those of Ni_2Pc_2/GO/Nf, Zn_2Pc_2/GO/Nf, Ni_2Pc_2/G/Nf, Zn_2Pc_2/G/Nf and Ni_2Pc_2/Tm/Nf, Zn_2Pc_2/Tm/Nf in the whole process of cathodic oxygen reduction, the ORR values of current densities for $Fe_2(OAc)_2Pc_2$/GO/Nf, Co_2Pc_2/GO/Nf and $Mn_2(OAc)_2Pc_2$/GO/Nf at the all potentials are larger than those Ni_2Pc_2/GO/Nf and Zn_2Pc_2/GO/Nf. The J_L (3.80 mA cm^{-2}) of the $Fe_2(OAc)_2Pc_2$/GO/Nf is larger than those of Co_2Pc_2/GO/Nf (2.49 mA cm^{-2}), Ni_2Pc_2/GO/Nf (2.92 mA cm_{-2}) and Zn_2Pc_2/GO/Nf (2.26 mA cm-^{2}). Moreover, the E_0 and $E_{1/2}$ of the $Fe_2(OAc)_2Pc_2$/GO/Nf complex are -0.11 V and -0.25 V, respectively. These values of the $Fe_2(OAc)_2Pc_2$/GO/Nf complex are nearly equal to those of $Fe_2(OAc)_2Pc_2$/G/Nf catalyst (E_0=-0.13V and $E_{1/2}$ =-0.30 V, respectively).

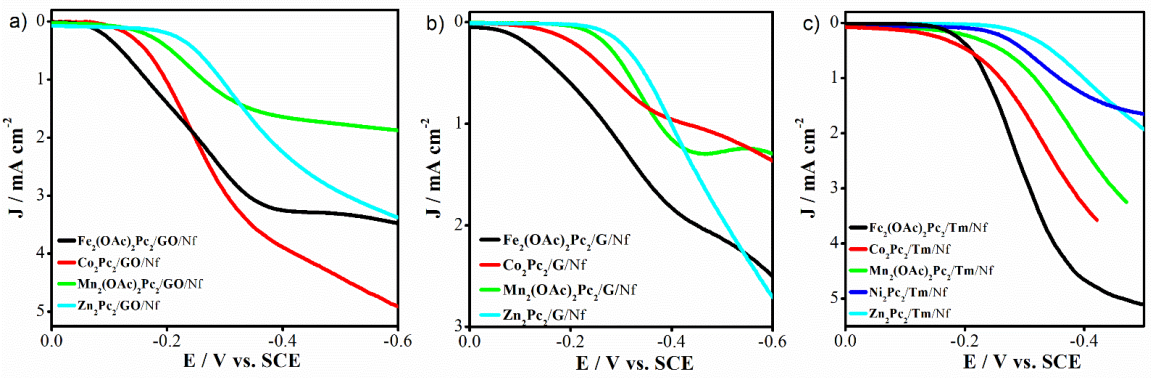

Figure 78 RDE voltammograms recorded with **(A)** M_2Pc_2/GO/Nf catalyst materials **(B)** M_2Pc_2/G/Nf catalyst materials **(C)** M_2Pc_2/Tm/Nf (M= $Fe_2(OAc)_2Pc_2$ (**2b**), Co_2Pc_2 (**2a**), $Mn_2(OAc)_2Pc_2$ (**2c**) Ni_2Pc_2 (**2d**) ve Zn_2Pc_2 (**2e**))modified glassy carbon electrodes in 0.1 M KOH solution for electro catalyticORR (rotation speed 2500rpm).

Table 16 Electro catalytic activities of (**2a-2e**) complexes for ORR according to the parameters of onset potential (E_o), diffusion current density (J_L) and half-wave potential ($E_{1/2}$) (according to SCE).

Catalysts	**E_oV (vs. SCE)**	**J_L / mA cm^{-2}**	**$E_{1/2}$ / V (vs. SCE)**
$Fe_2(OAc)_2Pc_2$/Fl/Nf	-0.02	6.74	-0.17
$Fe_2(OAc)_2Pc_2$/Vc/Nf	-0.07	7.40	-0.20
$Fe_2(OAc)_2Pc_2$/GO/N	-0.06	3.28	-0.22
$Fe_2(OAc)_2Pc_2$/G/Nf	-0.07	2.16	-0.28
$Fe_2(OAc)_2Pc_2$/Tm/Nf	-0.16	4.95	-0.28

To further examine the ORR electro catalytic activity of the catalysts, RDE curves of $Fe_2(OAc)_2Pc_2$/Vc/Nf, $Fe_2(OAc)_2Pc_2$/Fl/Nf, $Fe_2(OAc)_2Pc_2$/GO/Nf, $Fe_2(OAc)_2Pc_2$/G/Nf and $Fe_2(OAc)_2Pc_2$/Tm/Nf catalysts were performed as presented in **Figure 79**. The onset and half-wave potentials for $Fe_2(OAc)_2Pc_2$/Fl/Nf (-0.10 V and -0.23 V) were close to that for $Fe_2(OAc)_2Pc_2$/Vc/Nf (-0.09 V and -0.25 V), and more positive than that for $Fe_2(OAc)_2Pc_2$/GO/Nf, $Fe_2(OAc)_2Pc_2$/G/Nf and $Fe_2(OAc)_2Pc_2$/Tm/Nf indicating that $Fe_2(OAc)_2Pc_2$/Fl/Nf possesses a highly efficient ORR electro catalytic activity.

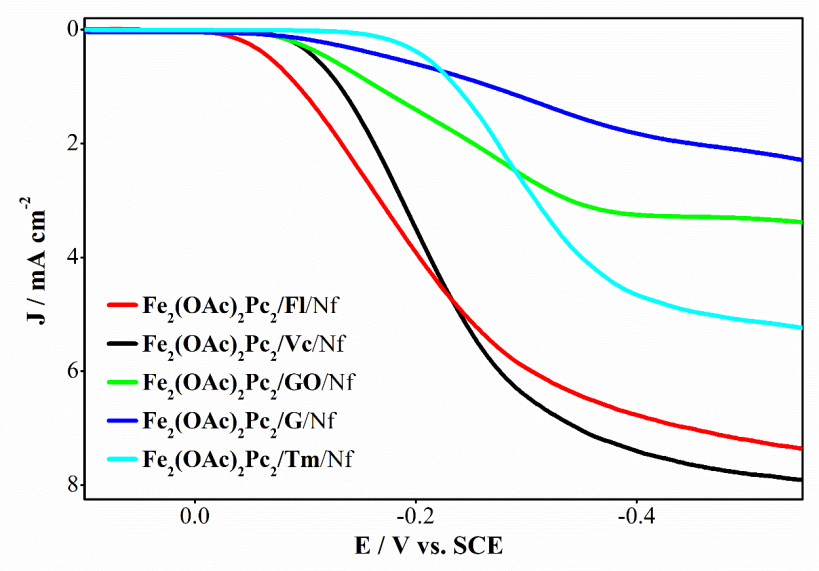

Figure 79 RDE voltammograms recorded with $Fe_2(OAc)_2Pc_2$/VC/Nf, $Fe_2(OAc)_2Pc_2$/Fl/Nf, $Fe_2(OAc)_2Pc_2$/GO/Nf, $Fe_2(OAc)_2Pc_2$/G/Nf and $Fe_2(OAc)_2Pc_2$/Tm/Nf) modified glassy carbon electrodes in 0.1 M KOH solution for electro catalytic ORR (rotation speed 2500rpm).

To further examine the ORR electro catalytic activity of the catalysts, RDE curves of $Fe_2(OAc)_2Pc_2$/Fl/Nf, $Fe_2(OAc)_2Pc_2$/VC/Nf and Pt/C/Nf catalysts were performed as presented in **Figure 80**. The onset and half-wave potentials for $Fe_2(OAc)_2Pc_2$/Fl/Nf (-0.10 V and -0.23 V) were close to that for benchmark Pt/C (-0.02 V and -0.17 V), and more positive than that for $Fe_2(OAc)_2Pc_2$/Vc/Nf, indicating that $Fe_2(OAc)_2Pc_2$/Fl/Nf possesses a highly efficient ORR electro catalytic activity.

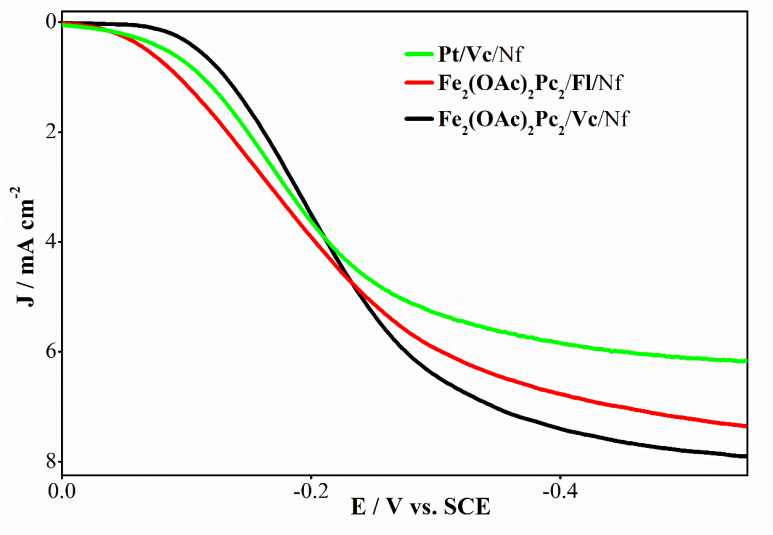

Figure 80 RDE voltammograms recorded with Pt/Vc/Nf, $Fe_2(OAc)_2Pc_2$/VC/Nf and $Fe_2(OAc)_2Pc_2$/Fl/Nf modified glassy carbon electrodes in 0.1 M KOH solution for electro catalyticORR (rotation speed 2500rpm).

3.10. Investigation of the electro catalytic performances for Oxygen evolution reaction (OER) of Ball Type Dinuclear Substituted (2a-2e) compounds in alkali medium

In order to evaluate the OER activity, RDE tests of carbon samples in O_2 saturated and 0.1 M KOH electrolyte, under a rotation rate of 2500 rpm were performed at scan rate of 5 mV s^{-1}.

Table 17 Electro catalytic OER performances of catalyst materials.

Catalysts	**E_0 V (vs. SCE)**	**J / mA cm^{-2}**
$Fe_2(OAc)_2Pc_2$/Vc/Nf	0.37	3.91
Co_2Pc_2/Vc/Nf	0.37	1.87
$Mn_2(OAc)_2Pc_2$/Vc/Nf	0.34	0.82
Ni_2Pc_2/Vc/Nf	0.53	0.40
Zn_2Pc_2/Vc/Nf	0.55	0.42
$Fe_2(OAc)_2Pc_2$/Fl/Nf	0.43	8.74
Co_2Pc_2/Fl/Nf	0.27	5.28
$Mn_2(OAc)_2Pc_2$/Fl/Nf	0.28	4.73
Ni_2Pc_2/Fl/Nf	0.32	3.56
Zn_2Pc_2/Fl/Nf	0.48	2.87

By comparison, the redox active and redox inactive metals had also been tested under the same test conditions, as shown **Figure 81**. Obviously, the OER activities of the $Fe_2(OAc)_2Pc_2$/Vc/Nf, Co_2Pc_2/Vc/Nf and $Mn_2(OAc)_2Pc_2$/Vc/Nf are much higher than those of Ni_2Pc_2/Vc/Nf and Zn_2Pc_2/Vc/Nf in the whole process of cathodic oxygen oxidation, the OER values of current densities for $Fe_2(OAc)_2Pc_2$/Vc/Nf, Co_2Pc_2/Vc/Nf and $Mn_2(OAc)_2Pc_2$/Vc/Nf at the all potentials are larger than those Ni_2Pc_2/Vc/Nf and Zn_2Pc_2/Vc/Nf. The J_L value (3.99 mA cm^{-2}) of the $Fe_2(OAc)_2Pc_2$/Vc/Nf is larger than those of Co_2Pc_2/Vc/Nf (1.87 mA cm^{-2}), Ni_2Pc_2/Vc/Nf (0.40 mA cm^{-2}) and Zn_2Pc_2/Vc/Nf(0.42 mA cm^{-2}). Moreover, the E_0 of the $Fe_2(OAc)_2Pc_2$/Vc/Nf complex is 0.37 V.

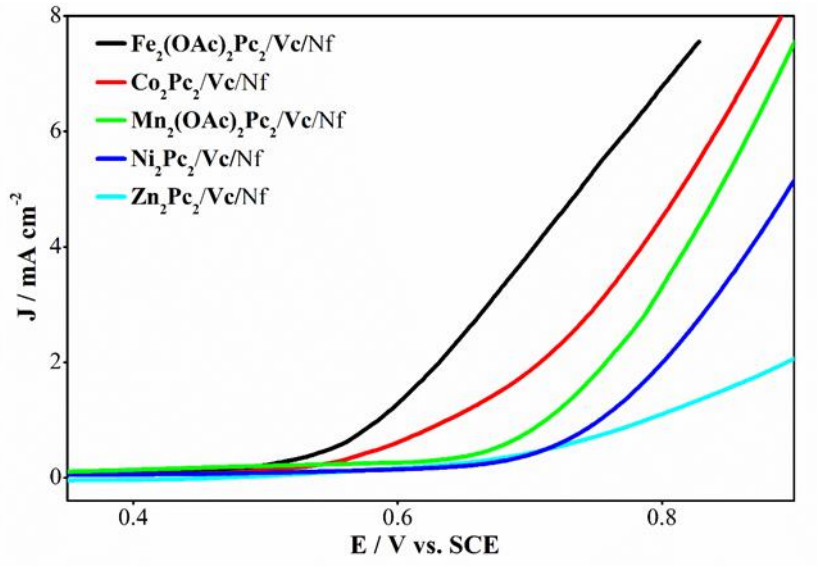

Figure 81 RDE voltammograms recorded with M_2Pc_2/Vc/Nf (M= $Fe_2(OAc)_2Pc_2$ (**2b**), Co_2Pc_2 (**2a**) $Mn_2(OAc)_2Pc_2$ (**2c**), Ni_2Pc_2 (**2d**) ve Zn_2Pc_2 (**2e**)modified glassy carbon electrodes in 0.1 M KOH solution for electro catalytic OER (Rotation speed: 2500 rpm).

OER activity of these $Fe_2(OAc)_2Pc_2$/Fl/Nf, Co_2Pc_2/Fl/Nf, $Mn_2(OAc)_2Pc_2$/Fl/Nf and Zn_2Pc_2/Fl/Nf were evaluated in 0.1 M KOH aqueous solution. (**Figure 82** and **Table 17**). The OER activities of the $Fe_2(OAc)_2Pc_2$/Fl/Nf, Co_2Pc_2/Fl/Nf and $Mn_2(OAc)_2Pc_2$/Fl/Nf are much higher than those of Ni_2Pc_2/ Fl /Nf and Zn_2Pc_2/ Fl /Nf in the whole process of cathodic oxygen oxidation, the OER values of current densities for $Fe_2(OAc)_2Pc_2$/Fl/Nf, Co_2Pc_2/ Fl /Nf and $Mn_2(OAc)_2Pc_2$/Fl /Nf at the all potentials are larger than those Ni_2Pc_2/Fl/Nf and Zn_2Pc_2/Fl/Nf. The J_L value (8.74 mA cm^{-2}) of the $Fe_2(OAc)_2Pc_2$/Fl/Nf is larger than those of Co_2Pc_2/Fl/Nf (5.28 mA cm^{-2}), Ni_2Pc_2/ Fl/Nf (3.56 mA cm^{-2}) and Zn_2Pc_2/Fl/Nf (2.87 mA cm^{-2}). Moreover, the E_0 of the $Fe_2(OAc)_2Pc_2$/ Fl /Nf complex is 0.43 V.

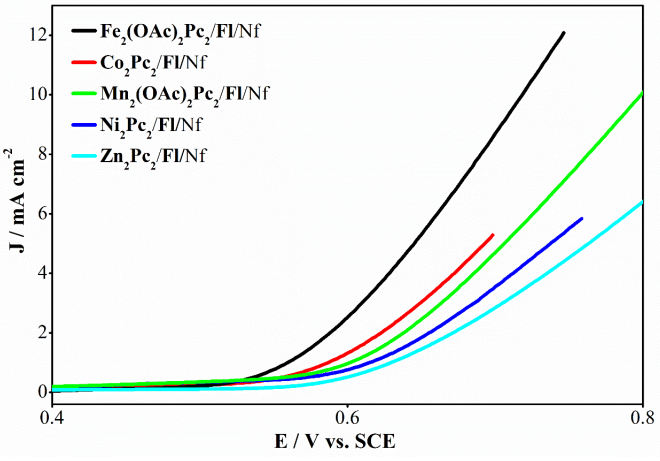

Figure 82 RDE voltammograms recorded with M_2Pc_2/Vc/Nf (M= $Fe_2(OAc)_2Pc_2$ (**2b**), Co_2Pc_2 (**2a**), $Mn_2(OAc)_2Pc_2$ (**2c**) Ni_2Pc_2 (**2d**) ve Zn_2Pc_2 (**2e**)) modified glassy carbon electrodes in 0.1 M KOH solution for electro catalytic OER (Rotation speed: 2500 rpm).

Table 18 Electro catalytic OER performances of catalyst materials.

Catalysts	E_o V (vs. SCE)	J / mA cm^{-2}
$Fe_2(OAc)_2Pc_2$/Fl/Nf	0.43	8.74
$Fe_2(OAc)_2Pc_2$/Vc/Nf	0.37	3.91
$Fe_2(OAc)_2Pc_2$/GO/Nf	0.55	3.56
$Fe_2(OAc)_2Pc_2$/G/Nf	0.53	2.15
$Fe_2(OAc)_2Pc_2$/Tm/Nf	0.52	0.71

To further examine the OER electro catalytic activity of the catalysts, RDE curves of $Fe_2(OAc)_2Pc_2$/Vc/Nf, $Fe_2(OAc)_2Pc_2$/Fl/Nf, $Fe_2(OAc)_2Pc_2$/GO/Nf, $Fe_2(OAc)_2Pc_2$/G/Nf and $Fe_2(OAc)_2Pc_2$/Tm/Nf catalysts were performed as presented in **Figure 83**. The onset potentials for $Fe_2(OAc)_2Pc_2$/Fl/Nf (0.43V) was close to that for $Fe_2(OAc)_2Pc_2$/Vc/Nf (0.37 V), and more positive than that for $Fe_2(OAc)_2Pc_2$/GO/Nf, $Fe_2(OAc)_2Pc_2$/G/Nf and $Fe_2(OAc)_2Pc_2$/Tm/Nf indicating that $Fe_2(OAc)_2Pc_2$/Fl/Nf possesses a highly efficient OER electro catalytic activity.

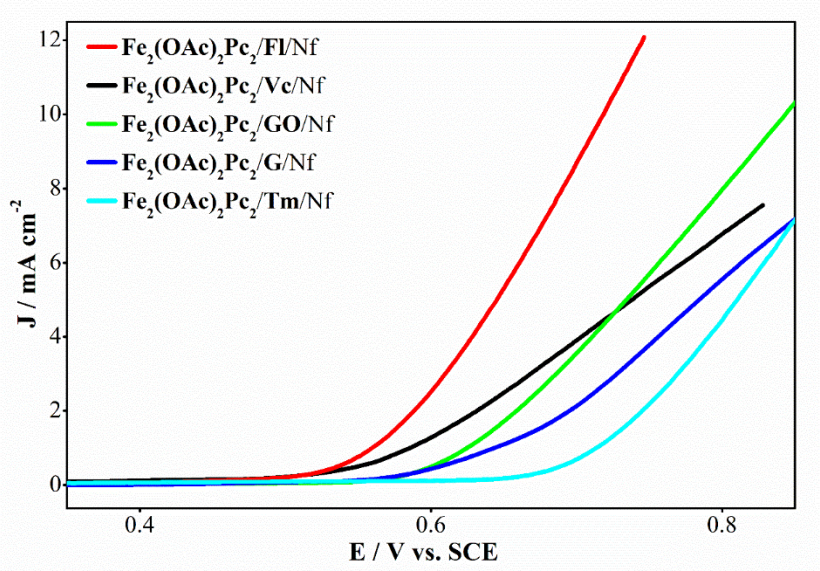

Figure 83 RDE voltammograms recorded with $Fe_2(OAc)_2Pc_2$/VC/Nf, $Fe_2(OAc)_2Pc_2$/Fl/Nf, $Fe_2(OAc)_2Pc_2$/GO/Nf, $Fe_2(OAc)_2Pc_2$/G/Nf and $Fe_2(OAc)_2Pc_2$/Tm/Nf modified glassy carbon electrodes in 0.1 M KOH solution for electro catalytic OER (Rotation speed: 2500 rpm).

In **Figure 84**, RDE recorded in O2 saturated 0.1M KOH solution for electro catalytic

OERof IrO_2/Nf, Pt/Vc/Nf, $Fe_2(OAc)_2Pc_2$/Fl/Nf and $Fe_2(OAc)_2Pc_2$/Vc/Nf catalysts. The current density J values of IrO_2/Nf, Pt/Vc/Nf and $Fe_2(OAc)_2Pc_2$/Fl/Nf catalysts at E=0.70 V are higher than $Fe_2(OAc)_2Pc_2$/Vc/Nf catalysts. It can be seen in **Figure 84.** current density of $Fe_2(OAc)_2Pc_2$/Fl/Nf catalyst at E=0.70 V in 0.1M KOH solution saturated with O_2 in an environment similar to Zinc Air battery operating conditions for OER J=8.74 mA cm^{-2} belonging to Pt/Vc/Nf catalyst It is seen that it is better than J=6.05 mA cm^{-2}. The J=10.35 mA cm^{-2} value of the IrO_2/Nf catalyst is quite good. Among the catalysts containing ball type dinuclear structure, the catalyst closest to the current density of the IrO_2/Nf catalyst is the $Fe_2(OAc)_2Pc_2$/F1/Nf catalyst. The more negative starting potential of the $Fe_2(OAc)_2Pc_2$/Vc/Nf catalyst isE_o=0.37 V, the E_o=0.43 V of the $Fe_2(OAc)_2Pc_2$/Fl/Nf catalyst and the E_o=0.49 V of the Pt/Vc/Nf catalyst is more negative. However, the $Fe_2(OAc)_2Pc_2$/Vc/Nf catalyst is more positive than the E_o=0.15 V value of the IrO_2/Nf catalyst, but it is the catalyst containing the ball type dinuclear structure with the closest value to the IrO_2/Nf catalyst in this parameter (**Table 19**).

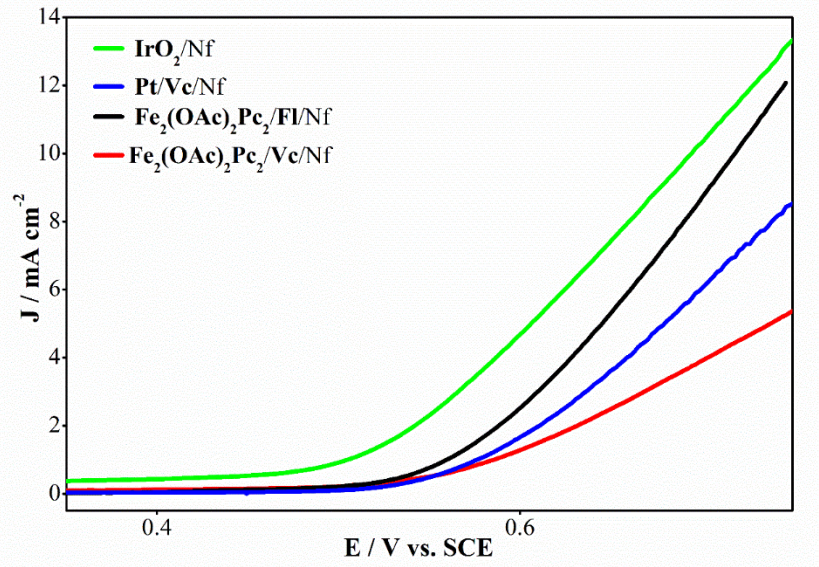

Figure 84 RDE voltammograms recorded with IrO_2/Nf, Pt/Vc/Nf, $Fe_2(OAc)_2Pc_2$/VC/Nf and $Fe_2(OAc)_2Pc_2$/Fl/Nf modified glassy carbon electrodes in 0.1M KOH solution for electro catalytic OER (Rotation speed: 2500 rpm).

Table 19 Electro catalytic OER performances of catalyst materials.

Catalysts	E_o V (vs. SCE)	J / mA cm^{-2}
IrO_2/Nf	0.15	10.35
Pt/Vc/Nf	0.49	6.05

$Fe_2(OAc)_2Pc_2$/Vc/Nf	0.37	3.91
$Fe_2(OAc)_2Pc_2$/Fl/Nf	0.43	8.74

The $Fe_2(OAc)_2Pc_2$/Fl/Nf and $Fe_2(OAc)_2Pc_2$/Fl/Nf catalysts suggest a good and inexpensive alternative catalysts for Zinc Air battery applications.

3.11. SEM, XPS and EDS spectrum of Dinuclear Substituted $Fe_2(OAc)_2Pc_2$ compound

Figure 85(A-C) shows the SEM images of VC, $Fe_2(OAc)_2Pc_2$ (**2b**) and $Fe_2(OAc)_2Pc_2$/Vc/Nf. **Figure 85A** and **85B** indicate that the particle sizes of catalyst active material VC and $Fe_2(OAc)_2Pc_2$ (**2b**) are different to each other. SEM, as well as other complementary techniques such as EDS, provided evidence of the formation of molecular materials in a micro-scale that can be extrapolated to typical electro synthesis cells in order to obtain larger amounts of these materials. On the other hand, it appears that $Fe_2(OAc)_2Pc_2$ (**2b**) complex dispersed homogeneously in the carbon-based supporting material.

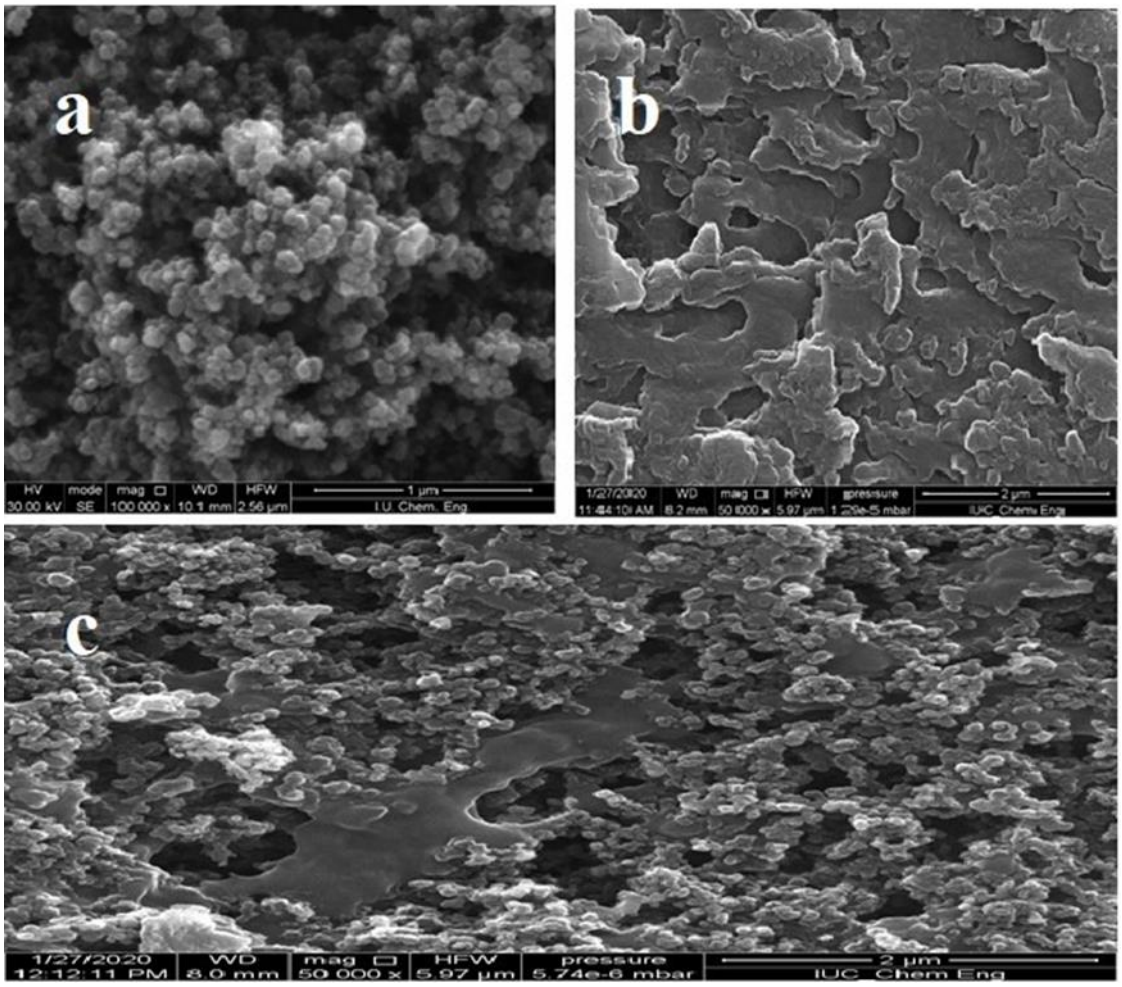

Figure 85 SEM images of **(A)** Vc **(B)** $Fe_2(OAc)_2Pc_2$ **(2b)** **(C)** $Fe_2(OAc)_2Pc_2$/Vc

Figure 86A and **86B** showed the EDS mapping images of $Fe_2(OAc)_2Pc_2$ (**2b**) with the uniform distribution of C, N, O and Fe elements on the surface, which indicated that the $Fe_2(OAc)_2Pc_2$ (**2b**) particles uniformly covered the surface. Homogeneous distribution of the catalyst active and conductive carbon materials is expected to have a positive effect on their catalytic performance in this study.

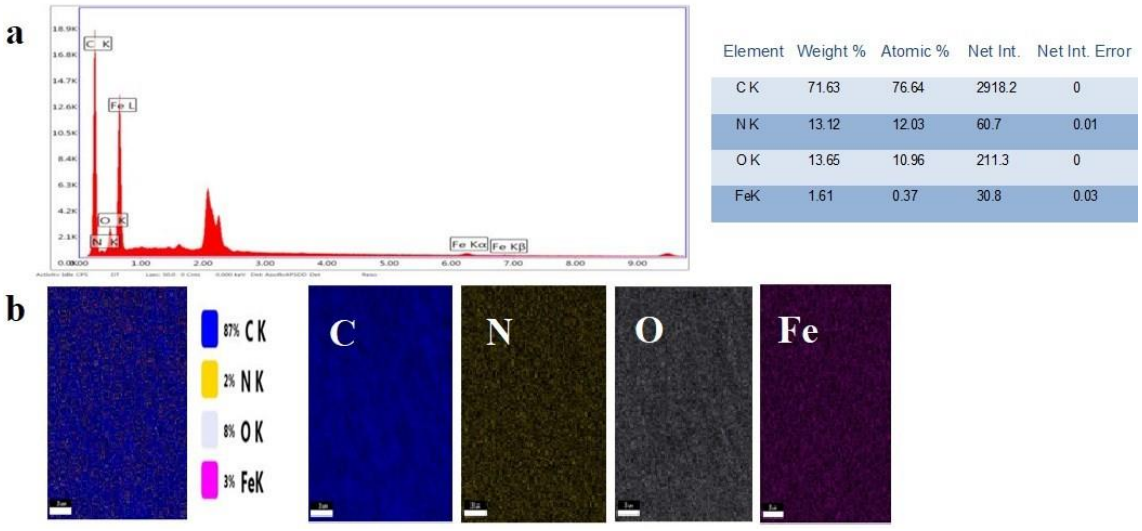

Figure 86 (A) EDS spectrum and **(B)** EDS elemental mapping of C, N, O, Fe and overall distribution on the outer surface of $Fe_2(OAc)_2Pc_2$/Vc.

The morphology and size of the catalysts were studied by SEM analysis **(Figure 87)**. These results showed homogeneous but irregular electrodeposit material where the presence of the starting elements can be noticed. For instance, it appears that $Fe_2(OAc)_2Pc_2$ (**2b**) complex dispersed homogeneously in the carbon-based supporting material. Microstructure analysis by SEM indicates that the $Fe_2(OAc)_2Pc_2$ (**2b**) particles are regular bulk **(Figure 87C)**. It is worth to mention that the largest amount of carbon found in the sample came from the electrode surface, as it is almost entirely composed of carbon atoms.

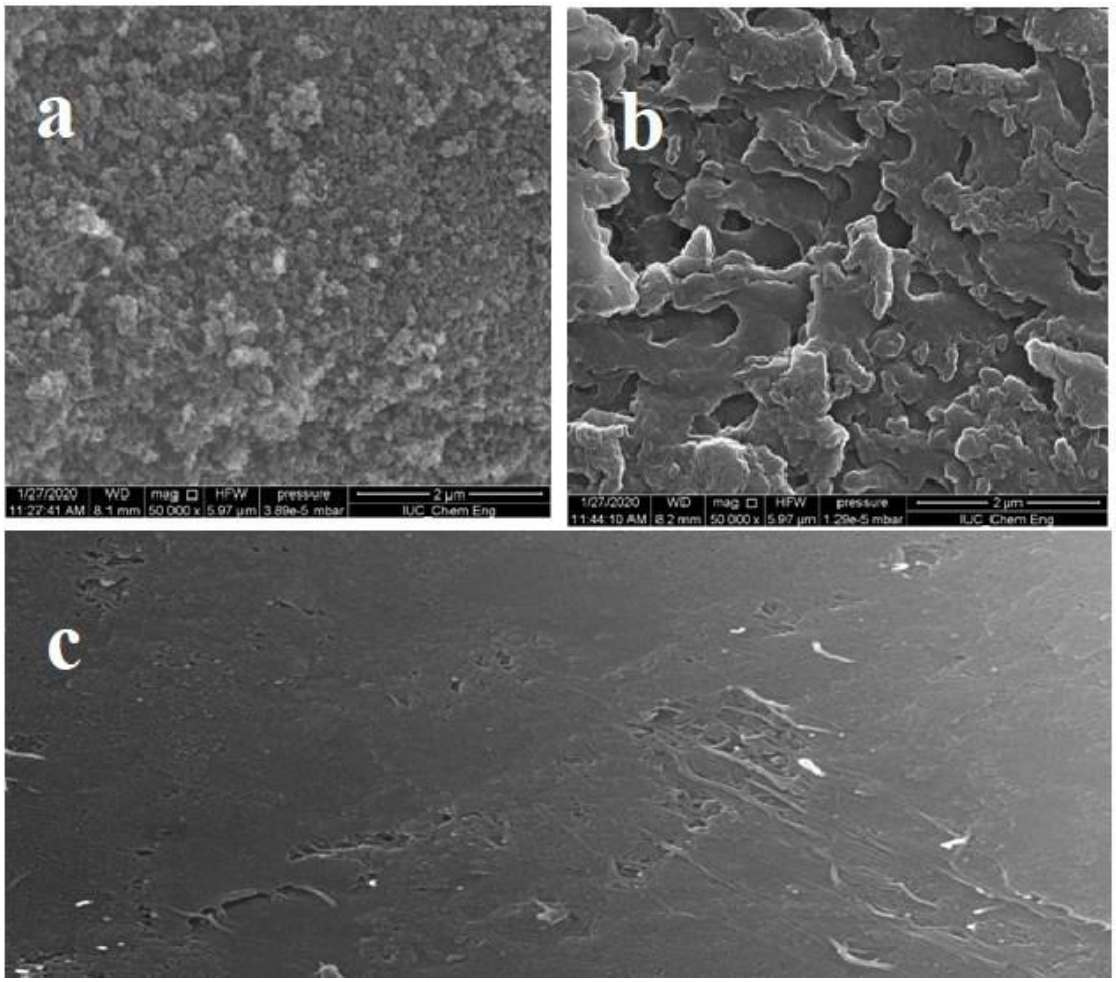

Figure 87 SEM images of **(A)** Fullerene **(B)** $Fe_2(OAc)_2Pc_2$ **(2b)** (**C)** $Fe_2(OAc)_2Pc_2$/ Fl

On the other hand, the carbon, nitrogen, oxygen and iron contents of the Fe_2Pc_2-based catalyst are presented by the EDS spectra in **Figure 88**. **Figure 88B** displays the elemental mapping of C, N, Fe, and overall distribution of the $Fe_2(OAc)_2Pc_2$/Fl mixture. It is worth to mention that Fl is the largest portion comparing all other particles found in the sample. EDS-mapping analysis verifies the homogenization of the iron atoms in the $Fe_2(OAc)_2Pc_2$ (**2b**) structure dispersed on the Fl.

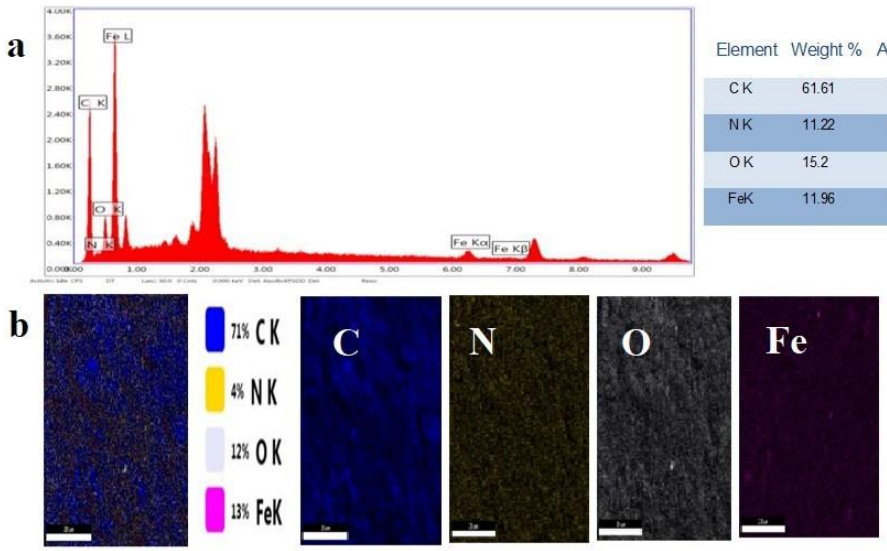

Figure 88 (**A)** EDS spectrum and **(B)** EDS elemental mapping of C, N, O, Fe and overall distribution on theouter surface of $Fe_2(OAc)_2Pc_2$/ Fl.

The high resolution N1s spectra was shown in **Figure 89.** The high resolution N1s spectra for (A) Fe(OAc)Pc (**1b**), (B) $Fe_2(OAc)_2Pc_2$, (**2b**) (C) Fe(OAc)Pc/Fl and (D) $Fe_2(OAc_{)2}Pc_2$/Fl catalysts showed main peaks at 398.85, 398.34, 399.02 eV and 399.18 eV respectively. As a maker for edge plane exposure, N was principally found on the edge of the carbon layer and exposed more active sites, which was related to higher catalytic activity of ORR.

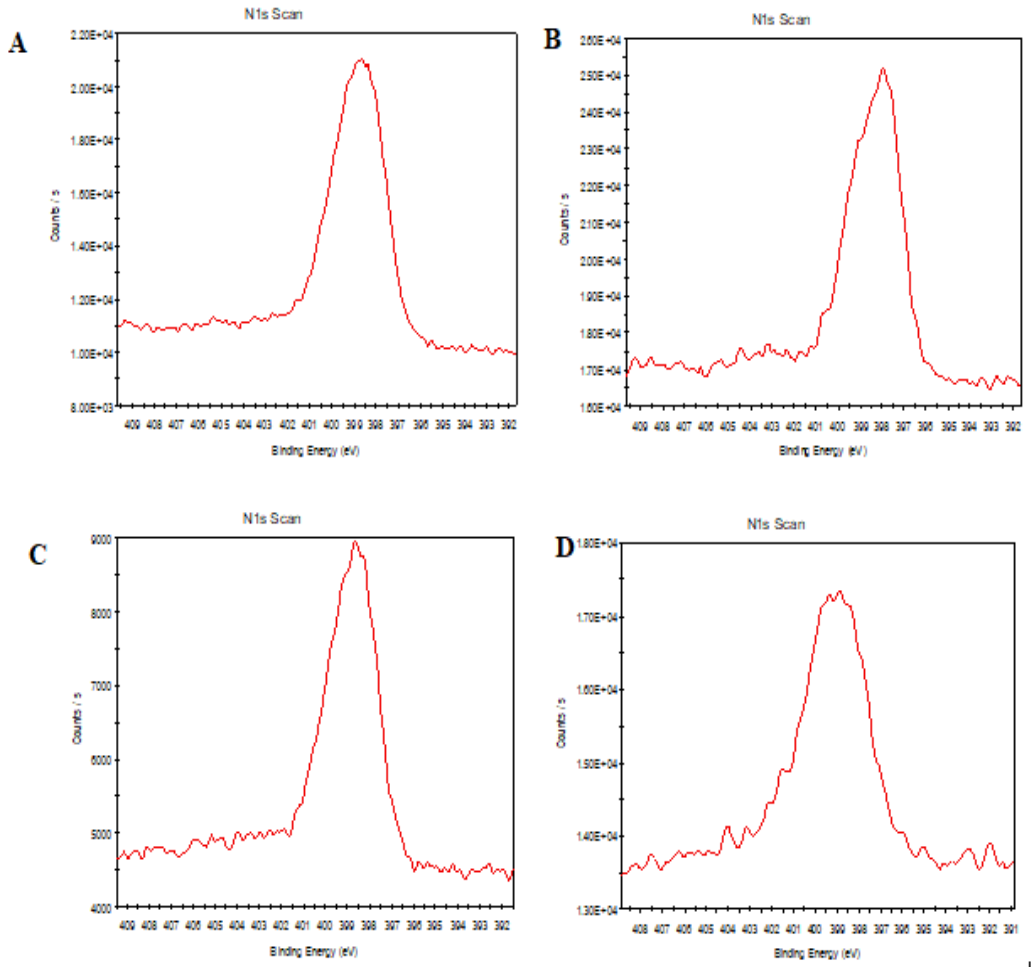

Figure 89 XPS detailed core-level spectra in the N1s region for **(A)** Fe(OAc)Pc **(1b)**, **(B)** $Fe_2(OAc)_2Pc_2$ **(2b)** **(C)** Fe**(OAc)**Pc/Fl and **(D)** $Fe_2(OAc)_2Pc_2$/Fl catalysts

The high resolution C1s spectra was shown in **Figure 90**. For catalysts (A) Fe(OAc)Pc (**1b**), (B) $Fe_2(OAc)_2Pc_2$ (**2b**) (C) Fe(OAc)Pc/Fl and (D) $Fe_2(OAc)_2Pc_2$/Fl - the high resolution C1s spectra showed main peaks approximately at 284.8 eV for all of them [102].

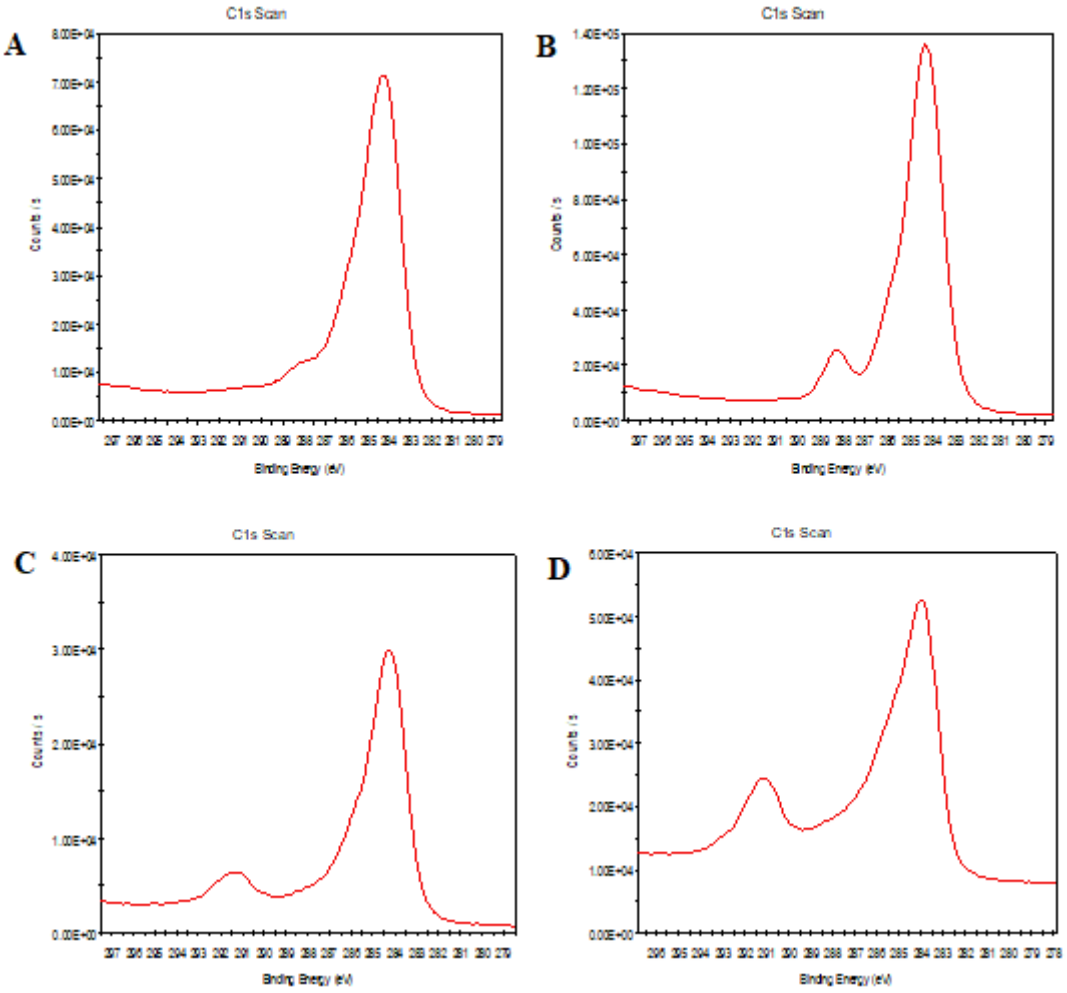

Figure 90 XPS detailed core-level spectra in the C1s region for **(A**) Fe(OAc)Pc **(1b)** , **(B)** $Fe_2(OAc)_2Pc_2$, **(2b)** **(C)** Fe**(OAc)**Pc/Fl and **(D)** $Fe_2(OAc)_2Pc_2$/Fl catalysts

The high resolution O1s spectra were shown in **Figure 91.** The high resolution O1s spectra for (A) Fe(OAc)Pc (**1b**), (B) $Fe_2(OAc)_2Pc_2$ (**2b**) (C) Fe(OAc)Pc/Fl and (D) Fe_2(OAc)2Pc2/Fl catalysts showed main peaks at 532.32 eV, 532.22 eV, 532.25 eV and 531.33 eV respectively. It was noteworthy that the C, O, N, Fe elements appear in XPS spectra at 284.81, 531.33, 399.18, 688.29 eV, indicating that $Fe_2(OAc)_2Pc_2$/Fl has been tracked.

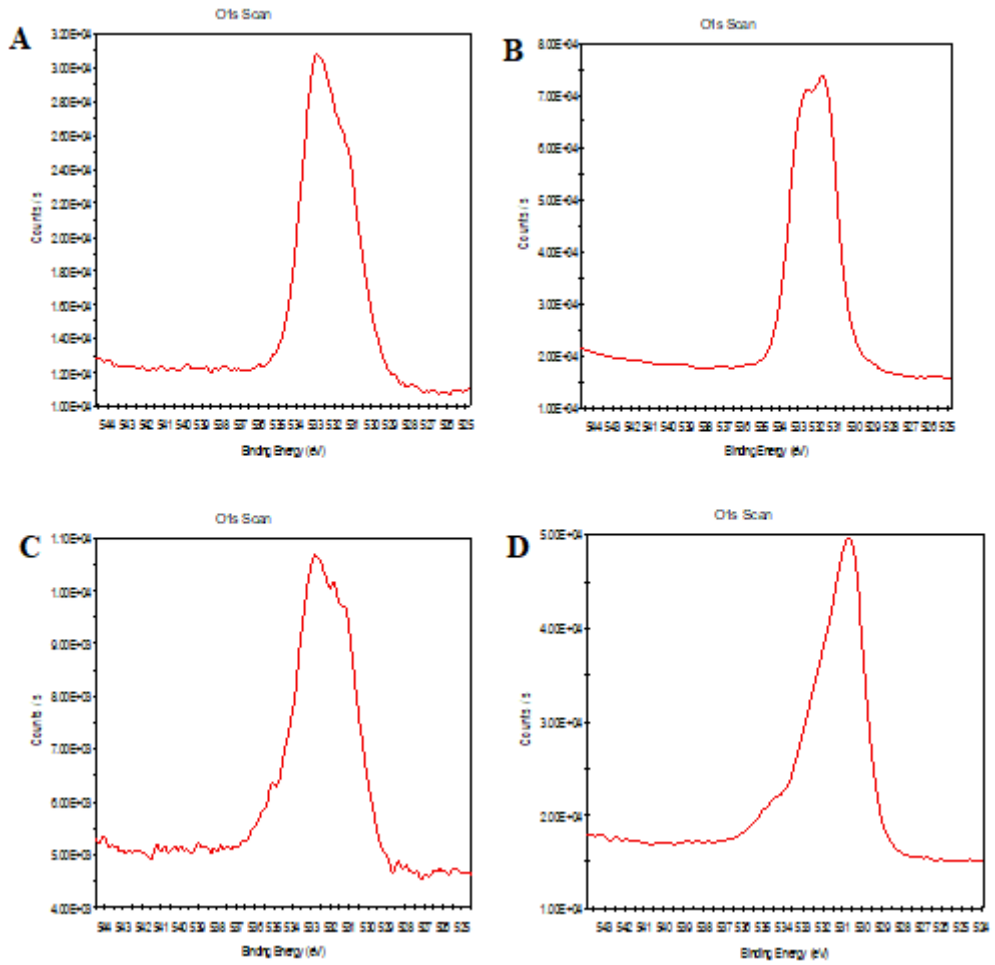

Figure 91 XPS detailed core-level spectra in the O1s region for **(A)** Fe(OAc)Pc **(1b)** , **(B)** $Fe_2(OAc)_2Pc_2$ **(2b) (C)** Fe**(OAc)**Pc/Fl and **(D)** $Fe_2(OAc)_2Pc_2$/Fl catalysts

3.12. Zinc-air battery tests with catalysts of mono and ball-type dinuclear substituted metal phthalocyanine compounds.

Research involving the direct testing of catalyst materials within a complete cell is infrequent. This study evaluated the electro catalytic performance of the Fe(OAc)Pc/Fl/Nf and Fe(OAc)Pc/Vc/Nf catalysts in the air cathode of a custom-built Zn-air battery. The primary Zn-air battery's performance was assessed through galvanodynamic tests, employing Fe(OAc)Pc/Fl/Nf and Fe(OAc)Pc/Vc/Nf as catalysts on the porous air cathode under ambient atmospheric conditions. These assessments were subsequently repeated using a commercial Pt/C catalyst for comparison. Both batteries exhibit open circuit potentials of 1.40 V, aligning closely with the theoretical expectation. Moreover, the voltages of these batteries are deemed acceptable until the current density reaches 100 mA cm^{-2} **(Figure 92)**

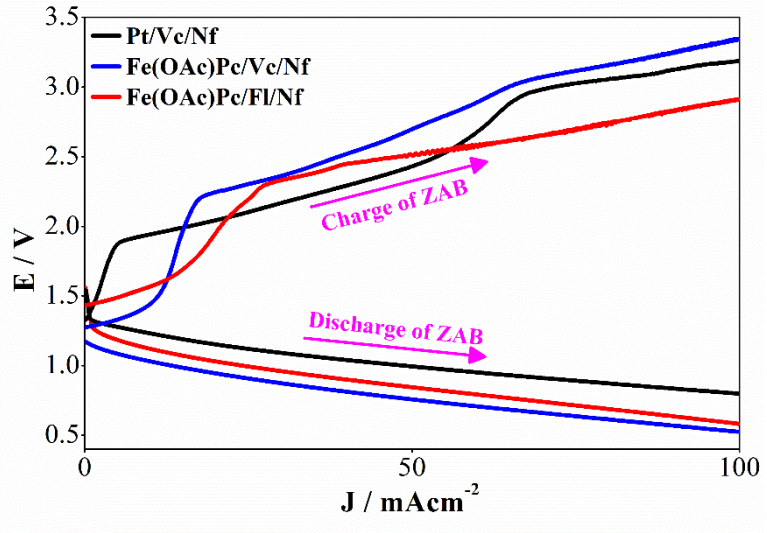

Figure 92 Galvanodynamic charge and discharge polarization curves

For both rechargeable batteries, featuring Pt/C and Fe(OAc)Pc/Fl catalysts, open circuit potentials were nearly 1.40 V and the voltages of both batteries remained adequate until the current density attained 100 mA/cm². The initial decline in cell voltage at the onset of charging and discharging process might be attributed to activation polarization. It is noteworthy that the zinc-air battery exhibits a relatively low polarization, even at current densities of up to 100 mA cm², when compared to other rechargeable zinc-air battery technologies [54]. The findings obtained from **Figure 92** indicated that the charge and discharge battery voltages of Fe(OAc)Pc/Fl exhibited considerably lower over potentials across all measured current densities especially when compared to Fe(OAc)Pc/Vc. Fe(OAc)Pc/Fl showed a considerable superiority over Fe(OAc)Pc/Vc in terms of both charge and discharge processes particularly at higher current densities. These findings consistent with the theory that the morphology of Fe(OAc)Pc/Fl along with its partially overlapping interactions contribute to enhance charge transport properties, which in turn reduced the over potentials that have been observed. A discharge voltage for Fe(OAc)Pc/Fl catalyst was close to 0.7 V while the charge voltage was around 2.7 V. The commercial viability of Fe(OAc)Pc/Fl as an effective electro catalyst was demonstrated by its comparable galvanodynamic discharge and notably enhanced charge voltages in relation to the Pt/C catalyst, particularly at higher current densities (**Figure 92**). The galvanostatic cycling performance of Fe(OAc)Pc/Vc/Nf and Pt/C catalyzed ZABs is depicted in **Figure 93**. The batteries were operated at a current density of 10 $mAcm^{-2}$, with each charge and discharge cycle lasting for a duration of 20

mits During cycle period, the initial charging and discharging voltages for the Pt/C based rechargeable zinc-air battery were recorded at 2.3 V and 1.2 V, respectively whereas the Fe-based catalyst exhibited potentials of 2.5 V for charging and 0.9 V for discharging. In the initial cycles, the charge-discharge performance of the Fe-catalyzed battery closely approximates that of the widely recognized catalyst, Pt/C.

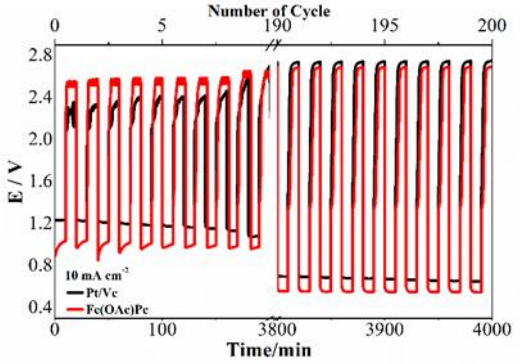

Figure 93 Galvanostatic cycling performances (the first 10 and the last 10 cycles) of rechargeable ZABs with Fe(OAc)Pc/Vc/Nf and Pt/C catalysts.

The specific discharge capacity of the Zn-air battery, as shown in **Figure 94**, is associated with the primary catalysts Fe(OAc)Pc/Vc/Nf and Fe(OAc)Pc/Fl/Nf at a specified current density. In these tests, a predetermined mass of zinc plate was employed as the anode, and the battery was operated until the anode was fully consumed. The theoretical specific capacity of Zn-air battery is 820 mAhg-1 [90] and the theoretical specific energy density value is 1084 Wh kg^{-1} [91,92]. The specific capacities of the batteries were recorded as 717 mA hg^{-1} for Pt/Vc/Nf, 703 mA hg^{-1} for Fe(OAc)Pc/Vc/Nf, 713 mA hg^{-1} for Fe(OAc)Pc/Fl/Nf based catalyst when tested at a current density of 40 mA cm^{-2}. On the other hand, the specific energy values were obtained as 703 Wh kg^{-1} for Pt/Vc/Nf is, 674.9 Wh kg^{-1} for Fe(OAc)Pc/Vc/Nf, 670.2 Wh kg^{-1} for Fe(OAc)Pc/Fl/Nf at the current density of 40 mA cm^{-2}. Specific capacity values obtained with catalysts containing iron phthalocyanine in the literature are given below: 791 $mAhg^{-1}$ for FePc/CoPc heterostructure [93], 725 $mAhg^{-1}$ for FePc/NC-1000 [94], 712 $mAhg^{-1}$ for FePc-P/MWCNTs-A [95] 808 $mAhg^{-1}$ for FePc-NHCS-500 [96], 758 $mAhg^{-1}$ for FePc/HCoNC [97], 651 $mAhg^{-1}$ for Pt/Vc/Nf [98] and. Specific energy density values in the literature are 995 Wh kg^{-1} for FePc-NHCS-500 [99], 831 Wh kg^{-1} for FePc/CoPc heterostructure [100]. The Zn-Air performances obtained in this study are consistent with the literature.

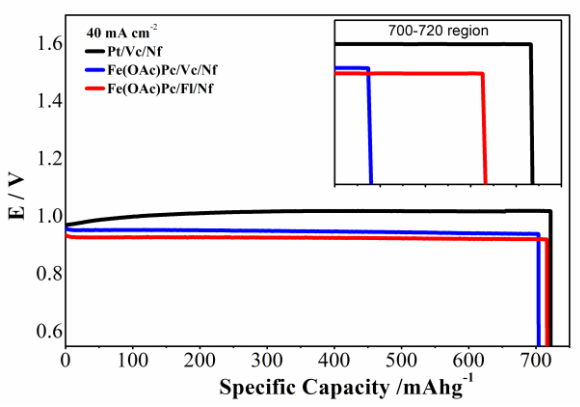

Figure 94 The specific capacities of primary ZABs for low and high currentdensities.

Numerous studies have documented the electro catalytic performance of metal phthalocyanine-based catalysts in relation to the ORR. However, it is noteworthy that the majority of these investigations rely on data obtained from half-cell measurements. Research that evaluates the catalyst materials directly within a full cell setup remains infrequent. This study focused on assessing the electro catalytic performance of the ORR for the $Fe_2(OAc)_2Pc_2$/Fl/Nf and $Fe_2(OAc)_2Pc_2$/Vc/Nf catalysts in the air cathode of a self- assembled zinc-air battery. The performance tests for the primary zinc-air battery,which incorporated $Fe_2(OAc)_2Pc_2$/Fl/Nf and $Fe_2(OAc)_2Pc_2$/Vc/Nf as catalysts on the porous air cathode, were performed galvanodynamically in an ambient environment. Additionally, these tests were replicated using a commercial Pt/C catalyst for comparative purposes. Both batteries exhibit open circuit potentials of 1.35 V, which is in proximity to the theoretical value. Moreover, the voltages of these batteries are deemed acceptable until the current density attains 100 mA cm^{-2}. The galvanodynamic discharge polarization curves for these batteries clearly illustrate that the performance levels of $Fe_2(OAc)_2Pc_2$/Vc/Nf and $Fe_2(OAc)_2Pc_2$/Fl/Nf are align closely with those of Pt/Vc atlower current densities, particularly under 20 mA cm^{-2}.

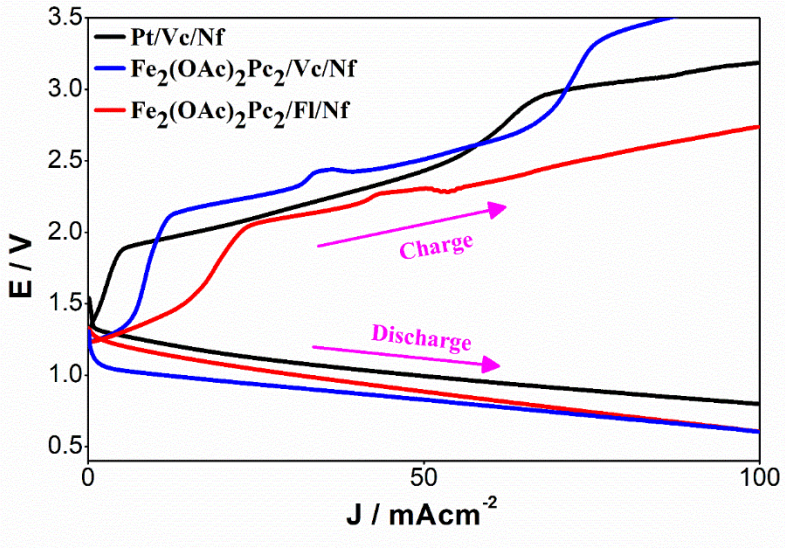

Figure 95 Galvanodynamic charge and discharge polarization curves.

The primary and rechargeable ZAB performance of $Fe_2(OAc)_2Pc_2$/Vc/Nf and $Fe_2(OAc)_2Pc_2$/Fl/Nf catalyst have been tested with galvanodynamic and galvanostatic techniques in a homemade ZAB prototype on ambient atmosphere. Charge and discharge profile of Pt/C catalyst was also tested for comparison. As shown in **Figure 95**, the open circuit potentials for both rechargeable batteries including Pt/C, $Fe_2(OAc)_2Pc_2$/Vc/Nf and $Fe_2(OAc)_2Pc_2$/Fl/Nf catalysts are 1.40 V, which is indicative of thefact that all batteries are identical without polarization. Also, the performances of ZABs were acceptable until the current density reached 100 $mAcm^{-2}$. Charge polarization ofthe battery with $Fe_2(OAc)_2Pc_2$/Fl/Nf catalyst is competitive with that of the one including Pt/C as the catalyst, at all current densities. On the other hand, $Fe_2(OAc)_2Pc_2$/Fl/Nfcatalyst has good performance at higher and lower current densities during discharge process. The battery including $Fe_2(OAc)_2Pc_2$/Fl/Nf catalyst has superior charging performance with relatively low polarization throughout all current densities, with respect to $Fe_2(OAc)_2Pc_2$/Vc/Nf catalyst.

Figure 96 illustrates galvanostatic cycling performances of $Fe_2(OAc)_2Pc_2$/Vc/Nf and Pt/C catalyzed ZABs. Each battery was operated with a current density of 20 $mAcm^{-2}$ and 20-minute duration time for each charge-discharge stage. For the first 10 cycles, charge-discharge performance of the $Fe_2(OAc)_2Pc_2$/Vc/Nf catalyzed battery is almost nearof the known most popular catalyst, Pt/C. Furthermore, during ZAB applications, $Fe_2(OAc)_2Pc_2$/Vc/Nf catalyst exhibited good electrochemical stability with charge and discharge voltage loss of about 0.20 V at the end of 200 cycles.

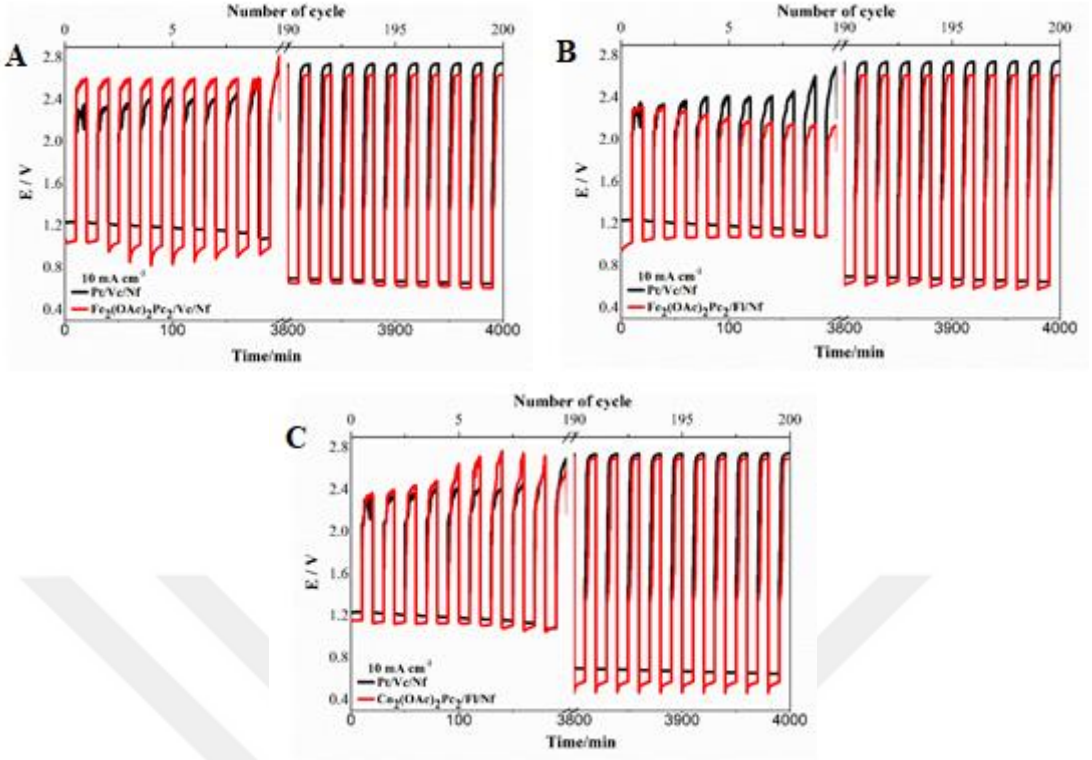

Figure 96 Galvanostatic cycling performances (the first 10 and the last 10 cycles) of rechargeable ZABs with **A)** $Fe_2(OAc)_2Pc_2$/Vc/Nf **B)** $Fe_2(OAc)_2Pc_2$/Fl/Nf and **C)** Co_2Pc_2/Fl/Nf with Pt/C catalysts.

The specific discharge capacity of the Zn-air battery, as shown in **Figure 97**, is associated with the catalysts $Fe_2(OAc)_2Pc_2$Vc/Nf and $Fe_2(OAc)_2Pc_2$/Fl/Nf at a specified current density. In these tests, a designated mass of zinc plate was employed as the anode, and the battery was operated until the anode was fully consumed. The theoretical specific capacity of Zn-air battery is 820 mAhg-1 [90] and the theoretical specific energy density value is 1084 Wh kg^{-1} [91,92]. The specific capacities of the batteries were recorded as 717 mA hg^{-1} for Pt/Vc/Nf, 715 mA hg^{-1} for $Fe_2(OAc)_2Pc_2$/Vc/Nf and 716 mA hg^{-1} for $Fe_2(OAc)_2Pc_2$/Fl/Nf based catalyst when tested at a current density of 40 mA cm^{-2}.On the other hand, the specific energy values were obtained as 703 Wh kg^{-1} for Pt/Vc/Nf, 674.2 Wh kg^{-1} for $Fe_2(OAc)_2Pc_2$/Vc, and 708.8 Wh kg^{-1} for $Fe_2(OAc)_2Pc_2$/Fl at the current density of 40 mA cm^{-2}. Specific capacity values obtained with catalysts containing iron phthalocyanine in the literature are given below: 791 $mAhg^{-1}$ for FePc/CoPc heterostructure [93], 725 $mAhg^{-1}$ for FePc/NC-1000 [94], 712 $mAhg^{-1}$ for FePc-P/MWCNTs-A [95] 808 $mAhg^{-1}$ for FePc-NHCS-500 [96], 758 $mAhg^{-1}$ for FePc/HCoNC [97], 651 $mAhg^{-1}$ for Pt/Vc/Nf [98] and. Specific energy

density values in the literature are 995 Wh kg^{-1} for FePc-NHCS-500 [99], 831 Wh kg^{-1} for FePc/CoPc heterostructure [100]. The Zn-Air performances obtained in this study are consistent with the literature.

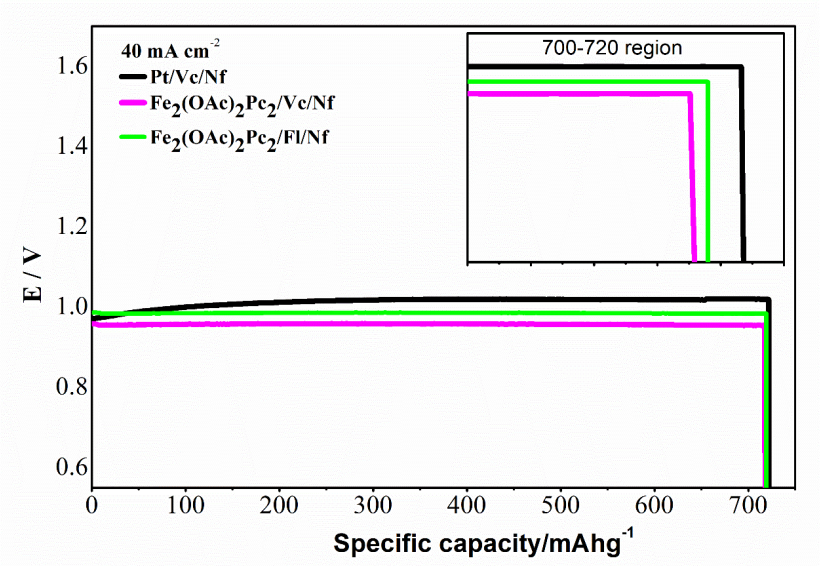

Figure 97 The specific capacities of primary ZABs for low and high current densities.

In this study, electro catalytic and ZAB performances of non-precious dinuclear complexes have been tested and compared. $Fe_2(OAc)_2Pc_2$/Vc/Nf and $Fe_2(OAc)_2Pc_2$/Fl/Nf complex supported with VC and Fl showed extraordinary performance due to its unique molecular structure and redox properties. This performance can be further increased by modification of the bridging units in the structure and/or use of different carbon-based supporting materials such as GO, reduced graphene oxide (rGO) and carbon Nano tubes (CNTs). The homogenization of the catalyst-active and conductive carbon materials is also known to be very effective on the performance. Thus, the modification of the main M_2Pc_2 skeleton is expected to enhance its dispersive properties in a certain solvent suitable for the dispersion of the carbon material. These evaluations and the results of this study encourage us to design new phthalocyanine-based catalysts and test their battery performances in our continuing studies.

The findings of this study indicate that employing the dimeric ball-type configuration significantly enhances the catalytic activity of MPc-based materials in the realm of oxygen electro catalysis. The presence of two redox-active metal centers within the

dimeric ball-type M_2Pc_2 complexes facilitates a stronger interaction with dioxygen molecules, thereby improving their efficacy in oxygen electro catalysis. Notably, when Fe(II) is selected as the central metal, the catalytic performance approaches that of commercial Pt/C. Consequently, the ball-type $Fe_2(OAc)_2Pc_2$/Vc/Nf and $Fe_2(OAc)_2Pc_2$/Fl/Nf complexes investigated in this study demonstrate potential as effective oxygen electro catalysts for primary zinc-air batteries.

3.13. Comparison of findings of mononuclear and dinuclear ball type phthalocyanine complexes

The electrochemical and *in situ* spectroelectrochemical analysis revealed that dinuclear ball-type complexes exhibited richer redox behavior compare to mononuclear complexes. Dinuclear ball-type complexes displayed redox processes with one or two electron transfers due to the two MPc units and formed mixed-valence species. Thus, mixed-valence splitting can be observed in redox process and the split process occurs with one electron. On the other hand, if there is no mixed-valence species, the process happens with two electron transfers and this behavior is observed as broad peaks in CV and SWV. Therefore, dinuclear ball-type complexes have richer redox properties than mononuclear ones.

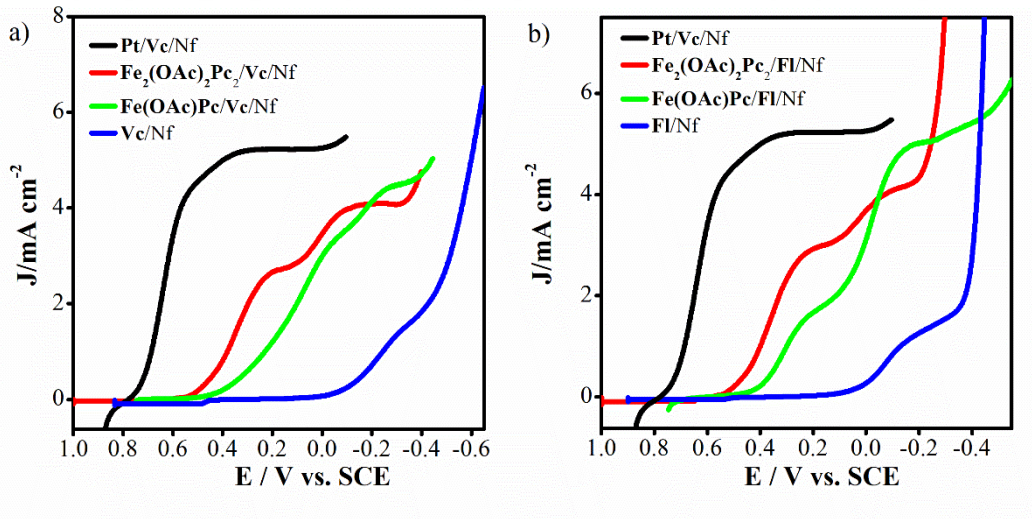

Figure 98 RDE polarization curves for comparing with **(A)** MPc/Vc/Nf and **(B)** MPc/Fl/Nf modified glassy carbon electrodes in 0.5 M H_2SO_4 solution saturated with O_2 for electro catalytic ORR (Rotation speed: 2500 rpm).

Fig. 98A and 98B presents the polarization curve that highlights the catalytic activity of each complex with respect to the ORR in acid solution. The findings of this study indicate that employing the ball-type configuration significantly enhances the catalytic

activity of MPc-based materials in oxygen electro catalysis. The presence of two redox-active metal centers in dimeric ball-type M_2Pc_2 complexes evidently strengthens their interaction with dioxygen molecules, thereby improving their efficacy in oxygen electro catalysis.

The onset potential and the limiting current densities of ORR catalysts decreased in the following order: Fe> Mn >Co > Ni > Zn for all the supporting carbon (Vc, GO, G, Tm and Fl). The anticipated redox behavior of the central metals in macrocycles was likely to be crucial in determining the electro catalytic performance of these catalyst composites. The redox mechanisms taking place at the metal centers facilitate the interaction with dioxygen molecules, which in turn lead to the formation of suitable intermediates for the electro catalytic ORR [33-39]. Therefore, the relatively high catalytic performance exhibited by the Fe, Co and Mn complexes can be explained by the redox-active characteristics of their respective metal centers.

The catalytic performance of the Fe(OAc)Pc/Fl/Nf, Fe(OAc)Pc/Vc/Nf, $Fe_2(OAc)_2Pc_2$/Fl/Nf and $Fe_2(OAc)_2Pc_2$/Vc/Nf complexes markedly superior to that of the other MPc complexes. The analysis of the E_0, $E_{1/2}$, and J_L values associated with ORR revealed that Fe(OAc)Pc/Fl/Nf and $Fe_2(OAc)_2Pc_2$/Fl/Nf showed higher catalytic activity which owing to its advantageous combination of sufficient surface area together with high electrical conductivity inherent to Fl [43-47]. The onset potentials of Fe(OAc)Pc/Fl/Nf and $Fe_2(OAc)_2Pc_2$/Fl/Nf were significantly closer to Pt/Vc/Nf in OER in alkaline solutions [43-47]. Thus, the excellent performance observed in both ORR and OER suggest that the Fe(OAc)/Fl/Nf and $Fe_2(OAc)_2Pc_2$/Fl/Nf catalysts have the potential to act as an electro catalyst in alkaline conditions for metal-air batteries. $Fe_2(OAc)_2Pc_2$/Fl/Nf catalyst showed better catalytic performance than Fe(OAc)/Fl/Nf catalyst due to its superior electro catalytic activity originating from the interaction of two MPc units with dioxygen molecule.

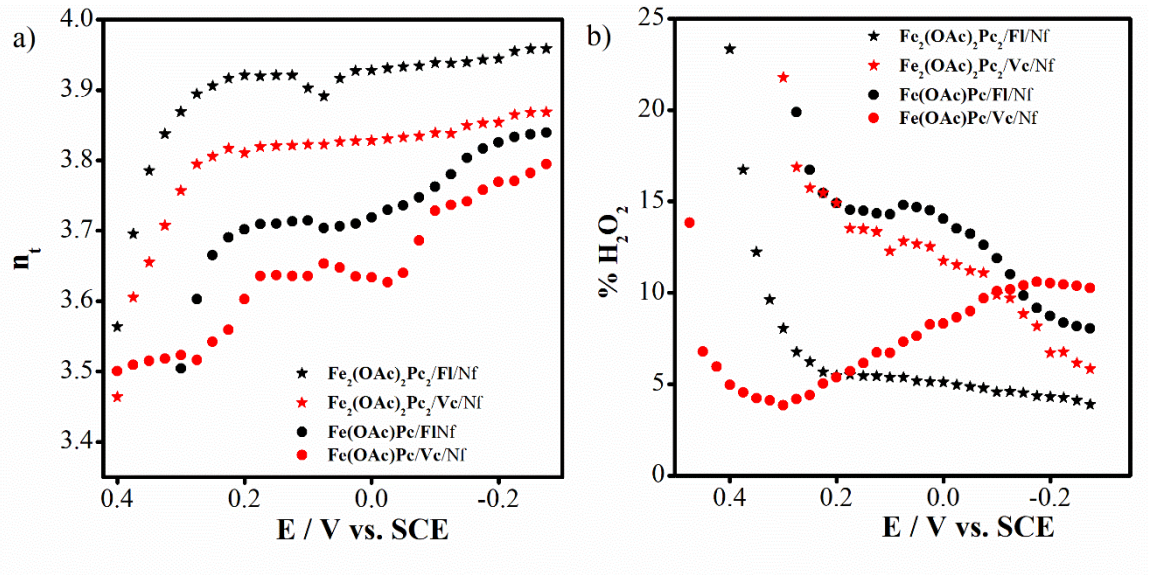

Figure 99 (A) Variation of the total number of electrons transferred with the disk potential for $Fe_2(OAc)_2Pc_2$/Fl/Nf modified electrodes **(B)** Variation of the % H_2O_2 formed for $Fe_2(OAc)_2Pc_2$/Fl/Nf modified electrodes with the disk potential (accordingto Ering = 0.95 V vs SCE).

In Figure 99, the number of electrons transferred nt and the percentage of hydrogen peroxide produced are illustrated as functions of potential. These measurements distinctly demonstrated that the participation of two cofacial redox-active metal centers within the M_2Pc_2 structure significantly improved the electro catalytic performance. This improvement was ascribed to the generation of M(III)-O-O-M(III) species, which occurred due to the robust interaction between the redox-active metal centers and dioxygen. This interaction not only hindered the production of H_2O_2 but also facilitated a direct four-electron transfer mechanism.

In accordance with n_t, the ORR for all catalysts proceeds through a four-electron pathway that produces only water, in addition to two separate two-electron pathway that first generate hydrogen peroxide, which is then convert into water. In an acidic medium, the ORR can proceed via a four-electron pathway, resulting in the production of water, or through a two-electron pathway that results in the formation of hydrogen peroxide.

It is particularly evident that the ORR facilitated by the $Fe_2(OAc)_2Pc_2$/Fl/Nf based electrode in acid generates a substantially greater quantity of water in contrast to that of hydrogen peroxide compare to Fe(OAc)Pc/Fl/Nf catalyst. Increase in voltage corresponds to a rise in the n_t value for $Fe_2(OAc)_2Pc_2$/Fl/Nf (reaching 3.96 and 4% H_2O_2) and Fe(OAc)Pc/Fl/Nf (reaching 3.85 and 10% H_2O_2) at the limiting diffusion

current plateau, thereby indicating that water being the predominant product.

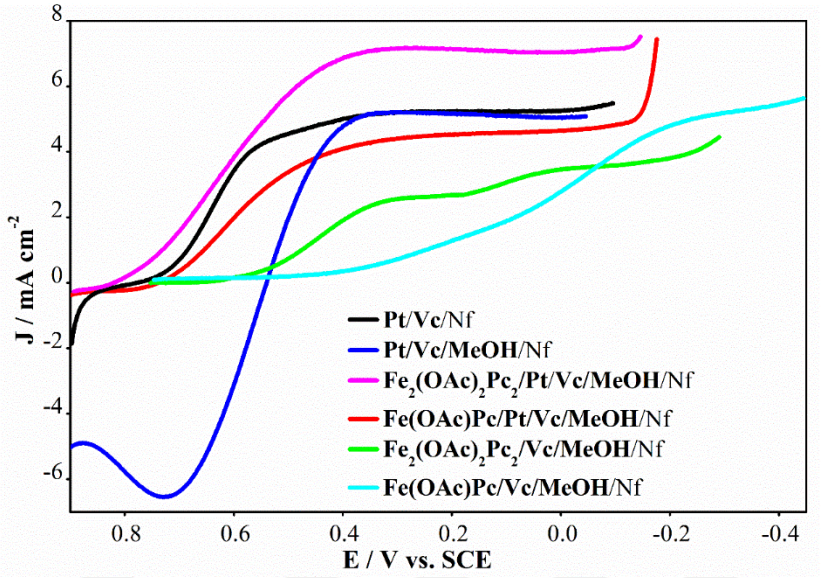

Figure 100 RDE polarization curves for comparing with Pt/Vc/Nf, Pt/Vc/Nf /MeOH, $Fe_2(OAc)_2Pc_2$/Vc/Nf and $Fe_2(OAc)_2Pc_2$/Pt/Vc/Nf/MeOH and Fe(OAc)Pc/Pt/Vc/Nf/MeOH modified glassy carbon electrodes in 0.5 M H_2SO_4 solution saturated with O_2 for electro catalytic ORR in the presence and absence of methanol (Rotation speed: 2500 rpm).

The polarization curves presented in **Figure 100** were obtained from an O_2-saturated electrolyte, showcasing the effects of methanol presence and absence on the Pt- and mono and ball type dinuclear Pcs based catalysts. The $Fe_2(OAc)_2Pc_2$/Vc/Nf and Fe(OAc)Pc/Vc/Nf based catalyst demonstrates a considerably superior tolerance to methanol than Pt-based catalyst. The polarization curves of $Fe_2(OAc)_2Pc_2$/Vc/Nf and Fe(OAc)Pc/Vc/Nf in acid for the ORR, were unaffected by the presence of 1.0 M methanol in the electrolyte. Unlike them, the presence of 1.0 M methanol into the electrolyte of a platinum-based electrode caused the oxygen reduction potential to shift towards negative values. A notable methanol oxidation current was detected throughout a wide potential range, thereby completely blocking the catalytic activity of Pt-based catalysts for the ORR within the potential range of 0.65–0.80 V versus SCE. The $Fe_2(OAc)_2Pc_2$/Vc/Nf based catalyst demonstrates a considerably superior tolerance to methanol than Fe(OAc)Pc/Vc/Nf and Pt-based catalyst and can serve as a promising alternative for platinum-based catalysts for the oxygen reduction reaction within direct methanol fuel cell applications.

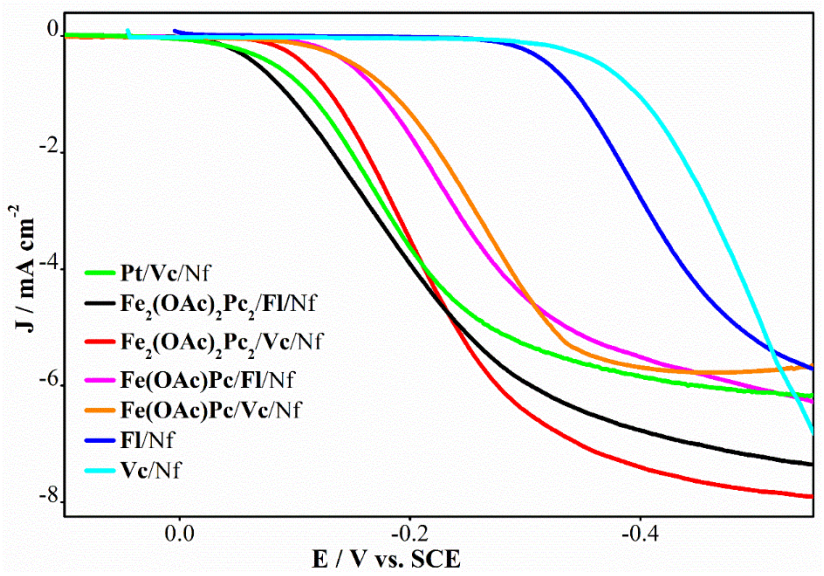

Figure 101 RDE voltammograms for comparing with Pt/Vc/Nf, $Fe_2(OAc)_2Pc_2$/VC/Nf and $Fe_2(OAc)_2Pc_2$/Fl/Nf, Fe(OAc)Pc/Fl/Nf and Fe(OAc)Pc/VC/Nf modified glassy carbon electrodes in 0.1 M KOH solution for electro catalyticORR (rotation speed 2500rpm).

The RDE curves for the mono and ball type dinuclear Pc catalysts for ORR at 2500 rpm in O_2-saturated 0.1 M KOH solutions with a scan rate of 5 mV s^{-1} were shown in **Figure 101**. The role of cofacial dual central metals is crucial for the effectiveness of the M_2Pc_2 structure as an electro catalyst for the ORR. It can be inferred that the oxidation of both dual and cofacial Fe(II) centers within the M_2Pc_2-type dimeric structure results in the generation of Fe(III)-O-O-Fe(III) per Oxo species. This formation is anticipated to reduce the rate of hydrogen peroxide (HO_2^-) production while simultaneously enhancing the rate of hydroxide (OH^-) production due to the facilitation of the cleavage of the O–O bond. Consequently, the $Fe_2(OAc)Pc_2$ (**2b**) catalyst demonstrates remarkably high catalytic activity for ORR, rivaling that of the commercial 40% Pt/C catalyst. Additionally, it significantly lowers the activation over potential for the ORR, primarily facilitating the reaction through a direct four-electron pathway to produce hydroxide ions at the majority of the catalytic sites.

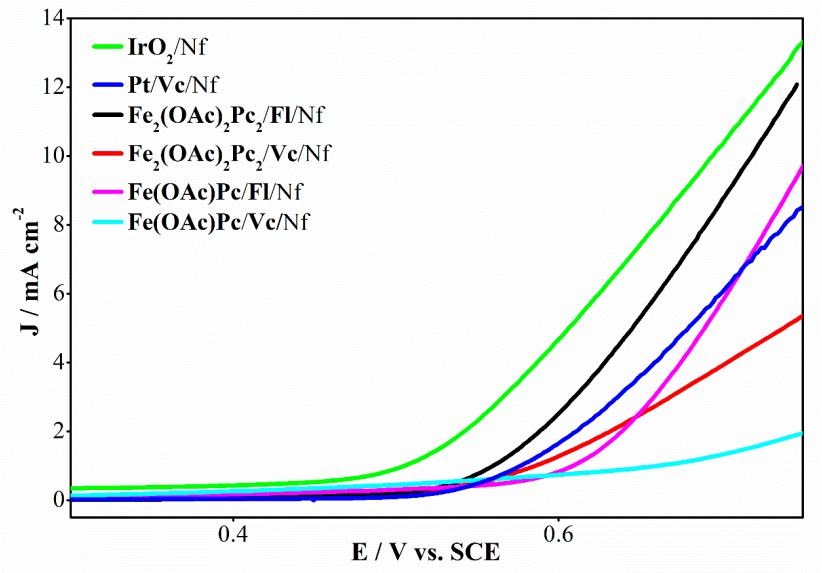

Figure 102 RDE voltammograms for comparing with IrO_2/Nf, Pt/Vc/Nf, $Fe_2(OAc)_2Pc_2$/VC/Nf, $Fe_2(OAc)_2Pc_2$/Fl/Nf, Fe(OAc)Pc/VC/Nf and Fe(OAc)Pc/Fl/Nf modified glassy carbon electrodes in 0.1M KOH solution for electro catalytic OER (Rotation speed: 2500 rpm).

In addition to the ORR activity, the analysis of OER activity cannot be overlooked for catalysts. **Figure 102** showed the OER activities for mono and ball type dinuclear Pc catalyst. It was concluded from these measurements of this study, the dual Fe^{2+} centers, which exhibit high nucleophilicity and are encircled by pyrrolic nitrogen atoms within the $Fe_2(OAc)_2Pc_2$ structure, are likely to engage effectively with OH^- ions, thereby facilitating significant OER activity and reversibility. The $Fe_2(OAc)_2Pc_2$ (**2b**) complex, when supported by Fl, demonstrated exceptional performance attributed to its distinctive molecular structure and redox characteristics.

4. CONCLUSION

In this study, the redox behavior of peripherally 2,4-di-tert-butyl-6-(3,4-dicyanophenoxy) phenolate substituted mononuclear metallophthalocyanines (CoPc (**1a**), Fe(OAc)Pc (**1b**), Mn(OAc)Pc (**1c**), NiPc (**1d**) and ZnPc (**1e**)) and 4,4'-(3,5-di-tert-butyl-1,2-phenylene) bis(oxy) substituted dinuclear ball-type phthalocyanine compounds (Co_2Pc_2 (**2a**), $Fe_2(OAc)_2Pc_2$ (**2b**), $Mn_2(OAc)_2Pc_2$ (**2c**), Ni_2Pc_2 (**2d**), and Zn_2Pc_2 (**2e**)) has been characterized by the voltammetric techniques of CV, SWV, and CPC. In situ spectroelectrochemical measurements were also performed for analysis of spectral changes and thus, color transitions occurring throughout the redox processes of MPcs. The electro catalytic performance of these compounds for ORR and OER was tested by RDE and bipotentiostatic RRDE voltammetry measurements in both acid and alkaline media for fuel cell and as Zn-air battery systems. Characterization of the catalysts, consisting of MPcs, Vc and Fl was analyzed via SEM, EDS and EDS-Mapping analysis techniques. The concluding remarks obtained from the evaluation of all electrochemical studies are listed below:

The investigation into the electrochemical and spectroelectrochemical properties of various mononuclear and dinuclear ball type phthalocyanine complexes (**1a-1e**) and (**2a-2e**) in DMSO/TBAP and DCM/TBAP electrolytes revealed that complexes including cobalt, iron, manganese exhibited significant redox activity along with notable spectral and color variations compare to nickel and zinc ones. While NiPc (**1d**), ZnPc (**1e**), Ni_2Pc_2 (**2d**) and Zn_2Pc_2 (**2e**) demonstrated phthalocyanine ring based redox processes, CoPc (**1a**), Fe(OAc)Pc (**1b**), Mn(OAc)Pc (**1c**), Co_2Pc_2 (**2a**), $Mn_2(OAc)Pc_2$ (**2c**) and $Fe_2(OAc)Pc_2$ (**2b**) showed additional metal centered redox behaviors. The main reason of this dissimilarity in the voltammetric performance of redox active metal centered complexes since the d orbitals of them laying between the LUMO and HOMO levels of the phthalocyanine ligand. Moreover, rare redox processes M^{IV}/M^{III} and M^{III}/M^{II} were observed for Fe(OAc)Pc (**1b**), Mn(OAc)Pc (**1c**), $Mn_2(OAc)Pc_2$ (**2c**) and $Fe_2(OAc)Pc_2$ (**2b**) complexes since their metal center were in +3 oxidation state [48,66]. Due to the arrange of axial position by the neutralizing and/or donor solvent molecules, the potentials of MPcs are greatly affected. Oxidation state of iron and manganese metal ions in Fe(OAc)Pc (**1b**), Mn(OAc)Pc (**1c**), $Mn_2(OAc)Pc_2$ (**2c**) and $Fe_2(OAc)Pc_2$ (**2b**) complexes was 3+, whereas the cobalt metal center is in the oxidation state of 2+ in

CoPc (**1a**) and Co_2Pc_2 (**2a**). Because of the essentiality of neutralization of the oxidation state three (3^+), one axial site of iron and manganese complexes is occupied by OAc. Moreover, these results were supported by observing carbonyl groups of Fe and Mn in IR spectroscopy.

Dinuclear ball type complexes with strong intermolecular interaction between two MPc units formed mixed-valence species with one electron transfers. Two MPc units in complexes that do not form mixed-valence species showed a simultaneous two-electron transfer redox behavior. Broader peaks in CV and SWV revealed this two-electron behavior. Thus, dinuclear ball type complexes had richer redox properties due to mixed-valence species than mononuclear complexes (**Table 1**, **Table 2** and **Table 12**).

The electrochemical an in situ spectroelectrochemical analysis of the mononuclear and dinuclear ball type complexes showed that Fe(OAc)Pc (**1b**) and $Fe_2(OAc)Pc_2$ (**2b**) complexes displayed better redox properties among the complexes with same molecular structure. The enhanced redox responses of Fe(OAc)Pc (**1b**) and $Fe_2(OAc)Pc_2$ (**2b**) are crucial for their potential technological applications, particularly in electro sensing, electrochromic and electro catalytic technological fields.

All redox responses of mononuclear complexes shift to more negative potentials in DMSO because of its polarization effect compare to DCM (**Table 1**, **Table 2**). $E_{1/2}$ value for the Fe(OAc)Pc (**1b**) complexes are mostly in agreement with those of the previously reported Pc complexes [42, 43]. Because of the polarization effect of DMSO, each redox pair of Mn(OAc)Pc (**1c**) have slightly much negative half-wave potentials in coordinating DMSO/TBAP electrolyte than those in DCM/TBAP electrolyte system. In comparison with CoPc (**1a**) and Fe(OAc)Pc (**1b**) complexes, for CV and SWV method, the shifting of redox potential for Mn(OAc)Pc (**1c**) compound is minor if coordinating DMSO/TBAP electrolyte is applied in place of non-coordinating DCM/TBAP electrolyte.

The findings obtained from the electro catalytic measurements indicated that the catalysts including Fe, Co and Mn metals for all the supported carbon materials, showed higher catalytic activity than catalysts with Ni and Zn. Their better catalytic performance can be attributed to the redox active metal-centers that additionally interaction with O_2 molecules [19,50]. Furthermore, dinuclear ball type molecular structure provided better catalytic effect compare to mono nuclear structure due to the

interaction of two MPc units in complexes with O_2. The catalysts including iron metal-centered complexes displayed better catalytic behavior among all. On the other hand, Fl carbon material provided better catalytic effect than VC, G, GO, and Tm due to the sufficient surface area and high electrical conductivity of Fl [43-47]. Thus, Fe(OAc)Pc/Fl/Nf and $Fe_2(OAc)_2Pc_2$/Fl/Nf catalyst showed the better performances in catalytic test and $Fe_2(OAc)_2Pc_2$/Fl catalyst was the best [93, 99, 100].

Zn-air battery performance tests of catalysts showing better electro catalytic activity were performed. The findings displayed that Fe(OAc)Pc/Fl/Nf in catalysts including mononuclear complexes and $Fe_2(OAc)_2Pc_2$/Fl/Nf in catalyst with dinuclear ball type ones attracted attention with better Zn-air battery performances in terms of both charge and discharge processes particularly at higher current densities. The theoretical specific capacity of Zn-air battery is 820 mAhg-1 [90] and the theoretical specific energy density value is 1084 Wh kg^{-1} [91,92]. The specific capacities of the batteries were recorded as 717 mA hg^{-1} for Pt/Vc/Nf, 703 mA hg^{-1} for Fe(OAc)Pc/Vc/Nf, 713 mA hg^{-1} for Fe(OAc)Pc/Fl/Nf, 715 mA hg^{-1} for $Fe_2(OAc)_2Pc_2$/Vc/Nf and 716 mA hg^{-1} for $Fe_2(OAc)_2Pc_2$/Fl/Nf based catalyst when tested at a current density of 40 mA cm^{-2}. On the other hand, the specific energy values were obtained as 703 Wh kg^{-1} for Pt/Vc/Nf is, 674.9 Wh kg^{-1} for Fe(OAc)Pc/Vc/Nf, 670.2 Wh kg^{-1} for Fe(OAc)Pc/Fl/Nf, 674.2 Wh kg^{-1} for $Fe_2(OAc)_2Pc_2$/Vc, and 708.8 Wh kg^{-1} for $Fe_2(OAc)_2Pc_2$/Fl at the current density of 40 mA cm^{-2}. Specific capacity values obtained with catalysts containing iron phthalocyanine in the literature are given below: 791 $mAhg^{-1}$ for FePc/CoPc heterostructure [93], 725 $mAhg^{-1}$ for FePc/NC-1000 [94], 712 $mAhg^{-1}$ for FePc-P/MWCNTs-A [95] 808 $mAhg^{-1}$ for FePc-NHCS-500 [96], 758 $mAhg^{-1}$ for FePc/HCoNC [97], 651 $mAhg^{-1}$ for Pt/Vc/Nf [98] and. Specific energy density values in the literature are 995 Wh kg^{-1} for FePc-NHCS-500 [99], 831 Wh kg^{-1} for FePc/CoPc heterostructure [100]. The Zn-Air performances obtained in this study are consistent with the literature.

5. REFERENCES

[1] O. Dolotova, N. Bundina, O. Kaliya, E. Lukyanets, Manganese phthalocyanine coordination chemistry: recent results and present status, Journal of Porphyrins and Phthalocyanines 1(4) (1997) 355-366.

[2] M. Coates, T. Nyokong, X-ray photoelectron spectroscopy analysis of the effect of alkyl- and arylthio substituents on manganese phthalocyanines for self-assembled monolayer formation on gold, Electrochemistry Communications 31 (2013) 104-107.

[3] N.B. McKeown, Phthalocyanine Materials: Synthesis, Structure and Function, Cambridge University Press1998.

[4] F. Matemadombo, S. Griveau, F. Bedioui, T. Nyokong, Electrochemical Characterization of Self-Assembled Monolayer of a Novel Manganese Tetrabenzylthio-Substituted Phthalocyanine and Its Use in Nitrite Oxidation, Electroanalysis: An International Journal Devoted to Fundamental and Practical Aspects of Electroanalysis 20(17) (2008) 1863-1872.

[5] Leznoff, C.C.; Lever, A.B.P. (Eds.): "*Phthalocyanines: Properties and Applications*", Vol.1-4, VCH Publishers Inc., New York, USA, **(1989, 1992, 1993, 1996)**.

[6] N. Chebotareva, T. Nyokong, Metallophthalocyanine catalysed electroreduction of nitrate and nitrite ions in alkaline media, Journal of applied electrochemistry 27(8) (1997) 975-981.

[7] K.I. Zagal, J.H.: "Metallophthalocyanines as catalysts in electrochemical reactions", Coordination Chemistry Reviews, 119 (1992) 89-136.

[8] P.N. Mashazi, P. Westbroek, K.I. Ozoemena, T. Nyokong, Surface chemistry and electro catalytic behaviour of tetra-carboxy substituted iron, cobalt and manganese phthalocyanine monolayers on gold electrode, Electrochimica acta 53(4) (2007) 1858-1869.

[9] N. Sehlotho, T. Nyokong, Effects of ring substituents on electro catalytic activity of manganese phthalocyanines towards the reduction of molecular oxygen, Journal of Electroanalytical Chemistry 595(2) (2006) 161-167.

[10] G. Ariel Valiente, M. Marco César, C. Maria Eugenia. Phthalocyanines as Molecular

Scaffolds to Block Disease-Associated Protein Aggregation, May 2016, Accounts of Chemical Research 49(5)

[11] N. Chebotareva, T. Nyokong, First-row transition metal phthalocyanines as catalysts for water electrolysis: a comparative study, Electrochimica acta 42(23-24) (1997) 3519-3524.

[12] J. Oni, P. Westbroek, T. Nyokong, Voltammetric detection of vitamin B1 at carbon paste electrodes and its determination in tablets, Electroanalysis: An International Journal Devoted to Fundamental and Practical Aspects of Electroanalysis 14(17) (2002) 1165-1168.

[13] B. Akkurt, A. Koca, E. Hamuryudan, Synthesis, in situ spectroelectrochemistry and in situ electrocolorimetry of electrochromic octakis (chloroethylsulfanyl) phthalocyaninatomanganese (III) chloride, New Journal of Chemistry 33(11) (2009) 2248-2254.

[14] S. Gupta, T.N. Misra, Manganese phthalocyanine for the detection of fish freshness by its trimethylamine emission, Sensors and Actuators B: Chemical 41(1-3) (1997) 199-202.

[15] O. Dolotova, O. Yuzhakova, L. Solovyova, E. Shevchenko, V. Negrimovsky, E. Lukyanets, O. Kaliya, Water-soluble manganese phthalocyanines, Journal of Porphyrins and Phthalocyanines 17(08n09) (2013) 881-888.

[16] I.E. Brumboiu, R. Totani, M. de Simone, M. Coreno, C. Grazioli, L. Lozzi, H.C. Herper, B. Sanyal, O. Eriksson, C. Puglia, Elucidating the 3d electronic configuration in manganese phthalocyanine, The Journal of Physical Chemistry A 118(5) (2014) 927-932.

[17] G. Mbambisa, P. Tau, E. Antunes, T. Nyokong, Synthesis and electrochemical properties of purple manganese(III) and red titanium(IV) phthalocyanine complexes octa-substituted at non-peripheral positions with pentylthio groups, Polyhedron 26(18) (2007) 5355-5364.

[18] J. Janczak, R. Kubiak, M. Śledź, H. Borrmann, Y. Grin, Synthesis, structural investigations and magnetic properties of dipyridinated manganese phthalocyanine, MnPc (py) 2, Polyhedron 22(19) (2003) 2689-2697.

[19] R. Ağcaabat, C. Seslikaya, V. Fındık, S.S. Erdem, Z. Odabaş, Systematically investigation of the effect of backsubstituted methoxy groups on the spectral and acid sensing properties of thiobridged phthalocyanines, New Journal of Chemistry (2023) Submit manuscript.

[20] R. Li, X. Zhang, P. Zhu, D.K.P. Ng, N. Kobayashi, J. Jiang, Electron-Donating or -Withdrawing Nature of Substituents Revealed by the Electrochemistry of Metal-Free Phthalocyanines, Inorganic Chemistry 45(5) (2006) 2327-2334.

[21] K.I. Ozoemena, T. Nyokong, Novel amperometric glucose biosensor based on an ether-linked cobalt(II) phthalocyanine–cobalt(II) tetraphenylporphyrin pentamer as a redox mediator, Electrochimica Acta 51(24) (2006) 5131-5136.

[22] V. Mani, R. Devasenathipathy, S.-M. Chen, S.-T. Huang, V.S. Vasantha, Immobilization of glucose oxidase on graphene and cobalt phthalocyanine composite and its application for the determination of glucose, Enzyme and Microbial Technology 66 (2014) 60-66.

[23] D. Akyüz, A. Koca, An electrochemical sensor for the detection of pesticides based on the hybrid of manganese phthalocyanine and polyaniline, Sensors and Actuators B: Chemical 283 (2019) 848-856.

[24] O. Koyun, S. Gorduk, M. Gencten, Y. Sahin, A novel copper(ıı) phthalocyanine-modified multiwalled carbon nanotube-based electrode for sensitive electrochemical detection of bisphenol A, New Journal of Chemistry 43(1) (2019) 85-92.

[25] H. Xu, J. Xiao, B. Liu, S. Griveau, F. Bedioui, Enhanced electrochemical sensingof thiols based on cobalt phthalocyanine immobilized on nitrogen-doped graphene, Biosensors and Bioelectronics 66 (2015) 438-444.

[26] M.K.S. Monteiro, S.S.M. Paiva, D.R. da Silva, V.J.P. Vilar, C.A. Martínez-Huitle, E.V. dos Santos, Novel cork-graphite electrochemical sensor for voltammetric determination of caffeine, Journal of Electroanalytical Chemistry 839 (2019) 283-289.

[27] C.-L. Lin, C.-C. Lee, K.-C. Ho, Spectroelectrochemical studies of manganese phthalocyanine thin films for applications in electrochromic devices, Journal of Electroanalytical Chemistry 524-525 (2002) 81-89.

[28] C. Solis, E. Baigorria, M.E. Milanesio, G. Morales, E.N. Durantini, L. Otero, M.

Gervaldo, Electrochemical polymerization of EDOT modified Phthalocyanines and their applications as electrochromic materials with green coloration, and strong absorption in the Near-IR, Electrochimica Acta 213 (2016) 594-605.

[29] E. Baturhan Orman, M.B. Sağlam, A.R. Özkaya, Novel peripherally substituted metal-free, zinc (II), and cobalt (II) phthalocyanines with 1,1'-thiobis(2-napthol) and additional tetraphthalonitrile groups: Synthesis, aggregation behavior, electrochemical redox and electro catalytic oxygen reducing properties, Synthetic Metals 263 (2020) 116351.

[30] N. Kocyigit, U.E. Ozen, M. Ozer, B. Salih, A.R. Ozkaya, O. Bekaroglu, Electro catalytic Activity of Novel Ball-Type Metallophthalocyanines with Trifluoro Methyl Linkages in Oxygen Reduction Reaction and Application as Zn-Air Battery Cathode Catalyst, Electrochimica Acta 233 (2017) 237-248.

[31] Ü.E. Özen, E. Doğan, M. Özer, Ö. Bekaroğlu, A.R. Özkaya, Communication—High-performance and non-precious bifunctional oxygen electro catalysis with binuclearball-type phthalocyanine based complexes for zinc-air batteries, Journal of The Electrochemical Society 163(9) (2016) A2001.

[32] İ. Koç, M. Özer, A.R. Özkaya, Ö. Bekaroğlu, Electro catalytic activity, methanol tolerance and stability of perfluoroalkyl-substituted mononuclear, and ball-type dinuclear cobalt phthalocyanines for oxygen reduction in acidic medium, Dalton Transactions (32) (2009) 6368-6376.

[33] İ. Koç, M. Çamur, M. Bulut, A.R. Özkaya, Electro catalytic Performances of Carbon Supported Metallophthalocyanine and Pt/Metallophthalocyanine Catalysts Towards Dioxygen Reduction in Acidic Medium, Catalysis Letters 131(3) (2009) 370-380.

[32] Koca, Copper phthalocyanine complex as electro catalyst for hydrogen evolution reaction, Electrochemistry Communications 11(4) (2009) 838-841.

[34] E.B. Orman, Z. Odabaş, A.R. Özkaya, High Electrochemical Versatility and Applicability with Metal Phthalocyanines Carrying Peripheral 2,3-dihydro-1H-inden-5-yloxy Substituents: Rich Redox Behavior, Oxygen Electrocatalysis and Electrochromism, Journal of The Electrochemical Society 165(9) (2018) h530-h548.

[35] K.P. Madhuri, N.S. John, Supercapacitor application of nickel phthalocyanine

nanofibers and its composite with reduced graphene oxide, Applied Surface Science 449 (2018) 528-536.

[36] H. Karaca, Redox chemistry, spectroelectrochemistry and catalytic activity of novel synthesized phthalocyanines bearing four Schiff bases on the periphery, Journal of Organometallic Chemistry 822 (2016) 39-45.

[37] C.G. Claessens, U. Hahn, T. Torres, Phthalocyanines: From outstanding electronic properties to emerging applications, The Chemical Record 8(2) (2008) 75-97.

[38] V. Mani, R. Devasenathipathy, S.-M. Chen, J.-A. Gu, S.-T. Huang, Synthesis and characterization of graphene-cobalt phthalocyanines and graphene-iron phthalocyanine composites and their enzymatic fuel cell application, Renewable Energy 74 (2015) 867-874.

[39] H. Yalazan, Y.E. Maden, A. Koca, H. Kantekin, Multi-step syntheses, electrochemistry and spectroelectrochemistry of peripheral CoII, CuII and MnIIICl phthalocyanines bearing pyrazoline, Journal of Molecular Structure 1269 (2022) 133788.

[40] H. Yalazan, H. Kantekin, Ö. Budak, A. Koca, Non-peripheral tetra methoxylated pyrazoline bearing CoII, CuII and MnIIICl phthalocyanines: Syntheses, electrochemistry and spectroelectrochemistry, Journal of Organometallic Chemistry 973-974 (2022) 122405.

[41] R. Bayrak, S.K. Ataşen, I. Yılmaz, İ. Yalçın, M. Erman, Y. Ünver, İ. Değirmencioğlu, Synthesis and Spectro-Electrochemical Properties of New Metallophthalocyanines Having High Electron Transfer Capability, Journal of Molecular Structure 1231 (2021) 129677.

[42] S. Şahin, Ö. Akdağ, E.B. Orman, Z. Odabaş, A.R. Özkaya, Electrochemical and in-situ spectroelectrochemical properties of novel (5-(tert-butyl)-2-((3,4-dicyanophenoxy)methyl)phenyl)methanolate substituted mononuclear metal phthalocyanines, Journal of Molecular Structure 1276 (2023) 134769.

[43] Y.E. Maden, G.G. Köse, G.K. Karaoğlan, A. Koca, Electrochemical and spectroelectrochemical characterizations of phthalocyanines bearing peripherally tetra-4-carboxyethylenephenoxy anchoring groups and usage as photosensitizers of dye-sensitized solar cell, Journal of Electroanalytical Chemistry 929 (2023) 117104.

[44] S. Şahin, Ö. Akdağ, Z. Odabaş, A.R. Özkaya, Ball type (4-(tert-butyl)-1,2-phenylene)dimethanolate bridged dinuclear metallo phthalocyanines: Synthesis, characterization, electrochemistry, and in situ spectroelectrochemistry, Polyhedron 258 (2024) 117042.

[45] A.M. Sevim, S. Çakar, M. Özacar, A. Gül, Electrochemical and photovoltaic properties of highly efficient solar cells with cobalt/zinc phthalocyanine sensitizers, Solar Energy 160 (2018) 18-24.

[46] R. Słota, G. Dyrda, Z. Hnatejko, J. Karolczak, Z. Stryła, Effect of air-absorbed oxygen and moisture on the chemical stability of photoexcited Mg, Zn and Eu phthalocyanines in dimethylformamide, Journal of Porphyrins and Phthalocyanines 10(01) (2006) 43-54.

[47] T. Furuyama, K. Satoh, T. Kushiya, N. Kobayashi, Design, Synthesis, and Properties of Phthalocyanine Complexes with Main-Group Elements Showing Main Absorption and Fluorescence beyond 1000 nm, Journal of the American Chemical Society 136(2) (2014) 765-776.

[48] S. Altun, A. Altındal, M. Bulut, Synthesis, characterization and dielectric properties of novel axial coumarin-substituted titanium(IV) phthalocyanines, Polyhedron 49(1) (2013) 41-49.

[49] S. Altun, Z. Odabaş, A. Altındal, A.R. Özkaya, Coumarin-substituted manganese phthalocyanines: synthesis, characterization, photovoltaic behaviour, spectral and electrochemical properties, Dalton Transactions 43(21) (2014) 7987-7997.

[50] C.C. Leznoff, L.S. Black, A. Hiebert, P.W. Causey, D. Christendat, A.B.P. Lever, Red manganese phthalocyanines from highly hindered hexadecaalkoxyphthalocyanines, Inorganica Chimica Acta 359(9) (2006) 2690-2699.

[51] M.J. Cook, J. McMurdo, D.A. Miles, R.H. Poynter, J.M. Simmons, S.D. Haslam,

[52] R.M. Richardson, K. Welford, Monolayer behaviour and Langmuir–Blodgett film properties of some amphiphilic phthalocyanines: factors influencing molecular organisation within the film assembly, Journal of Materials Chemistry 4(8) (1994) 1205-1213.

[53] R.D. George, A.W. Snow, J.S. Shirk, W. Barger, The alpha substitution effect on

phthalocyanine aggregation, Journal of Porphyrins and Phthalocyanines (2012).

[54] F.A. Kılıçarslan, A. Erdoğmuş, Ö. Budak, A. Koca, Synthesis, characterization, electrochemistry and spectroelectrochemistry of new non-peripherally substituted lutetium bis phthalocyanines, Inorganica Chimica Acta 561 (2024) 121870.

[55] A.M. Bond, 2.15 - Electrochemistry: General Introduction, in: J.A. McCleverty,

[56] T.J. Meyer (Eds.), Comprehensive Coordination Chemistry II, Pergamon, Oxford, 2003,pp. 197-222.

[57] A.B.P. Lever, P.C. Minor, Electrochemistry of main-group phthalocyanines, Inorganic Chemistry 20(11) (1981) 4015-4017.

[58] A.B.P. Lever, S. Licoccia, K. Magnell, P. Minor, B. Ramaswamy, Mapping of the Energy Levels of Metallophthalocyanines via Electronic Spectroscopy, Electrochemistry, and Photochemistry, ACS Symp. Series. 201 (1982) 21.

[59] M. Stillman, C.C. Leznoff, A.B.P. Lever, Phthalocyanine, Principles and Properties1 (1989).

[60] A.B.P. Lever, J.P. Wilshire, Electrochemistry of iron phthalocyanine complexes in nonaqueous solvents and the identification of five-coordinate iron(I) phthalocyanine derivatives, Inorganic Chemistry 17(5) (1978) 1145-1151.

[61] F. Bedioui, S. Griveau, T. Nyokong, A. John Appleby, C.A. Caro, M. Gulppi, G. Ochoa, J.H. Zagal, Tuning the redox properties of metalloporphyrin- and metallophthalocyanine-based molecular electrodes for the highest electro catalytic activity in the oxidation of thiols, Physical Chemistry Chemical Physics 9(26) (2007) 3383-3396.

[62] Y. Wu, Z. Jiang, X. Lu, Y. Liang, H. Wang, Domino electroreduction of CO(2) to methanol on a molecular catalyst, Nature 575(7784) (2019) 639-642.

[63] X. Zhang, Y. Wang, M. Gu, M. Wang, Z. Zhang, W. Pan, Z. Jiang, H. Zheng, M. Lucero, H. Wang, G.E. Sterbinsky, Q. Ma, Y.-G. Wang, Z. Feng, J. Li, H. Dai, Y. Liang, Molecular engineering of dispersed nickel phthalocyanines on carbon nanotubes for selective CO2 reduction, Nature Energy 5(9) (2020) 684-692.

[64] J.-P. Zhong, Y.-J. Fan, H. Wang, R.-X. Wang, L.-L. Fan, X.-C. Shen, Z.-J. Shi, Copper phthalocyanine functionalization of graphene nanosheets as support for

platinum nanoparticles and their enhanced performance toward methanol oxidation, Journal of Power Sources 242 (2013) 208-215.

[65] M. Peterson, Synthesis, Characterization, and Electrochemical Properties of Metallophthalocyanines for Use in Energy Storage Applications., UC Santa Barbara, 2021.

[66] K. Kadish, K. Smith, R. Guilard, The porphyrin handbook: Phthalocyanines: Spectroscopic and electrochemical characterization, 2012.

[67] J.C. Swarts, E.H.G. Langner, N. Krokeide-Hove, M.J. Cook, Synthesis and electrochemical characterisation of some long chain 1,4,8,11,15,18,22,25-octa-alkylated metal-free and zinc phthalocyanines possessing discotic liquid crystalline properties, Journal of Materials Chemistry 11(2) (2001) 434-443.

[68] M. L'Her, A. Pondaven, 104 - Electrochemistry of Phthalocyanines, in: K.M.Kadish, K.M. Smith, R. Guilard (Eds.), The Porphyrin Handbook, Academic Press, Amsterdam, 2003, pp. 117-169.

[69] T. Nyokong, Electronic Spectral and Electrochemical Behavior of Near Infrared Absorbing Metallophthalocyanines, in: J. Jiang (Ed.), Functional Phthalocyanine Molecular Materials, Springer Berlin Heidelberg, Berlin, Heidelberg, 2010, pp. 45-87.

[70] B. Agboola, K.I. Ozoemena, P. Westbroek, T. Nyokong, Synthesis and electrochemical properties of benzyl-mercapto and dodecyl-mercapto tetrasubstituted manganese phthalocyanine complexes, Electrochimica Acta 52(7) (2007) 2520-2526.

[71] J. Zhu, Y. Shen, F. Gu, J. Tao, J. Zhang, Preparation and photovoltaic properties of near-infrared absorbing manganese(II) phthalocyanine polymer films, Materials Letters 61(6) (2007) 1296-1298.

[72] J. Obirai, T. Nyokong, Synthesis, electrochemical and electro catalytic behaviour of thiophene-appended cobalt, manganese and zinc phthalocyanine complexes, Electrochimica Acta 50(27) (2005) 5427-5434.

[73] J. Obirai, T. Nyokong, Electrochemical studies of manganese tetraamminophthalocyanine monomer and polymer, Electrochimica Acta 49(9) (2004) 1417-1428.

[74] S. Knecht, K. DÜRr, G. Schmid, L.R. Subramanian, M. Hanack, Synthesis and

properties of soluble phthalocyaninatomanganese(III) complexes, Journal of Porphyrins and Phthalocyanines 03(04) (1999) 292-298.

[75] J. Obirai, T. Nyokong, Electrochemical and catalytic properties of chromium tetraaminophthalocyanine, Journal of Electroanalytical Chemistry 573(1) (2004) 77-85.

[76] B. Köksoy, O. Soyer, E.B. Orman, A.R. Özkaya, M. Bulut, Synthesis, electrochemistry and In situ spectroelectrochemistry of novel tetra dimethyl 5-oxyisophthalate substituted Co(II), Mn(III), and μ-oxo-dimer Fe(III) phthalocyanines, Dyes and Pigments 118 (2015) 166-175.

[77] E.B. Orman, Z. Yazar, M. Pişkin, Z. Odabaş, A.R. Özkaya, Novel 2,6-dimethoxyphenoxy alpha substituted phthalocyaninato metal complexes: Electrochemistry, In situ spectroelectrochemistry and oxygen electro catalysis, SyntheticMetals 290 (2022) 117139.

[78] H.Y. Yenilmez, Ö. Akdağ, A.M. Sevim, A. Koca, Z.A. Bayır, Electrochemical, spectroelectrochemical characterization and electropolymerization of 2-(4-methyl-1,3-thiazol-5-yl)ethoxy-substituted manganese and indium phthalocyanines, Polyhedron 99 (2015) 244-251.

[79] M. Arıcı, D. Arıcan, A.L. Uğur, A. Erdoğmuş, A. Koca, Electrochemical and spectroelectrochemical characterization of newly synthesized manganese, cobalt, iron and copper phthalocyanines, Electrochimica Acta 87 (2013) 554-566.

[80] A.B.P. Lever, P.C. Minor, J.P. Wilshire, Electrochemistry of manganese phthalocyanine in nonaqueous media, Inorganic Chemistry 20(8) (1981) 2550-2553.

[81] M.N. Yaraşir, M. Kandaz, A. Koca, B. Salih, Polytopic cation receptor functional phthalocyanines: Synthesis, characterization, electrochemistry and metal ion binding, Polyhedron 26(5) (2007) 1139-1147.

[82] Ö. İpsiz, H.Y. Yenilmez, K. Kaya, A. Koca, Z.A. Bayır, Carbazole-substituted metallo-phthalocyanines: Synthesis, electrochemical, and spectroelectrochemical properties, Synthetic Metals 217 (2016) 94-101.

[83] M. Canlıca, I.N. Booysen, T. Nyokong, Synthesis and electrochemical behavior of novel peripherally and non-peripherally substituted ball-type cobalt phthalocyanine complexes, Polyhedron 30(3) (2011) 522-528.

[84] N. Daban, E.B. Orman, L. Meyancı, A. Altındal, M. Özer, A.R. Özkaya, Electrochemical, spectroelectrochemical, electro catalytic oxygen reducing, and heavy metal ion sensing properties of novel tetrakis-[4-((2, 8-bis (trifluoromethyl) quinolin-4-yl) oxyl)] substituted metallophthalocyanines, Journal of Molecular Structure 1250 (2022) 131707.

[85] G.S. Amitha, S. Vasudevan, Optical and electrochemical properties of peripherally substituted chromium and manganese phthalocyanines, Polyhedron 212 (2022) 115591.

[86] A.A. Esenpınar, A.R. Özkaya, M. Bulut, Synthesis and electrochemical properties of crown ether functionalized coumarin substituted cobalt and copper phthalocyanines, Journal of Organometallic Chemistry 696(24) (2011) 3873-3881.

[87] N. Farajzadeh, D. Akyüz, A. Koca, M.B. Koçak, Synthesis, electrochemistry and in situ spectroelectrochemistry of novel tetra- and octa-substituted metallophthalocyanines bearing peripherally 4-(trifluoromethoxy)phenoxy groups, Polyhedron 177 (2020) 114264.

[88] S.G. Feridun, E.B. Orman, Ü. Salan, A.R. Özkaya, M. Bulut, Synthesis, characterization, and electrochemical and in-situ spectroelectrochemical properties of novel peripherally and non-peripherally 7-oxy-3-(3,4-dimethoxyphenyl) coumarin substituted phthalocyanines, Dyes and Pigments 160 (2019) 315-327.

[89] C.C. Leznoff, L.S. Black, A. Hiebert, P.W. Causey, D. Christendat, A. Lever, Red manganese phthalocyanines from highly hindered hexadecaalkoxyphthalocyanines, Inorganica chimica acta 359(9) (2006) 2690-2699.

[90] K. Roy, A. Rana, J.N. Heil, B.M. Tackett, J.E. Dick, For Zinc Metal Batteries, How Many Electrons go to Hydrogen Evolution? An Electrochemical Mass Spectrometry Study, Angew Chem Int Ed Engl 63(11) (2024) e202319010.

[91] J. Pan, Y.Y. Xu, H. Yang, Z. Dong, H. Liu, B.Y. Xia, Advanced Architectures and Relatives of Air Electrodes in Zn–Air Batteries, Advanced Science 5(4) (2018) 1700691.

[92] S. Tao, S. Xiang, Y. Yu, H. Lan, C. Liu, J. Zhang, Regulating electron region of central Fe atom in iron phthalocyanine by N, S-doped carbon nanofibers as efficient oxygen reduction catalysts for high-performance Zn-air battery, Carbon 220 (2024) 118893.

[93] Z.-L. Wang, D. Xu, J.-J. Xu, X.-B. Zhang, Oxygen electrocatalysts in metal–air batteries: from aqueous to nonaqueous electrolytes, Chemical Society Reviews 43(22) (2014) 7746-7786.

[94] H. Zhang, Z. Zhang, Z. Zhang, Y. Li, Y. Hou, P. Liu, B. Xu, H. Zhang, Y. Liu, J. Guo, Highly dispersed ultrasmall iron phthalocyanine molecule clusters confined by mesopore-rich N-doped hollow carbon nanospheres for efficient oxygen reduction reaction and Zn-air battery, Chemical Engineering Journal 469 (2023) 143996.

[95] Y. Wu, J. Chen, J. Liu, L. Zhang, R. Abazari, T.-T. Li, J. Qian, Iron phthalocyanine coupled with Co-Nx sites in carbon nanostraws for Zn-Air batteries, Chemical Engineering Journal 503 (2025) 158343.

[96] Y. Ma, J. Li, X. Liao, W. Luo, W. Huang, J. Meng, Q. Chen, S. Xi, R. Yu, Y. Zhao, L. Zhou, L. Mai, Heterostructure Design in Bimetallic Phthalocyanine Boosts Oxygen Reduction Reaction Activity and Durability, Advanced Functional Materials 30(50) (2020) 2005000.

[97] Z.-y. Mei, S. Cai, G. Zhao, X. Zou, Y. Fu, J. Jiang, Q. An, M. Li, T. Liu, H. Guo, Boosting the ORR active and Zn-air battery performance through ameliorating the coordination environment of iron phthalocyanine, Chemical Engineering Journal 430 (2022) 132691.

[98] A. Dong, Y. Lin, Y. Guo, D. Chen, X. Wang, Y. Ge, Q. Li, J. Qian, Immobilization of iron phthalocyanine on MOF-derived N-doped carbon for promoting oxygen reduction in zinc-air battery, Journal of Colloid and Interface Science 650 (2023) 2056-2064.

[99] Umit Ergin Ozen, Elvan Dogan, Metin Ozer, Ozer Bekaroglu, and Ali Rıza Ozkaya, Communication—High-Performance and Non-Precious Bifunctional Oxygen Electrocatalysis with Binuclear Ball-Type Phthalocyanine Based Complexes for Zinc-Air Batteries, Journal of The Electrochemical Society, 163 (9) A2001-A2003 (2016)

[100] N. Koçyiğit, Ü.E. Özen, M. Özer, B. Salih, A.R. Özkaya, Ö. Bekaroğlu, Electrocatalytic Activity of Novel Ball-Type Metallophthalocyanines with Trifluoro Methyl Linkages in Oxygen Reduction Reaction and Application as Zn-Air Battery Cathode Catalyst, Electrochimica Acta 233 (2017) 237-248.

[101] A. Dong, Y. Lin, Y. Guo, D. Chen, X. Wang, Y. Ge, Q. Li, J. Qian, Immobilization

of iron phthalocyanine on MOF-derived N-doped carbon for promoting oxygen reduction in zinc-air battery, Journal of Colloid and Interface Science 650 (2023) 2056-2064.

[102] K. Jae Hyung , S. Young Jin , J. Hu Young , J. Sang Hoon , Roles of Fe–N x and Fe–Fe 3 C@C Species in Fe–N/C Electrocatalysts for Oxygen Reduction Reaction, ACS Applied Materials & Interfaces 9(11), February 2017

Papers Presented from the Thesis

- 29th Annual meeting of the international society of Electrochemistry, Czech Republic, 2021

Electrochemical, Spectro-electrochemical and Electro- Catalytic Properties of Novel Di-nuclear Ball type Metallo Phthalocyanines Involving Tertiary Butyl and Oxo Bridging Groups, 2021, 10.13140/RG.2.2.19837.49122

- 29th Annual meeting of the international society of Electrochemistry, Czech Republic, April 2021

Electrochemical, Spectro-electrochemical and Electro-Catalytic Properties of New Mononuclear Metallo Phthalocyanines Involving Tertiary Butyl and Oxo Bridging Groups, 2021, 10.13140/RG.2.2.31581.54243

- 13th International conference on Electrochemistry in Barcelona, Spain, may, 2017

Electrochemical and Electro-Catalytic Oxygen Reducing Properties of Metal Phthalocyanines Involving Tertiary Butyl and Oxo Bridging Groups. Tarifa Kaniz et al., J BiosensBioelectron 2019, Volume 10.

CURRICULUM VITAE

Name : Tarifa KANIZ

Native Language : Bangla

Foreign Language: English, Turkish, Hindi, Urdu

Papers;

- “Electrochemical and *In-situ* exhibited spectroelectrochemical properties of novel 4,40.625*pt′*0.625*pt*-(3,5-di-tert-butyl-1,2- phenylene)bis(oxy) substituted ball-type phthalocyanine compounds. Synthetic Metals, 297 (2023) 117408”. Safinaz Sahin, Tarifa Kaniz, Efe Baturhan Orman, Zafer Odabas, Ali Rıza Özkaya.
- “Electrochemical and In-situ spectroelectrochemical properties of novel mononuclear 2,4-di-tert-butyl-6-(3,4-dicyanophenoxy)phenolate substituted metallophthalocyanine compounds. Polyhedron, 1 october, 2023, 116541”. Safinaz Sahin, Tarifa Kaniz, Efe Baturhan Orman, Zafer Odabas, Ali Rıza Özkaya.